Interpretation of magnetic anomalies using the pseudogravimetric transformation and other methods, with application to tertiary volcanic centres in N-W Scotland

Dhammika Ariyakumara Tantrigoda

INTERPRETATION OF MAGNETIC ANOMALIES USING THE PSEUDOGRAVIMETRIC TRANSFORMATION AND OTHER METHODS, WITH APPLICATION TO TERTIARY VOLCANIC CENTRES IN N-W SCOTLAND

by

Dhammika Ariyakumara Tantrigoda

A thesis submitted for the degree of
Doctor of Philosophy in the University of Durham

Graduate Society

May 1982

ABSTRACT

A method of transforming magnetic anomalies into pseudogravimetric anomalies which uses fast Fourier transforms and a method of interpreting gravity anomalies in three dimensions using a non-linear optimization technique which involves automatic end corrections are developed.

These methods have been used to interpret the complicated aeromagnetic anomalies over the Mull, Skye and Blackstones Bank Tertiary igneous centres of N.W.Scotland. One inch aeromagnetic maps over the complexes have been digitized at 1 km intervals covering 32 x 32 km^2 (Mull and Blackstones Bank) or 64 x 64 km^2 (Skye).

The strongly magnetized rocks of the Mull complex extends in the preferred model to a depth of 2.1 km with normal magnetization of 6.7 A/m. This body is smaller in depth and areal extent than the gravity model of the complex. The magnetic model of the Skye complex consists of two strongly magnetized bodies of opposite polarity and a weakly magnetized region corresponding to the Red Hills granites. A reversely magnetized body of depth extent in the range 1.5km - 3.0km with a modelling magnetization of 4.9 A/m can be identified with the basic and ultrabasic rocks of the Cuillin centre. Normally magnetized body probably represents more weakly magnetized deep seated body which underlains the whole complex and extends to a modelled depth of 14 km with a modelling magnetization of 1.1 A/m. This composite model has approximately equal dimensions to the dense rocks of the gravity model. The main body of the Blackstones Bank magnetic model extends to a depth of 15 km with reverse magnetization of 0.93 A/m. A shallow normally magnetized body occurs within this to depth of the order of 1.0km - 5.0km with a magnetization in the range 0.0A/m-2.47 A/m. The composite model has approximately equal dimensions to the gravity model.

Intense negative anomalies over the lavas and over some intrusive

rocks demonstrate the strong remanent magnetization of these rocks. The magnetic interpretations show that basic and ultrabasic rocks are strongly magnetized and large in volume and the granitic rocks are small in volume, shallow and weakly magnetized. Generally, the magnetic interpretations agree with previous gravity interpretations.

ACKNOWLEDGEMENTS

My thanks are due to Professor M.H.P.Bott for his supervision and many helpful discussions and suggestions in connection with this study. The aeromagnetic data used in the present study was obtained from the I.G.S. with the help of Dr.D.J.Masson-Smith and this is gratefully acknowledged. I also would like to thank Dr.C.H.Emeleus for many useful discussions on the geology of N.W.Scotland and Mr.R.Phillips for helping with the analysis of polished rock specimens from the Isle of Mull and Drs.A.E.Mussett and P.Dagley for discussion on paleomagnetism of Mull.

I would like to thank my colleagues in the Department of Geological Sciences for the help given to me during the course of this study. In particular, Mr.M.D.Linton for advice in problems relating to mathematics, Mr. C.O.Ofoegbu, Mr.C.Uruski, Mr.J.Faithfull and Mr.G.Waghorn for reading the manuscript of this thesis and for interesting discussions.

I am grateful to my wife, Ramani Uppalawanna for her patience, encouragement and assistance in digitizing, drafting and proof reading.

I would also like to thank my parents for providing me with financial assistance for the first year and the Association of Commonwealth Universities for the award of a Commonwealth Scholarship for the last two years of this study.

Finally, I offer my thanks to Mrs. C.Rowes for typing this thesis.

CONTENTS

CHAPTER 1

INTRODUCTION

1.1 Scope of the Study

The main purpose of this study is to develop a method of transforming magnetic anomalies into pseudogravimetric anomalies, a concept which was introduced by Baranov (1957), and to use this method with other methods of magnetic interpretation to interpret the aeromagnetic anomalies over some of the Tertiary volcanic centres of N.W.Scotland. The method of pseudogravimetric transformation using fast Fourier transforms which was developed in this study is discussed in detail in chapter 2. Since the pseudogravimetric anomaly gives the equivalent gravity effect due to a magnetized body which would be caused by a fictitious density contrast proportional to actual magnetization contrast at each point of the body, interpretation of such anomalies must be performed using gravity methods. Automatic and semi-automatic methods of three dimensional gravity interpretation which use the end corrections are developed to interpret the pseudogravimetric anomalies and are presented in chapter 3. Two dimensional automatic methods of magnetic interpretation used in this study are also discussed in this chapter. The aeromagnetic anomalies over three Tertiary igneous centres of N.W. Scotland, Mull, Skye and Blackstones Bank, are selected to apply the method of pseudogravimetric transformation that is developed in this study. The resulting pseudogravimetric anomalies are interpreted and compared with previous geophysical and geological studies of these areas.

This chapter introduces the concept of pseudogravity and gives a general introduction to the Tertiary igneous centres of N.W.Scotland.

1.2 Pseudogravimetric Transformation of Magnetic Anomalies

If a body has a magnetization contrast J and a density contrast

ρ producing a local magnetic potential V and a gravity potential U at an external point, and further if the ratio $\underline{J}/\rho$ is constant throughout the body, then these two potentials will be connected by the well known relation of Poisson

$$V = -\frac{\underline{J} \cdot \underline{\nabla U}}{4\pi\rho G} \qquad 1.2.1$$

where G is the gravitational constant. If γ and $\underline{s}$ are unit vectors along the direction of magnetization of the body and along the direction of the earth's total magnetic field respectively, then the magnetic anomaly T(x,y,z) at an external point due to the body can be written as

$$T(x,y,z) = \frac{\mu_o J}{4\pi\rho G} \frac{d^2U}{dsd\gamma} \qquad 1.2.2$$

where μ_o is the permeability of free space. This equation connects the magnetic anomaly of a body with its gravitational potential provided that $\underline{J}/\rho$ is a constant. In practice this is most unlikely to be the case. If, however, we assume a fictitious density contrast so that $\underline{J}/\rho$ is a constant then we can use 1.2.2 to calculate a theoretical gravity potential from a given magnetic anomaly. From this theoretical gravity potential we can then derive a theoretical gravity anomaly. Such an anomaly is called a pseudogravimetric anomaly. This will not be the true gravity anomaly of the body, but rather is a gravity-like anomaly wholly derived from the true magnetic anomaly. If we choose as our fictitious density contrast the value

$$\rho = \frac{\mu_o J}{4\pi G} \qquad 1.2.3$$

1.2.2 takes the simple form

$$T(x,y,z) = \frac{d^2U}{dsd\gamma} \qquad 1.2.4$$

The pseudogravimetric potential U is calculated by integration of

1.2.4. By taking the vertical derivative of this potential the pseudogravimetric anomaly is found.

The pseudogravimetric transformation of an aeromagnetic anomaly removes its asymmetry due to the inclination of the magnetization vector and the inclination of the earth's total magnetic field. The pseudogravimetric anomaly is therefore symmetrical with respect to the causative body. The characteristic presence of short wavelength features in magnetic anomalies causes problems in interpretation. The pseudogravimetric transformation acts as a filter for the short wavelength anomalies and so removes this difficulty. In addition, it allows us to perform the interpretation using gravity methods which are more straightforward to apply than magnetic methods. The pseudogravimetric anomaly is thus a useful aid to the interpretation of complicated magnetic anomalies.

1.3 Tertiary Igneous Centres of N.W.Scotland

The north-western part of Scotland is one of the areas of the North Atlantic or Thulean province which were subjected to intense volcanic activity about 50-65 m.y. ago during the early Tertiary (Richey et al., 1961, Stewart, 1965, Evans et al. 1973). In each volcanic centre activity characteristically occurred in two stages; extrusion of basaltic lava followed by intrusion of plutonic bodies forming central intrusive complexes. Intrusion of dyke swarms took place during, after and probably also before the intrustion of plutonic bodies. There are two different views about the way in which basaltic lavas have been erupted. Judd (1874) proposed that the lavas were erupted from central volcanoes. Geikie (1897) alternatively suggested that the lavas were extruded by fissure eruption with the dykes in these regions as feeders. Recent studies show that Greenland and North Europe

started to split about 52 m.y. ago as dated by magnetic anomaly 24 (Hailwood et al., 1979). This splitting may be related to the Tertiary igneous activity of the Thulean province (Bott, 1973).

In N.W. Scotland Tertiary igneous complexes can be found in central Skye, Mull, Rhum, Arran, Ardnamurchan and in the St.Kilda group of islands (Figure 1.1). There are several other submerged igneous complexes such as the Blackstones Bank in the sea areas around N.W.Scotland (Figure 1.1). These central complexes consist of various intrusive bodies such as ring dykes, multiple cone sheets, dykes, sills, volcanic plugs, large layered intrusions and products of explosive vents. A wide range of rock types, varying from granitic to ultrabasic, can be observed in the Tertiary igneous complexes. Each of the complexes had a centre, or focus of activity, around which most of the igneous intrusions occurred and in most cases the centre of activity has migrated from place to place within the complex. In Ardnamurchan, Mull and Arran the centre of activity has moved twice, once in Rhum and three times in Skye. A more detailed account of the geology of the three central complexes selected for the application of the present method of pseudogravimetric transformation is given in chapters 4,5 and 6.

Study of surface geology alone is not sufficient to understand the deep structure of the igneous complexes. Geophysical techniques such as gravity and magnetic methods are useful in obtaining such details. All central complexes are characterized by near circular positive gravity anomalies. The observed maximum Bouguer anomaly over the Tertiary volcanic centres are in the range 50-73 mgal, except over the Blackstones Bank which has a maximum Bouguer anomaly of 140 mgal. Interpretation of gravity anomalies over the complexes shows that these

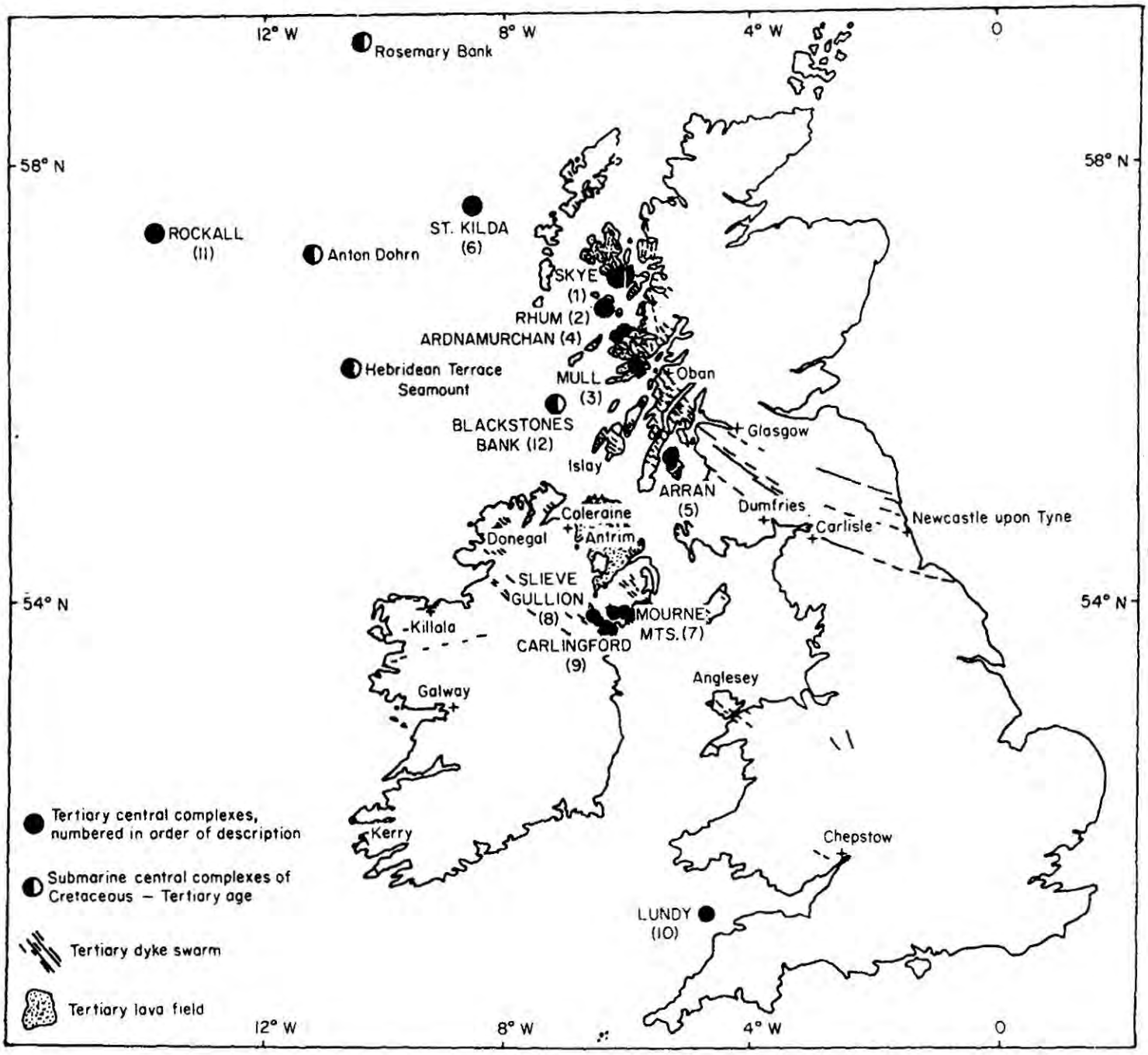

Figure 1.1 Map of the British Isles and surroundings showing the distribution of Tertiary central complexes, submarine centres of Tertiary or Cretaceous age, together with the distribution, on land, of Tertiary dyke swarms and lavas *from* Emeleus (1982).

are underlain by basic and ultrabasic bodies extending to a great depth (Bott and Tuson, 1973, McQuillin, et al., 1975). The aeromagnetic anomaly maps over the Tertiary igneous complexes prepared by the Institute of Geological Sciences of Great Britain show intense positive and negative anomalies (see Figure 4.1, 5.1 and 6.1), suggesting that the complexes are underlain by massive magnetized bodies. Owing to the presence of a large number of near surface intrusions and adjacent lavas, the aeromagnetic anomalies take an extremely complicated form making their interpretation difficult using normal magnetic methods. The pseudogravimetric transformation method introduced in this chapter is very useful in interpreting magnetic anomalies of this nature.

CHAPTER 2

THEORY OF PSEUDOGRAVIMETRIC TRANSFORMATION OF MAGNETIC ANOMALIES

2.1 Introduction

This chapter describes a method of performing the pseudogravimetric transformation of magnetic anomalies using Fourier transforms. This method, which was developed by P.V.Stavrev, was brought to the author's attention by Professor M.H.P.Bott. An independent development of the same method by the author is presented here. This method is basically similar to the Cordell and Taylor (1971) method of pseudogravimetric transformation although the method of derivation is different and the final formula takes a different form. The reliability of the method of pseudogravimetric transformation developed in this chapter is examined by applying it to a magnetic field calculated from a known simple structure and comparing the resulting pseudogravimetric anomaly with the calculated gravity anomaly due to the same structure assuming that it has a density contrast equal to the fictitious density constrast of the pseudogravimetric transformation. A review of previous methods of performing pseudogravimetric transformation is given in 2.2. Some practical problems involved in the present method are discussed in 2.7.

2.2 A Review of Methods of Performing Pseudogravimetric Transformations

Baranov (1957) first introduced the pseudogravimetric transformation of magnetic anomalies. His method involves a double integration of the vertical derivative of 1.2.4 along the opposite direction to the magnetization vector and along the opposite direction to the earth's total field. He also presented a practical way of computing the pseudogravimetric anomaly and its vertical derivatives using numerical

grids. There are two disadvantages of this method; it does not take into account the direction of remanent magnetization, and it fails when the inclination of the magnetization vector is less than 30^{o}.

Bott et al.(1966) presented a two-dimensional method of performing the pseudogravimetric transformation which takes into account the direction of remanent magnetization and is valid for any inclination of the magnetization vector. In this method magnetic and gravimetric potentials and fields are considered as complex functions whose transformation is performed using the Cauchy-Riemann equations and Poisson's relationship. This method can also be used to estimate the remanent direction of magnetization. Bott et al. used this method to estimate the direction of remanent magnetization of the Lambay magnetic anomaly in the West Irish Sea.

A two-dimensional method of performing pseudogravimetric transformation using the equivalent layer theorem has been given by Bott and Ingles (1972). This method relates a magnetic anomaly and its pseudogravimetric anomaly to a common fictitious layer. This fictitious layer is divided into a series of compartments having rectangular cross-sections whose magnetization is calculated by inverting the observed magnetic anomaly. The pseudogravimetric anomaly is computed by assigning to each compartment a suitable density contrast proportional to the magnetization. This method can also be used to calculate the pseudomagnetic anomaly starting from the gravity anomaly and it can be easily extended to the three-dimensional case.

Cordell and Taylor (1971) performed the pseudogravimetric transformation using Fourier transforms. In this method they derived the relationship between the Fourier transform of the magnetic anomaly

and the pseudogravimetric anomaly using Poisson's relationship. These two transforms are connected by a factor in the frequency domain depending on the magnetization to density ratio, direction of magnetization, and the direction of earth's total field. By multiplying the Fourier transform of the magnetic anomaly by this factor and applying a phase shift, the Fourier transform of the pseudogravimetric anomaly can be found and by taking its inverse transform the pseudogravimetric anomaly can be determined. Cordell and Taylor used this method to transform magnetic anomalies over a North Atlantic seamount into pseudogravimetric anomalies.

Gunn (1972) described a method of performing linear transformations on gravity and magnetic fields by using Weiner filters. A Weiner filter converts a given input into a specified output in such a way that the sum of the squares of the difference between the specified output and the actual output is a minimum. This method can be used to perform the pseudogravimetric transformation of magnetic anomalies, where the specified output should be the gravity anomaly due to a model body which has approximately the same dimensions as the geological feature causing the magnetic anomaly. Therefore unlike the methods described earlier, this approach requires some knowledge of the dimensions of the geological features which cause the anomaly.

Shuey (1972) presented a method of calculating pseudogravimetric anomalies by using Hilbert transforms. He showed that the vertical gradient of the pseudogravimetric anomaly can be written as a linear combination of the magnetic anomaly and its Hilbert transform. The vertical integration of this linear combination yields the pseudogravimetric anomaly. The success of this technique depends on the accuracy of the

computer programs which perform Hilbert transforms. The computer routines developed by Shuey give accurate results except at the edges of the profile. Since this is a fault of most of the methods discussed previously, it is unlikely to be a serious disadvantage.

The most recent method of three-dimentional pseudogravimetric transformation known to the author is published by Savinisky (1976). This method involves two line integrations similar to Baranov's method. In this case the result is valid for any direction of the induced magnetization. However, it still fails to take into account the remanent direction of magnetization.

Another technique which removes distortion in a magnetic field has been developed by various authors (Baranov and Naudy, 1964, Bhattacharyya, 1965, Kanasewich and Agarwal, 1970, Baranov, 1975). This method is known as the reduction of the magnetic anomaly to the pole and it gives the magnetic anomaly of the causative body as if it were at the magnetic North pole. The mathematical calculations involved in this method are similar to that of pseudogravimetric transformation. The first step involves the recovery of the potential U of 1.2.2 by carrying out two line integrations and the second step involves the calculation of the anomaly reduced to the pole by taking its second vertical derivative. We can clearly see that the anomaly reduced to the pole is just a quantity proportional to the pseudogravimetric vertical gradient. This method is useful when comparing magnetic anomalies measured at different magnetic latitudes.

2.3 Derivation of the formula which performs the pseudogravimetric transformation

This section describes a method of performing the pseudogravimetric

transformation using Fourier transforms. The equation 1.2.4 given in chapter 1 states the relationship between the magnetic anomaly T(x,y,z) and the pseudogravimetric potential U(x,y, z).

$$T(x,y,z) = \frac{d^2U}{d\,s\,d\,\gamma} \qquad 2.3.1$$

where $\underline{s}$ and $\underline{\gamma}$ are unit vectors along the earth's total magnetic field and along the direction of magnetization. It is assumed that the body causing the anomaly has a constant fictitious density contrast ρ given by

$$\rho = \frac{\mu_o J}{4\pi G} \qquad 2.3.2$$

where,

J = magnitude of the magnetization contrast of the body,

G = gravitational constant.

Firstly, the pseudogravimetric potential U is recovered by successively integrating 2.3.1 along directions opposite to the earth's total magnetic field ($-\underline{s}$) and the magnetization vector ($-\underline{\gamma}$). Then by taking its vertical derivative, the pseudogravimetric anomaly can be found. To do this integration it is necessary to represent the magnetic anomaly as a function of s and γ. By solving Laplace's equation in Cartesian coordinates the magnetic anomaly can be obtained as a function of x,y and z which are related to s and γ. Then by transforming the variables s and γ to z the magnetic anomaly can be integrated with respect to z to obtain the pseudogravimetric potential.

Let XYZ be a right-handed rectangular Cartesian coordinate system with the X-axis pointing towards north and Z-axis pointing vertically downwards. Let us also assume that all magnetized

material producing magnetic anomalies is situated below the XY plane ($z > 0$). It is possible to write the magnetic anomaly $T(x,y,z)$ ($z < 0$), by solving Laplace's equation, as (Bhattacharyya, 1965)

$$T(x,y,z) = \sum_{k_1=o}^{\infty} \sum_{k_2=o}^{\infty} \exp\{2\pi(\frac{k_1^2}{L_x^2} + \frac{k_2^2}{L_y^2})^{\frac{1}{2}} z\}(A_{k_1} \cos \frac{2\pi x k_1}{L_x}$$

$$+ B_{k_1} \sin \frac{2\pi x k_1}{L_x})(C_{k_2} \cos \frac{2\pi y k_2}{L_y} + D_{k_2} \sin \frac{2\pi y k_2}{L_y}) \qquad 2.3.3$$

where,

L_x, L_y = fundamental wavelengths in X and Y directions,

k_1, k_2 = 0,1,2, ... ,

$A_{k_1}, B_{k_1}, C_{k_2}, D_{k_2}$ = coefficients of the Fourier series expansion.

It is useful to write the Fourier series expansion in the above equation in exponential form, since it allows the use of a fast Fourier transform algorithm in the ensuing computation. By expressing the Fourier series expansion in 2.3.3. in the exponential form, it can be written

$$T(x,y,z) = \sum_{k_1=-\infty}^{\infty} \sum_{k_2=-\infty}^{\infty} \exp\{2\pi(\frac{k_1^2}{L_x^2} + \frac{k_2^2}{L_y^2})^{\frac{1}{2}} z\}$$

$$\cdot F(k_1,k_2) \exp\{2\pi i (\frac{k_1 x}{L_x} + \frac{k_2 y}{L_y})\} \qquad 2.3.4$$

where,

$F(k_1, k_2)$ = complex Fourier series coefficients.

If a square magnetic anomaly map of length L is digitised at equal intervals (Δx) at N^2 points, then T(x,y,z) can be represented approximately by

$$T(x,y,z) = \sum_{k_1=-p}^{q} \sum_{k_2=-p}^{q} F(k_1,k_2) \exp\{\frac{2\pi i}{N}(k_1 x + k_2 y)\}$$

$$\exp\{\frac{2\pi}{N}(k_1^2 + k_2^2)^{\frac{1}{2}} z\} \qquad 2.3.5$$

where,

p = (N-1)/2 and q = (N-1)/2 when N is odd

p = N/2 -1 and q = N/2 when N is even

In the above equation x,y and z are in units of digitizing interval Δx. Substituting for T(x,y,z) in 2.3.1 from 2.3.5 gives

$$\frac{d^2U}{ds d\gamma} = \sum_{k_1=-p}^{q} \sum_{k_2=-p}^{q} F(k_1,k_2) \exp\{\frac{2\pi i}{N}(k_1 x + k_2 y)\}$$

$$\cdot \exp\{\frac{2\pi}{N}(k_1^2 + k_2^2)^{\frac{1}{2}} z\} \qquad 2.3.6$$

Let us assume that the magnetic anomaly is known at an elevation z_1, ($z_1 < 0$) and $\vec{AB}$ (Figure 2.1) is in the direction of earth's total magnetic field. First 2.3.6 is integrated from $B(x_1,y_1,z_1)$ to minus infinity.

If A(x,y,z) ($z < 0$) is a variable point and $B(x_1,y_1,z_1)$ is a

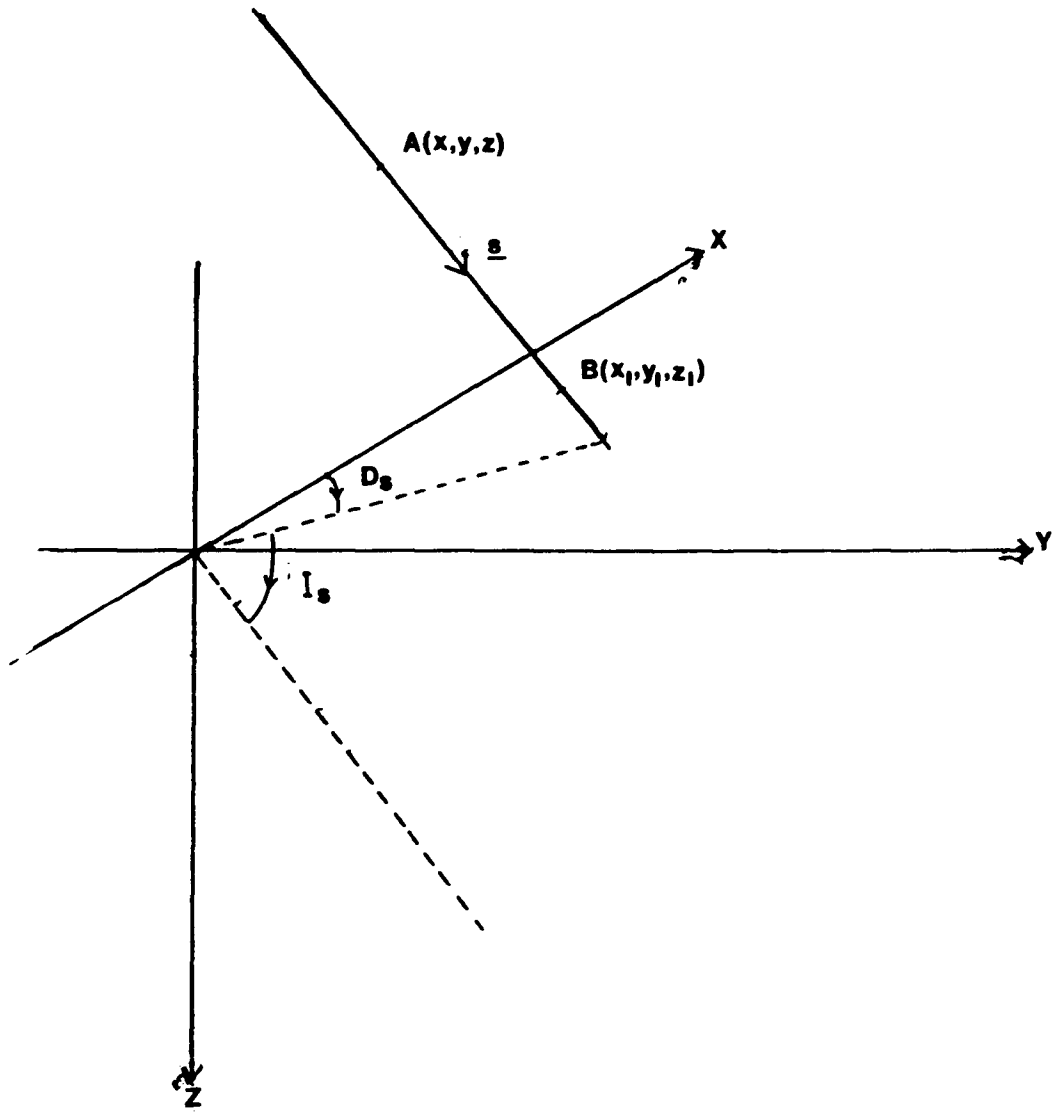

Figure 2.1 Coordinate system chosen for the derivation of pseudogravimetric transformation formula. s indicates the direction of earth's total magnetic field.

fixed point on the line AB, the equation of AB can be written as

($I_s \neq 0$, $D_s \neq 0$)

$$\frac{x - x_1}{\cos I_s \cos D_s} = \frac{y - y_1}{\cos I_s \sin D_s} = \frac{z - z_1}{\sin I_s} = s \qquad 2.3.7$$

where,

I_s = inclination of the earth's total field,

D_s = declination of the earth's total field,

s = AB

Substituting for x and y in terms of x_1, y_1, z_1, z, I_s and D_s in 2.3.6 from 2.3.7 and using the relationship $\frac{d}{ds} = \sin I_s \frac{d}{dz}$ gives

$$\frac{d^2U}{dz d\gamma} = \frac{1}{\sin I_s} \sum_{k_1} \sum_{k_2} F(k_1, k_2) \exp[(P_{12} + i\psi_1)z + i\{-\psi_1 z_1 + \frac{2\pi}{N}(k_1 x_1 + k_2 y_1)\}]$$

where,

$$\psi_1 = \frac{2\pi}{N}(k_1 \cos D_s + k_2 \sin D_s) \cot I_s,$$

$$P_{12} = \frac{2\pi}{N}(k_1^2 + k_2^2)^{\frac{1}{2}}.$$

Assuming there is no contribution to U from an infinite slab $\frac{dU}{d\gamma}$ at minus infinity is zero.

$$\therefore -\left(\frac{dU}{d\gamma}\right)_{z_1} = \frac{1}{\sin I_s} \int_{z_1}^{-\infty} \sum_{k_1} \sum_{k_2} F(k_1, k_2)$$

$$\cdot \exp\left[(P_{12} + i\psi_1)z + i\{-\psi_1 z_1 + \frac{2\pi}{N}(k_1 x_1 + k_2 y_1)\} \right] dz$$

$$\therefore \left(\frac{dU}{d\gamma}\right)_{z_1} = \frac{1}{\sin I_s}\left[\sum_{k_1}\sum_{k_2}\frac{F(k_1,k_2)}{(P_{12}+i\psi_1)}\exp\{(P_{12}+i\psi_1)z\right.$$

$$\left.- i\psi_1 z_1 + \frac{2\pi i}{N}(k_1 x_1 + k_2 y_1)\}\right]_{-\infty}^{z_1}$$

Since the expression inside the square brackets tends to zero as z tends to minus infinity,

$$\left(\frac{dU}{d\gamma}\right)_{z_1} = \frac{1}{\sin I_s}\sum_{k_1}\sum_{k_2}\frac{F(k_1,k_2)}{(P_{12}+i\psi_1)}\exp\{(P_{12}+i\psi_1)z_1$$

$$- i\psi_1 z_1 + \frac{2\pi i}{N}(k_1 x_1 + k_2 y_1)\}$$

$$= \frac{1}{\sin I_s}\sum_{k_1}\sum_{k_2}\frac{F(k_1,k_2)}{(P_{12}+i\psi_1)}\exp\{\frac{2\pi i}{N}(k_1 x_1 + k_2 y_1)\}\exp(P_{12} z_1)$$

Since this equation is valid for any point (x_1, y_1, z_1) on or above the xy plane, it can be written

$$\left(\frac{dU}{d\gamma}\right)_{z\leq o} = \frac{1}{\sin I_s}\sum_{k_1}\sum_{k_2}\frac{F(k_1, k_2)}{(P_{12}+i\psi_1)}\exp\{\frac{2\pi i}{N}(k_1 x + k_2 y)\}$$

$$\cdot\exp(P_{12} z) \qquad 2.3.8$$

Using a similar line of argument it is possible to integrate 2.3.8 with respect to γ to recover the pseudogravimetric potential U, which gives

$$U(x,y,z) = \frac{1}{\sin I_s \sin I_\gamma} \sum_{k_1} \sum_{k_2} F(k_1,k_2) \frac{P_{12}^2 - \psi_1 \psi_2 - iP_{12}(\psi_1 + \psi_2)}{(P_{12}^2 - \psi_1 \psi_2)^2 + P_{12}^2(\psi_1 + \psi_2)^2}$$

$$\cdot \exp(P_{12}z) \quad \exp\left\{\frac{2\pi i}{N}(k_1 x + k_2 y)\right\} \qquad 2.3.9$$

Where,

$\psi_2 = \frac{2\pi}{N}(k_1 \cos D_\gamma + k_2 \sin D_\gamma) \operatorname{Cot} I_\gamma$,

I_γ = inclination of the magnetization vector,

D_γ = declination of the magnetization vector.

Now the pseudogravimetric anomaly $\frac{dU}{dz}$ can be written as

$$\Delta g(x,y,z)_{z\leq o} = \frac{1}{\sin I_s \sin I_\gamma} \sum_{k_1} \sum_{k_2} F(k_1,k_2) \frac{P_{12}^3 - P_{12}\psi_1\psi_2 - iP_{12}^2(\psi_1 + \psi_2)}{(P_{12}^2 - \psi_1 \psi_2)^2 + P_{12}^2(\psi_1 + \psi_2)^2}$$

$$\cdot \exp(P_{12} z) \quad \exp\left\{\frac{2\pi i}{N}(k_1 x + k_2 y)\right\} \qquad 2.3.10$$

$$\therefore \Delta g(x,y,z)_{z\leq o} = \sum_{k_1} \sum_{k_2} F^1(k_1,k_2) \exp\left\{\frac{2\pi i}{N}(k_1 x + k_2 y)\right\} \qquad 2.3.11$$

where,

$$F^1(k_1,k_2) = F(k_1,k_2)\, A(k_1,k_2,I_s,I_\gamma,D_s,D_\gamma)$$

$$A(k_1,k_2,I_s,I_\gamma,D_s,D_\gamma) = \frac{1}{\sin I_s \sin I_\gamma} \frac{P_{12}^3 - P_{12}\psi_1\psi_2 - iP_{12}^2(\psi_1 + \psi_2)}{(P_{12}^2 - \psi_1\psi_2)^2 + P_{12}^2(\psi_1 + \psi_2)^2}$$

$$\cdot \exp(P_{12}z)$$

The expression on the right hand side of 2.3.11 has the same form as an inverse Fourier transform.

In transforming a given magnetic anomaly map into pseudogravimetric anomalies, the forward Fourier transform $(F(k_1,k_2))$ of the magnetic anomaly map needs to be obtained. Then each of the Fourier series coefficients, $F(k_1,k_2)$, is multiplied by the factor $A(k_1,k_2,\ldots)$ to find $F^1(k_1,k_2)$ and then by taking the inverse transform the pseudogravimetric anomaly is obtained. A fast Fourier transform algorithm is used to obtain the Fourier transform of the magnetic anomaly. Usually in calculating the Fourier coefficients of an N-sampled vector, it requires N^2 complex multiplications and additions. The fast Fourier transform algorithm (Cooley and Tukey, 1964) reduces the number of calculations from N^2 to $N \log_2 N$. Since the magnetic anomaly map usually used is a two-dimensional one with a large number of samples, the use of a fast Fourier transform algorithm substantially reduces the computing time.

2.4 An Alternative Way of Deriving the Pseudogravimetric Transformation Formula

An alternative way of deriving the pseudogravimetric transformation formula is by differentiation instead of integration. This method was suggested by Bott (private communications). The way of deriving this is indicated below and the symbols used here are the same as in the earlier derivation. Since the magnetic anomaly $T(x, y,z)$ and corresponding pseudogravimetric potential $U(x,y,z)$ both satisfy Laplace's equation

$$T(x,y,z) = \sum_{k_1=-p}^{q} \sum_{k_2=-p}^{q} F(k_1,k_2)\exp\{\frac{2\pi i}{N}(k_1x + k_2y)\} \exp(P_{12}z)\} \qquad 2.4.1$$

$$U(x,y,z) = \sum_{k_1=-p}^{q} \sum_{k_2=-p}^{q} F^1(k_1,k_2)\exp\{\frac{2\pi i}{N}(k_1x + k_2y)\}\exp(P_{12}z) \qquad 2.4.2$$

If $\underline{l}$, $\underline{m}$ and $\underline{n}$ are unit vectors along x,y and z axes (Figure 2.1) $\underline{s}$ and $\underline{\gamma}$ can be written as

$$\underline{s} = (\underline{l}\ \cos I_s \cos D_s,\ \underline{m}\ \cos I_s \sin D_s,\ \underline{n}\ \sin I_s) \qquad 2.4.3$$

$$\underline{\gamma} = (\underline{l}\ \cos I_\gamma \cos D_\gamma,\ \underline{m}\ \cos I_\gamma \sin D_\gamma,\ \underline{n}\ \sin I_\gamma) \qquad 2.4.4$$

From the Poisson's relationship we have

$$V = \frac{-J}{4\pi\rho G}\ \underline{\gamma} \cdot \underline{\nabla}\ U$$

Substituting for $\underline{\gamma}$ and $\underline{U}$ in the above equation from 2.4.4 and 2.4.2 respectively

$$V = \frac{-J}{4\pi\rho G} \sum_{k_1} \sum_{k_2} F^1(k_1,k_2)(\underline{l}\ \cos I_\gamma \cos D_\gamma + \underline{m}\ \cos I_\gamma \sin D_\gamma + \underline{n}\ \sin I_\gamma)$$

$$\cdot(\underline{l}\ \frac{2\pi i}{N} k_1 + \underline{m}\ \frac{2\pi i}{N} k_2 + \underline{n}\ P_{12})\ \exp\{\frac{2\pi i}{N}(k_1 x + k_2 y)\}\ \exp(P_{12} z)$$

$$= \frac{-J}{4\pi\rho G} \sum_{k_1} \sum_{k_2} F^1(k_1,k_2)(\frac{2\pi i k_1}{N} \cos I_\gamma \cos D_\gamma + \frac{2\pi i k_2}{N} \cos I_\gamma \sin D_\gamma$$

$$+ P_{12} \sin I_\gamma)\ \exp\{\frac{2\pi i}{N}(k_1 x + k_2 y)\}\ \exp(P_{12} z)$$

$$= \frac{-J \sin I_\gamma}{4\pi\rho G} \sum_{k_1} \sum_{k_2} F^1(k_1,k_2)(P_{12} + i\psi_1)\ \exp\{\frac{2\pi i}{N}(k_1 x + k_2 y)\}\ \exp(P_{12} z)$$

$$T(x,y,z) = -\mu_o\ \underline{s} \cdot \underline{\nabla} V$$

$$= \frac{\mu_o J \sin I_\gamma}{4\pi\rho G} \sum_{k_1} \sum_{k_2} F^1(k_1,k_2)(P_{12} + i\psi_1)(\underline{l}\ \cos I_s \cos D_s + \underline{m}\ \cos I_s \sin D_s + \underline{n}\ \sin I_s)$$

$$\cdot(\underline{l}\ \frac{2\pi i k_1}{N} + \underline{m}\ \frac{2\pi i k_2}{N} + \underline{n}\ P_{12})\ \exp\{\frac{2\pi i}{N}(k_1 x + k_2 y)\}\ \exp(P_{12} z)$$

$$T(x,y,z) = \frac{\mu_o J \sin I_\gamma}{4\pi\rho G} \sum_{k_1} \sum_{k_2} F^1(k_1,k_2)(P_{12} + i\psi_1)\left(\frac{2\pi i k_1}{N} \cos I_s \cos D_s\right.$$

$$\left. + \frac{2\pi i k_2}{N} \cos I_s \sin D_s + P_{12} \sin I_s\right) \exp\left\{\frac{2\pi i}{N}(k_1 x + k_2 y)\right\} \exp(P_{12} z)$$

$$= \frac{\mu_o J \sin I_\gamma \sin I_s}{4\pi\rho G} \sum_{k_1} \sum_{k_1} F^1(k_1,k_2)(P_{12} + i\psi_1)(P_{12} + i\psi_2)$$

$$\cdot \exp\left\{\frac{2\pi i}{N}(k_1 x + k_2 y)\right\} \exp(P_{12} z)$$

By selecting the value

$$\rho = \frac{\mu_o J}{4\pi G}$$

for the fictitious density contrast, above equation can be written as

$$T(x,y,z) = \sin I_s \sin I_\gamma \sum_{k_1} \sum_{k_2} F^1(k_1,k_2)(P_{12} + i\psi_1)(P_{12} + i\psi_2)$$

$$\cdot \exp\left\{\frac{2\pi i}{N}(k_1 x + k_2 y)\right\} \exp(P_{12} z) \qquad 2.4.5$$

Since 2.4.1 and 2.4.5 represent the same magnetic anomaly

$$F(k_1,k_2) = F^1(k_1,k_2)(P_{12} + i\psi_1)(P_{12} + i\psi_2) \sin I_s \sin I_\gamma$$

for $k_1,k_2 = -p.....o.....q$

Substituting the coefficients $F^1(k_1,k_2)$ in 2.4.2 in terms of $F(k_1,k_2)$, P_{12}, ψ_1, ψ_2, $\sin I_s$ and $\sin I_\gamma$ gives

$$U(x,y,z) = \frac{1}{\sin I_s \sin I_\gamma} \sum_{k_1} \sum_{k_2} \frac{F(k_1,k_2)}{(P_{12} + i\psi_1)(P_{12} + i\psi_2)} \exp\left\{\frac{2\pi i}{N}(k_1 x + k_2 y)\right\}$$

$$\cdot \exp(P_{12} z)$$

$$\therefore \Delta g = \frac{dU}{dz} = \frac{1}{\sin I_s \sin I_\gamma} \sum_{k_1} \sum_{k_2} \frac{F(k_1,k_2)\, P_{12}}{(P_{12} + i\psi_1)(P_{12} + i\psi_2)} \exp\left\{\frac{2\pi i}{N}(k_1 x + k_2 y)\right\}$$

$$\cdot \exp\,(P_{12} z)$$

$$= \frac{1}{\sin I_s \sin I_\gamma} \sum_{k_1} \sum_{k_2} \frac{F(k_1,k_2)\{P_{12}^{\,2} - \psi_1\psi_2 - i\,(\psi_1 + \psi_2)\, P_{12}\} P_{12}}{(P_{12}^{\,2} - \psi_1\psi_2)^2 + P_{12}^{\,2}(\psi_1 + \psi_2)^2}$$

$$\cdot \exp\left\{\frac{2\pi i}{N}(k_1 x + k_2 y)\right\} \exp\,(P_{12} z)$$

$$\Delta g = \frac{1}{\sin I_s \sin I_\gamma} \sum_{k_1} \sum_{k_2} F(k_1,k_2) \frac{P_{12}^{\,3} - P_{12}\psi_1\psi_2 - i\, P_{12}^{\,2}\,(\psi_1 + \psi_2)}{(P_{12}^{\,2} - \psi_1\psi_2)^2 + P_{12}^{\,2}(\psi_1 + \psi_2)^2}$$

$$\cdot \exp\left\{\frac{2\pi i}{N}(k_1 x + k_2 y)\right\} \exp\,(P_{12} z) \qquad 2.4.6$$

This formula is the same as the formula which was obtained previously (2.3.11) by integration.

2.5 Testing of the Method

The Fortran routine PSGC which uses a fast Fourier transform algorithm has been written to perform the pseudogravimetric transformation and has been used to test the validity of the preceding method. The test involved converting the magnetic anomalies due to a sphere into pseudogravimetric anomalies and comparing the results with the calculated gravity anomaly due to the same sphere having a density contrast equal to the fictitious density contrast used in

the pseudogravimetric transformation. Figures 2.2 and Figure 2.3 give the magnetic anomaly and the pseudogravimetric anomaly due to the sphere. Figure 2.4 gives the real gravity anomaly due to the same sphere having a density contrast equal to the fictitious density contrast of the pseudogravimetric transformation. Cross-sections of the gravity and the pseudogravimetric anomalies are depicted in Figure 2.5. It can be seen from this diagram that the background level of the pseudogravimetric anomaly is depressed compared to the true gravity anomaly. This discrepancy between the two anomalies can be explained as follows. In the derivation of the pseudogravimetric transformation formula (by integration) it was assumed that there is no contribution to the pseudogravimetric potential U from an infinite slab. A given magnetic anomaly can be produced either by a finite body or by the combination of an infinite slab and the same body. This is because the magnetic anomaly due to an infinite slab is zero. Therefore the calculated pseudogravimetric anomaly is uncertain by the pseudogravimetric effect due to an infinite slab. Since the gravity effect due to an infinite slab is a constant depending on the density contrast and the thickness of the slab, the regional level of the calculated pseudogravimetric anomaly is uncertain by a constant value. If the background level of the pseudogravimetric anomaly is increased by a constant amount, then the pseudogravimetric anomaly can be made to coincide with the gravity anomaly (Figure 2.5) except at the edges of the profile. This method was tested further for a range of magnetization and earth's total field directions by using the same test. It was found that the method works satisfactorily for any value of the azimuth of two directions. The results were not good when the

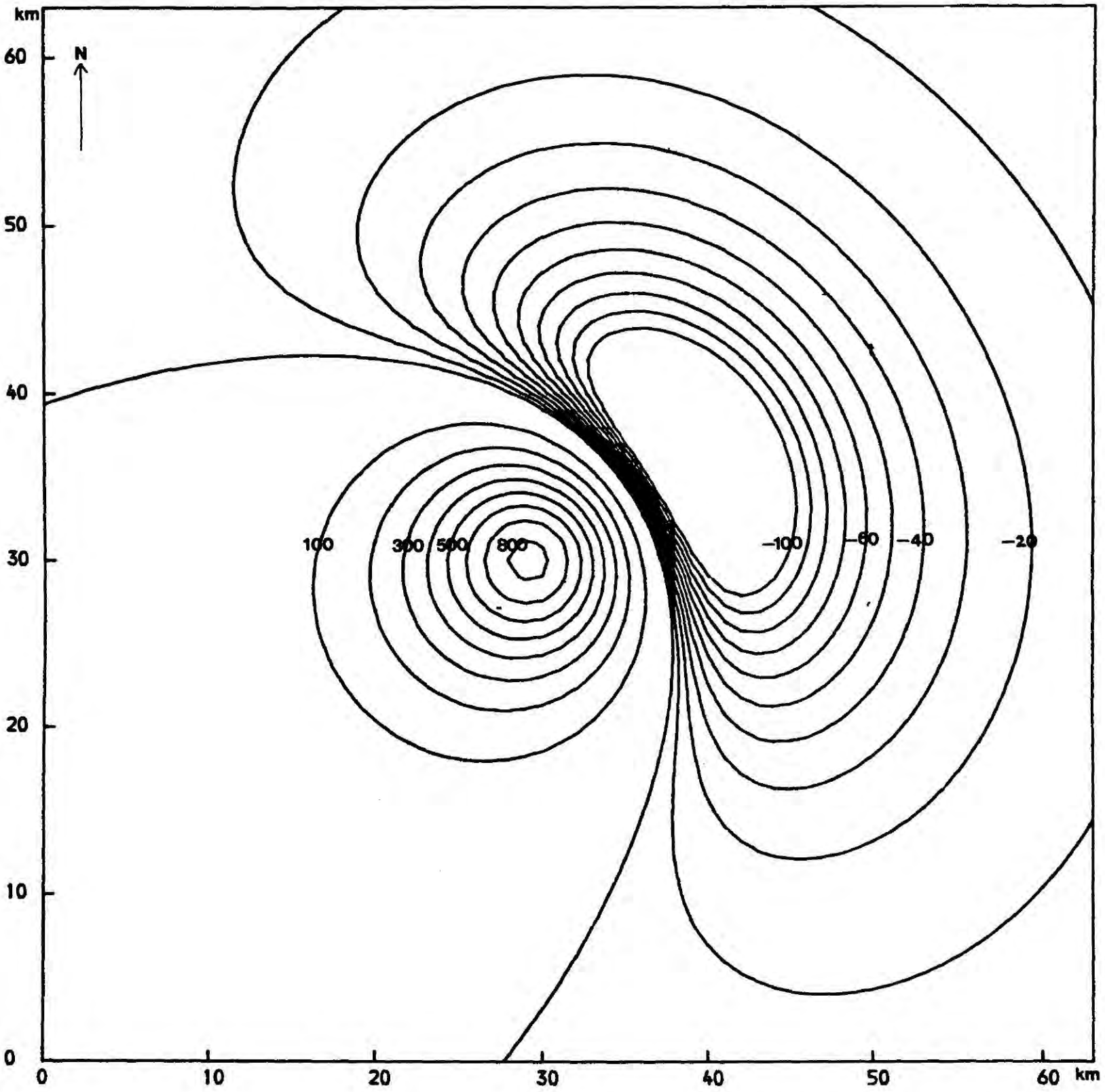

Figure 2.2 Magnetic anomaly due to a sphere having a radius of 5 km and magnetization of 1o A/m. Inclination and declination of the magnetization vector=5o°,3o°. Inclination and declination of the earth's total magnetic field=7o°,4o°. Contours in gamma.

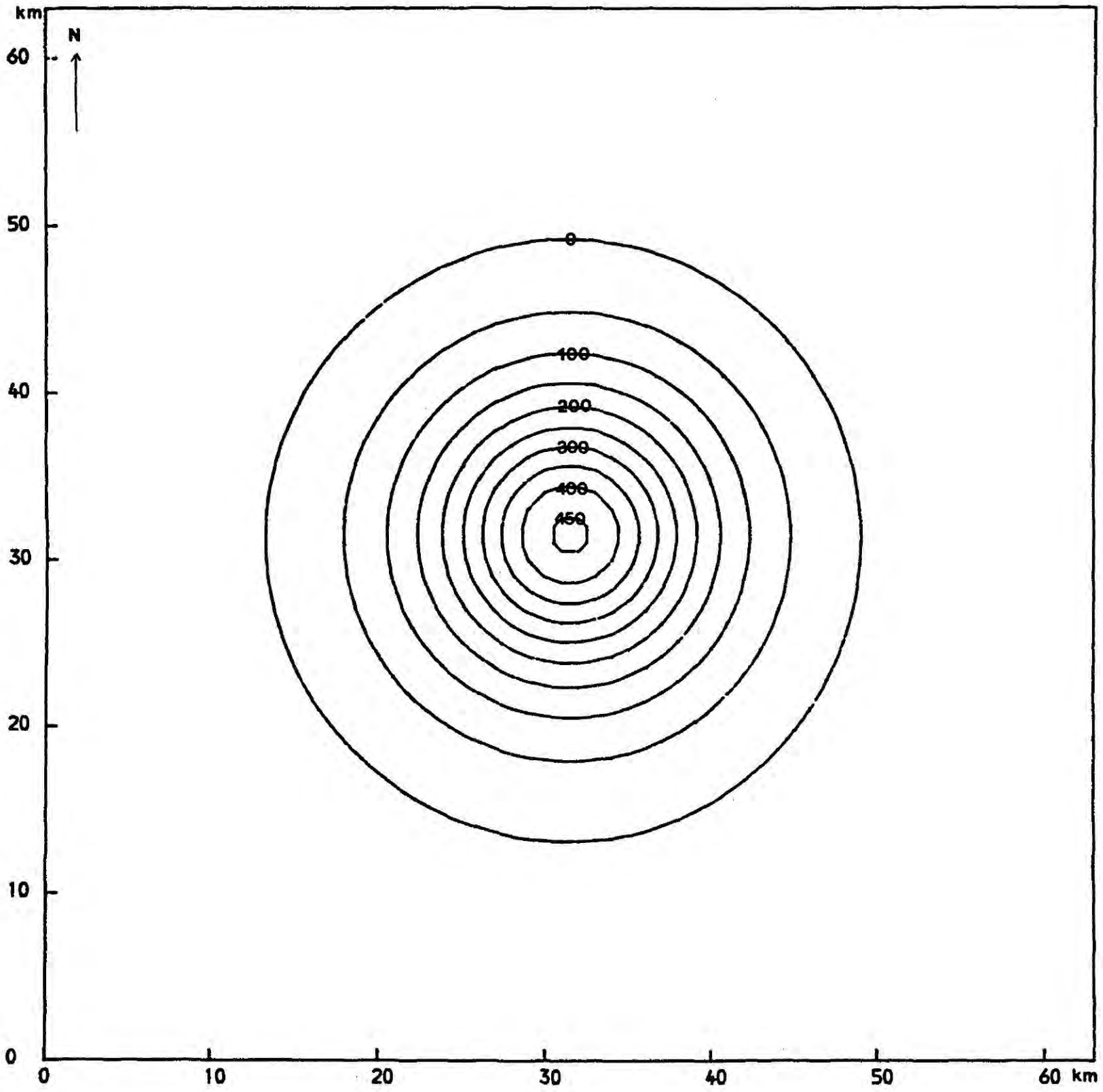

Figure 2.3 Pseudogravimetric anomaly of the magnetic anomaly shown in Figure 2.2. Contours in mgal.

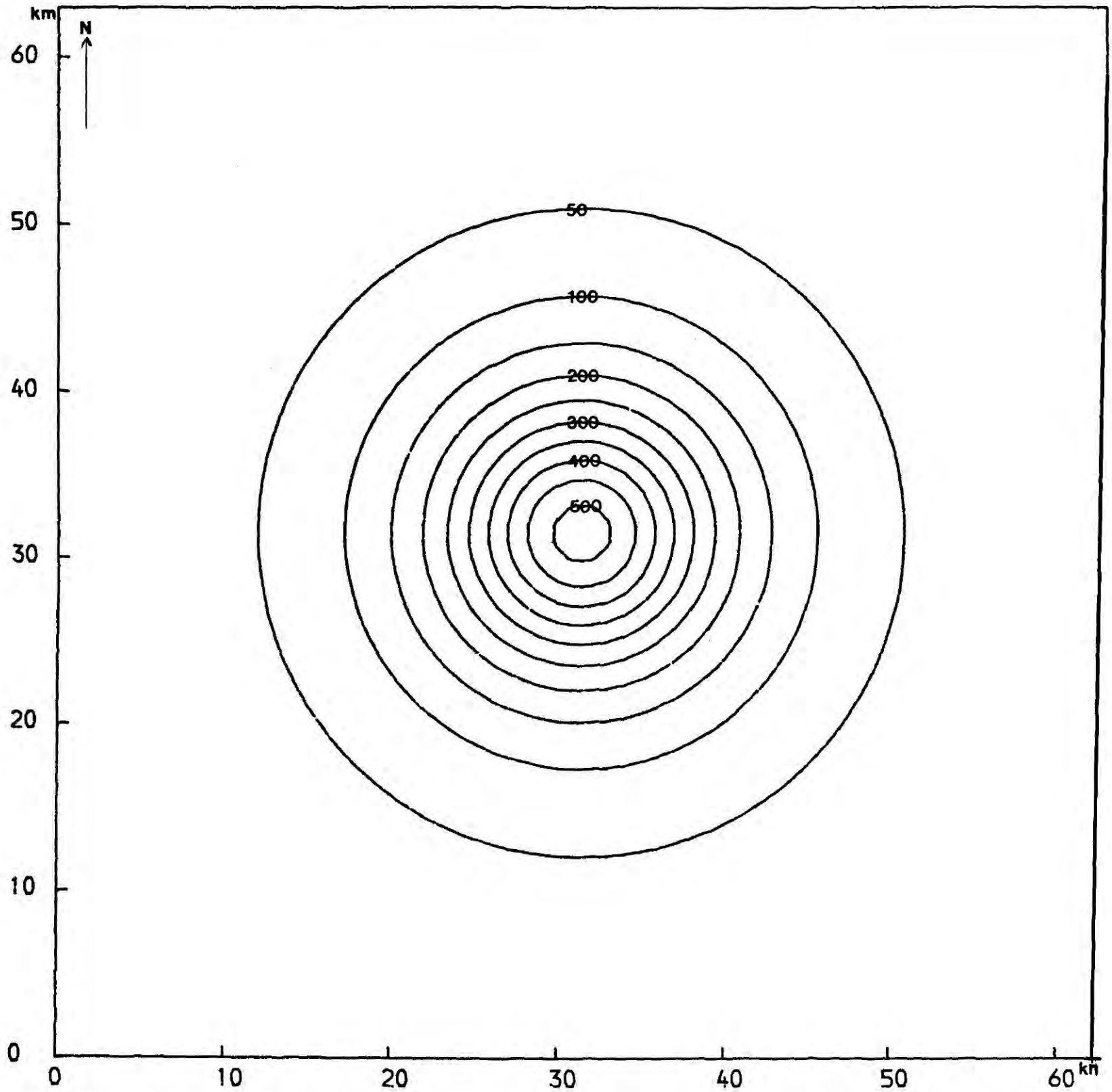

Figure 2.4 Calculated gravity anomaly due to the sphere described in Figure 2.2, assuming that it has a density contrast equal to the fictitious density contrast of the pseudogravimetric transformation. Contours in mgal.

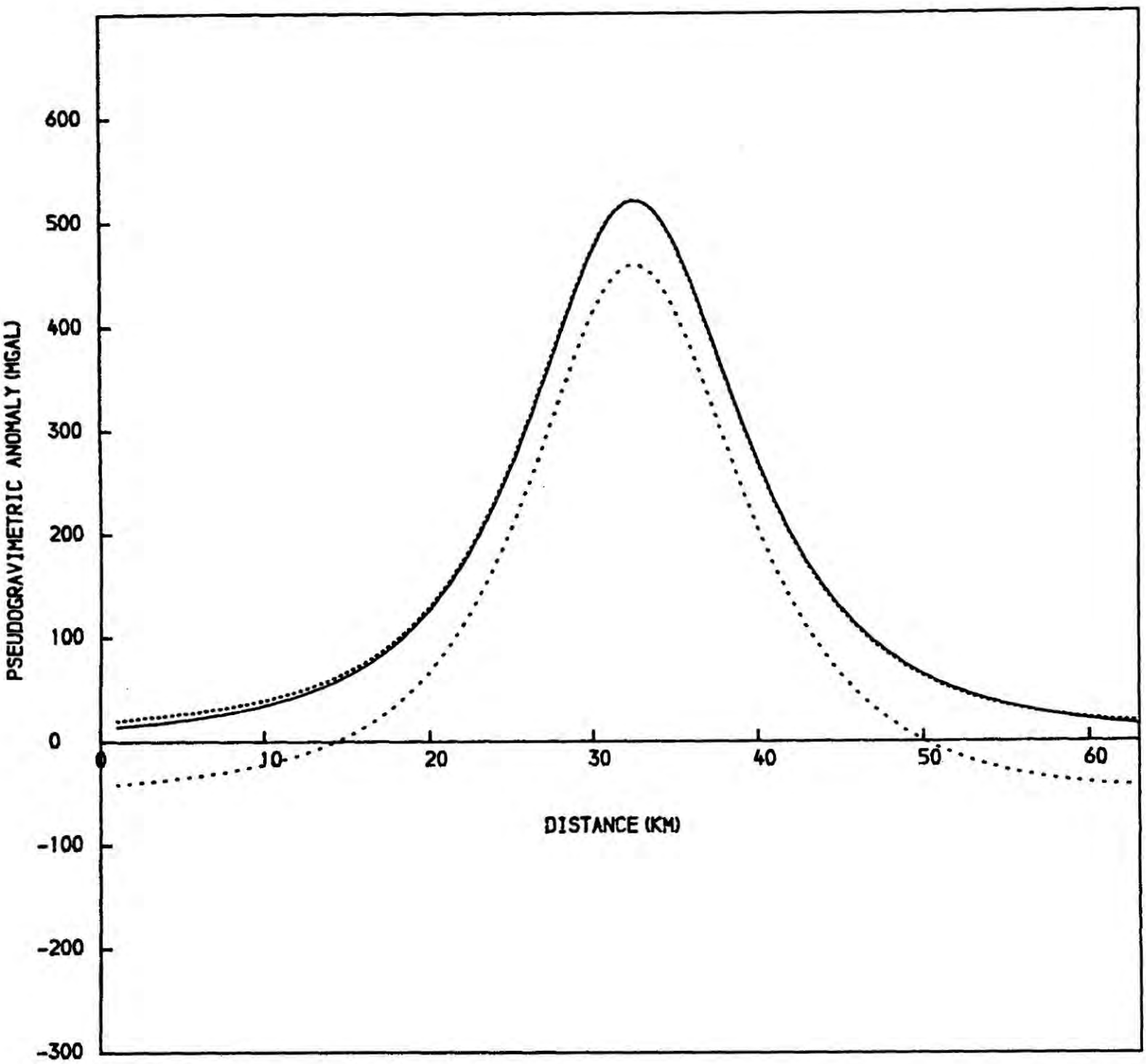

Figure 2.5 Comparison of pseudogravimetric(Figure 2.3) and gravity (Figure 2.4) anomalies.

..... A cross section of the pseudogravimetric anomaly.

——— A cross section of the gravity anomaly.

.....— A cross section of the pseudogravimetric anomaly when regional level is raised by 62.0 mgal.

inclination of either directions were less than 20^{o} (Figure 2.6 and Figure 2.7). Therefore this method works fairly well except at the edges of the profile when the inclination of the earth's total field and the inclination of the magnetization vector are less than 20^{o}. A listing of the program PSGC is given in the Appendix A1.

2.6 Analogue to Digital Conversion of the Anomaly Map

To apply the pseudogravimetric transformation method of 2.3 a square portion of an aeromagnetic anomaly map is selected. The values of the anomaly are then found at nodes of an equally spaced grid. Since a fast Fourier transform algorithm is used, this grid should have 2^{m} (m = integer, m$>$ 1) nodes on each side. However, if the selected square does not have sides with 2^{m} nodes, then each side should be expanded to such a square with zero values for the anomaly at all additional points. Sampling or digitizing can be done by laying an equally spaced grid drawn on a transparent paper on the magnetic anomaly map and finding the values of the anomaly at the nodes. There are two ways of finding the values of the anomaly at the nodes. The first is by direct interpolation of contours. The second is by using the bicubic spline interpolation method (Bhattacharyya, 1969). It is possible to achieve the necessary accuracy by the first method if it is done with some care.

2.7 Discussion

In 2.5 it was shown that the pseudogravimetric transformation method developed in this chapter works satisfactorily. However there are some practical problems involved in using this method, some of which are inherent in the application of the discrete Fourier transforms. This section is devoted to a discussion of these problems and the ways of overcoming them.

2.7.1 Aliasing Effect

Sampling a continuous function at a certain interval

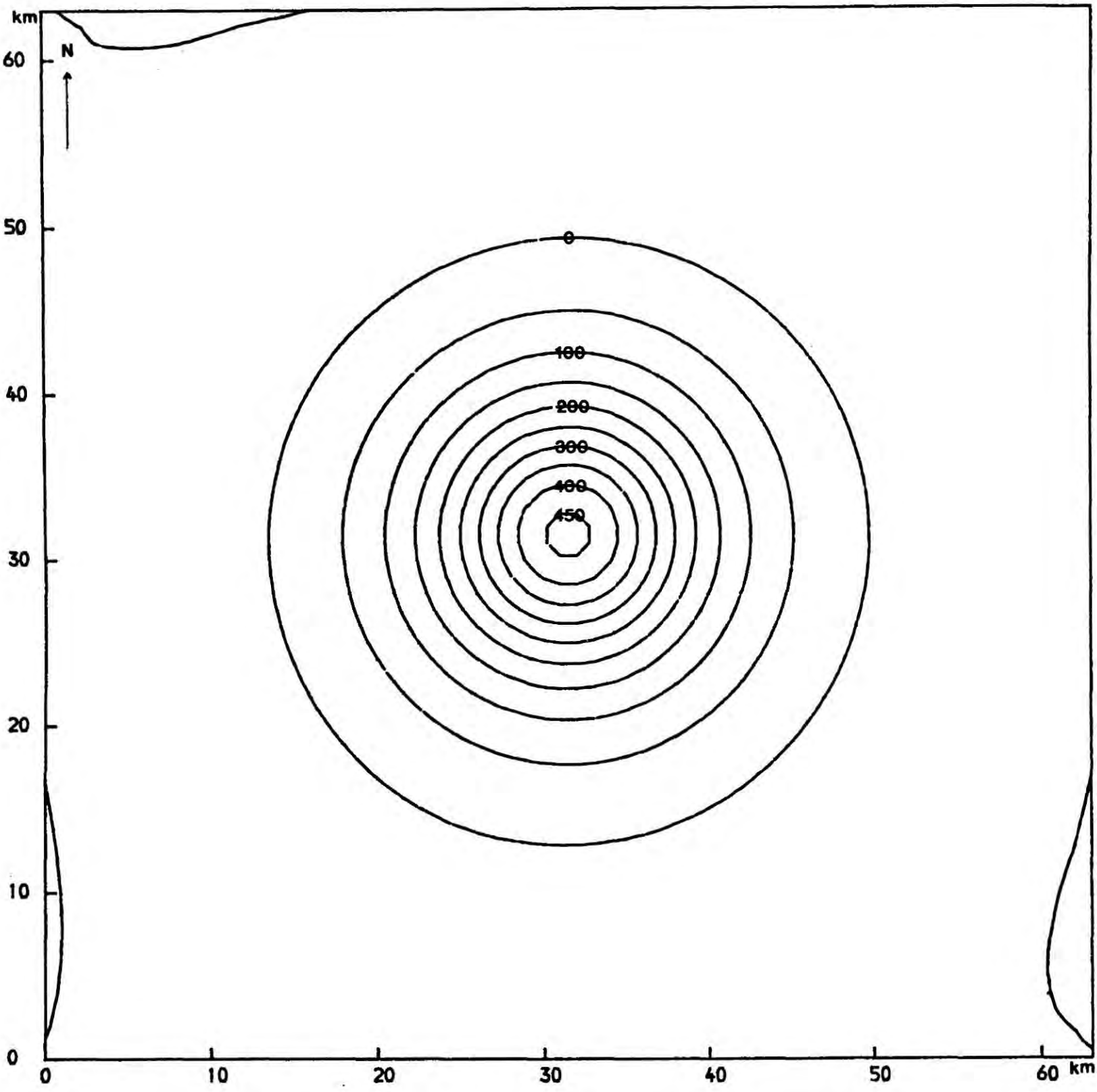

Figure 2.6 Pseudogravimetric anomaly due to a magnetized sphere having a radius of 5 km and magnetization of 1o A/m. Inclination and declination of the magnetization vector = 15°,3o°. Inclination and declination of the earth's total magnetic field = 7o°,4o°. Contours in mgal.

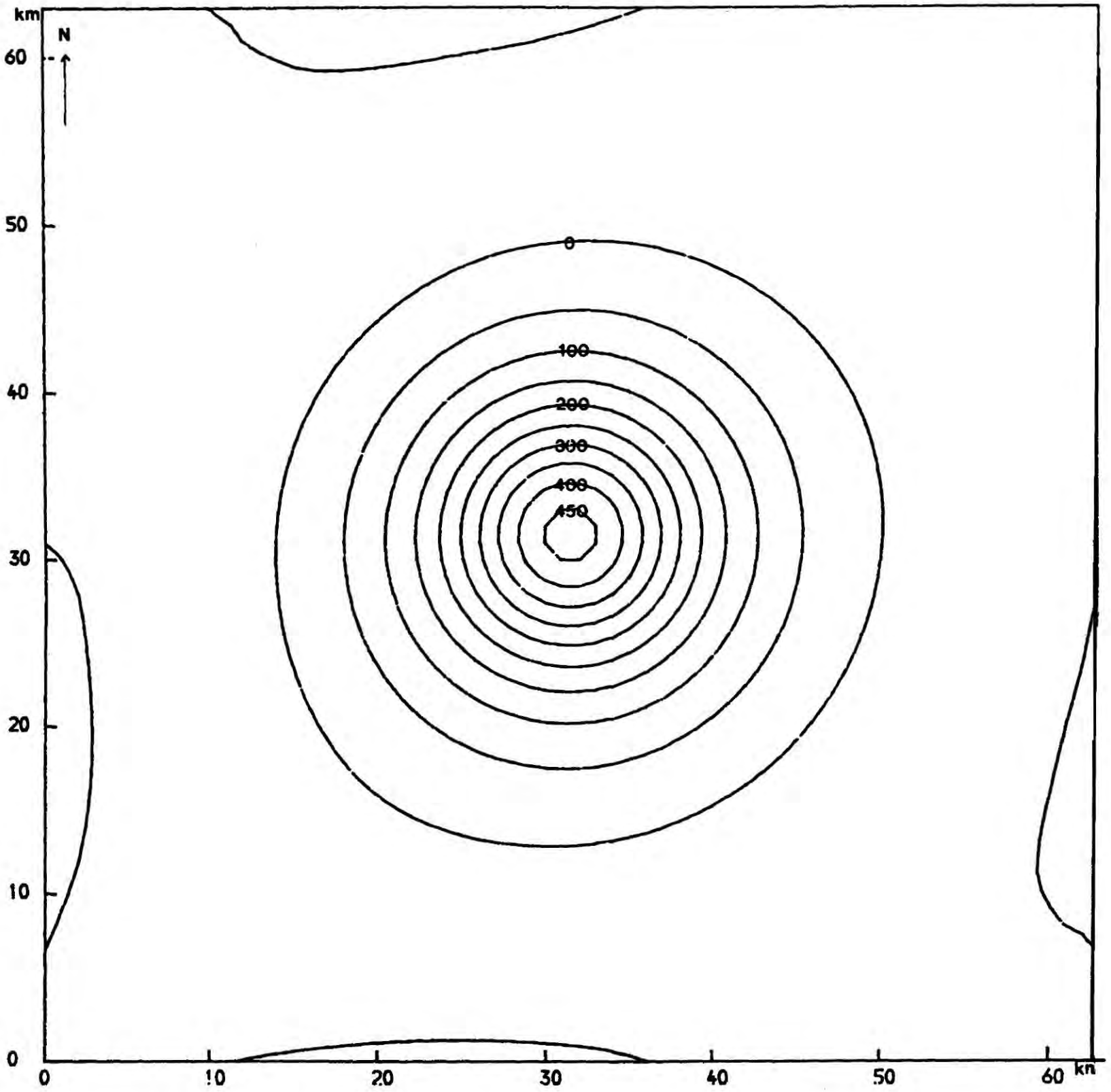

Figure 2.7 Pseudogravimetric anomaly due to a magnetized sphere having a radius of 5 km and magnetization of 1o A/m. Inclination and declination of the magnetization vector = 5o°, 3o°. Inclination and declination of the earth's total magnetic field = 15°, 4o°. Contours in mgal.

determines the maximum frequency that can be uniquely defined by the sampled function (Blackman and Tukey, 1959). This frequency is known as the Nyquist frequency and is equal to half the value of the sampling frequency. Frequencies greater than the Nyquist frequency impersonate the lower frequencies and this is known as the alaising effect. Therefore it is necessary to remove the frequencies greater than the Nyquist frequency or decrease the sampling interval such that the Nyquist frequency is equal to or greater than the highest frequency component present in the function.

2.7.2 Truncation Effects

When a square portion of an aeromagnetic anomaly map is selected for the pseudogravimetric conversion, sharp discontinuities are introduced to the anomaly at the sides of the square. Sampling this function with a given frequency is equivalent to truncation of the function in the frequency domain beyond the Nyquist frequency. Under such conditions it is not possible to reconstruct the sharp edges of the anomaly with a limited number of frequencies. The effect of this truncation in the frequency domain is to introduce spurious oscillations in the spatial domain around the region of the discontinuity. This is known as the Gibb's phenomenon and it can be very clearly observed for the case of a step function (Bracewell, 1965). The effect due to the Gibb's phenomenon can be reduced by decreasing the sampling interval. Another way of overcoming this problem is by selecting a large portion of the anomaly centred around the feature of interest. Since the Gibb's phenomenon only affects the edges of the function where there are discontinuities, the region of the anomaly of interest remains unchanged.

Selecting a square portion of an aeromagnetic anomaly map for the

pseudogravimetric transformation is equivalent to the truncation of the of the anomaly (function) at the sides of the square. This truncation of the function in the spatial domain introduces spurious oscillations to the function in the frequency domain. For simplicity this problem is discussed here with reference to the one dimensional case. The effect due to a truncation of a function in the spatial domain is the same as multiplication of the function by a rectangular window. In the frequency domain this is equivalent to the convolution of the Fourier transform of the function with the Fourier transform of a rectangular window. Since the Fourier transform of a rectangular window is a sine cardinal function (sinf/f), this will introduce some ripples at the edges of the function in the frequency domain (Figure 2.8). If the length of the rectangular window is increased then its Fourier transform, the sine cardinal function, tends towards a delta function, in which case the ripples at the edges of the function in the frequency domain are reduced. Therefore it is possible to reduce this inability by selecting a large portion of the anomaly map for the pseudogravimetric transformation. Another way of reducing this problem is by cosine tapering the data (Kanasewich, 1975).

2.7.3 Even and Odd Symmetries of real and imaginary parts of a Fourier Transform

Another important factor that should be borne in mind when performing the pseudogravimetric transformation using Fourier transforms is to arrange real and imaginary parts of the Fourier transform with the proper symmetry in such a way that the computed pseudogravimetric anomaly is completely real. The Fourier transform of a real function has a symmetrical real part and antisymmetrical imaginary part. So

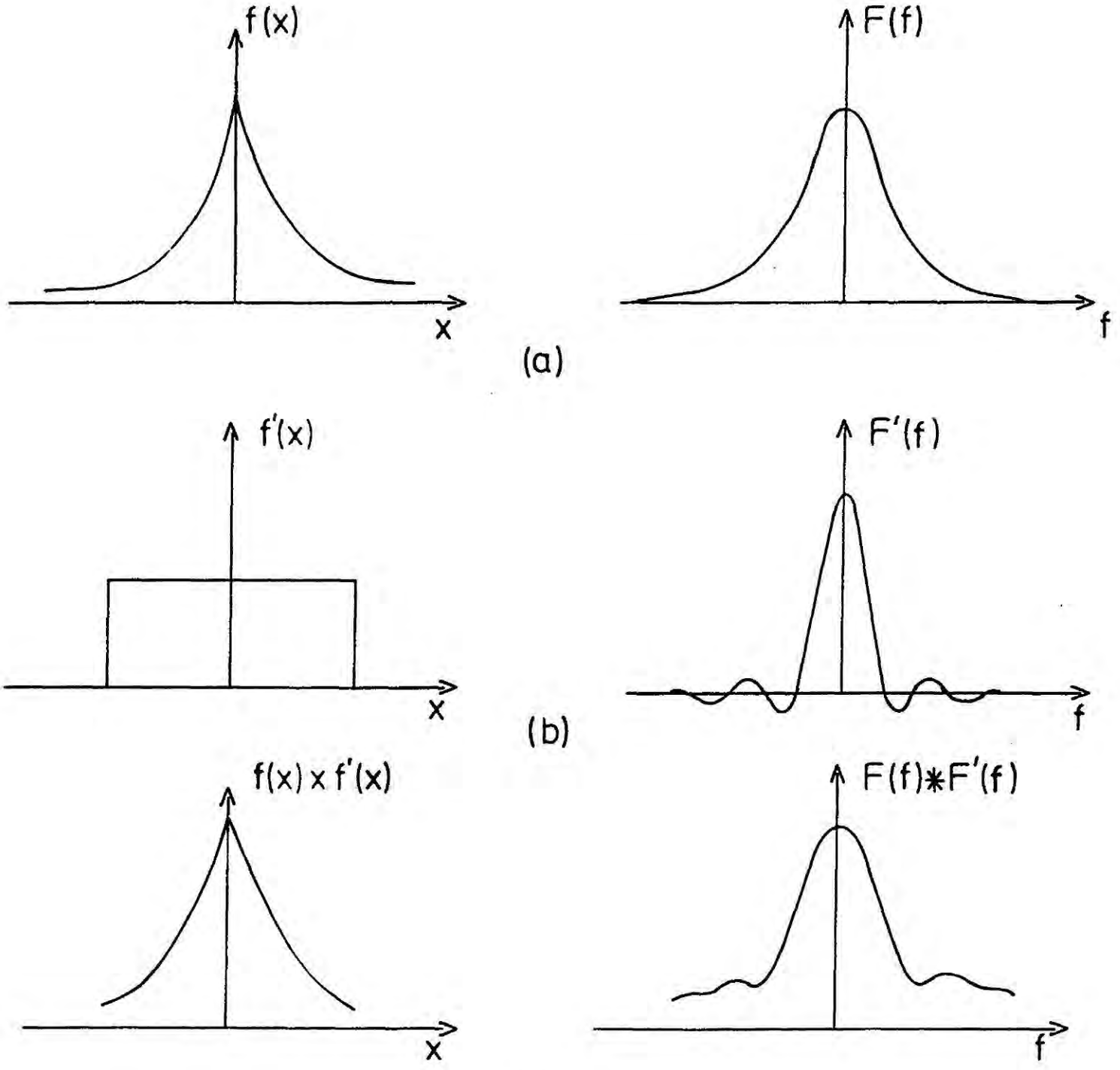

Figure 2.8 Illustration of the effects on the frequency domain function due to the truncation of the spatial domain function.

(a) Spatial domain function and its Fourier transform(frequency domain function).

(b) Rectangular window and its Fourier transform.

(c) Truncated spatial domain function and its Fourier transform.

$*$ Convolution.

when trying to recover the original function which is real from its Fourier transform, it is necessary to arrange terms in the real part of the Fourier transform to have even symmetry and terms in the imaginary part to have odd symmetry. In the one dimensional case this can be done by folding the real part about the Nyquist frequency and folding and flipping, (reversing the polarity), the imaginary part about the same frequency (Brigham, 1974). In the case of the imaginary part it is also necessary to set the amplitude of the Nyquist frequency to zero in order to obtain the odd symmetry. If this precaution were not taken the function would be double valued at this point. This procedure can easily be extended to the two dimensional case by considering the two dimensional array of Fourier coefficients as a series of one dimensional arrays parallel to each other. Terms in real and imaginary parts of a two dimensional array (8x8) are arranged with the required symmetry by using this procedure. This is illustrated in Figure 2.9. By identifying the symmetries in these two arrays, the following sequence of steps should be followed to obtain this symmetry in practice.

Real part

a) Arrange the first row and the first column of the array in the same way as in the one dimensional case.

b) Then fold the array about F_{Nx}.

c) Then fold the results of (b) about F_{Ny}.

Imaginary Part

a) Same as in (a) above

b) Then fold and flip the array about F_{Nx}.

c) Then fold and flip the results of (b) about F_{Ny}.

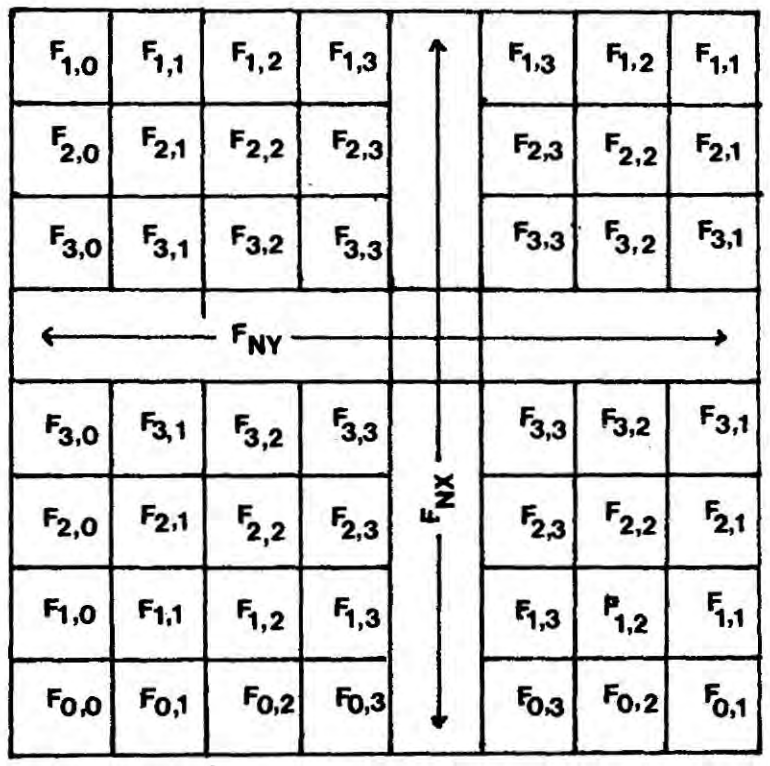

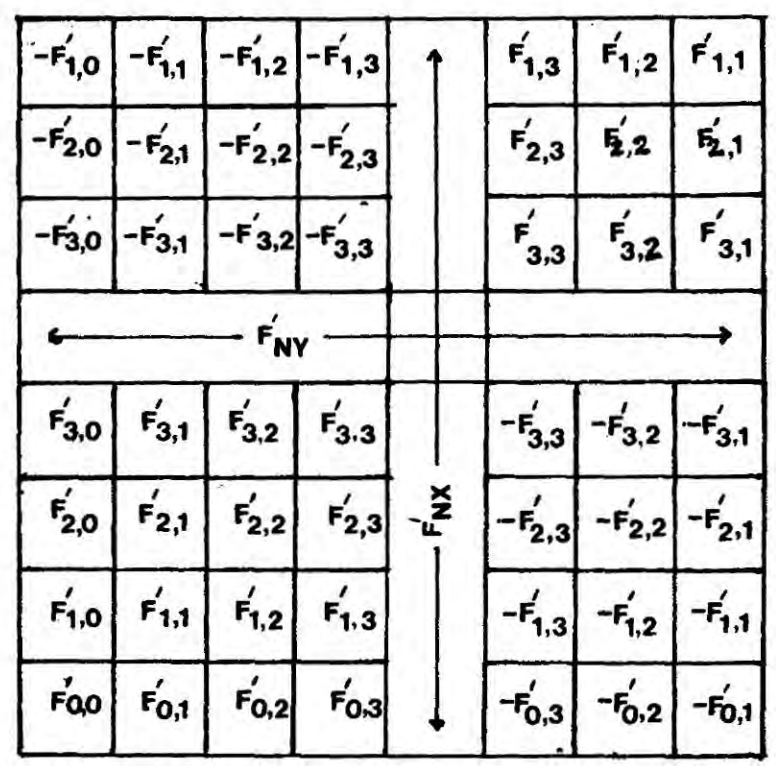

Figure 2.9 Even and odd symmetries of the real and imaginary parts of a Fourier transform of a real two dimensional function. F represents the amplitude of each frequency. F_{NX}, F_{NY}, F'_{NX}, F'_{NY} represent the amplitudes of Nyquist frequencies along X and Y directions of real and imaginary parts.

where ,

F_{Nx} = Nyquist frequency for the x-direction

F_{Ny} = Nyquist frequency for the y-direction

Finally the amplitudes of F_{Nx}' and F_{Ny}' of the imaginary part are set to zero as in the one dimensional case.

CHAPTER 3

INTERPRETATION OF GRAVITY AND MAGNETIC ANOMALIES

3.1 Introduction

Interpretation of gravity and magnetic anomalies involves the determination of the shape and other physical properties, such as density contrast and magnetization, of a subsurface structure causing an anomaly. Usually geological features causing an anomaly have complicated shapes. In interpretation therefore we only intend to find an approximate shape which explains large-scale features of the causative body.

Most of the work discussed in this thesis involves interpretation of magnetic and pseudogravimetric anomalies. Interpretation of magnetic anomalies in two dimensions was performed using a non-linear optimization technique. As indicated in the preceding chapter, interpretation of pseudogravimetric anomalies has to be performed by using gravity methods. The conventional trial-and-error modelling method and a non-linear optimization technique were both used in interpreting pseudogravimetric anomalies in three dimensions using the end correction method (Nettleton, 1940). These methods are discussed in detail below. The end correction factor for the interpretation of magnetic anomalies is derived in 3.2. The problem of non-uniqueness in the gravity and magnetic interpretation is discussed in 3.4.

3.2 The End Correction Method

Usually we make several approximations in interpreting gravity and magnetic anomalies. One of them is to assume that the body causing the anomaly has a constant cross-section and an infinite strike. Such a two-dimensional interpretation is not adequate when one horizontal

dimension of the body is not large compared to the other. However, three-dimensional interpretation involves lengthy calculations and therefore consumes a large amount of computing time. Nettleton (1940) suggested an approximate method of calculating gravity or magnetic anomalies due to three-dimensional bodies to overcome this problem. This method involves making an end correction to the two-dimensional calculations.

In calculating the gravity or magnetic anomaly due to a body using the end correction method, firstly the body is divided into a number of horizontal prisms. Then the gravity or magnetic anomaly due to each prism is calculated considering prisms as two-dimensional bodies. The next step is to calculate an end correction factor for each prism, for each field point at which we are going to find the anomaly. This is calculated by assuming that the mass or the magnetic moment of each prism is concentrated along its axis.. If the gravity or magnetic anomaly at a point due to such a line mass, or a line of dipoles, is F, and F_∞ is the anomaly due to the same line if it extends to infinity in both directions, then the end correction factor for the calculation of the anomaly due to the corresponding prism at that point is F/F_∞ . Multiplying the gravity or magnetic anomaly due to each prism, obtained under the assumption that these are two-dimensional bodies, by the corresponding end correction factor and adding the results yields an approximation to the anomaly due to the body at each field point. By increasing the number of prisms it is possible to achieve any degree of accuracy required.

The end correction factor for the computation of gravity anomalies has been given by Nettleton (1940). If R is the perpendicular distance from the field point to the axis of a prism and y is the half

length of the prism, then the end correction factor for the calculation of the gravity anomaly due to the prism is (see Figure 3.1)

$$\frac{F}{F_\infty} = \frac{1}{\sqrt{1 + (\frac{y}{R})^2}} \qquad 3.2.1$$

The derivation of the end correction factor for the computation of magnetic anomalies is much more complicated than the gravity case because the direction of magnetization and the direction of earth's total magnetic field are both involved in the derivation. Winter (1972) and Bott (private communications) derived the end correction factor for the case of magnetics. It was found that the derivation given by Winter (1972) is cumbersome and involves some minor errors and therefore the end correction factor for the computation of magnetic anomalies is rederived here. The derivation below is based on Bott (private communications).

Let A_1A_2 in Figure 3.2 be a finite line of dipoles parallel to the Y axis, $\underline{J}(J_x, J_y, J_z)$ be the magnetic moment per unit length of the line, $U(x,y,z)$ be the gravity potential due to the line at $P(x,y,z)$ and $\underline{S}(S_x,S_y,S_z)$ be the unit vector along the direction of the earth's total magnetic field. Let us also assume that the mass per unit length of the line is equal to $\mu o/4\pi G$; where μo is the permeability of free space and G is the gravitational constant. By using the Poisson's relationship (chapter 1) the magnetic anomaly F due to the line of dipoles at the point $P(x,y,z)$ can be written as

$$F = \underline{S}.\underline{\nabla}(\underline{J}.\underline{\nabla}U)$$

$$= S_xJ_x \frac{\partial^2 U}{\partial x^2} + S_yJ_y \frac{\partial^2 U}{\partial y2} + S_zJ_z \frac{\partial^2 U}{\partial z^2} + (S_xJ_y + S_yJ_x) \frac{\partial^2 U}{\partial x \partial y}$$

$$+ (S_xJ_z + S_zJ_x) \frac{\partial^2 U}{\partial x \partial z} + (S_yJ_z + S_zJ_y) \frac{\partial^2 U}{\partial z \partial y} \qquad 3.2.2$$

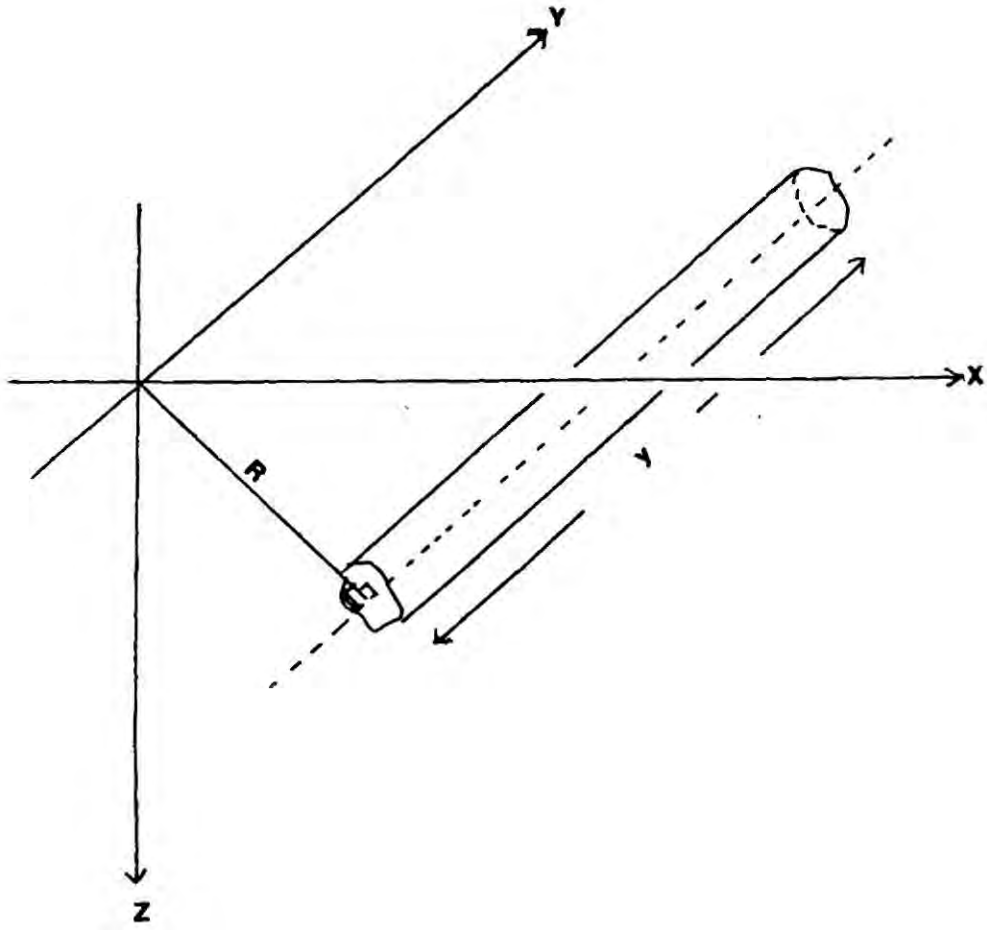

Figure 3.1 End correction factor for the computation of gravity anomalies due to three dimensional bodies.

R - Perpendicular distance from the field point to the axis of the prism.

y - Half length of the prism.

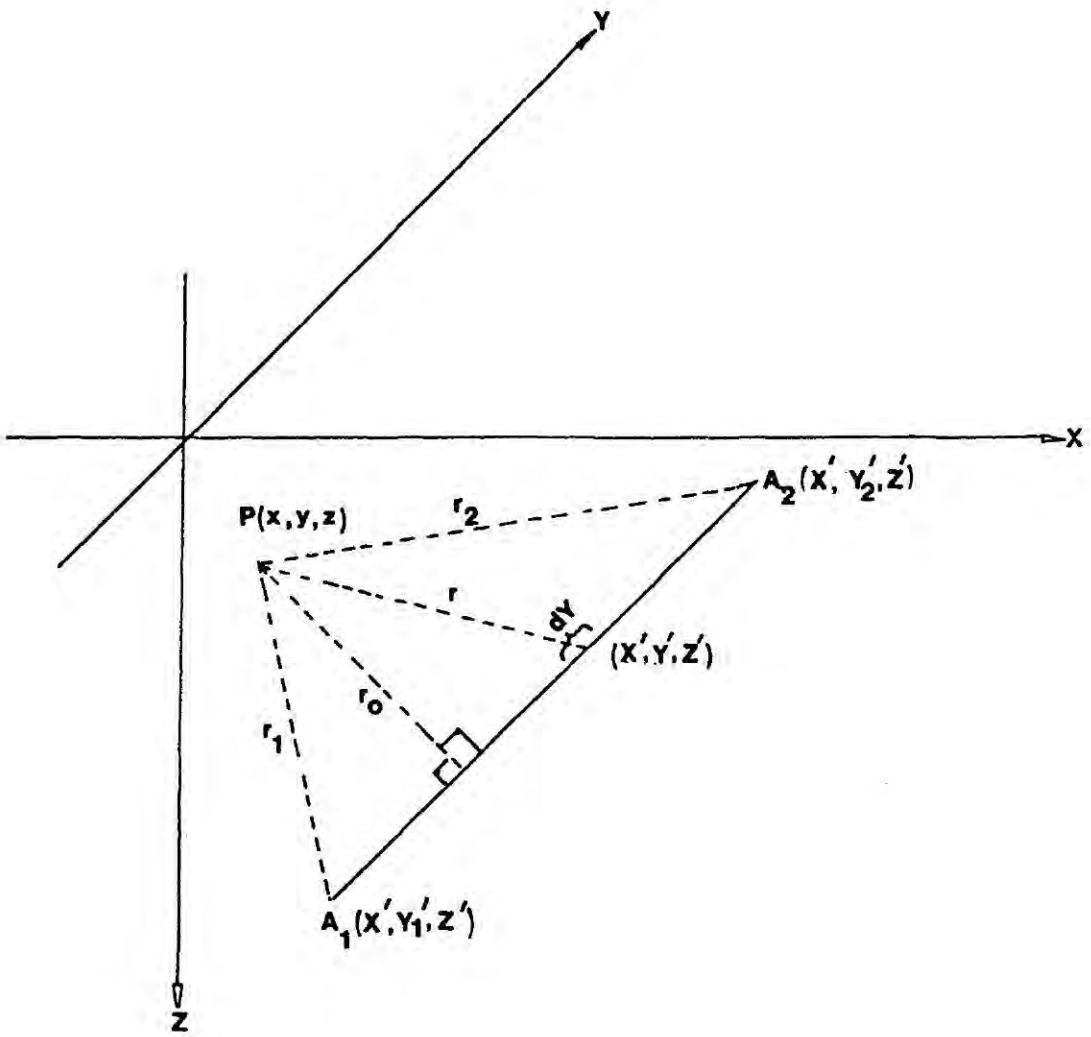

Figure 3.2 Gravity potential due to a finite line mass A_1A_2 at the point P(x,y,z).

To obtain F involves the determination of the six second derivatives of the gravitational potential U given by (Figure 3.2)

$$U = \int_{Y_1'}^{Y_2'} \frac{dY'}{\sqrt{r_o^2 + (Y'-y)^2}} \qquad 3.2.3$$

where,

$$r_o = \{(X' - x)^2 + (Z'- z)^2\}^{\frac{1}{2}}$$

substituting $Y = Y'-y$ in 3.2.3

$$U = \int_{Y_1'-y}^{Y_2'-y} \frac{dY}{\sqrt{r_o^2 + Y^2}} \qquad 3.2.4$$

Using Leibnitz's rule for differentiation under an integral sign,

$$\frac{\partial U}{\partial y} = \frac{1}{\sqrt{r_o^2 + (Y_2'-y)^2}} \frac{d}{dy}(Y_2-y) - \frac{1}{\sqrt{r_o^2 + (Y_1'-y)^2}} \frac{d}{dy}(Y_1-y)$$

$$= \frac{1}{r_1} - \frac{1}{r_2}$$

where,

$$r_1 = \{(X'-x)^2 + (Y_1'-y)^2 + (Z'-z)^2\}^{\frac{1}{2}}$$

$$r_2 = \{(X'-x)^2 + (Y_2'-y)^2 + (Z'-z)^2\}^{\frac{1}{2}}$$

Differentiating 3.2.4 w.r.t. x,

$$\frac{\partial U}{\partial x} = \int_{Y_1'-y}^{Y_2'-y} \frac{X'-x}{(r_o^2 + Y^2)^{3/2}}\, dY$$

By performing this integration using the substitution $Y = r_o \tan\theta$,

$$\frac{\partial U}{\partial x} = \frac{X}{r_o^2}\left(\frac{Y_2}{r_2} - \frac{Y_1}{r_1}\right)$$

where,

$$Y_1 = Y_1' - y,$$

$$Y_2 = Y_2' - y,$$

$$X = X' - x.$$

Similarly,

$$\frac{\partial U}{\partial z} = \frac{Z}{r_o^2}\left(\frac{Y_2}{r_2} - \frac{Y_1}{r_1}\right)$$

where,

$$Z = Z' - z.$$

When the first three partial derivatives are known, the six second partial derivatives can be determined easily and they are given below.

$$\frac{\partial^2 U}{\partial x^2} = \frac{\left(2X^2 - r_o^2\right)}{r_o^4}\left(\frac{Y_2}{r_2} - \frac{Y_1}{r_1}\right) + \frac{X^2}{r_o^2}\left(\frac{Y_2}{r_2^3} - \frac{Y_1}{r_1^3}\right) \qquad 3.2.5$$

$$\frac{\partial^2 U}{\partial y^2} = \frac{Y_1}{r_1^3} - \frac{Y_2}{r_2^3} \qquad 3.2.6$$

$$\frac{\partial^2 U}{\partial z^2} = \frac{\left(2Z^2 - r_o^2\right)}{r_o^4}\left(\frac{Y_2}{r_2} - \frac{Y_1}{r_1}\right) + \frac{Z^2}{r_o^2}\left(\frac{Y_2}{r_2^3} - \frac{Y_1}{r_1^3}\right) \qquad 3.2.7$$

$$\frac{\partial^2 U}{\partial x \partial y} = X\left(\frac{1}{r_1^3} - \frac{1}{r_2^3}\right) \qquad 3.2.8$$

$$\frac{\partial^2 U}{\partial z \partial y} = Z\left(\frac{1}{r_1^3} - \frac{1}{r_2^3}\right) \qquad 3.2.9$$

$$\frac{\partial^2 U}{\partial x \partial z} = \frac{2XZ}{r_o^4}\left(\frac{Y_2}{r_2} - \frac{Y_1}{r_1}\right) + \frac{XZ}{r_o^2}\left(\frac{Y_2}{r_2^3} - \frac{Y_1}{r_1^3}\right) \qquad 3.2.10$$

These derivatives for an infinite line of dipoles can be easily obtained by finding the limits of 3.2.5 to 3.2.10 when Y_1 tends to minus infinity and Y_2 tends a plus infinity. The six derivatives for this case are as follows:

$$\frac{\partial^2 U_\infty}{\partial x^2} = \frac{2(X^2-Z^2)}{r_o^4} \qquad 3.2.11$$

$$\frac{\partial^2 U_\infty}{\partial z^2} = \frac{2(Z^2-X^2)}{r_o^4} \qquad 3.2.12$$

$$\frac{\partial^2 U_\infty}{\partial x \partial z} = \frac{4XZ}{r_o^4} \qquad 3.2.13$$

$$\frac{\partial^2 U_\infty}{\partial y^2} = \frac{\partial^2 U_\infty}{\partial z \partial y} = \frac{\partial^2 U_\infty}{\partial x \partial y} = 0 \qquad 3.2.14$$

Combining 3.2.2 and 3.2.5 to 3.2.10, the magnetic anomaly due to the finite line of dipoles $A_1A_2(F)$ and combining 3.2.2 and 3.2.11 to 3.2.14 the magnetic anomaly due to the line of dipoles when it is infinitely long (F_∞) can be found. Hence the ratio F/F_∞ which gives the end correction factor can be calculated. In evaluating 3.2.5 to 3.2.7 it is only necessary to calculate two of them. By using the relationship $\nabla^2 U = 0$ (Laplace's equation) the third can be found.

Similarly by knowing either 3.2.11 or 3.2.12 the other can be found.

An interesting feature of this result is that the magnetic anomaly due to a finite line of dipoles can be greater than the infinite line of dipoles for certain values of X and Z. Therefore unlike the case of gravity, the end correction factor for the case of magnetics can be greater than unity for some values of X and Z. A Fortran routine which computes the end correction factor using the above equations is given in the Appendix A1.

It was shown above that it is necessary to divide a body into a number of sufficiently small horizontal prisms in order to use the end correction method accurately. This can be performed by dividing the cross-section of the body into a number of elements. Then each element becomes the cross-section of each prism. Usually the cross-section is divided into rectangular and triangular elements. The ensuing calculations require the coordinates of the nodes of each element. Since it is intended to use a trial-and-error method to perform the interpretation, it is necessary to find a separate set of coordinates of nodes each time the shape of the body is changed, which is obviously time consuming. Therefore it was decided to develop a computer routine which divides a given polygonal shape into a number of elements automatically. The Fortran routine BD was written for this purpose and it divides a polygonal shape having top and bottom sides parallel to the X-axis into a number of elements (Figure 3.3). The use of this routine for polygonal shapes which do not satisfy this condition is explained later. The routine BD first divides the polygonal shape into a series of strips having top and bottom sides parallel to the X axis. Each strip is then divided into a specified number of elements having top and bottom sides parallel to

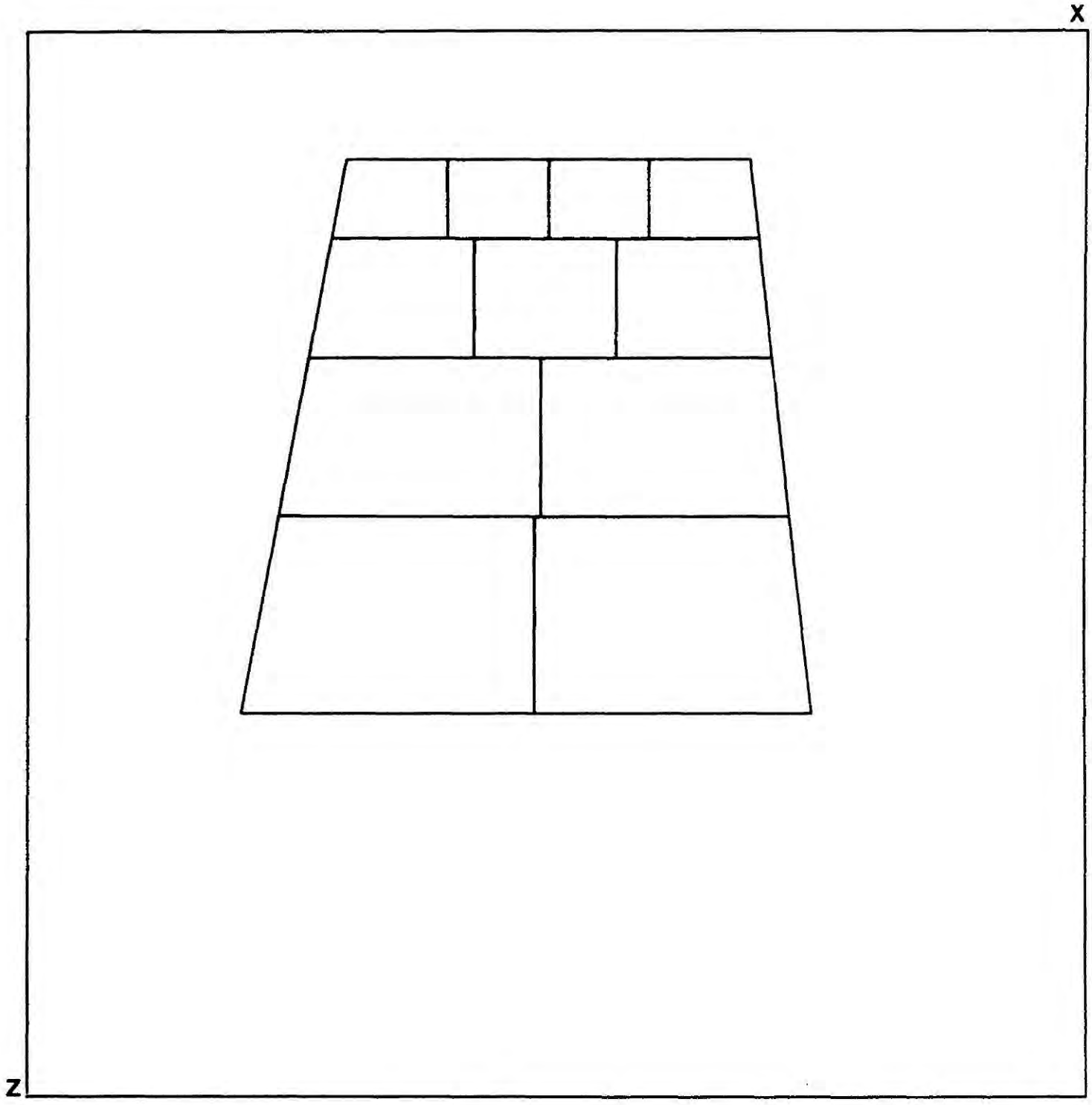

Figure 3.3 Way in which the subroutine BD divides a polygonal shape having top and bottom sides parallel to X axis.

the X axis. The following information has to be given as input data:

a) the coordinates of each node of the polygon;

b) number of horizontal strips the polygon has to be divided into (NS);

c) number of elements each strip has to be divided into ($N_1, N_2, \ldots N_{NS}$);

d) a number R which controls the relative thickness of each strip.

The routine BD gives the coordinates of nodes of each element and the centre of mass of each element, calculated by calling another routine CMASS, as the output. It is possible to reduce the computing time by having relatively large elements in the lower part of the body. This can be achieved by dividing the polygonal shape into horizontal strips having increasing thickness when going downwards and dividing the lower strips into comparatively smaller number of elements. The routine BD divides the body into a given number of horizontal strips in such a way that the thicknesses of strips form an arithmetic series. By using a number greater than zero as the common difference (R) of this series, it is possible for the horizontal strips to have increasing thicknesses when going downwards. The number of elements each strip has to be divided into ($N_1 N_2, \ldots N_{NS}$) has to be specified as input data. By using a decreasing set of values for $N_1, N_2, \ldots N_{NS}$ in the input data, the strips in the lower part of the body can be divided into fewer but wider elements. In this way it is possible to divide the whole polygonal shape into smaller elements at the upper part and larger elements in the lower part.

This routine can be used to divide a complicated shape such as given in Figure 3.4 into smaller elements. The structure shown in Figure 3.4 consist of two bodies, ABCDEFGH and BEDC. First the outer body AFGH is subdivided without considering the inner body BEDC

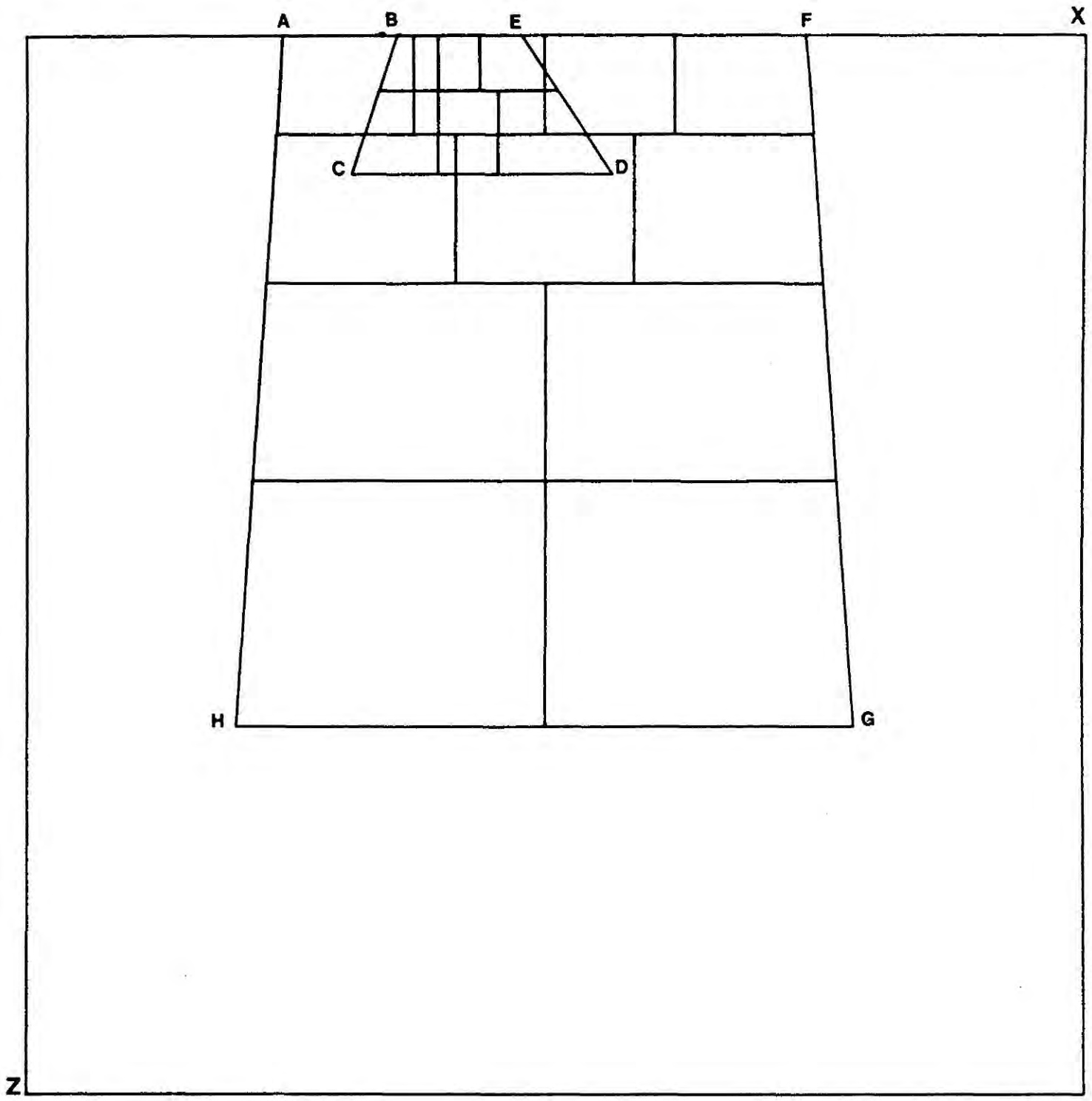

Figure 3.4 Way in which the subroutine BD divides a cross section of a geological structure consists of two bodies.

and its gravity or magnetic anomaly is calculated. Then BEDC is divided separately into smaller elements and the anomaly is calculated and added to the result obtained earlier. The actual density contrast or the magnetization of the inner body (BEDC) is the sum of two magnetizations or density contrasts used in the calculation.

Although the routine BD requires the body to have its top and bottom sides parallel to the X-axis, it is still possible to use it to divide bodies which do not satisfy this condition. The body ABCD given in Figure 3.5 has only its top side parallel to the X-axis. The quadrilateral ABCD can be regarded as the pentagon ABCDD' with the points D and D' coincided. Then the body ABCDD' has its top and bottom sides (AB and DD') parallel to the X-axis and the routine BD can be used to divide this body into a number of elements. Input data for the X and Z coordinates of the nodes of the polygon take the form (X_A, Z_A, X_B, Z_B, X_C, Z_C, X_D, Z_D, $X_{D'}$, $Z_{D'}$). By following a similar method, it is possible to divide a body which does not have the top side parallel to the X-axis.

When the cross-section of the body is divided into a series of elements it is then necessary to calculate the gravity or magnetic anomaly due to two dimensional prisms having these elements as cross-sections. This can be performed by using the two-dimensional polygonal prism methods of Talwani et al. (1959, 1964). Using Talwani et al. (1959) the Fortran routine SLAB was written to calculate the gravity anomaly due to a semi infinite slab and by the repeated application of this routine gravity anomaly due to a two-dimensional prism can be calculated. Bott (1975) wrote a PL1 routine to calculate the gravity anomalies due to similar bodies. Two programmes were run with the same data and gave identical results. The main Fortran program GREND was

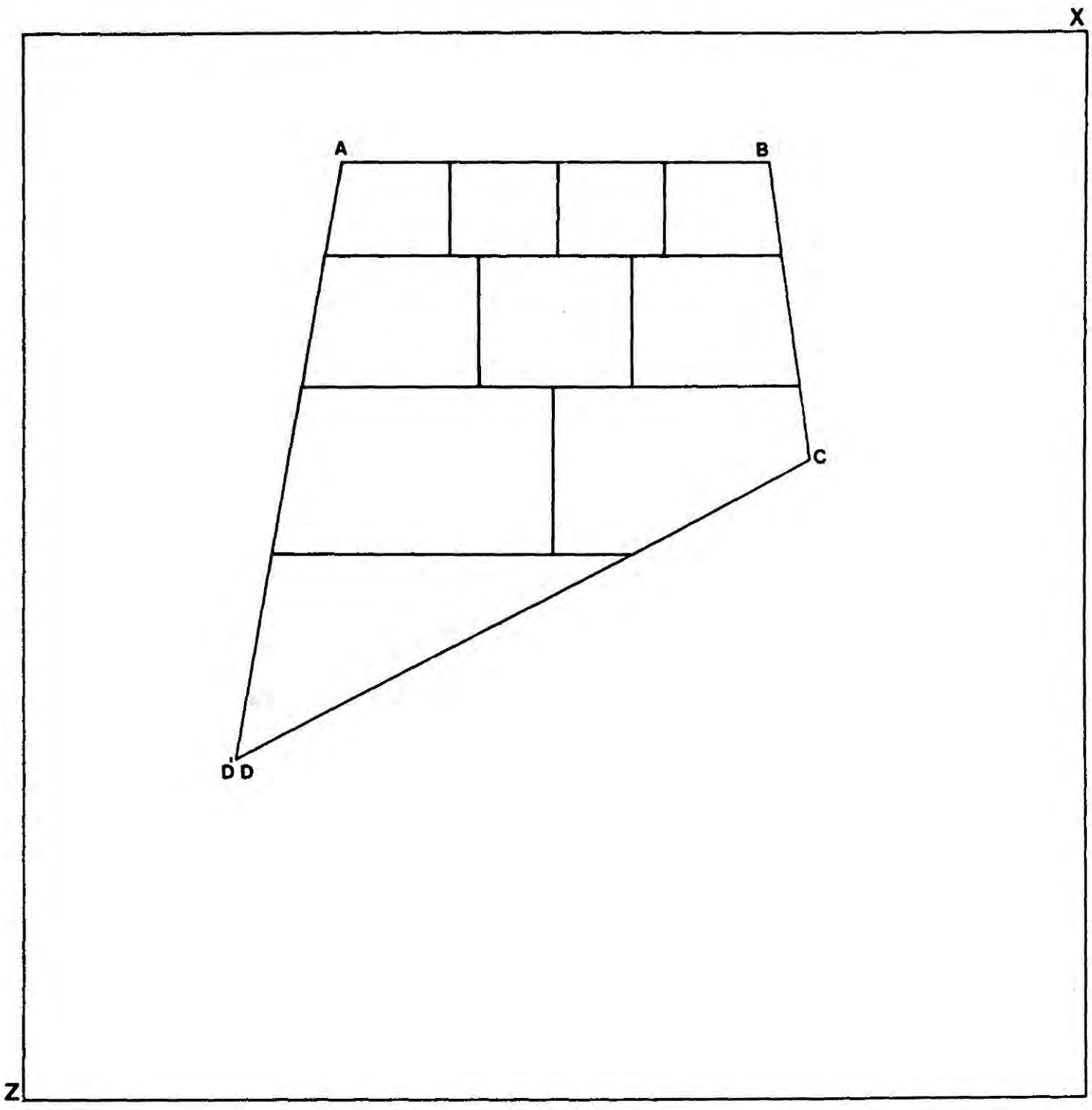

Figure 3.5 Way in which the subroutine BD divides a polygonal shape having only its top side parallel to X axis.

developed to perform gravity interpretation using the end correction method. This program uses subroutines BD, SLAB, CMASS and another routine, ENDCR, which calculates the end correction factors. The program GREND can be used at a computer graphics terminal to perform the interpretation. It gives two separate diagrams as the output. The first diagram shows the way in which the cross-section of the body is divided into a number of elements and the second gives the observed and calculated anomalies together with the cross-section of the model. The first diagram helps us to check whether dividing the cross-section of the body into smaller elements was done properly or not. A listing of this program is given in the Appendix A1.

3.3 Application of Non-Linear Optimization to the Interpretation of Magnetic Anomalies

3.3.1 Introduction

Trial-and-error modelling provides a useful method for gravity and magnetic interpretation in two dimensions and in three dimensions when the end correction method is used. However, the accuracy and speed of this method can be increased by using self-adjusting computer routines which perform the alterations of the shape and physical properties of the body and comparisons of observed and calculated anomalies automatically. Such computer routines can use non-linear optimization techniques.

There are several parameters involved in calculating gravity or magnetic anomalies due to a body. Parameters, such as coordinates of the points which define the shape of the body, are non-linear and parameters such as density contrast and magnetization are linear. For convenience, the regional level can also be considered as a linear parameter. A least-squares method can be used to evaluate the linear

parameters while the non-linear optimization technique can be used to evaluate the non-linear parameters (Al-Chalabi, 1970).

This section describes an application of non-linear optimization techniques in two-dimensional magnetic interpretation. A more detailed account of the use of these techniques in magnetic interpretation can be found in Al-Chalabi(1970). Talwani (1960) described a method of calculating gravity anomalies due to three-dimensional bodies defined by a set of horizontal contours. An attempt was made to perform a three-dimensional gravity interpretation by applying non-linear optimization to this method. During the early stages of developing a computer program to perform the interpretation it was found that this method consumes a large amount of computing time and therefore it was abandoned. However, the end correction method of calculating the gravity anomaly due to a three-dimensional body takes a comparatively small amount of time. Therefore the computer program GREND (see 3.2) which performs 3D gravity interpretations using end corrections was automated using a non-linear optimization technique.

3.3.2 Calculation of the Objective Function

Mathematically non-linear optimization involves a minimization of a function called the objective function. In practical problems this function usually measures the discrepancy between the calculated effect due to a theoretical model and observed results. We can define the objective function for magnetic interpretation in the following way.

Let $Fc_k(\alpha_1,\alpha_2,.....\alpha_n)$ be calculated magnetic anomaly due to an assumed model at the k^{th} fied point and Fo_k be the observed anomaly at the same point, where $\alpha_1, \alpha_2, ...\alpha_n$ are the parameters involved in calculating the magnetic anomaly due to the model. Then the objective

function $f(\beta)$ can be written as

$$f(\beta) = \sum_{k=1}^{n} (Fo_k - Fc_k)^2 \qquad 3.3.1$$

where n is the number of field points and β is the vector consisting of the parameters $\alpha_1, \alpha_2 \ldots\ldots \alpha_n$. The optimization technique seeks the minimum of this function by varying the parameters $\alpha_1, \alpha_2 \ldots\ldots \alpha_n$. Calculation of the objective function requires the magnetic anomaly due to the assumed model at all field points. This can be achieved by using the method discussed by Talwani and Heirtzler (1964). Using this method Fc_k for a two-dimensional body having a polygonal cross-section with m sides (see Figure 3.6) can be written as

$$Fc_k = J_x U_k + J_z V_k \qquad 3.3.2$$

where,

J_x, J_z = X and Z components of the magnetization,

$$U_k = 2\sum_{i=1}^{m} \{Q_i \sin I + P_i \cos I \cos(C-D)\},$$

$$V_k = 2\sum_{i=1}^{m} \{Q_i \cos I \cos(C-D) - P_i \sin I\},$$

$$P_i = \frac{z_{ji}^2}{z_{ji}^2 + x_{ij}^2} (\theta_i - \theta_j) + \frac{z_{ji} x_{ij}}{z_{ji}^2 + x_{ij}^2} \log\left(\frac{r_j}{r_i}\right),$$

$$Q_i = \frac{z_{ji} x_{ij}}{z_{ji}^2 + x_{ij}^2} (\theta_i - \theta_j) - \frac{z_{ji}^2}{z_{ji}^2 + x_{ij}^2} \log\left(\frac{r_j}{r_i}\right),$$

$j = i+1$ for $i = 1, 2, \ldots\ldots\ldots m-1$,
$j = 1$ for $i = m$

$$x_{ij} = x_i - x_j ,$$

$$z_{ji} = z_j - z_i ,$$

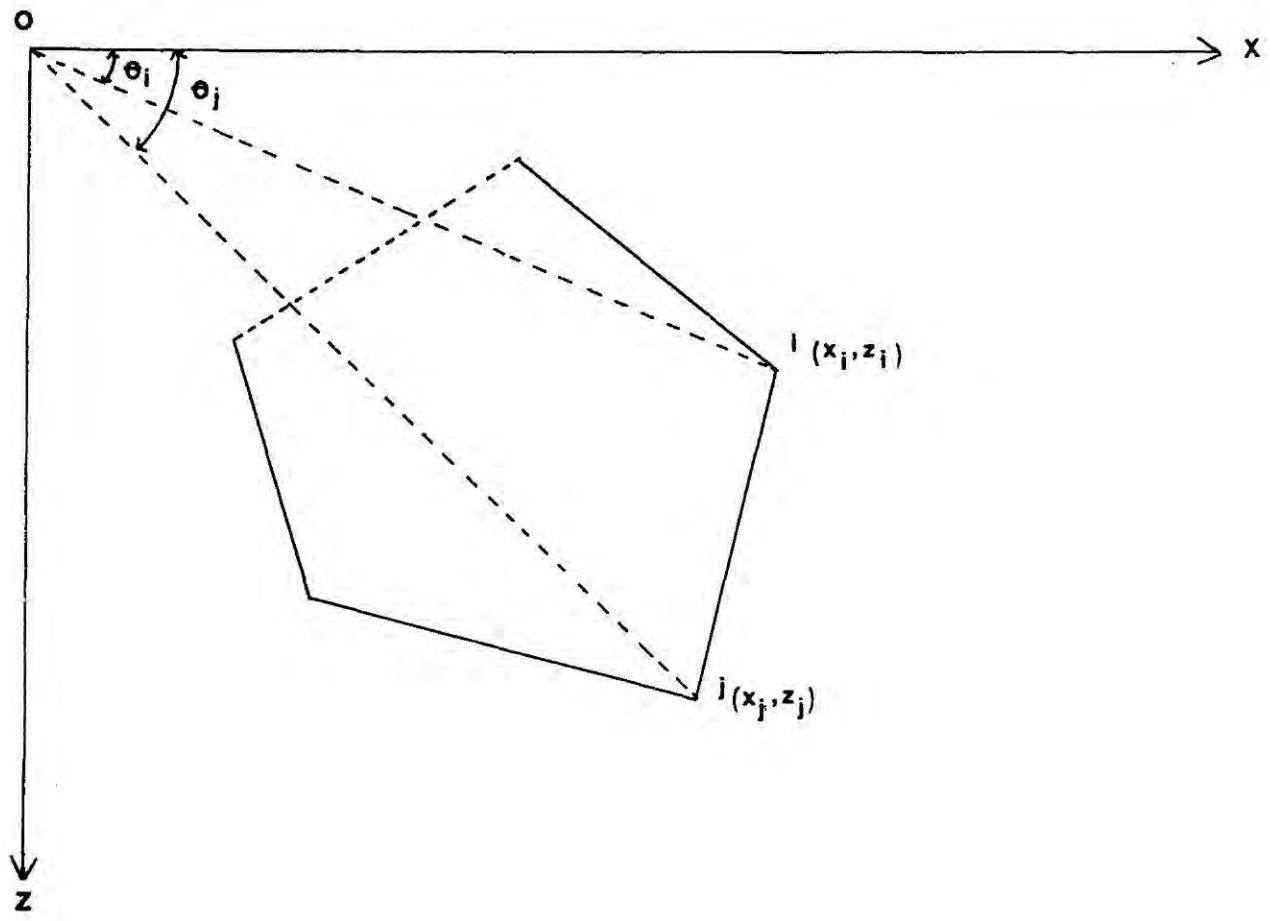

Figure 3.6 Magnetic anomaly due to a two dimensional body having a polygonal cross section.

$$r_i = (x_i^2 + z_i^2)^{\frac{1}{2}} \quad ,$$

$$r_j = (x_j^2 + z_j^2)^{\frac{1}{2}} \quad ,$$

I,D = inclination and declination of the earth's total field,

C = angle between the X-axis and geographic north measured clockwise from geographic north.

For θ_i and θ_j refer to the Figure 3.6.

If R is the constant regional level, then the objective function given in 3.3.1 can be written as

$$f(\beta) = \sum_{k=1}^{n} (Fo_k - J_X U_k - J_Z V_k - R)^2 \qquad 3.3.3$$

It is possible to treat linear parameters, such as magnetization (J_x and J_z) and the linear regional level R, as non-linear parameters and include their evaluation in the optimization process. The least-squares method is another way of evaluating these linear parameters. Details of this evaluation aregiven by Al-Chalabi (1970).

Usually the objective function has several minima. The lowest minimum is known as the global minimum and the minima other than the global minimum are known as local minima. In gravity and magnetic interpretation the location of the global minimum is sometimes a difficult task.

3.3.3 Optimization Techniques used in the Interpretation

Optimization techniques can be divided into two main categories, namely direct search methods and gradient methods. Gradient methods are methods which use the gradient of the objective

function in finding the minimum. Methods which are based only on the comparison of the value of the objective function in successive iterations are known as direct search methods. A Simplex method, (a direct search method), and a Quasi-Newton method, (a gradient method), were used in the application of non-linear optimization to magnetic interpretation. These two methods are discussed below.

3.3.3.1 The Simplex Method

A simplex in n-dimensional space is defined as a set of n+1 points in that space. The simplex is said to be regular if all the points of the simplex are mutually equidistant. In the case of two dimensional space the simplex is a triangle and in three dimensional case it is a tetrahedron. The simplex method of optimization was originally introduced by Spendley et al. (1962) and later improved by Nelder and Mead (1965). This improved version is now widely in use.

The Simplex method of Spendley et al. uses a regular simplex. This method first evaluates the value of the objective function at the vertices of a regular simplex. Then it forms a new simplex by reflecting the point having the largest value of the objective function in the centroid of the remaining vertices and this procedure is then successively repeated. If the point obtained by reflection still has the largest value of the function, then this point is discarded and a new point is obtained by reflecting the vertex having the second highest value of the function in the original simplex. At the vicinity of a minimum the simplex starts to rotate around one of its vertices. When this condition occurs, the method reduces the size of the distance between points of the simplex by half and repeats the procedure again. When the distance between points of the simplex reduces to a specified value, the centroid of the simplex is assumed to be the position of

the minimum of the function.

However, it is not essential to use a regular simplex in finding a minimum of a function. The simplex method of Nelder and Mead uses an irregular simplex, together with three basic operations which change the shape and size of the simplex. These basic operations are reflection, expansion and contraction. The operation reflection is similar to that discussed above. However it is no longer essential to have the distance from the centroid of the remaining points to the new point obtained by reflection and the distance from this centroid to the original point equal to each other. The ratio between these two distances are defined as the reflection coefficient. The expansion operation moves the point obtained by reflection away from the centroid of the remaining points. The ratio between distances to the centroid of remaining points from the point obtained by expansion and the original point (the point obtained by reflection) is known as the expansion coefficient, and is usually greater than one. The operation which brings a point obtained by reflection towards the centroid is known as contraction. The contraction operation is similar to the expansion operation, but in this case the coefficient is less than one.

Similar to the original Simplex method, Nelder and Mead's method first reflects the point having the largest value of the function about the centroid of the remaining points. If the new point gives a minimum, further search along the direction of the new point is made by using the expansion operation. If the function at the new point is greater than that at one of the remaining points, the search is done in the opposite direction using the contraction operation. At the vicinity of a minimum, the size of the simplex is reduced and the process is repeated. When the variance of the values of the

function at the vertices of the simplex is less than a specified value, the search is terminated and the centroid of the last simplex is assumed to be the position of the minimum. However, this kind of termination does not guarantee the absolute convergence of the function.

3.3.3.2 The Newton Method and Quasi-Newton Methods

Since the theory behind Quasi-Newton methods is mathematically involved, only the basic ideas of these methods are given here. Quasi-Newton methods can be regarded as an extension of the Newton method of optimization. Therefore Newton's method is described first.

Let $X^*(\alpha_1, \alpha_2, \ldots \alpha_n)$ be a minimum of the function f(X) and $X = X^* + h$, where $h = (h_1, h_2, \ldots h_n)$, be a point close to this minimum. In the neighbourhood of a minimum a function can be taken as being approximately quadratic (Wolfe, 1978). Let us also assume that H and g are the matrix of second partial derivatives at X^* (Hessian matrix), and the vector of partial derivatives at X (gradientvector) respectively. Using the second order Taylor series Box et al. (1969) showed that

$$X^* = X - H^{-1}g \qquad 3.3.4$$

Since the function behaves quadratically in the vicinity of a minimum, H is a constant. Therefore by calculating H at the point X and using this value in 3.3.4 X^* can be found. If X is not close to X^* the quadratic approximation to the objective function is not valid and therefore H is not a constant. The equation 3.3.4 cannot therefore be used to obtain the position of minimum directly. Nevertheless 3.3.4 can be used as an iterative rule

$$X_{k+1} = X_k - H^{-1} g \qquad 3.3.5$$

where X_k is the value of X after k iterations and H and g are evaluated at the same point X_k.

This method requires the matrix H to be non-singular and this condition is generally satisfied in the region close to the minimum. The greatest objection to this method is that it requires the computation of the matrix H and its inverse at each stage. Quasi-Newton methods overcome this problem by forming an approximation to H, and its inverse, from the information obtained from the iterative process. A detailed account of these methods is given by Broyden (1967).

3.3.3.3. Scaling and Constraints

Suitable scaling of non-linear variables in an optimization problem improves its efficiency. This scaling should be done in such a way that the non-linear variables have approximately the same value in the region of the minimum. The objective function for an unscaled problem is usually elongated, while that for suitably scaled problem takes an approximately hyper-spherical shape (Al-Chalabi, 1970). This symmetry of the objective function, when variables are scaled, makes the search easier and therefore more efficient.

In the interpretation of a magnetic anomaly we usually have some knowledge of the geology of the region around the causative body. This geological information can be used to give upper and lower limits to the variable parameters of the minimization. The search will then perform only within the region defined by these limits. Solving such a problem is known as constrained optimization. Contrained optimization

not only reduces computing time, it also preserves the geological reality of the model. Most of the constraints in magnetic interpretation are very simple ones. For example the depth to the top surface of a body is restricted to being greater than a given value, or the magnetization of a body should lie in a given range. The variable transformation method (Box, 1966) is useful in applying such constraints.

3.3.3.4 Programming Details

Two Fortran programs, MAG1 and MAG2 have been written to perform two dimensional magnetic interpretation using non-linear optimization. In these programs, the calculation of the magnetic anomaly due to the assumed model is performed by a Fortran subroutine called MAGAN which uses Talwani and Heirzler's two-dimensional polyonal method. MAG1 uses a Quasi-Newton method to perform the optimization. MAG1 considers linear parameters such as magnetization and the linear regional level as non-linear parameters and their evaluation is performed in the optimization process. MAG2 considers these parameters as linear parameters and they are evaluated using the least squares method. The optimization technique used in MAG2 is a simplex method. The Fortran program GREND described in 3.2. performs the gravity interpretation in three-dimensions using the end correction method. This program was modified to perform the interpretation automatically using a non-linear optimization technique. The modified program, OPGREND, automatically varies parameters of the body such as its body points and density contrast as well as the regional level of the anomaly and seeks a model which produces an anomaly closest to the observed anomaly. This program uses a quasi-Newton method as the optimization technique and it requires the parameters of the objective function to be scaled.

This program took a C.P.U. time of 10·8 seconds at the Durham University IBM 370/168 computer to produce the pseudogravimetric model of the Mull igneous complex shown in Figure 4.12.

The computer subroutines which perform the non-linear optimization were obtained from the Durham University 'NAG' Computer library. A listing of the programs discussed above together with instructions on how to use them is given in the Appendix A.1.

3.4 Ambiguity in Gravity and Magnetic Interpretation

A simple application of Gauss' theorem shows that the gravity anomaly due to a sphere and a concentric spherical shell are equal, provided that both of them have the same mass. This is not the only example which illustrates this situation of ambiguity. There can be several bodies which give rise to the same observed anomaly. This fact is equally true for magnetics. Therefore it is not possible to obtain a unique geological shape which satisfies a given gravity or magnetic anomaly. This ambiguity will increase due to the lack of sufficient observations and errors involved in them. However, by making suitable assumptions uniqueness can be achieved in certain cases.

Skeels (1947) illustrated the non-uniqueness in gravity interpretation by considering different bodies at different depths, having different density contrasts, producing the same anomaly. Roy (1962) discussed this problem using potential theory methods. Using the equivalent layer theorem he showed how given gravity or magnetic anomaly can be caused by an infinite number of density or magnetization distributions on a thin layer. He also investigated the non-uniqueness by considering interpretation as solving an integral equation in the following way. If XYZ is a Cartesian coordinate system having the Z-axis pointing vertically downwards, the gravity anomaly at (α, β, o) due to a density

distribution $\rho(x,y,x)$ below the XY plane can be written as

$$g(\alpha, \beta, 0) = G \int_{-\infty}^{\infty} \int_{-\infty}^{\infty} \int_{0}^{\infty} \frac{\rho(x,y,z)\, z \;\, d\,x\, dydz}{\{(x-\alpha)^2 + (y-\beta)^2 + z^2\}^{3/2}}$$

where G is the gravitational constant. There is no unique solution to $\rho(x,y,z)$ as it is a function of three variables (x,y,z) and g is only a function of two variables x and y. Measuring the anomaly on a number of planes at different heights will not improve the situation as they are not independent. If we assume ρ is a constant along the Z direction, theoretical conditions under which interpretation can be achieved uniquely are given by Smith (1961). However, this requires the complete knowledge of the anomaly on an infinite plane. Nevertheless there are certain situations where we can perform the interpretation uniquely, provided we have a sufficient amount of accurate data. One such situation is given by Bott (1960). If the anomaly is caused by a sedimentary basin and if its density contrast, which is assumed to be uniform, and its upper surface are known then it is possible to determine the lower surface uniquely. Two other such situations are, (Roy, 1962),

a) determination of density or magnetization distribution of a flat layer when it is at a known depth,

b) determination of the depth to a body having a known density contrast or magnetization and a known shape.

These examples illustrate how much the knowledge of geology of the region where the causative body is situated is important in reducing the ambiguity in interpretation. Al-Chalabi (1971) showed the possibility of interpreting a given gravity anomaly uniquely in terms of a two-dimensional body having a polygonal cross-section and an uniform density contrast. The assumption that any vertical line through the

body meets its boundary only twice i an important condition in this case. Otherwise the polygonal model is not unique (Smith, 1978).

The non uniqueness arising from experimental errors and an insufficient amount of observations has been investigated by Al-Chalabi (1971), using the non-linear optimization technique. He showed that when the length of the anomaly is decreased and the interval of observation is increased, new minima of the objective function corresponding to different models begin to appear. Experimental errors in the observations also cause similar results.

By considering all these factors we can say that when a sufficient amount of accurate observations are available, then using the knowledge of the geology around the structure causing the anomaly the ambiguity in interpretation reduces to a reasonable level.

CHAPTER 4

INTERPRETATION OF MAGNETIC ANOMALIES OVER THE MULL IGNEOUS COMPLEX

4.1 Introduction

This chapter presents an interpretation of aeromagnetic anomalies over the Mull igneous complex. Figure 4.1 shows the aeromagnetic anomaly map over this region. The most striking feature of this aeromagnetic anomaly map is the large, dominantly positive, anomaly over the Mull central intrusive complex. Outside this central anomaly, there are some negative anomalies which extend over the area covered with basaltic lavas. In addition to these, there is a ring of relatively short wavelength anomalies outside the complex. This ring consists of both positive and negative anomalies. The anomaly map (Figure 4.1) is a complicated one. Interpretation of the central anomaly was therefore performed by transforming it into pseudogravimetric anomalies by using the method discussed in chapter 2. The above mentioned relatively short wavelength anomalies around the complex were interpreted by using normal magnetic interpretation methods. The results of these interpretations are discussed and compared with the results of the most recent gravity interpretation of the Mull complex. Before going into details of these interpretations,the geology of the Mull complex and previous gravity and magnetic studies of the area are discussed.

4.2 Geology of the Mull Complex

The Tertiary igneous geology of Mull has been described and discussed in great detail by Bailey et al. (1924), Richey et al. (1961), Stewart (1965) and by Skelhorn (1969). The account given below is a summary of the work presented by these authors.

4.2.1 Basaltic Lavas

Most of Mull is covered with basaltic lavas of Tertiary age

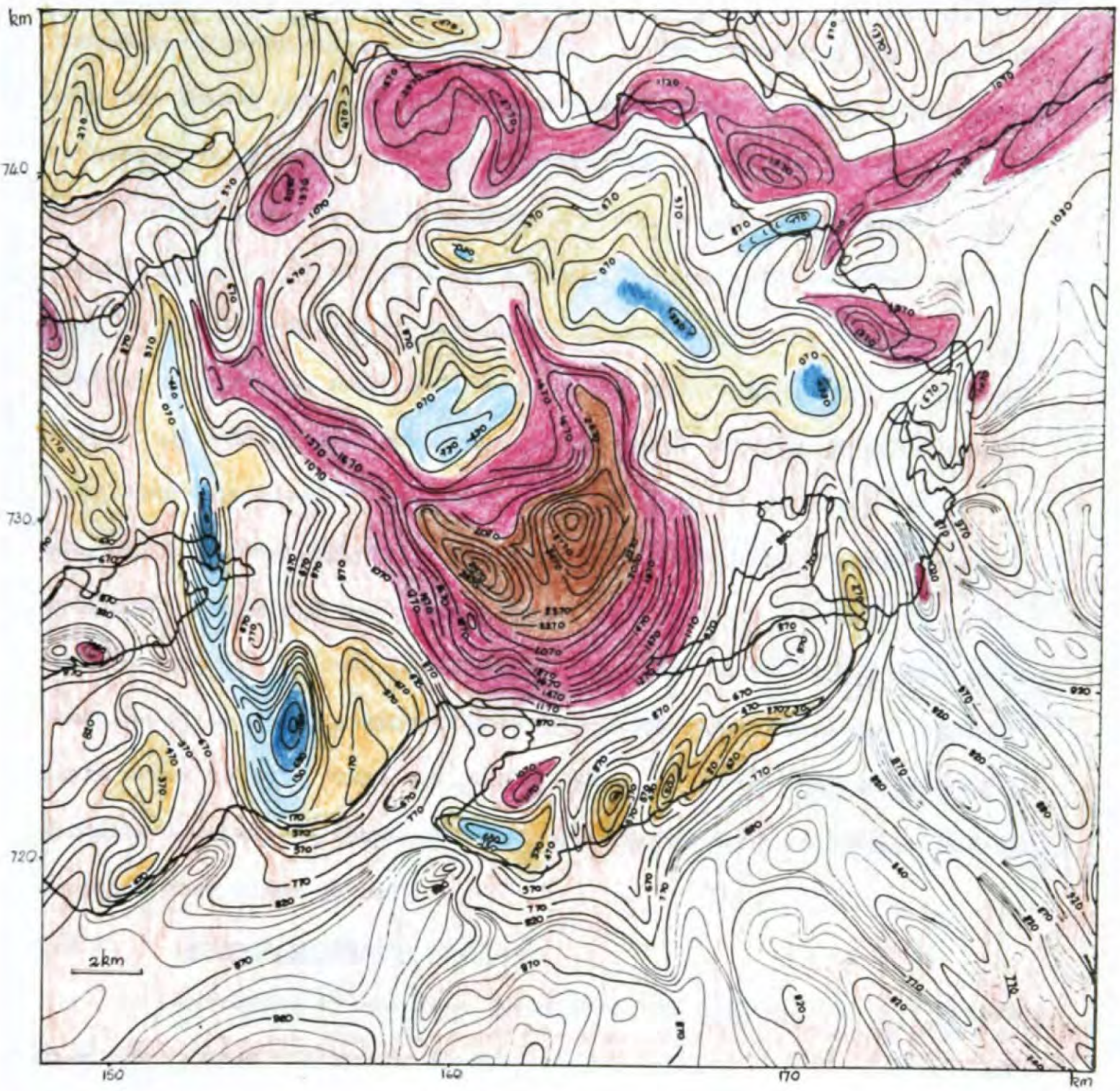

Figure 4.1 Aeromagnetic anomaly map over the Mull intrusive complex and surrounding lavas. Contours in gamma. Coordinates shown are national grid.

	7o-47o gamma		1o7o-2o7o gamma		7o- -73o gamma
	47o- 1o7o gamma		2o7o-3o7o gamma		below -73o gamma

and Figure 4.2 shows a part of this lava succession. These lavas overlie a thin layer of red mudstone which may have formed due to the lateritic weathering of basaltic ashes. Basaltic lavas in Mull are classified into two types; the plateau group and the central group. The central group, which was extruded later, overlies the plateau group, which is fully developed only in western Mull with a maximum thickness of about 915m (3000 ft) at Ben More. This group of lavas mainly consists of olivine basalts. The central group of lavas, which are mainly olivine poor basalts, can be seen in south-eastern Mull and in two subsided calderas (early south-eastern caldera and late north-western caldera, Figure 4.2) in central Mull. In central Mull three concentric zones of this group of lavas have been identified. The inner zone consists of olivine-poor or olivine-free non-porphyritic tholeiitic basalts while the middle zone consists of highly porphyritic basalts with felspar phenocrysts. The central type is not well developed in the outer zone. This zone mainly consists of sparsely porphyritic or non-porphyritic basalts. Pillow lavas occur in both outer and middle zones. The general absence of pyroclastic horizons throughout the lava successions indicates that the eruption took place quietly.

4.2.2 Central Intrusive Complex

Extrusion of basaltic lavas from the Mull volcano was followed by a complicated history of igneous events forming the central intrusive complex of Mull. During this period, the centre of activity moved twice from south-east to north-west. Originally activity centered at Glen More in the south-eastern caldera. With time it moved to Beinn Chaisgidle and from there, closer to Loch Bà. The whole igneous complex is symmetrical about the north-west axis along which the centre of

TERTIARY SURFACE ROCKS :—

Basalt-Lavas.

Agglomerate.

Mugearite-Lavas.

Common Central Types.

Big-Felspar Basalt.

Plateau Types.

TERTIARY INTRUSIONS (including Vent-Agglomerates, but omitting Sheets and Dykes) :—

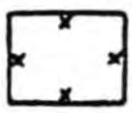

PRE-TERTIARY ROCKS :—

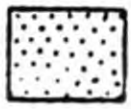

SIGNS :—

/s↙ Dips, in degrees.

Margins of Main Calderas.

Other Faults.

Limit of Pneumatolysis.

GENERALIZED SUCCESSION OF MULL LAVAS.

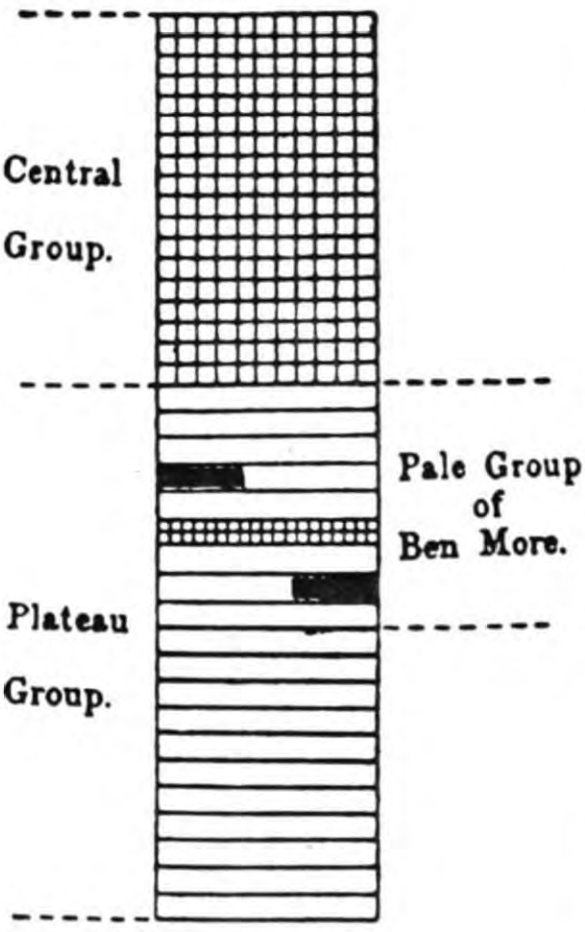

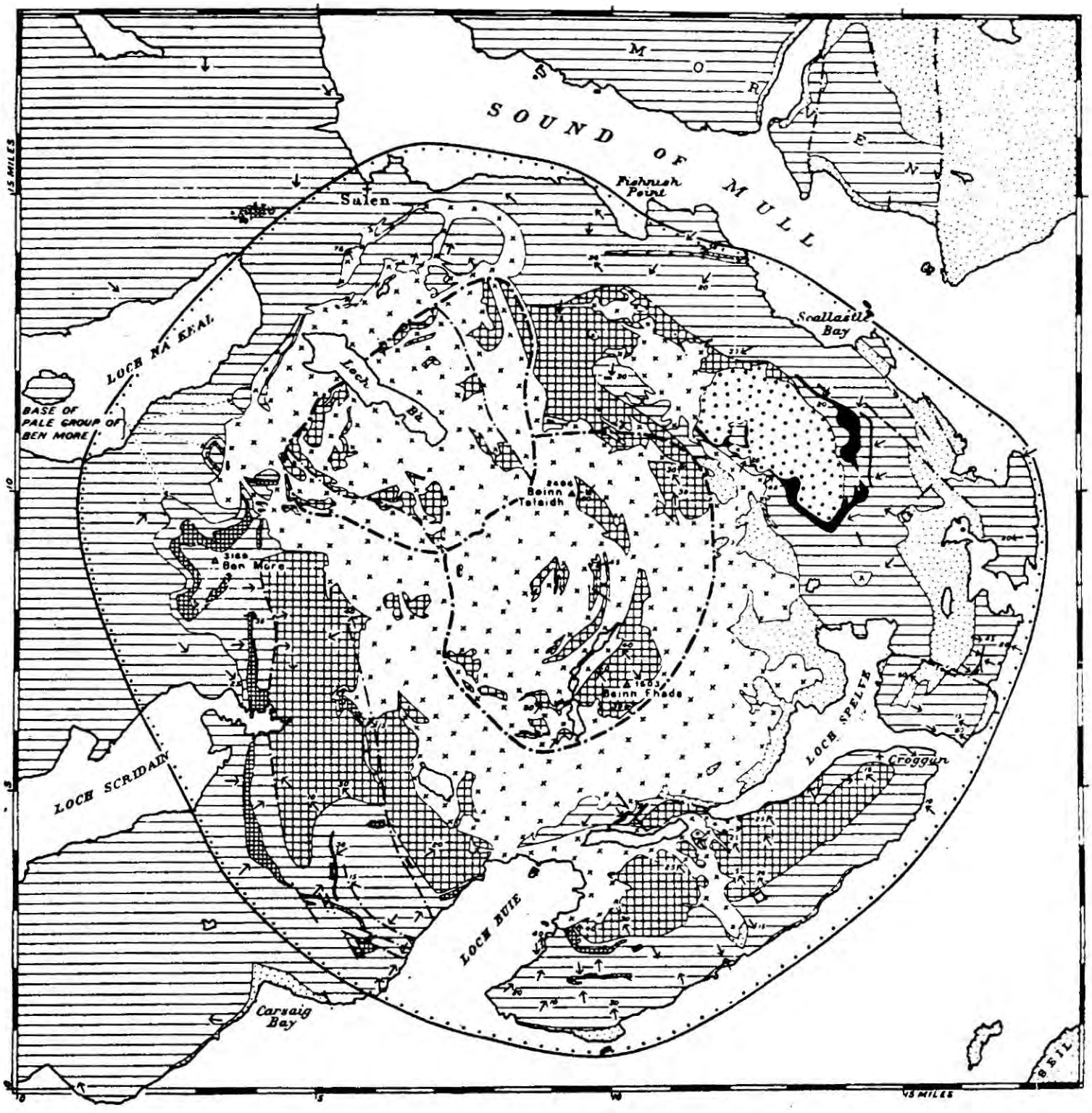

Figure 4.2 Map showing distribution of Tertiary lavas in central Mull from Bailey et al. (1924).

activity migrated. Figure 4.3 is a map which shows various intrusions associated with each of these centres. The original sequence of igneous events proposed by Bailey et al. (1924) and by Richey et al. (1961) has been slightly changed in view of recent research studies (Skelhorn,1969). It is the most recent interpretation that is adopted here and presented in chronological order.

Glen More Centre

The sequence of events is as follows:

1. Glass Bheinn and Derrynaculen granophyres.
2. Acid explosion vents.
3. Early Acid and Intermediate Cone Sheets.
4. Early Basic Cone Sheets.
5. Loch Usig granophyre and gabbro.
6. Ben Buie Layered Gabbro.

The geological map (Figure 4.3) shows that the Glass Bheinn and Derrynaculen granophyres are separated by the Ben Buie gabbro and a region covered with explosion vents. Since these vents contain fragments of granophyre, these two rock masses may have been connected originally. There is a series of concentric folds around the south-eastern caldera (Figure 4.3). The emplacement of the Glass Bheinn and Derrynaculen granophyres may be the cause of these folds. However, according to Skelhorn (1969) this folding took place due to a cylindrical magma chamber rising through the crust before the emplacement of the two granophyres. The petrogenesis of granitic rocks in the Mull complex has been studied by Walsh et al. (1979) by analysing major and trace elements. It was shown in this study, that

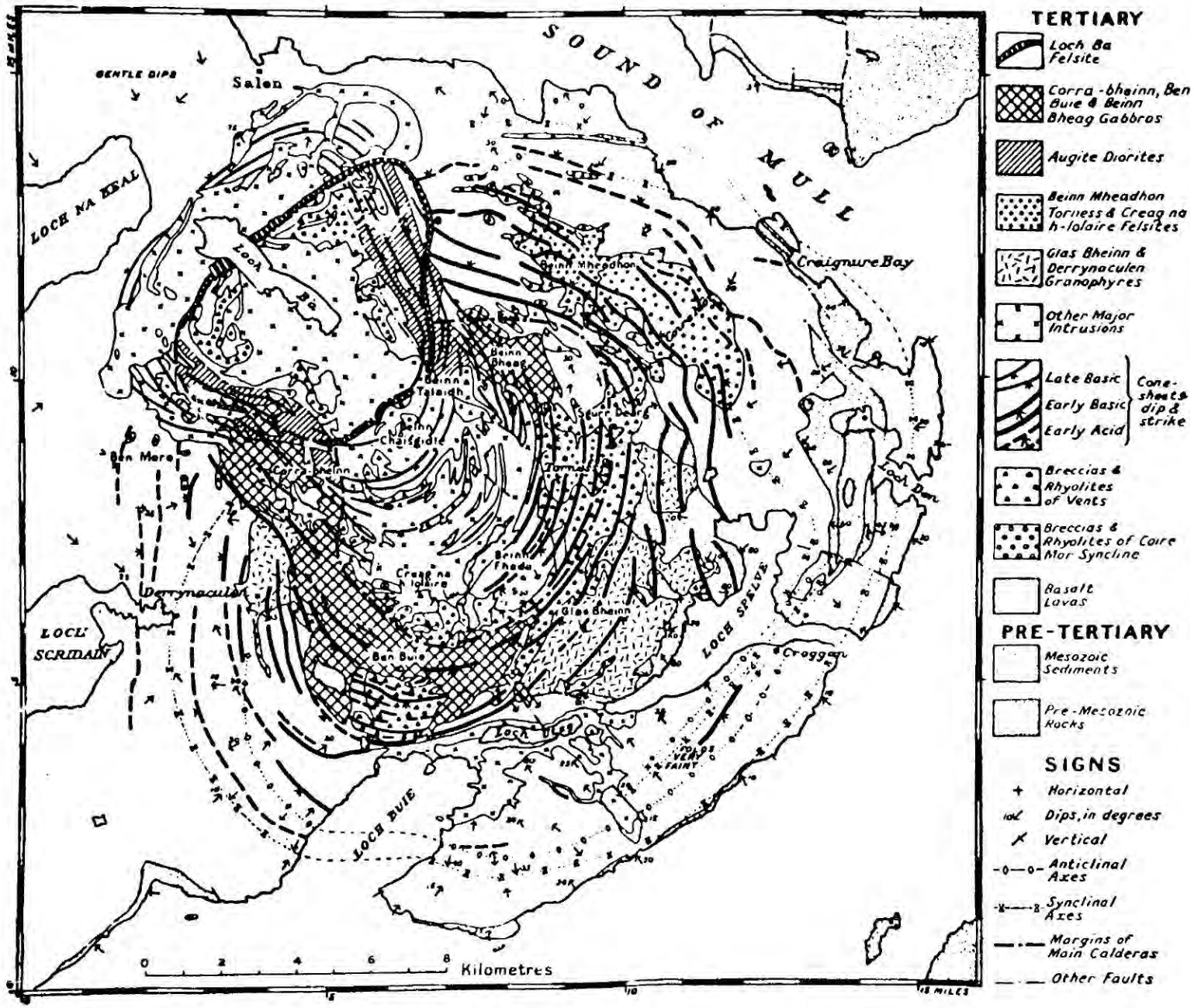

Figure 4.3 Geological map of Tertiary igneous complex of central Mull from Bailey et al. (1924).

However, olivine and bytownite/anorthite remain throughout as major components. This olivine content is fairly high, exceeding 50% of the bulk of the rocks. In places, concentration of olivine and chromiferous spinel has produced an ultrabasic rock closer to dunite. Microsopic studies have revealed that in some places, some olivine crystals are covered with dust like magnetite particles. The dominating component of the eurcite rocks of the Ben Buie gabbro is also olivine. Magnetite and chromiferous spinel occur in small amounts as scattered patches. Porphyritic rocks in the Ben Buie gabbro contain comparatively low amounts of olivine. Magnetite is present throughout the rock as large irregular crystals and granules.

The Beinn Bheag gabbro is another large mass of gabbro in the Mull complex. Since this intrusion is not included in the time sequence given by Skelhorn (1969), it is assumed that it was emplaced at the same time as the Ben Buie gabbro (Richey et al.,1961). This intrusion mainly consists of olivine gabbro with occasional large serpentized olivine. Some acid rocks occur in patches near the summit of Ben Bheag. Bailey et al. (1924) reported the presence of augite associated with magnetite in the acidic fractions.

Beinn Chaisgidle Centre

The sequence here is as follows:

1. Explosion vents.
2. Second suite of Early Acidic Cone Sheets.
3. Second suite of Early Basic Cone Sheets.
4. Corra-bheinn Layered gabbro.
5. Augite-diorite mass of Cruachan and Gaodhail.
6. Ring intrusions around Beinn Chaisgidle.
7. Late Basic Cone Sheets.

A major feature of this centre is the large number of ring intrusions around Beinn Chaisgidle having acidic, intermediate and basic compositions. The average width of these ring intrusions is about 157m (525 ft.) and usually they are separated from each other by the country rocks. The outermost and the largest of this suite is the Glen More ring dyke. At Cruach Choiredail the outcrop of this ring dyke becomes very steep and in this steep region as one passes up the mountain side, the rock type changes from basic to acidic through intermediate compositions. At the base, the rock type is olivine bearing quartz-gabbro and it changes to dioritic rocks at intermediate heights. At the summit of Cruach Choiredail, the rock type is granophyre. The authors of the Mull Memoir (Bailey et al., 1924) have explained this vertical variation of rock types as a result of a gravitational differentiation.

The Corra-bheinn layered gabbro is another major body which was intruded during the active period of the Beinn Chaisgidle centre. The layering of this rock dips towards the late caldera with very steep angles. The cause of this may be related to the subsidence of the nearby late caldera. As indicated by Bailey et al. (1924), these rocks are mainly olivine gabbro. Magnetic minerals such as magnetite occur from place to place as patches or crystals.

Loch Bà Centre

The sequence in this centre is as follows:

1. Glen Cannel Complex.
2. Early Beinn a'Ghràig Granophyre and Felsite masses.
3. Late Basic Cone Sheets.
4. Knock Granophyre.

5. Beinn a'Ghràig Granophyre.

6. Hybrid mass of Sorn nam Boc and Coille na Sroine.

7. Loch Ba Felsite Ring Dyke.

Dykes were intruded before, during and after the above time sequence.

A large portion of the area around this centre is covered by the massive Glen Cannel and Beinn a'Ghràig granophyres and the relatively small Knock granophyre. The Glen Cannel granophyre is either a stock or a thick sheet, while the other two are ring dykes (Richey et al., 1961). The Lock Bà felsite ring dyke is another conspicuous feature of this centre. This ring dyke which has almost complete outcrop is symmetrical about the north-west axis. Both inner and outer surfaces of the ring dyke dip towards the N.W. at angles between 70^{o} and 80^{o}. The Loch Ba ring dyke was intruded approximately along the margins of the north-western caldera which was subsiding at that time. On the south-western, north-eastern and the southern portions of the ring dyke there is a crush zone which must have been caused by this subsidence (Baily et al., 1924). According to Lewis (1968), this is a zone of gas brecciation, rather than a crush zone. He suggested that the cause was the explosive release of gases from the felsite magma acting on the country rock, before, during and after the emplacement of the Loch Bà ring dyke. There are some patches of central type lavas inside this ring dyke. The vertical distance between these lava patches and the plateau lavas at Ben More is about 915m(3000 ft.). Since the central type overlies the plateau type elsewhere, downthrow of the late caldera should be about 915m (3000ft.) (Richey et al., 1961).

4.2.3. Pneumatolysis and Hydrothermal Activity

It was pointed out by Bailey et al. (1924) that there is a zone of altered basaltic lavas around the central intrusive complex of Mull. Their field observations and microscopic studies have shown that there is no fresh olivine in most of the rocks inside this zone, and they also suggested that this alteration was due to pneumatolytic activity. Inside this zone of pneumatolysis (Figure 4.2), there are minute cracks in lavas and some of them are filled with minerals such as epidote and albite. Taylor and Forester (1971) and Forester and Taylor (1976) have found that most of the rocks inside the area covered by the limit of pneumatolysis are anomalously low in oxygen 18 isotope compared to igneous rocks in other parts of the world. They have explained this as being due to hydrothermal activity which must have taken place during the time the igneous centres of the complex were active. The meteoric ground water which is thought to have circulated around the igneous centres, had a very low O^{18} content and this water may have exchanged O^{16} for O^{18} with the rocks. Most of the rocks in the Mull complex should have been highly permeable to ground water due to numerous cracks and joints. The ground water in passing through these cracks and joints, became lighter or even vaporized due to the high temperatures of the complex and moved upwards. On cooling, it became denser and started sinking again (Figure 4.4). The resulting convective cells exchanged O^{16} for O^{18} within the rocks. Walker (1971) who did a study of amygdale mineral zones around the complex found that there is a zone of epidote minerals which approximately coincides with the zone of pneumatolysis and a zone of prehnite beyond that. It is likely that the high temperature and vapour pressure required for the

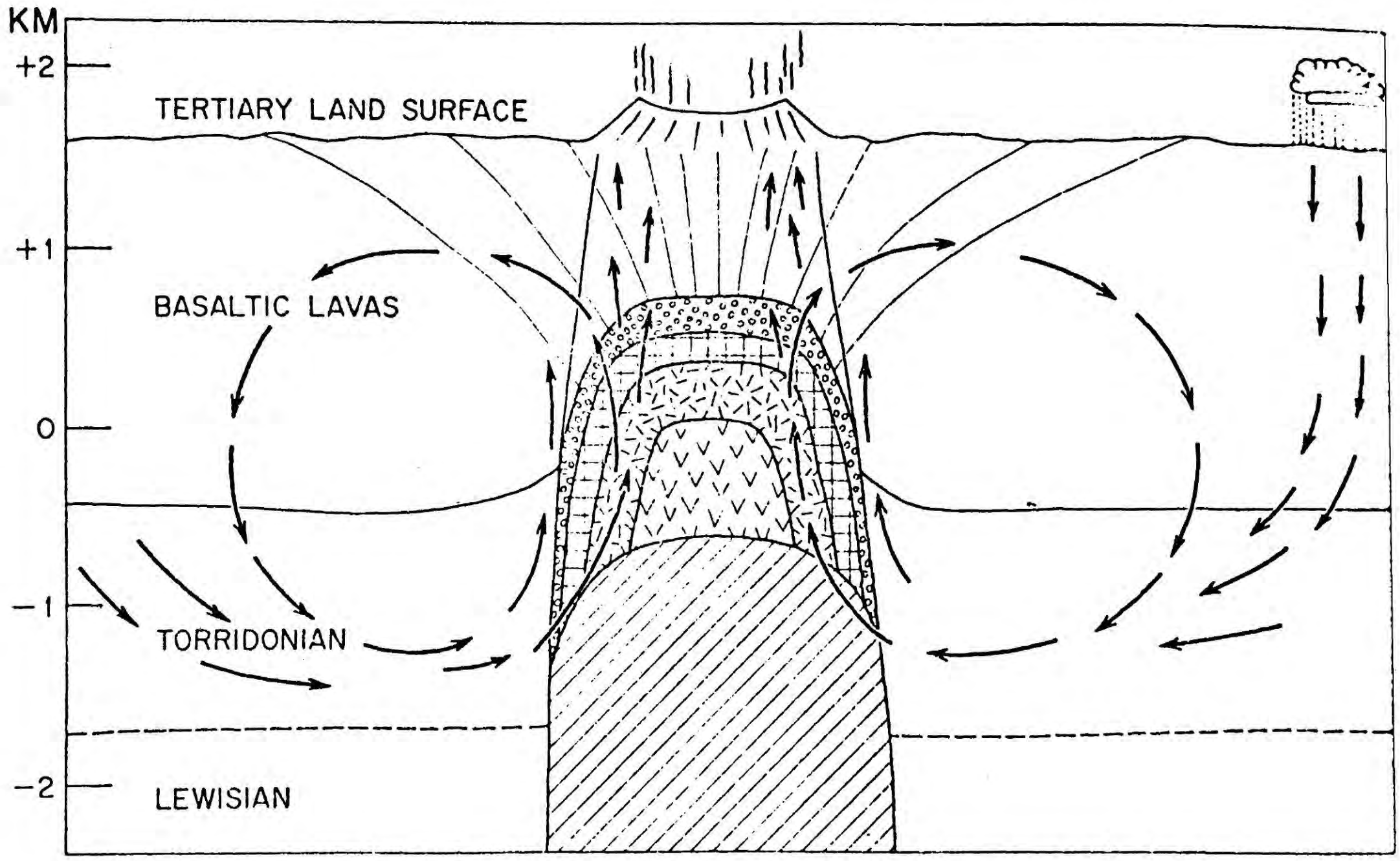

Figure 4.4 Hydrothermal circulations around a typical ring-dyke complex from Taylor and Forester(1971). The checked patterns indicate a series of ring dykes above a gabbro pluton.

formation of these minerals may have been supplied by the hydrothermal circulation.

4.2.4 Age of the Igneous Activity in Mull

Seward and Holttum (in Bailey et al., 1924) carried out a study of fossil flora from interbasaltic beds in Ardtun in Mull and came to the conclusion that they are of Eocene age. Results of more recent studies on the age of basaltic lavas in Mull using Potassium-Argon isotope methods by Miller and Brown (1961) have given an age in agreement with that of Seward and Holttum. According to Miller and Brown this igneous activity started in Palaeocene or Eocene period. Mussett et al. (1973) have shown by K-Ar age determination methods that the Mull lavas cannot be older than 62 m.y. The tentative age given for the N-W dyke swarm in Mull by them is in the interval 49-56 m.y.

4.3 Previous Gravity and Magnetic Studies of the Mull Complex

4.3.1 Gravity Studies

Tuson (1959) and Bott and Tuson (1973) carried out a gravity survey over the Mull igneous complex, and figure 4.5 gives the Bouguer anomaly map. This gravity anomaly map covers the area of the igneous complex and surrounding lavas and the Bouguer anomalies have a maximum value of 72 mgal at Glen More in the south-eastern caldera. The almost circular nature of the anomaly is distorted due to its elongation along a S.E. - N.W. axis. Distortion is also due to the presence of granitic rocks in the complex, which give rise to local negative anomalies. Tuson interpreted the subsurface structure which gives rise to the anomaly as a cylindrical body of density contrast 0.2 g/cm^3 which extends to a depth of 17km with a radius of 8 km. The difference between observed and calculated anomalies is as much as 10 mgal in

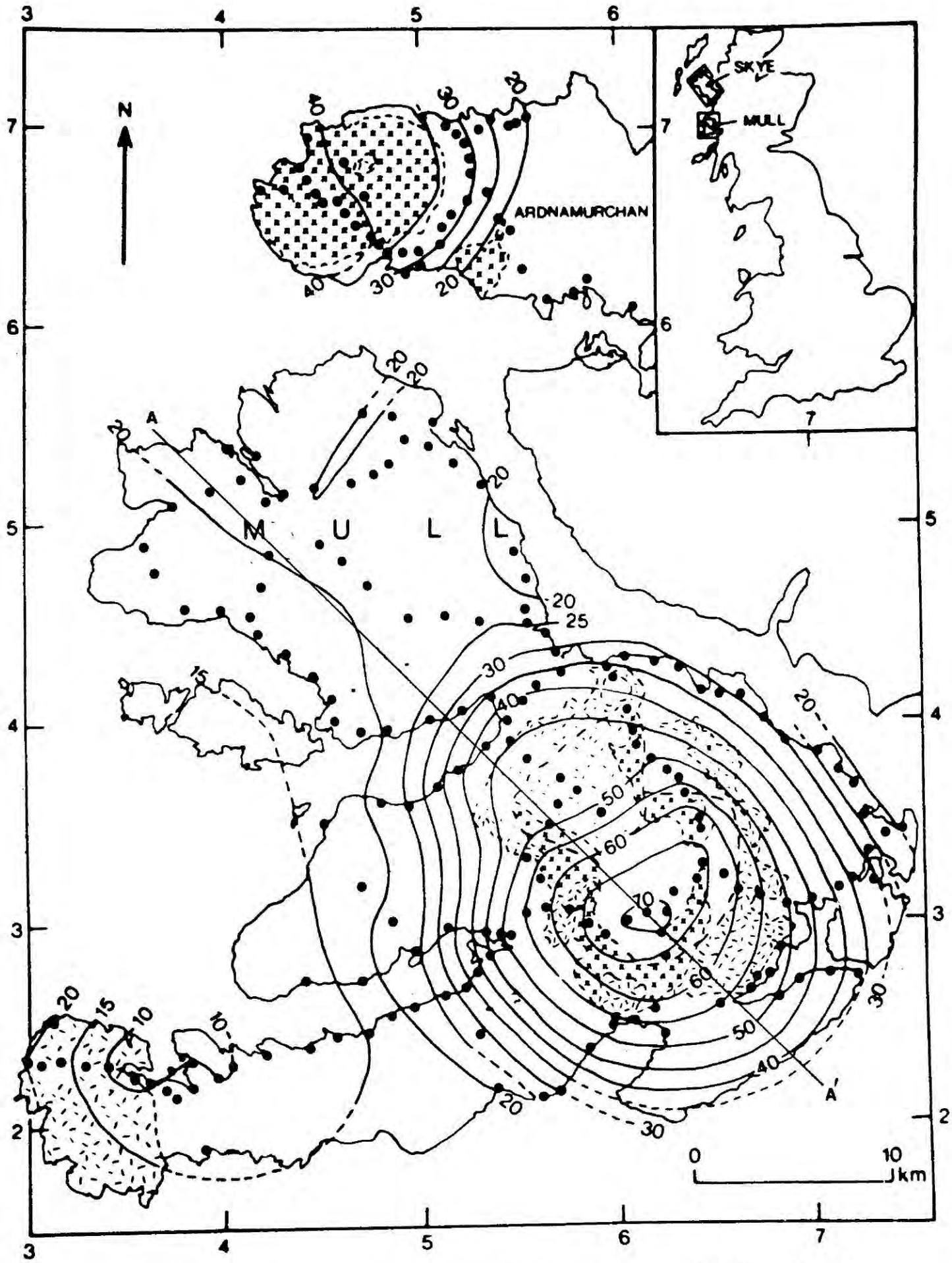

Figure 4.5 Bouguer anomaly map of the Isle of Mull, showing contours at 5 mgal intervals from Bott and Tuson(1973).

●, Gravity station; ×, gabbro; ⊠, granite.

certain places. Tuson explained some of these residuals as a result of negative gravity anomalies caused by the granitic rocks which were not considered in the interpretation and the rest as a result of the deviation of the shape of the subsurface mass from the assumed cylindrical shape. A similar interpretation of the Mull complex was presented by McQuillin and Tuson (1965). Bott and Tuson (1973) suggested that the subsurface structure of the Mull complex may take a shape similar to a truncated cone. It became clear from Tuson (1959), that it is necessary to perform a detailed three-dimensional interpretation, including the effects of granitic rocks, to obtain a clear picture of the subsurface structure of the Mull complex. In order to fulfill this requirement Bott (private communications) carried out a three-dimensional interpretation of the Mull complex using the end correction method (Nettleton, 1940). The results of this interpretation are presented in Figure 4.6 with the permission from the author (M.H.P.Bott). Figure 4.6 gives the results of the interpretation of the profile AA' of Figure 4.5, in terms of a basic body of rectangular plan perpendicular to the profile. This body which outcrops at the surface extends to a depth of 14km. The width (dimension of the body along the plane of Figure 4.6) of the body at the top surface is 16km and at the bottom it is 24km. The effect due to the granitic rocks was also incorporated in this interpretation and the estimated depth to which these subordinate granitic rocks extend is between 1.5-2.2km. Bott also interpreted another profile which passes through the centre of the complex and Ross of Mull. This profile has been interpreted in terms of a body which extends to 5.2 km using a somewhat higher density contrast. Using the results of these two interpretations, Bott came to the conclusion that

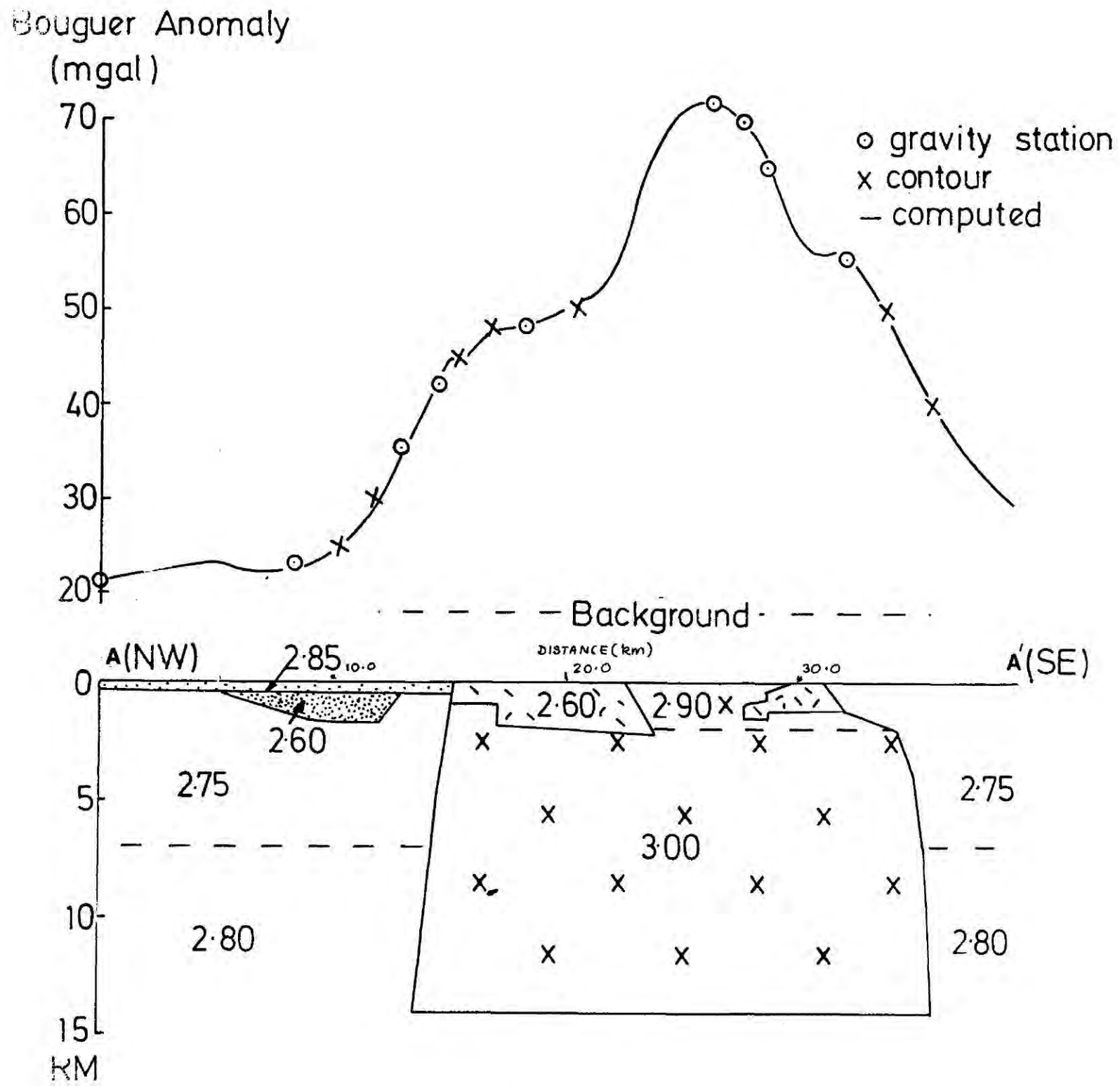

Figure 4.6 Interpretation of the sub-surface structure of the Mull igneous complex along AA'(Figure 4.5). from Bott(private communications) Density contrast in g/cm^3.

X , Gabbro; ⊠ , granite.

the central basic body in the Mull complex extends to a depth between 5 and 14km depending on the actual density contrast; i.e. depending on the relative proportions of basic and ultrabasic rocks in the body.

4.3.2. Magnetic Studies

Aeromagnetic anomaly maps over the Mull igneous complex (Figure 4.1) have been prepared by the Institute of Geological Sciences of Great Britain and they are available in one inch to one mile and quarter inch to one mile scales. Bennett (1968) reported a ground magnetic survey carried out by the same Institute. He also presented a qualitative interpretation of both aeromagnetic anomaly map and ground magnetic profiles. In this interpretation he supported the idea of having a condensed magma chamber in central Mull as proposed by Bailey et al.(1924) and by various authors who have performed gravity interpretations. Bennett tentatively estimated the depth to the top surface of this body as 3.0 km below sea level. There are several short wavelength magnetic anomalies outside the central complex that can be seen on the aeromagnetic anomaly map. Bennett explained these anomalies as being caused by a series of vertical or near vertical bodies outside the complex.

4.4 Interpretation of the Magnetic Anomalies Over the Central Complex

The magnetic anomaly map shown in Figure 4.1 was digitized at 1 km intervals and was transformed into pseudogravimetric anomalies using the method of chapter 2. The application of this pseudogravimetric transformation requires knowledge of the direction of magnetization of rocks in the region concerned. Bruckshaw and Vincenz (1954) studied the magnetic properties of lavas in the Isle of Mull and came to the conclusion that the direction of magnetization is on average opposite

to the present day earth's magnetic field. Vincenz (1954) showed that the rocks in the Mull central complex have two main directions of magnetization, one in the direction of the present day earth's field and the other in the opposite direction. Mussett et al. (1980) presented a summary of palaeomagnetic results of Mull lavas and intrusive rocks published by previous workers. The direction of the central axial dipole field, calculated from these results, is fairly close to the present direction of the earth's field in Mull (declination = 0^{o}, inclination = 71.8^{o}). From these results it can be concluded that most of the intrusive rocks and lavas in the Mull complex are magnetized aporoximately along the present direction of earth's field or along the opposite direction. Therefore the present direction of the earth's magnetic field was used in the pseudogravimetric conversion of magnetic anomalies over the Mull complex. In the resulting pseudogravimetric anomaly map, magnetic anomalies due to normally magnetized rocks appear as highs and those due to reversely magnetized rocks appear as lows.

The pseudogravimetric anomaly map obtained by transforming the magnetic anomaly map of Figure 4.1 is given in Figure 4.7. This pseudogravimetric anomaly is superimposed on a geological sketch of this region in order to illustrate the correlation between the geology and the anomaly(Figure 4.8). This anomaly map shows a positive anomaly over the central intrusive complex and negative anomalies over the basaltic lavas. The positive anomaly is intense over the Glen More and Beinn Chaisgidle centre and it is very weak over the Loch Ba centre which consists mainly of granitic rocks. The intense positive anomaly over the Glen More and Beinn Chaisgidle centres has very steep gradients indicating the shallow nature of the causative body. It is also useful

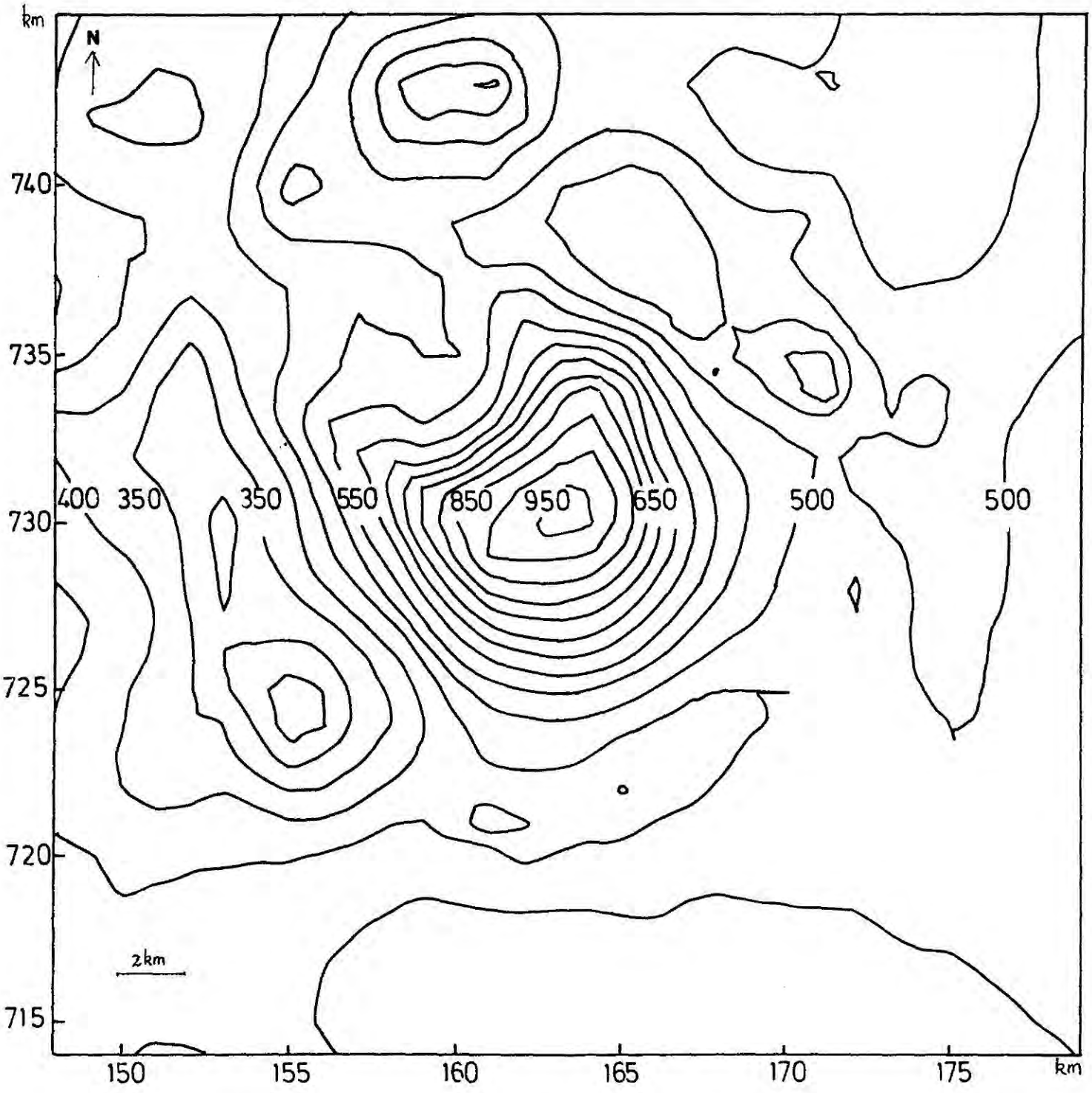

Figure 4.7 Pseudogravimetric anomaly map of the Mull central intrusive complex, showing contours at 50 mgal intervals. On this and subsequent related figures national grid is shown.

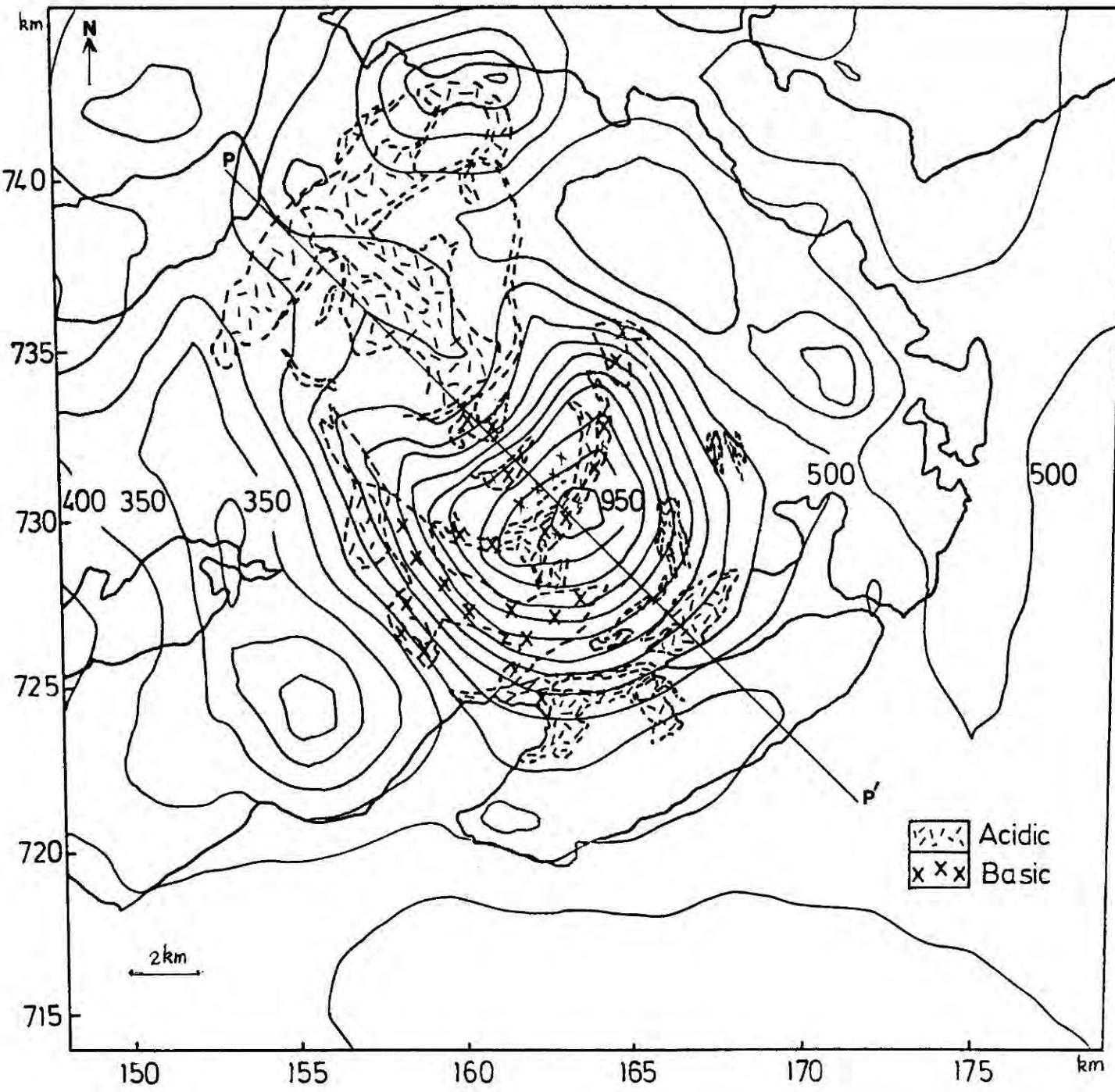

Figure 4.8 Correlation between the pseudogravimetric anomaly and the broad geology of Mull central intrusive complex.

to compare the pseudogravimetric anomaly with the real gravity anomaly map given in Figure 4.4. The maximum of the pseudogravimetric anomaly is situated over Glen More in the Mull complex and that of the gravity anomaly is situated about 3 km westward of this. Both the gravity and pseudogravimetric anomalies have fairly similar shapes. However, the extent of the gravity anomaly is much larger than the extent of the pseudogravimetric anomaly. To illustrate this more clearly the gravity and pseudogravimetric anomaly profiles taken along parallel lines are shown in Figure 4.9. The difference in extent of gravity and pseudogravimetric anomalies indicates that the body producing the gravity anomaly is much larger than the body producing the magnetic anomaly. More details about this can be found by comparing the results of interpretations of these two profiles.

It is clear from the central part of the pseudogravimetric anomaly that it must have been produced by a body having a shape close to a vertical cylinder. Normal two-dimensional interpretations may be insufficient to obtain the nature of the subsurface structure causing this anomaly. Therefore the interpretation was performed in terms of a three-dimensional body using the end correction method (chapter 3). The pseudogravimetric profile given in Figure 4.9 was used for this interpretation. First it was interpreted in terms of a 3-D body using end corrections using the Fortran routine GREND (chapter 3) which uses the trial and error method. The end correction method requires the trial model to be divided into a number of polygonal prisms (see 3.2) and Figure 4.10 shows the way in which division was performed. Results of this interpretation are given in Figure 4.11. This body has an approximate shape of a truncated cone and extends to a depth of 2.6 km and its magnetization is 6.0 A/m. The results of this interpretation were improved further by using the Fortran

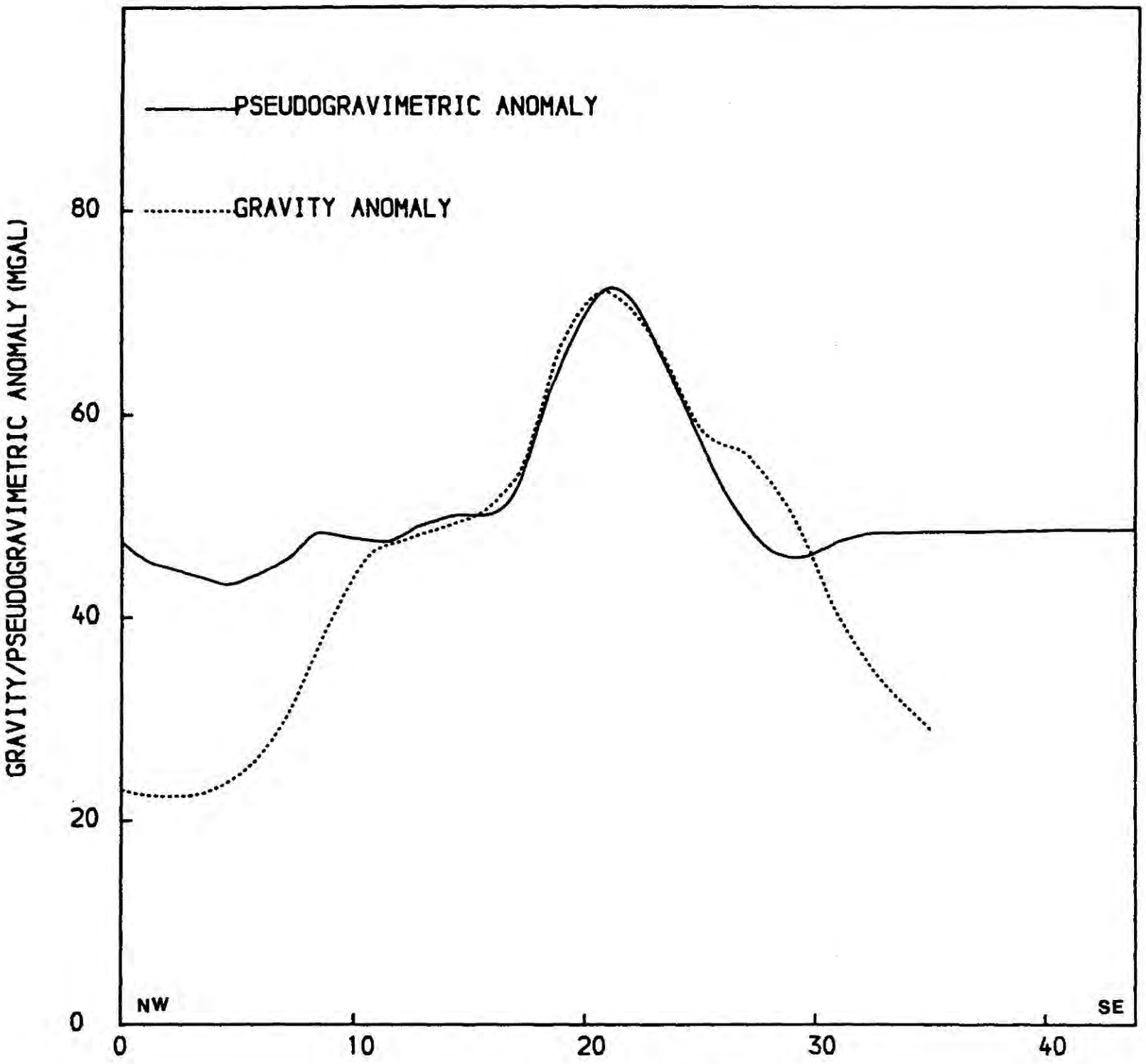

Rescaled

Figure 4.9 Pseudogravimetric and gravity anomaly profiles along PP'(Figure 4.8) and AA'(Figure 4.5) over Mull igneous complex. Lines PP' and AA' are parallel and close to each other.

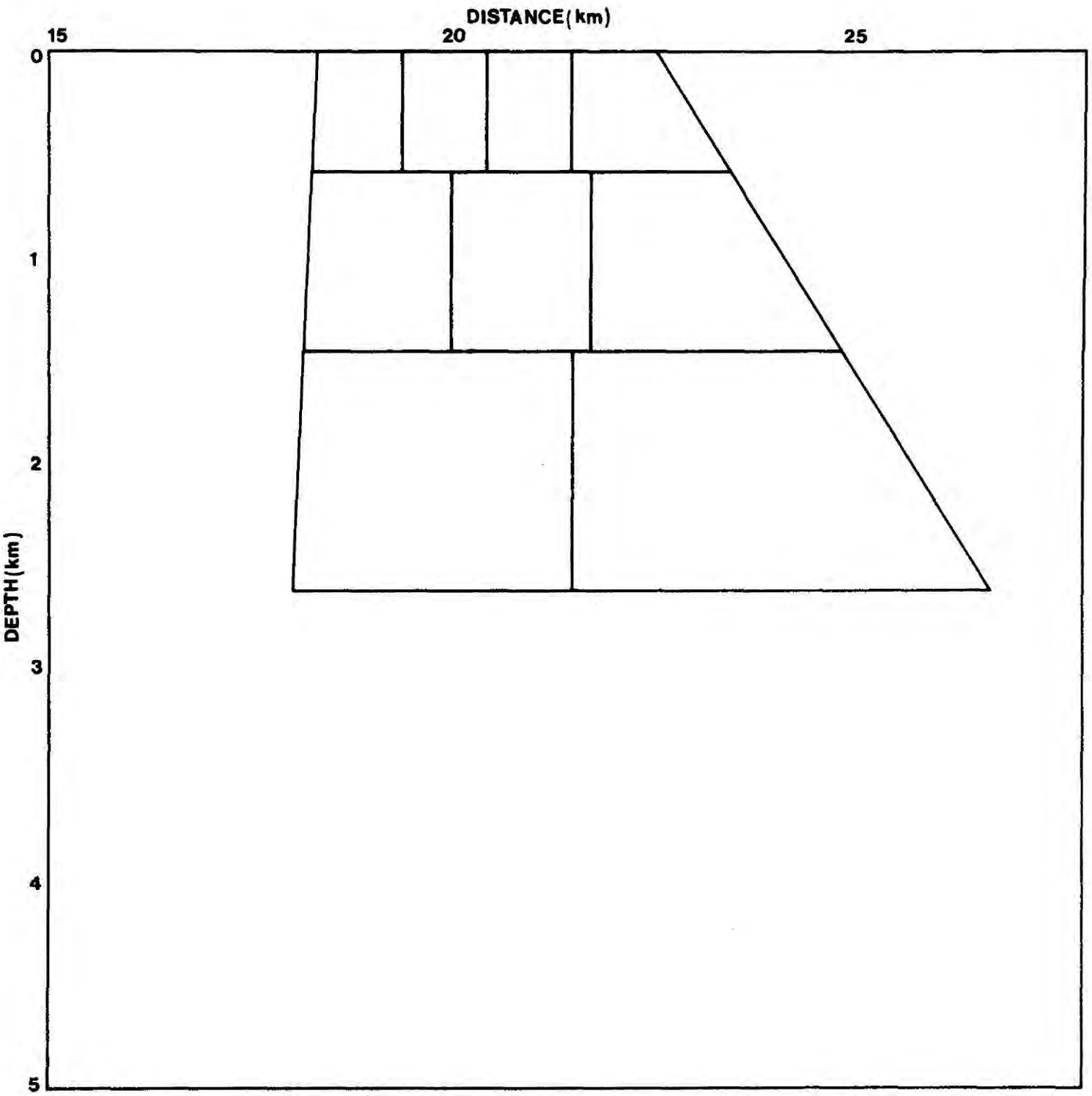

Figure 4.1o Subdivision of the model of Figure 4.11 for application of end corrections.

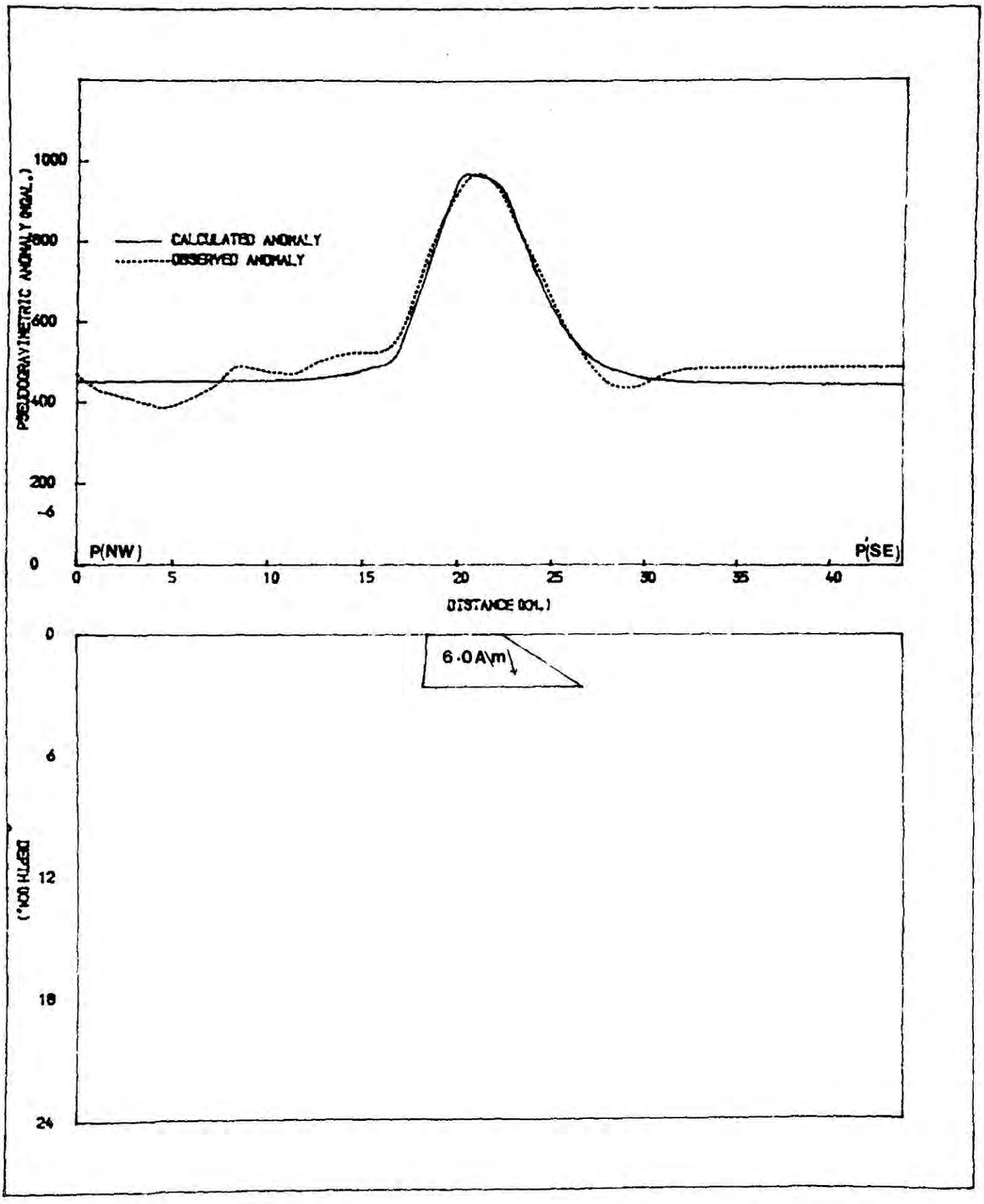

Figure 4.11 Interpretation of the pseudogravimetric profile PP' of Figure 4.8 using the program GREND.

routine OPGREND (chapter 3) which uses a non-linear optimization technique in interpreting gravity anomalies with end corrections. A cross-section of the optimal body obtained is shown in Figure 4.12 together with observed and calculated anomalies. The shape of the body approximates to a truncated cone as was suggested by the interpretation using GREND. The top surface of the body has a diameter of 3.7 km and the bottom surface of it has a diameter 10.7 km along the direction of the profile. The diameter of the top surface perpendicular to the profile is 5.0 km and that of the bottom surface is 6.0 km. The magnetization of the body is 6.7A/m and it extends to a depth of 2.1km. Owing to the ambiguity in gravity and magnetic interpretation (see 3.4) the model produced here is not unique and there can be several other models which equally satisfy observations. However, the main features of this model must be common to all possible models.

The most recent and complete gravity interpretation of the Mull complex has been performed by Bott (Figure 4.6). The profiles used for this interpretation and for the pseudogravimetric interpretation previously discussed are parallel and close to each other. It is therefore possible to compare the results of the two interpretations directly. The results of the two interpretations are given in Figure 4.13 at the same scale. From this diagram it is clear that the body which produces the gravity anomaly is much larger than the body which produces the magnetic anomaly.

4.5 Interpretation of Magnetic Anomalies Around the Central Anomaly

As indicated in the introduction there are some local negative magnetic anomalies over the regions covered with basaltic lavas which surround the central complex. Therefore it is possible that these anomalies may have been caused by the basaltic lavas.

The third type of magnetic anomalies in Mull is a ring of relatively

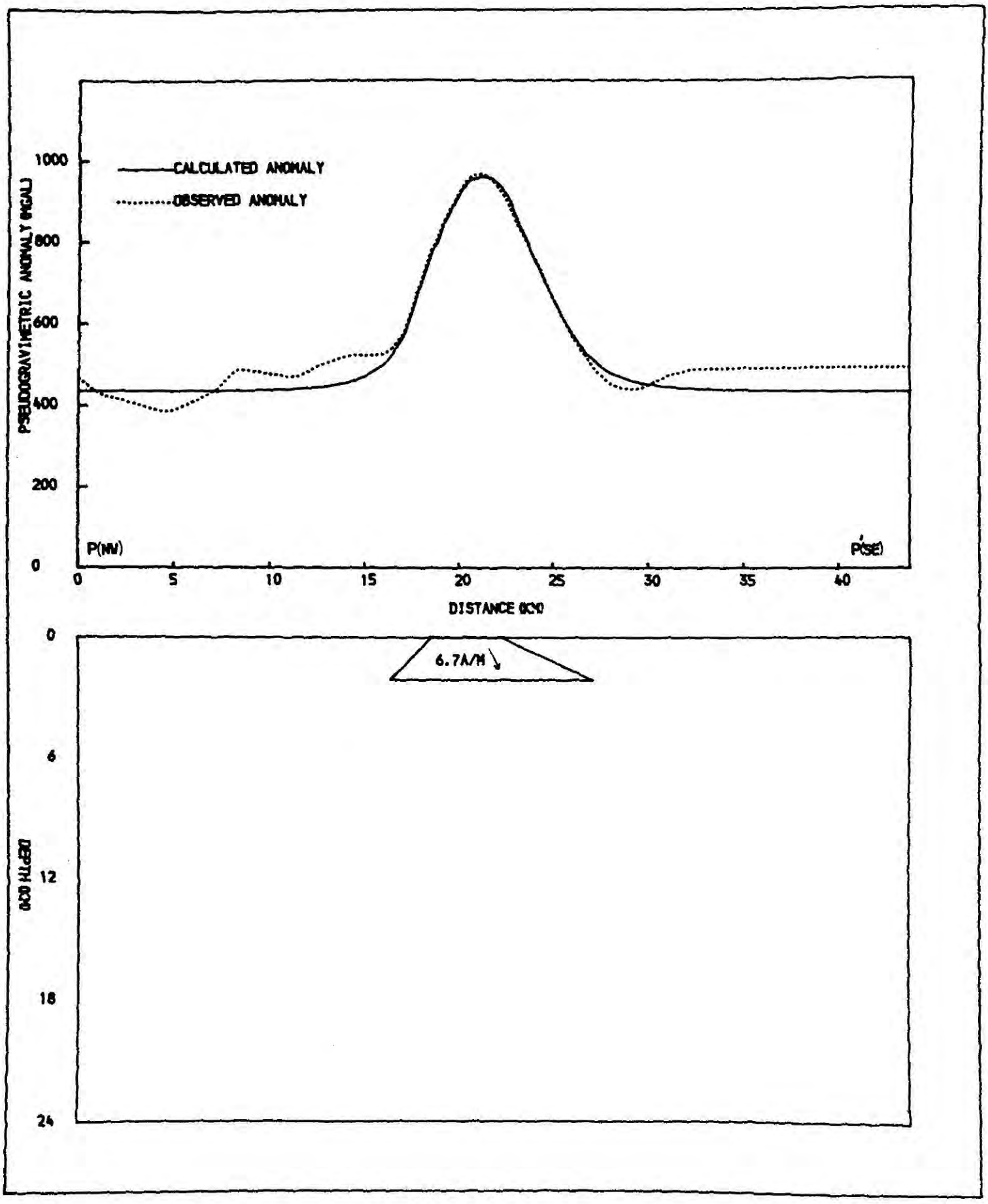

Figure 4.12 Interpretation of the pseudogravimetric profile PP'of Figure 4.8 using the program OPGREND.

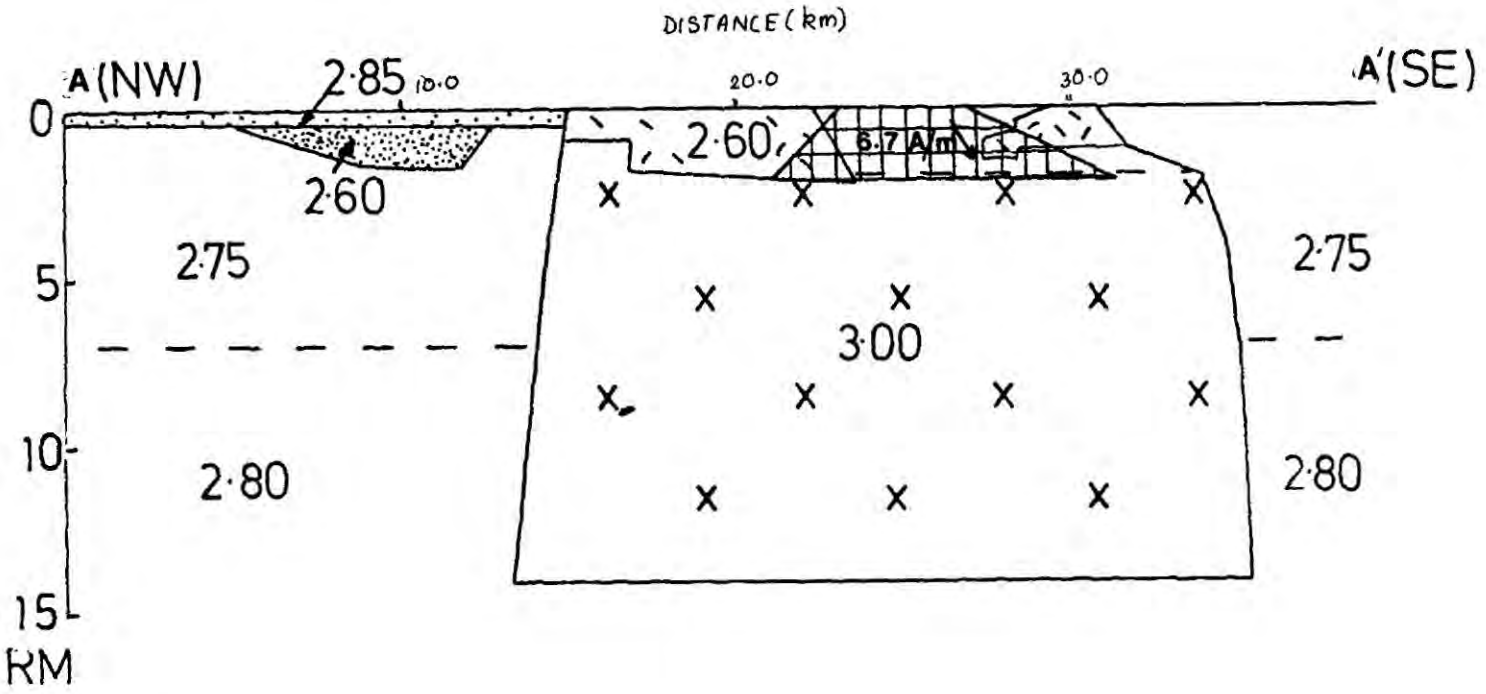

Figure 4.13 Results of the gravity(after Bott, private communications) and pseudogravimetric interpretations of the Mull complex. Density contrast in g/cm^3.

X , Gabbro; ⊠ , granite; ### , body obtained from the interpretation of the pseudogravimetric anomaly.

short wavelength positive and negative anomalies outside the central complex. In order to illustrate the correlation between these anomalies and the geology of the area, positions of these anomalies are marked with circles on the geological map in Figure 4.14. Most of these anomalies occur over the basaltic lavas. However, the extent of basaltic lavas is much larger than the wavelength of these anomalies. Nevertheless, there are certain areas where the lavas have been folded and the anomalies in such areas might be due to the folded lava structure. This idea was tested by calculating the anomaly due to the folded lava structure below the anomaly east of Loch Buie (Anomaly No.1, Figure 4.14), and comparing observed and calculated anomalies. A geological cross-section of this lava structure is given in Figure 4.15. The anomaly due to the lava structure was calculated assuming that it is a two-dimensional body and the observed and calculated anomalies are shown in Figure 4.16. It is clear from Figure 4.16 that there is no agreement between observed and calculated anomalies. Therefore these anomalies cannot be due to the folded lava structure and they may be due to a set of separate intrusions outside the complex.

Seven different anomalies were selected from the ring of short wavelength anomalies and they were interpreted in terms of 2D bodies having rectangular cross-sections. This interpretation was first performed using the PL1 routine MAGN (Bott,1975) and later on the results were improved further using the Fortran routines MAG1 and MAG2 (Chapter 3) which use non-linear optimization techniques. Results of these interpretations are depicted in Figure 4.17 to Figure 4.23. The main features of the bodies obtained by these interpretations are given in table 4.1. As can be seen in Figure 4.14, there are some intrusive bodies which outcrop below some of these anomalies. However, they are too small to account for these anomalies. Therefore

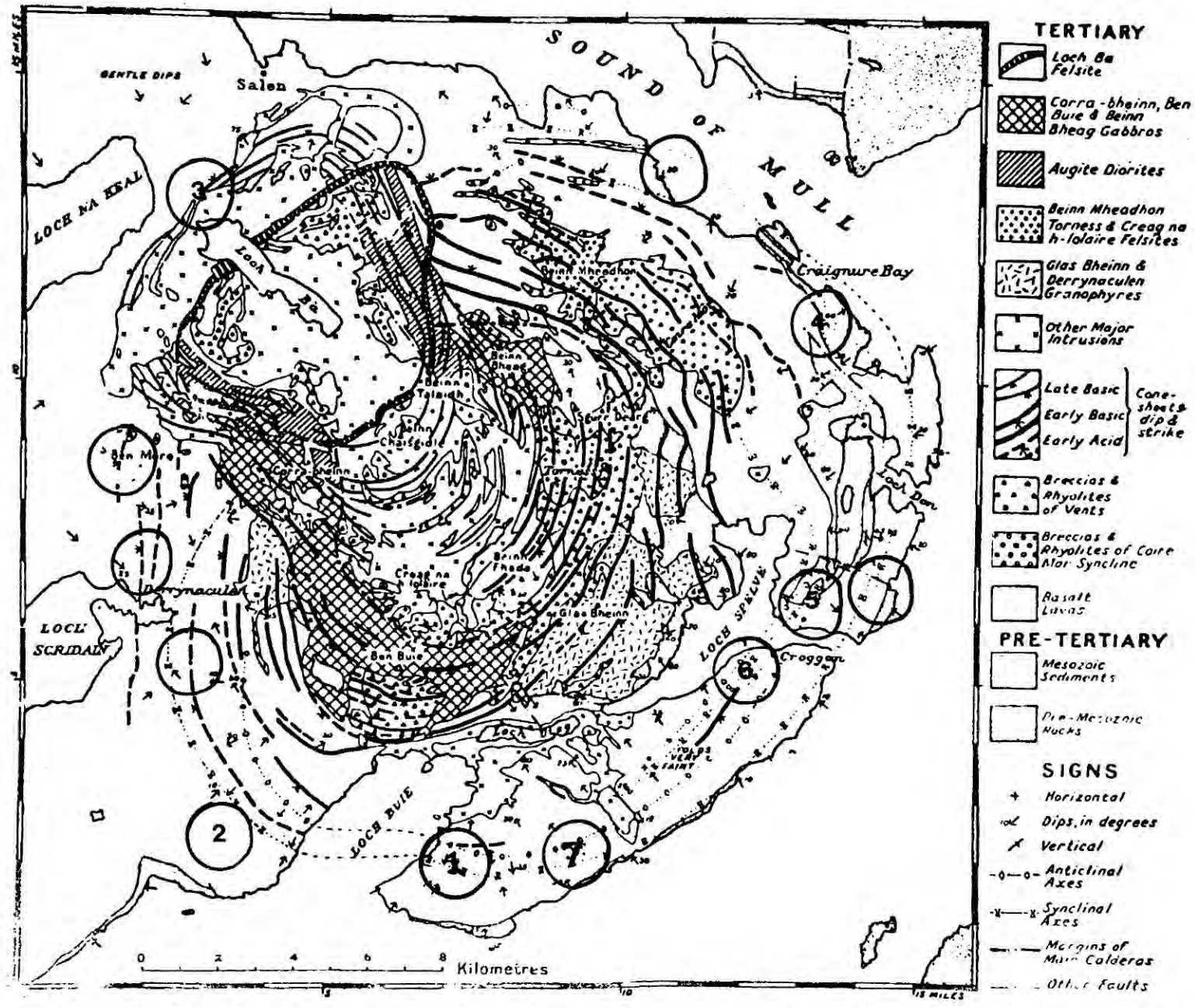

Figure 4.14 Locations of the ring of narrow magnetic anomalies outside the Mull central intrusive complex. Geological map is taken from Bailey et al.(1924).

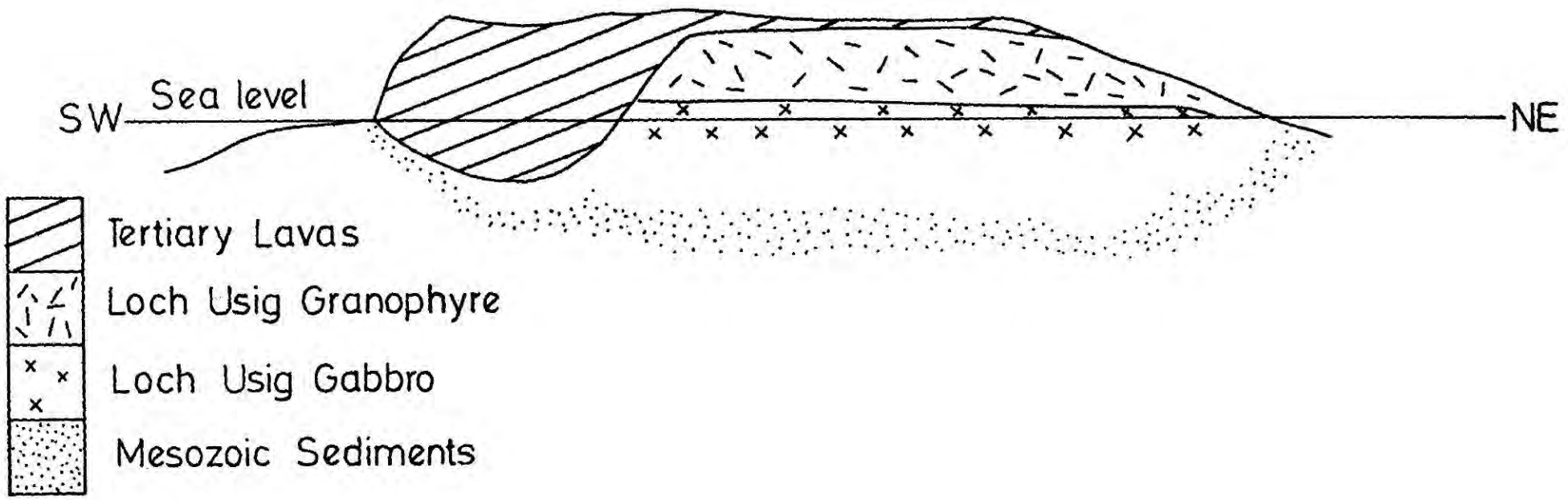

Figure 4.15 A geological cross-section of the folded lava structure situated east of Loch Buie.

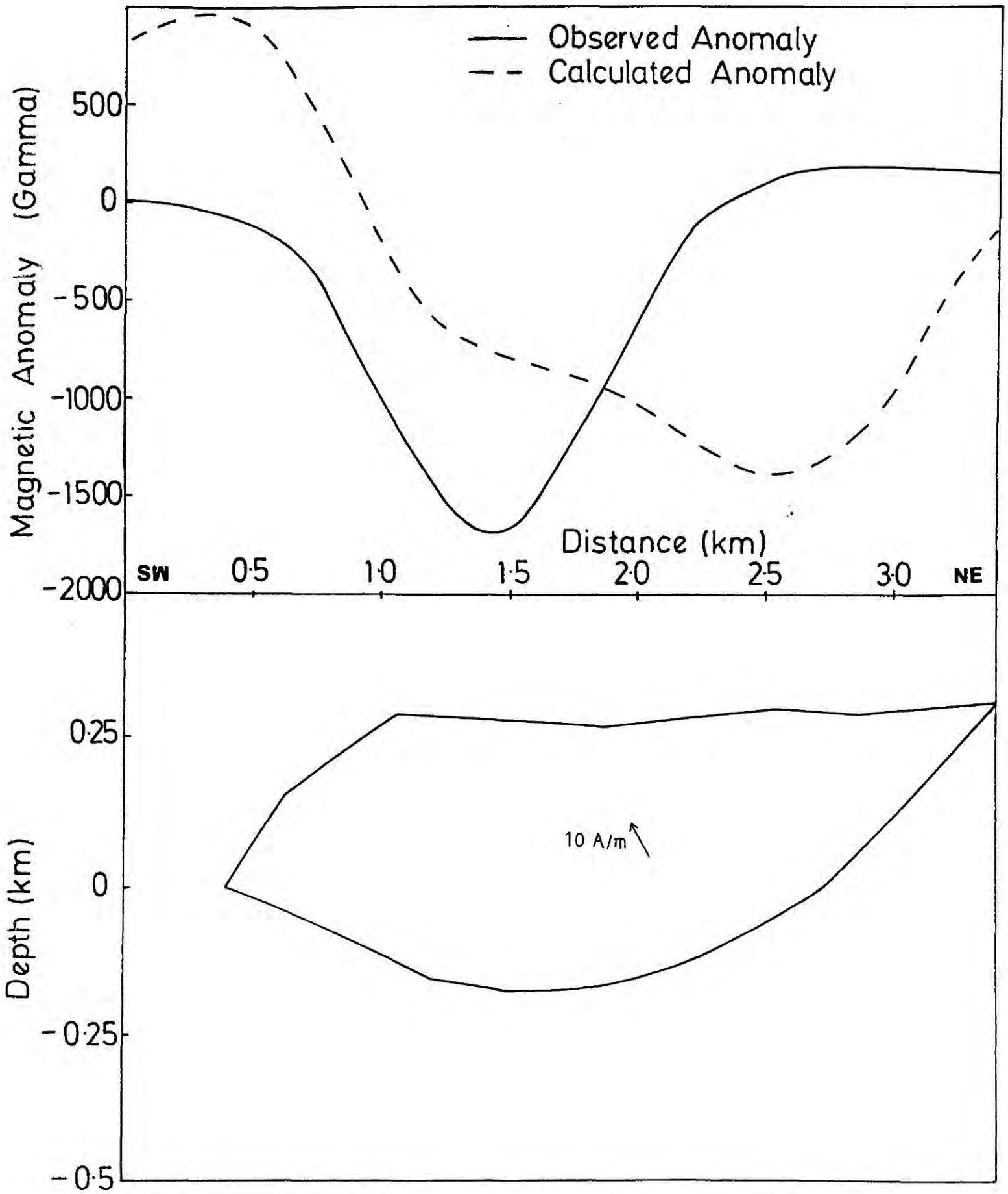

Figure 4.16 A profile of the magnetic anomaly No.1 of Figure 4.14 along the **SW-NE** direction and calculated magnetic anomaly due to the folded lava structure situated below the anomaly No.1.

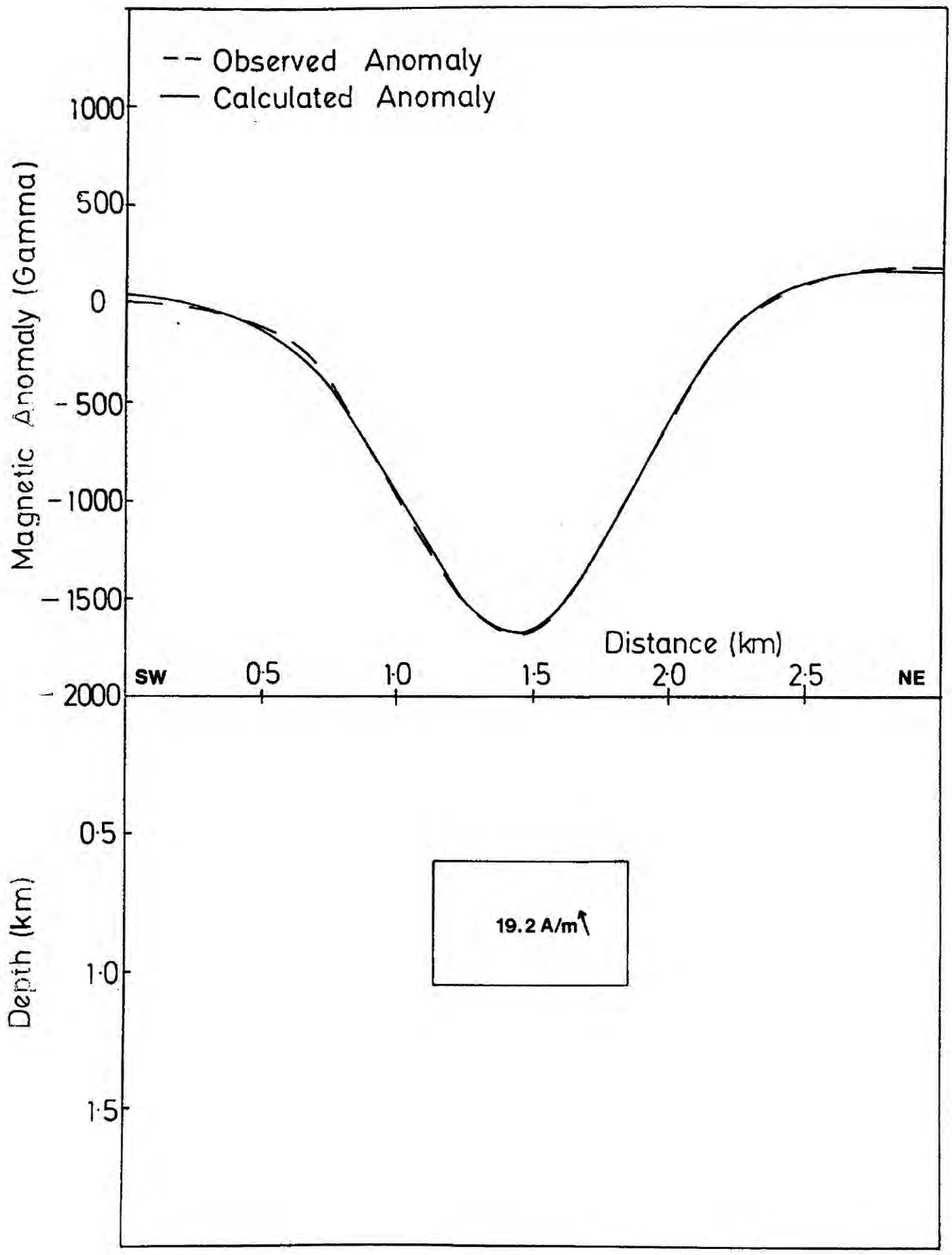

Figure 4.17 Interpretation of magnetic anomaly No.1 of Figure 4.14. Magnetization of the body = 19.2 A/m. Inclination of the magnetization vector = -88.6°.

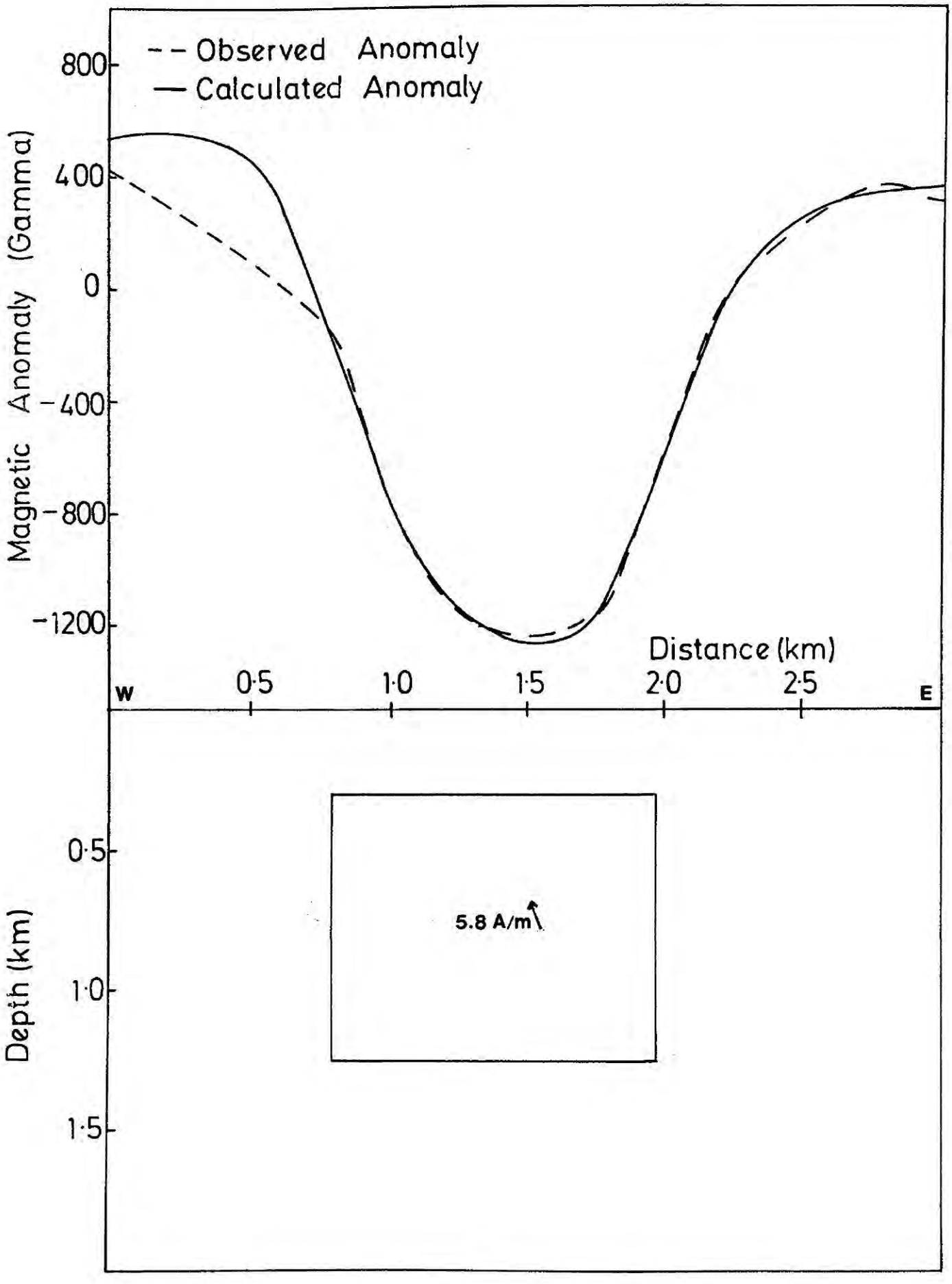

Figure 4.18 Interpretation of magnetic anomaly No.2 of Figure 4.14. Magnetization of the body = 5.8 A/m. Inclination of the magnetization vector = -81.5°.

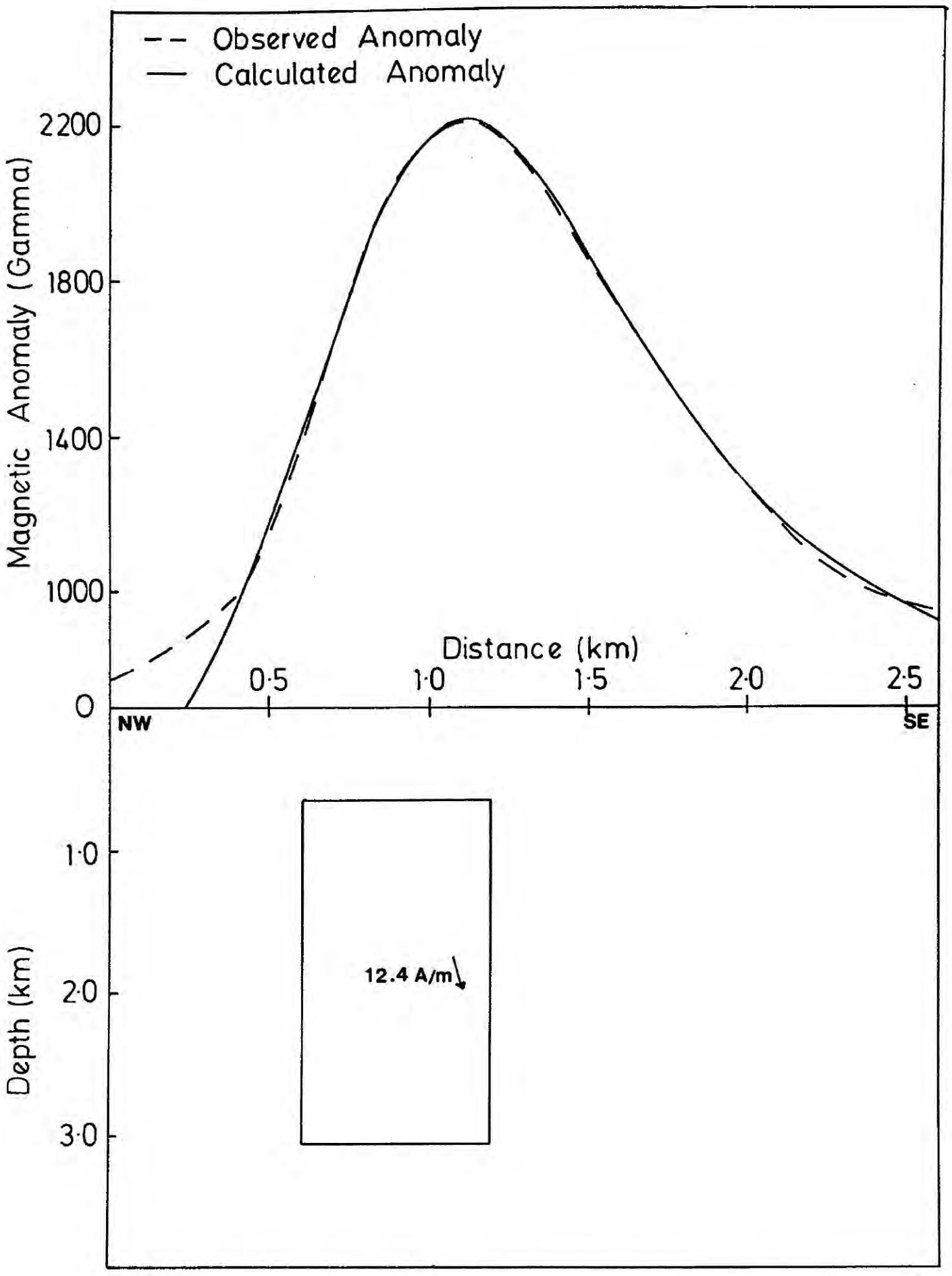

Figure 4.19 Interpretation of magnetic anomaly No.3 of Figure 4.14. Magnetization of the body = 12.4 A/m. Inclination of the magnetization vector = 70.6°.

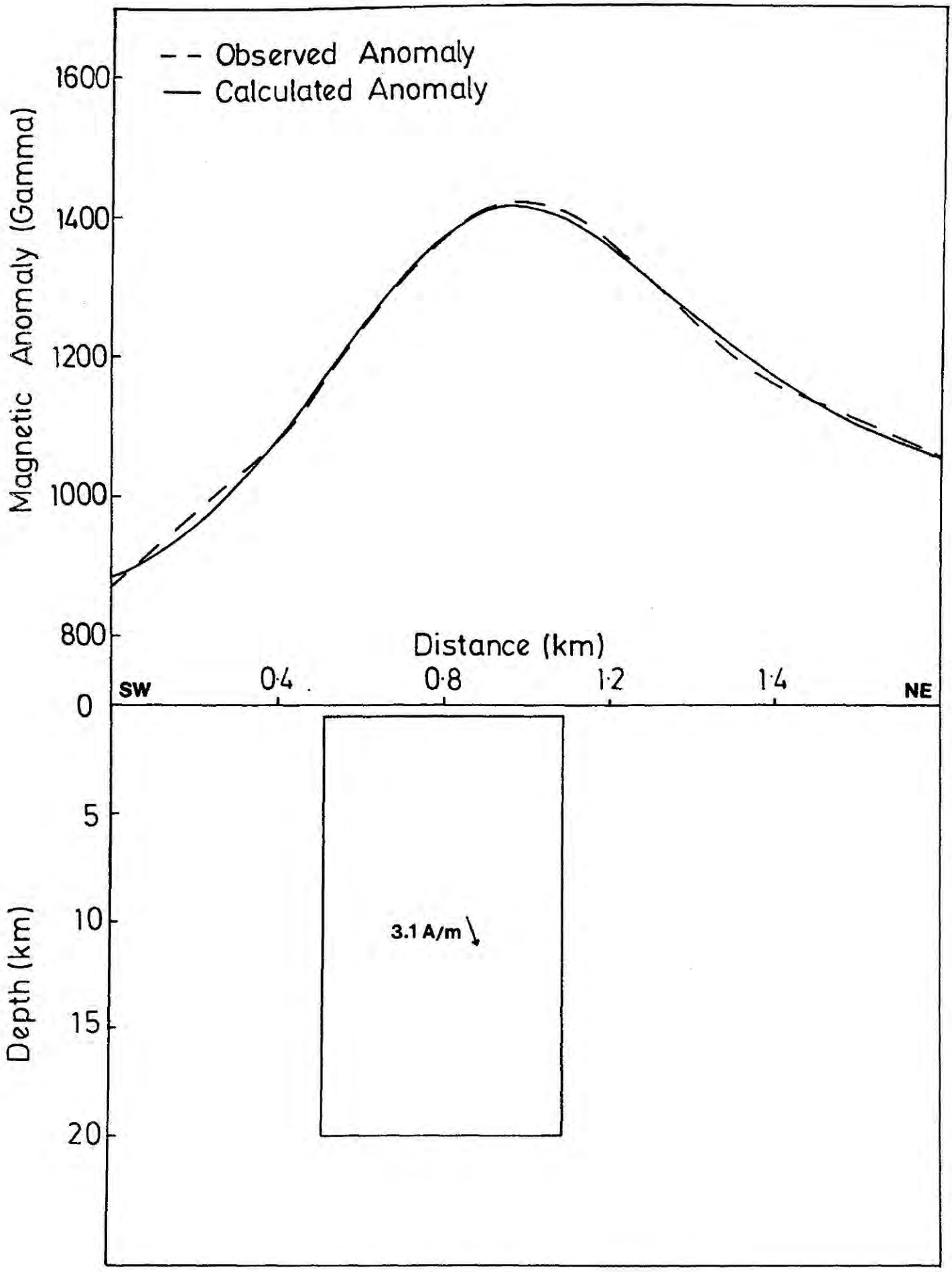

Figure 4.2o Interpretation of magnetic anomaly No.4 of Figure 4.14. Magnetization of the body = 3.1 A/m. Inclination of the magnetization vector = 48.8°.

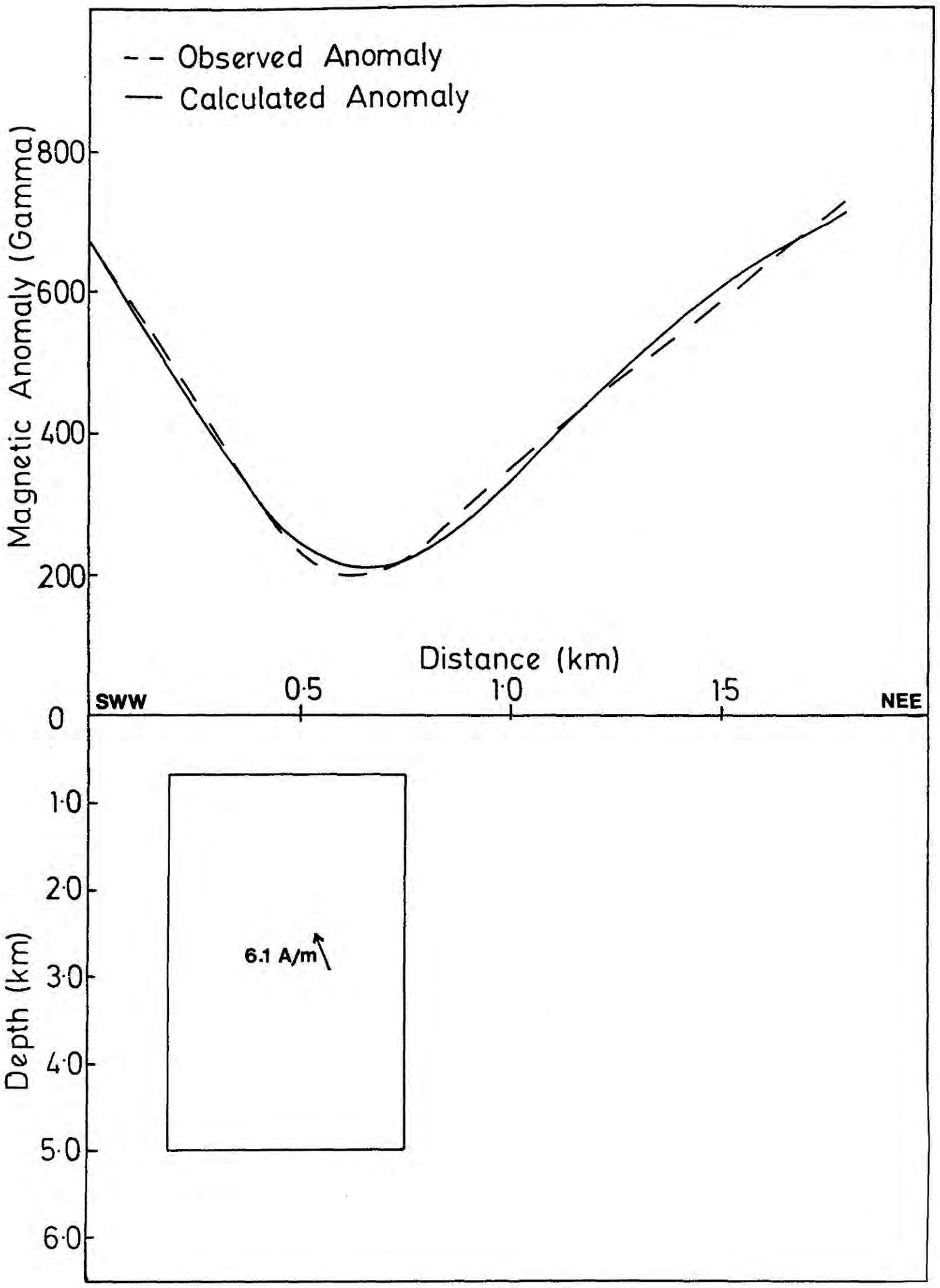

Figure 4.21 Interpretation of magnetic anomaly No.5 of Figu
Magnetization of the body = 6.1 A/m. Inclination of the magn
vector = -62.7°.

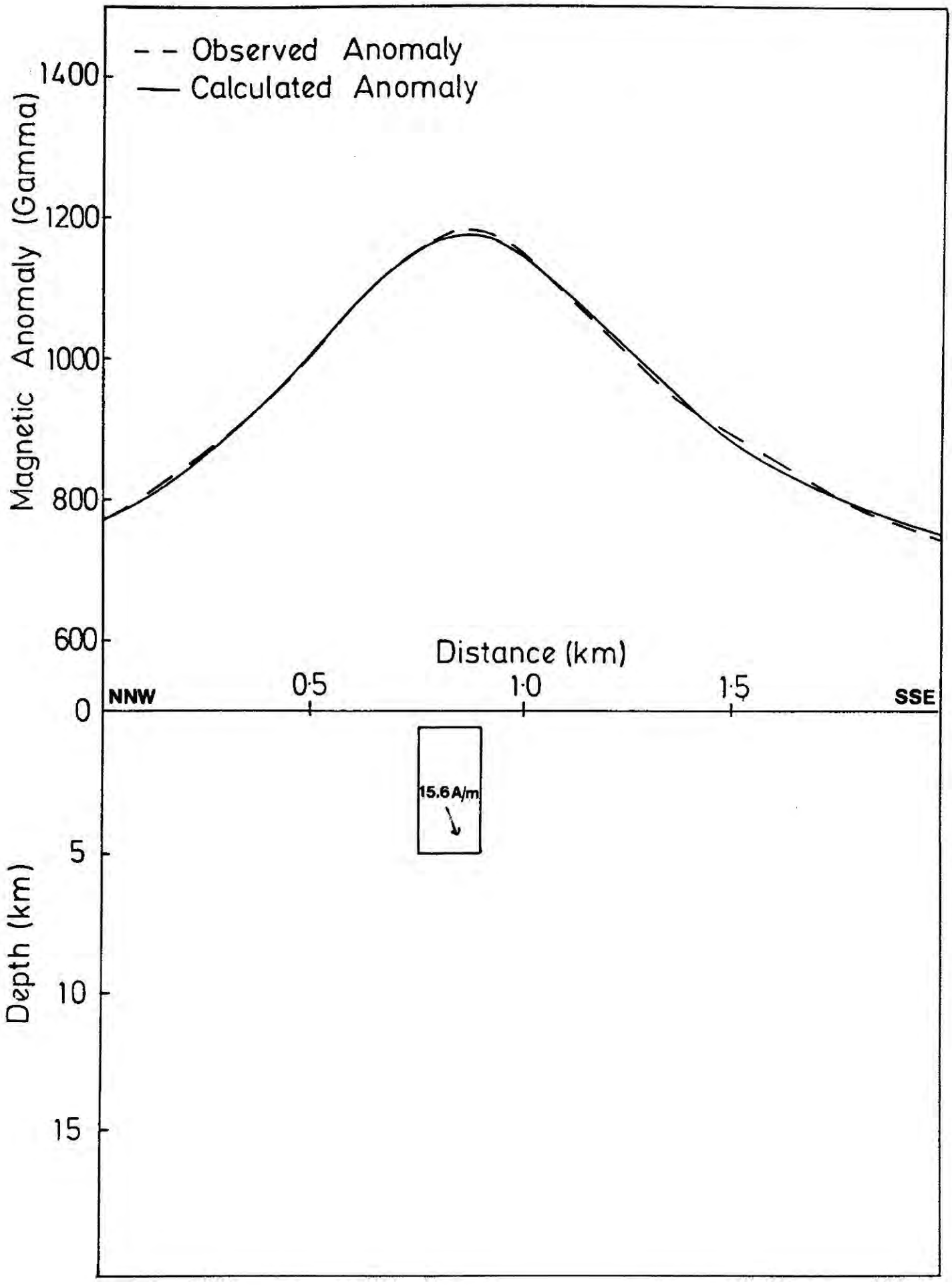

Figure 4.22 Interpretation of magnetic anomaly No.6 of Figure 4.14. Magnetization of the body = 15.6 A/m. Inclination of the magnetization vector = 64.4°.

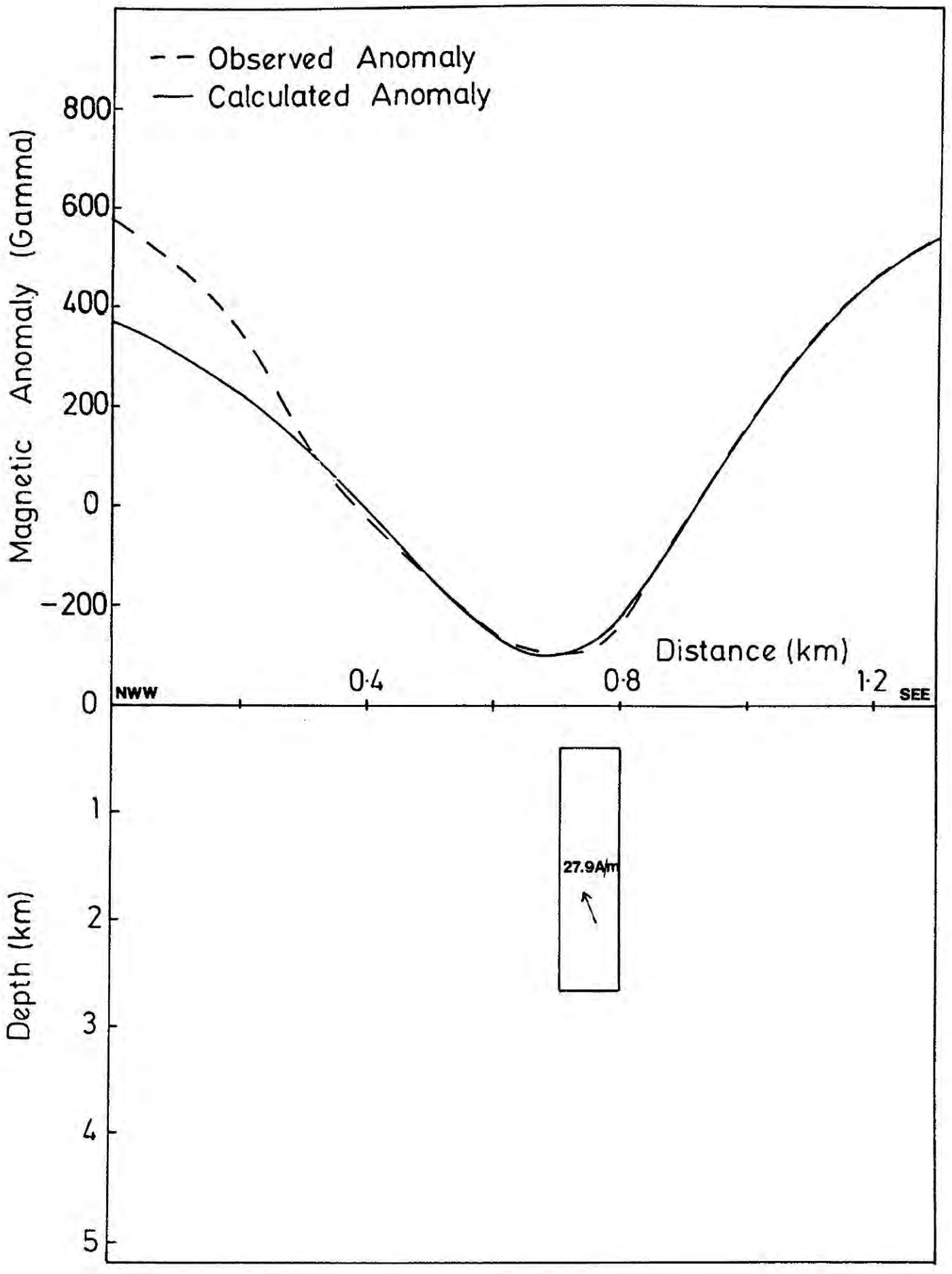

Figure 4.23 Interpretation of magnetic anomaly No.7 of Figure 4.14. Magnetization of the body = 27.9 A/m. Inclination of the magnetization vector = -77,9°.

TABLE 4.1

Anom. no.	Dirn. of the profile	Magnetization Mag.(A/m)	Inclination	Dimensions of the body (km) Width	Thickness	Depth to the top
1	SW-NE	19.2	-88.6^{o}	0.72	0.45	0.6
2	W-E	5.8	-81.5^{o}	1.17	0.95	0.3
3	NW-SE	12.4	70.6^{o}	0.59	2.4	0.64
4	SW-NE	3.1	48.8^{o}	0.58	19.5	0.52
5	SWW-NEE	6.1	-62.7^{o}	0.56	4.32	0.68
6	NNW-SSE	15.6	64.4^{o}	0.15	4.42	0.58
7	NWW-SEE	27.9	-77.9^{o}	0.10	2.26	0.4

this ring of relatively short wavelength anomalies may be produced by a set of intrusions which do not outcrop.

4.6 Results of a Ground Magnetic Survey

A ground magnetic survey was carried out using a proton magnetometer over the basaltic lavas situated between Loch Na Keal and Loch Bà and over the Loch Assapol fault (Figure 4.24) where basaltic lavas are faulted against older Moine rocks. It was found that there is a large scatter in the measurements taken over the basaltic lavas situated between Loch Na Keal and Loch Bà and therefore measurements are not suitable for the interpretation. The measurements taken over the Loch Assapol fault are shown in Figure 4.25 and Figure 4.26. It is clear from these two profiles that the lavas are reversely magnetized.

4.7 Discussion

It became evident from the interpretation of magnetic anomalies over the central intrusive complex of Mull that only the middle part of the complex around Glen More consists of highly magnetized rocks. These rocks are normally magnetized with an interpreted magnetization of 6.7 A/m and extend to a depth of 2.1 km. The highly magnetized central part and the surrounding weakly magnetized rocks both should have a high density as they produce an intense positive gravity anomaly. Since high density is a property of basic rocks, the central part of the complex should consist of basic rocks having a high content of magnetic minerals such as magnetite. The outer part of the complex should consist of basic rocks with a low content of magnetic minerals. There are three large basic bodies, which outcrop, in the outer part of the central complex of Mull. They are the Beinn Bheag layered gabbro, the Corra-bheinn layered gabbro and the Ben Buie layered gabbro. In the discussion of geology of Mull given in 4.2, it was shown that these three rock masses do not contain a high amount of magnetic

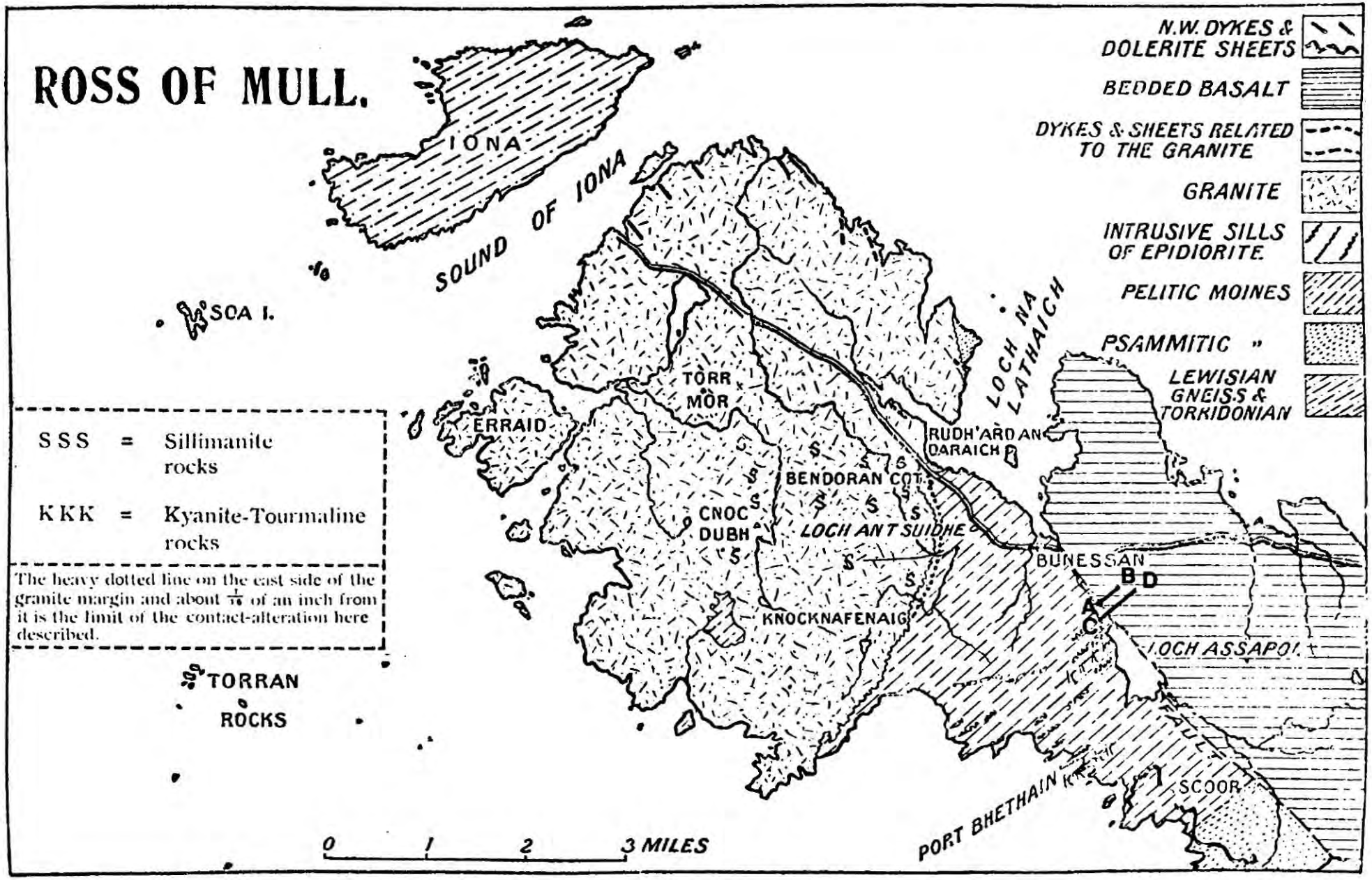

Figure 4.24 Locations of the magnetic survey lines (AB,CD).

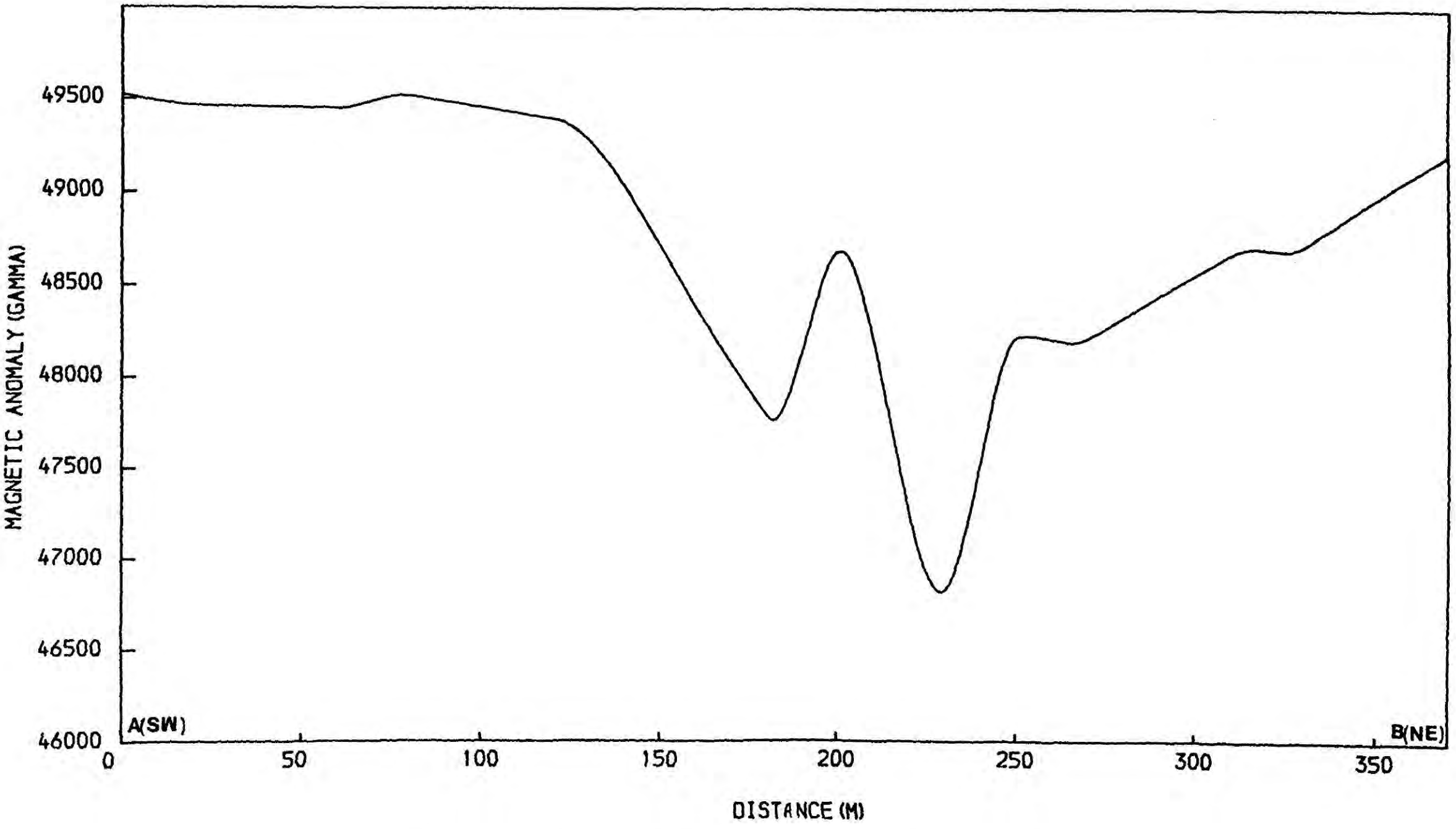

Figure 4.25 Magnetic anomaly profile AB over the Loch Assapol fault.

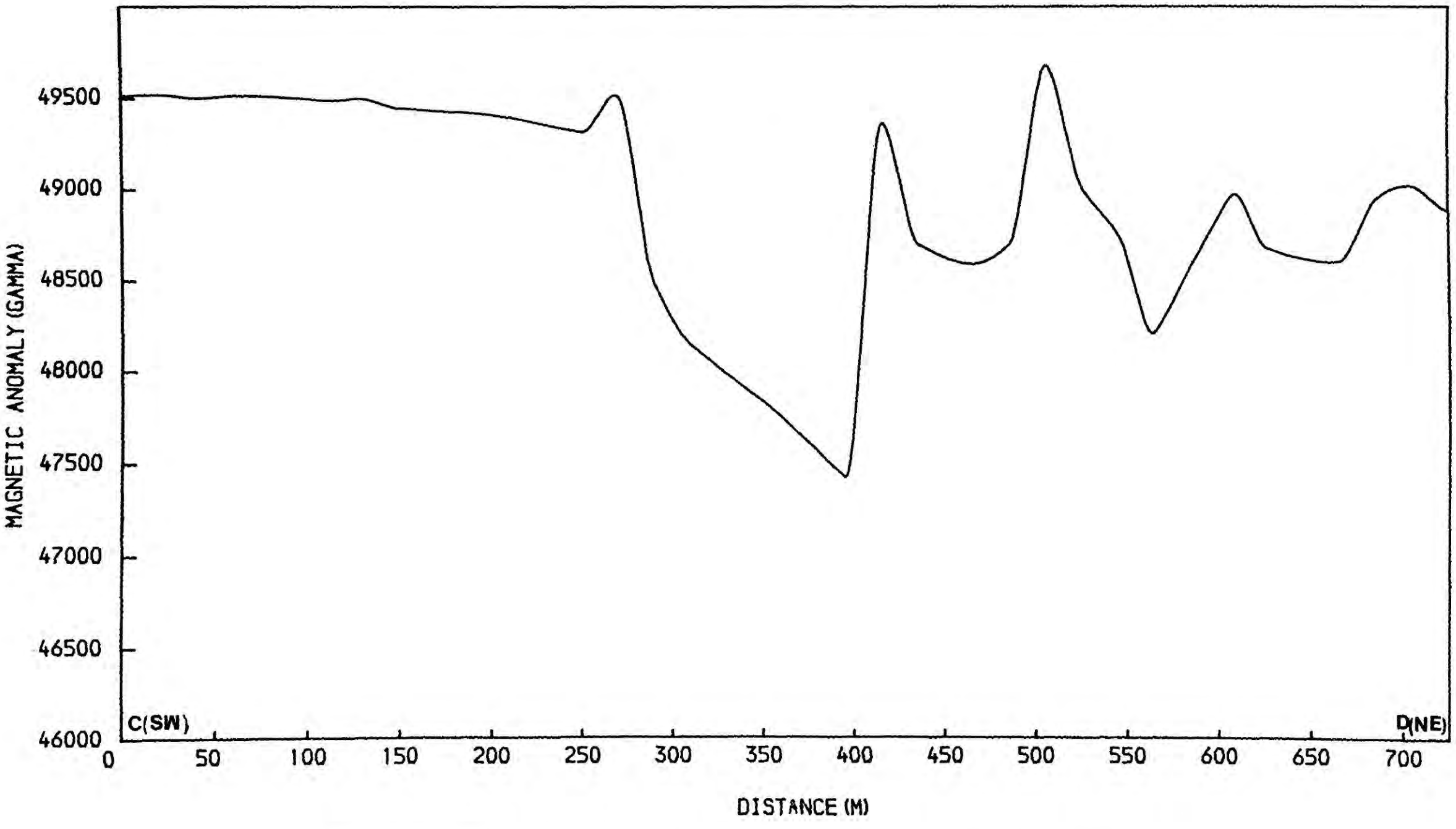

Figure 4.26 Magnetic anomaly profile CD over the Loch Assapol fault.

minerals. Nevertheless, they are fairly rich in olivine. These rocks could therefore be of high density particularly if their olivine content is high and at the same time do not show any strong magnetic properties. If olivine occurs in any quantity at depth, these rocks will produce a strong positive gravity anomaly, but little in the way of a magnetic anomaly. By contrast, in the middle part of the central complex there are numerous quartz dolerite and quartz gabbros which, while being composed of fairly dense minerals, also contain magnetic minerals such as magnetite and titaniferous magnetite (Bailey, et al., 1924). Polished rock specimens from the central part of the complex in the Durham University Geology Department rock collection showed the presence of a high amount of magnetite together with ilmenite lamellae when viewed with reflected light (R.Phillips, private communications). In addition, magnetic measurements performed by Vincenz (1954) and Mussett and Dagley (private communications) reveal that some of the rocks in the central part of the complex are highly magnetized. Therefore the middle part of the complex may be underlain by basic rocks having a high proportion of magnetic minerals. According to these facts, the model obtained for the central complex of Mull from the magnetic interpretation is consistent with the surface geology of the area.

It is revealed from the interpretation of the ring of relatively short wavelength anomalies that they are not due to lavas, but due to some shallow intrusive bodies outside the complex. Bennett (1968) who has presented a qualitative interpretation of ground and aeromagnetic anomaly maps of the Mull complex has also suggested the existence of such a series of vertical or near vertical bodies outside the complex.

Table 4.1 shows that these bodies have different directions of magnetization. This fact might suggest that these bodies were intruded at different times when there were different polarities in the earth's magnetic field. However, it is possible to change the original direction of magnetization of a body due to deuteric oxidation and hydrothermal activities (Ade-Hall et al.,1972). Therefore it is not possible to conclude that these bodies were intruded at different times when the earth's magnetic field had different polarities. As can be seen from Figure 4.13 these anomalies situated fairly close to the outer part of central intrusive complex. Therefore one might conclude that these bodies may have been intruded from the outer part of the central complex. However, this is unlikely since the outer part of the complex is weakly magnetized and these bodies are strongly magnetized. There is a large number of magnetized dykes inside and outside the central complex and some of them could have been feeders for these bodies.

The nature of the subsurface structure of the Mull complex revealed from this magnetic interpretation can be summarized as follows.

The subsurface structure of the Mull complex consists of a strongly and normally magnetized core surrounded by some weakly magnetized rocks. This strongly magnetized core is shallower than the surrounding weakly magnetized rocks. The centre of this magnetized core is situated close to the Glen More intrusive centre. The weakly magnetized part is surrounded by a ring of normally and reversely magnetized bodies. Basaltic lavas situated outside the central complex are reversely magnetized. The granitic rocks of the complex, which are situated outside the magnetized core, must be weakly magnetized.

INTERPRETATION OF MAGNETIC ANOMALIES OVER THE SKYE IGNEOUS COMPLEX

5.1 Introduction

An interpretation of magnetic anomalies over the Skye igneous complex is presented in this chapter. Figure 5.1 shows the aeromagnetic anomaly map over this complex. On this map there is a region of intense negative anomalies over the Cuillin centre and a region of extensive positive anomalies over the Western and Eastern Red Hills centres of the Skye igneous complex (see Figures 5.2 and 5.4). There are several negative anomalies and some positive anomalies over the northern region of Skye which is covered with basaltic lavas. As in case of Mull, interpretation was performed by transforming magnetic anomalies to the less complicated pseudogravimetric anomalies. A three-dimensional model for the subsurface structure of the Skye igneous complex was obtained by interpreting the pseudogravimetric anomaly using the end correction method (Nettleton, 1940). The results of this interpretation are presented in this chapter, preceded by a brief account of the Tertiary igneous geology of the Skye igneous complex and a review of previous gravity and magnetic studies performed on the area.

5.2 Tertiary Igneous Geology of Skye

The earliest recognisable volcanic activity in Skye was a period of pyroclastic activity producing agglomerates and tuffs (Harker, 1904, Anderson and Dunham, 1966). This was followed by the extrusion of basaltic lavas. At present these lavas can mainly be seen in northern, western and south-eastern Skye (Figure 5.2) and they cover an area of approximately 1500km^2. The greatest thickness of lavas occurs in northern Skye where it is over 600m (2000ft). This lava sequence extends seawards for several tens of kilometers beyond Skye towards the west and south-west (Figure 5.3). The present distribution of

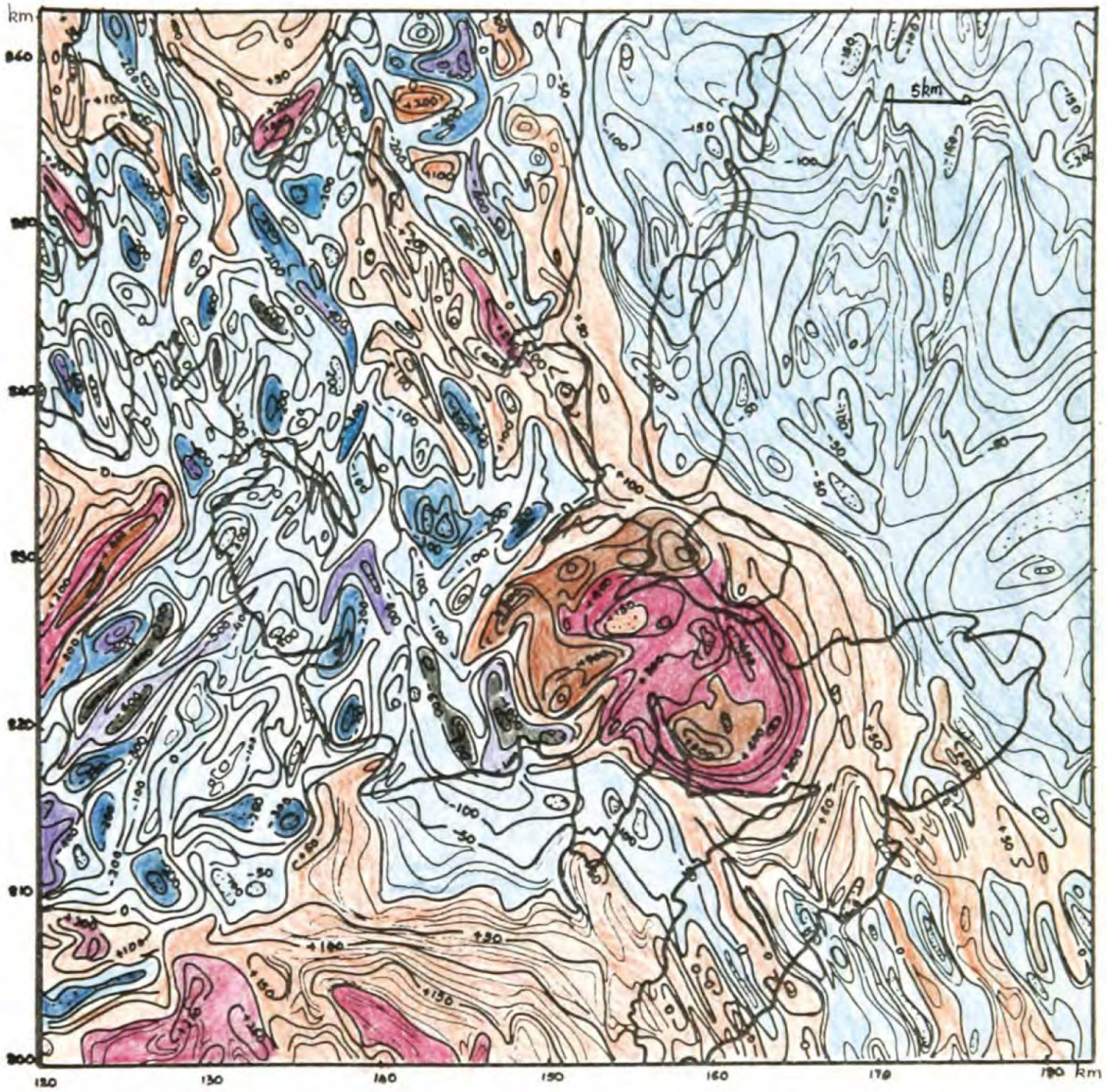

Figure 5.1 Aeromagnetic anomaly map over the Isle of Skye. Contours in gamma. Coordinates shown are national grid.

0 200 gamma

0 -200 gamma

-600 -1200 gamma

200 400 gamma

-200 -400 gamma

400 1000 gamma

-400 -600 gamma

Figure 5.2 Sketch map of geology of Skye from Bell (1976).

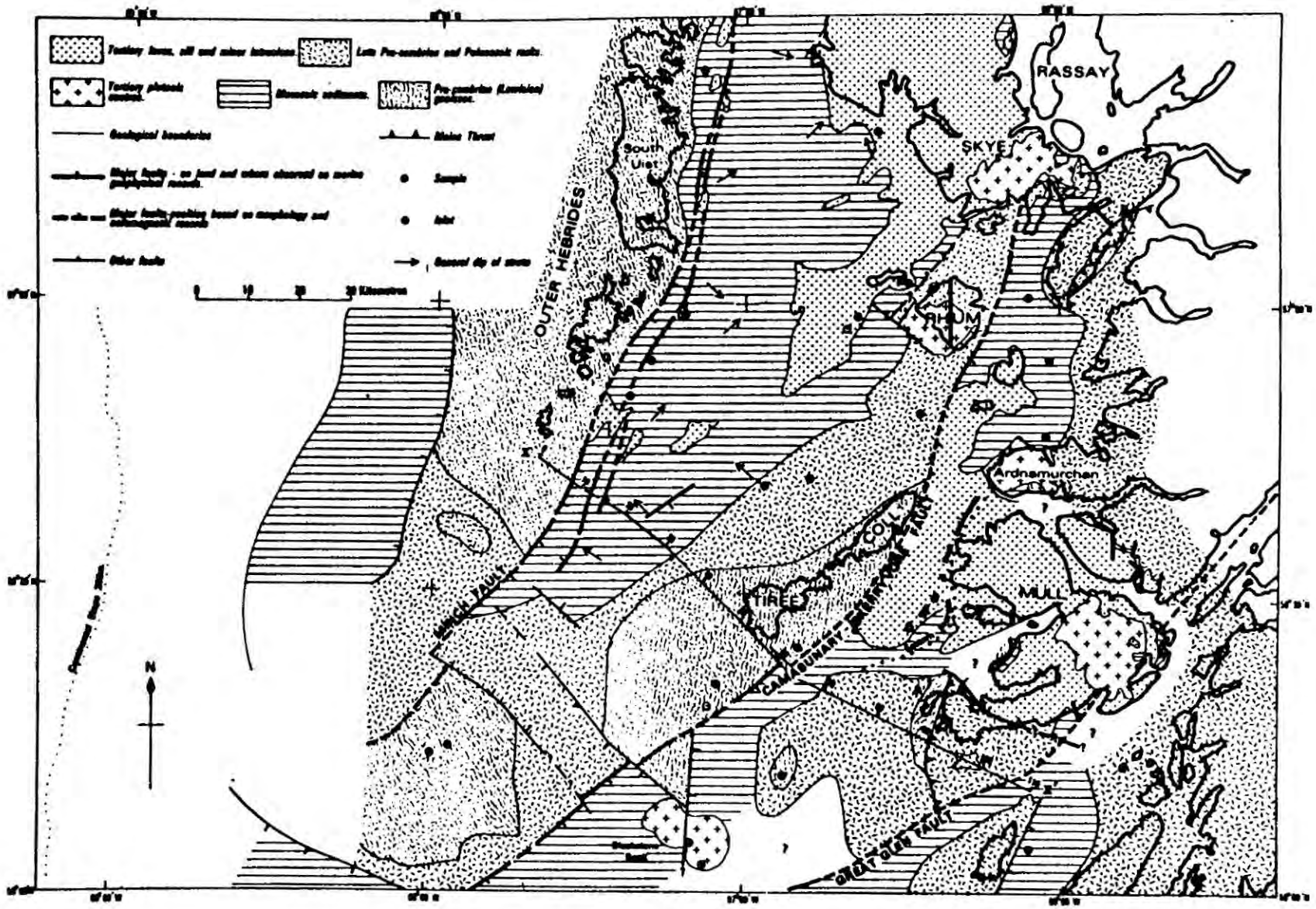

Figure 5.3 Pre-Quaternary geology of sea of Hebrides from McQuillin and Binns(1973).

lavas on Skye suggests that they have been extruded from several fissures related to a central volcano (Anderson and Dunham, 1966). Skye lavas consist mainly of olivine basalts. Mugearite and big-felspar mugearite basalts can be found in the upper part of the lava succession (Stewart, 1965).

Extrusion of basaltic lavas from fissures in Skye was followed by the intrusion of plutonic bodies. This intrusive activity was concentrated in four major centres in central Skye. In chronological order these are the Cuillin centre, the Strath na Creitheach centre, the Western Red Hills centre and the Eastern Red Hills centre. Figure 5.4 shows the various igneous intrusions associated with the four centres. The sequence of igneous events of the Skye complex has been given by Bell (1976) and by Emeleus (1982). The Cuillin centre consists of basic and ultrabasic rocks while the other three centres consist mainly of granitic rocks. In addition to the major intrusions around the four centres, minor intrusions such as dykes also took place throughout the time Skye igneous complex was active. These minor intrusions are mainly basic rocks and therefore basaltic magma must have been available throughout the history of the complex.

5.2.1 The Cuillin Centre

This centre consists mainly of layered and unlayered basic and ultrabasic rocks which cover an approximately circular area having a diameter of about 8 km. According to Harker (1904) the Cuillin Complex is a laccolith of ultrabasic rocks intruded by a subsequent gabbroic laccolith. Later work by Zinovieff (1958), Weedon (1961, 1965) and Wager and Brown (1968) on the layering of basic and ultrabasic rocks suggested that the layered rocks in the Cuillin centre resulted from crystal accumulation and differentiation within a magma chamber.

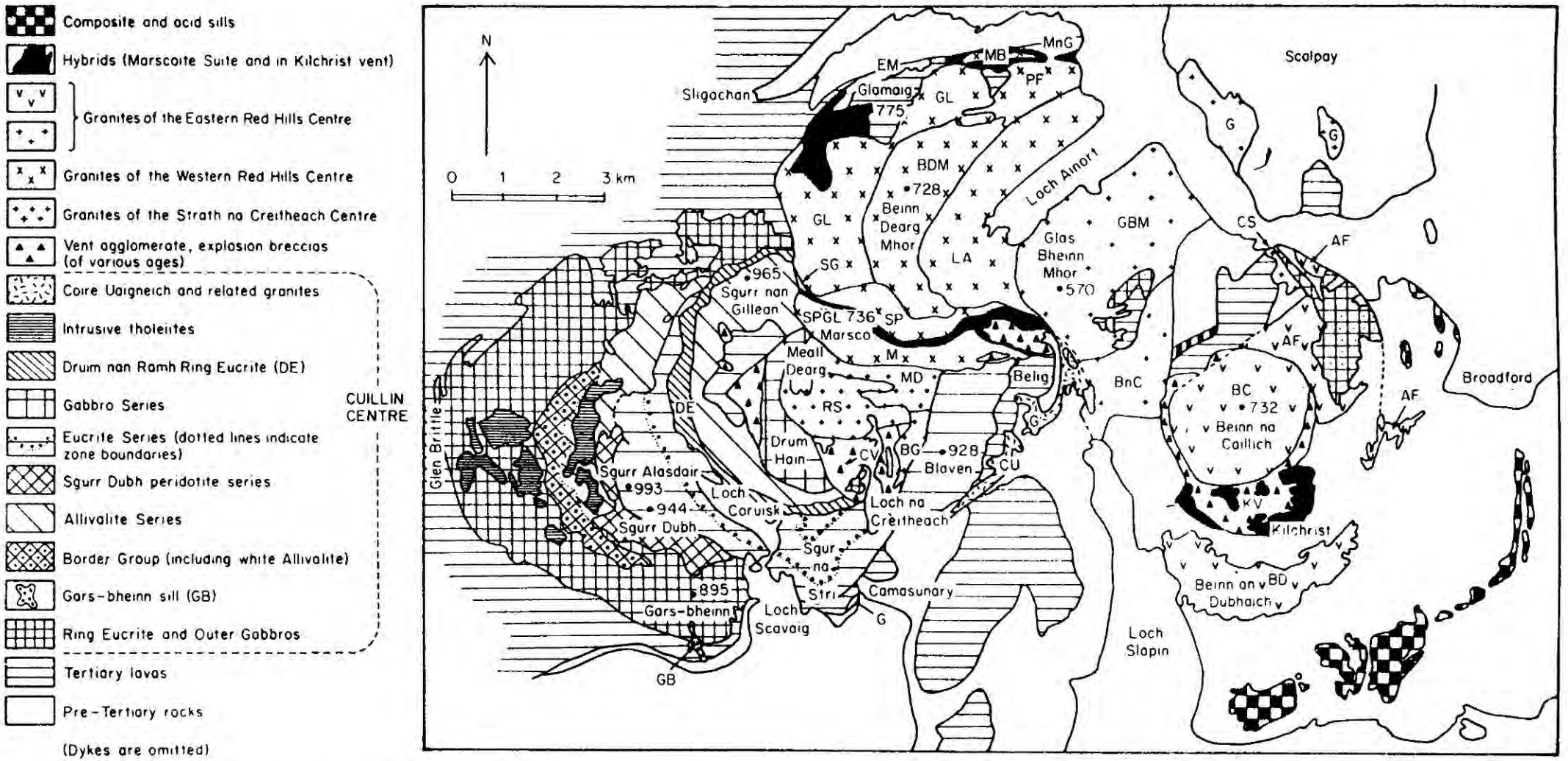

. Geological sketch map of the Skye central complex. Abbreviations: (i) Cuillin Centre: GB, Gars-bheinn ultrabasic sill; CU, granophyre of Coire Uaigneich; DE, Druim nam Ramh ring eucrite: (ii) Strath na Creitheach centre: CV, Loch na Creitheach vent; BG, Blaven epigranite; RS, Ruadh Stac epigranite; MD, Meall Dearg epigranite: (iii) Western Red Hills centre (see Figure 31.5); MnG, Maol na Gainmich epigranite; MB, Meall Buidhe epigranite; EM, Eas Mhor epigranite; GL, Glamaig epigranite; BDM, Beinn Dearg Mhor epigranite; LA, Loch Ainort epigranite; SP, Southern porphyritic epigranite; PF, porphyritic felsite; SG, Sligachan epigranite; M, Marsco epigranite: (iv) Eastern Red Hills centre: CS, Creag Strollamus epigranite; AF, Allt Fearna epigranite; GBM, Glas Bheinn Mhor epigranite; BnC, Beinn na Cro epigranite; KV, Kilchrist vent: BC, Beinn na Caillich epigranite; BD, Beinn an Dubhaich granite. G, other granites and granophyres. Heights indicated in metres. (

Figure 5.4 Geological sketch map of the Skye central complex *from* Emeleus (1982).

The southern, western and northern parts of the layered rocks are bounded by unlayered older rocks known as the outer gabbro and Garsbheinn gabbro (Figure 5.4). After the intrusion of these unlayered gabbros, a massive pool of basic magma was formed in the Cuillin area. Layered ultrabasic rocks (Sgur Dubh peridotite series and Allivalite series) and basic rocks (Eucrite series and Gabbro series) were formed from this magma. Relative vertical movements of various parts of the layered rocks and subsequent erosion are responsible for the present complicated structural arrangement of the Cuillin rocks (Wager and Brown, 1968). In addition to the major basic and ultrabasic rocks, intrusion of basic cone sheets and dykes took place during the time when the Cuillin centre was active. A few acid rocks such as Coire Uaigneich granophyre were emplaced during the late stages of this centre.

5.2.2 The Strath na Creitheach Centre

This is the smallest igneous centre in the Skye complex. It has the smallest area as well as the smallest number of intrusions compared to the other three centres. As indicated in 5.2.1 there are several cone sheets which cut the nearby Cuillin centre. Absence of such cone sheets in the Strath na Creitheach centre indicates that it is younger than the Cuillin centre. Furthermore, the granitic rocks of this centre trangressively cut the gabbroic rocks of the Cuillin centre (Figure 5.4) and this further substantiates its post Cuillin age. The earliest member of this centre is a semicircular volcanic vent, with blocks of gabbro and cone sheets, having an area of about 1,8km^2 (Bell, 1976). Ruadh Stac, Meall Dearg and Blaven granites (Figure 5.4) are the other members of the Strath na Creitheach centre.

5.2.3 The Western Red Hills Centre

Harker (1904) described the western Red Hills centre as a complex laccolith of granitic rocks. More recent studies by Richey et al.(1946, 1947), Wager et al.(1965), Bell (1966) have shown that this centre consists of several granitic intrusions. Absence of cone sheets, which can be found in large numbers in the Cuillin centre, in Western Red Hills demonstrates its post Cuillin age. Truncation of the Meall Dearg granite of the Strath na Creitheach centre by the Marsco epigranite of the Western Red Hills centre indicates its post Strath na Creitheach age. Presence of lavas over some granitic mountains in the Western Red Hills centre suggests that the original structural level of these rocks cannot be much higher than the present level. Contacts between country rocks and granites and between the major granites themselves are dipping outwards at angles between 30° and near vertical. Flat lying roof-like contacts between different granites can also be observed (Bell, 1966, Emeleus, 1982). In addition to these major granitic rocks, there are some gabbroic and hybrid rocks in this centre. Gabbroic rocks of the Western Red Hills centre have outcropped near Marsco and they were emplaced shortly before the emplacement of the earliest granitic member, the Glamaig epigranite, of this centre (Thompson, 1969). Hybrid rocks of the Western Red Hills centre also outcrop near Marsco. Harker (1904) gave the name marscoite to these hybrid rocks. Marscoite hybrid rocks exist together with some porphyritic felsite and ferrodiorite rocks and they are known as the marscoite suite of rocks. The marscoite suite of rocks, which takes the form of a narrow discontinuous ring dyke, cuts several granitic members of the Western Red Hills centre (Figure 5.4). Widespread occurrence of marscoite rocks in central Skye

suggests that marscoite may have been available as a separate magma (Bell, 1976). Wager et al.(1965) suggested that the marscoite magma must have been formed at depth due to the mechanical mixing of porphyritic felsite and ferrodiorite magmas. The origin of the ferrodiorite magma has been discussed by Wager and Vincent (1962). According to them, this magma has originated as a result of differentiation of basic magma of a mafic layered intrusion below the Western Red Hills centre.

5.2.4 The Eastern Red Hills Centre

This is the last major igneous centre in the Skye complex and it has been least well studied of the four centres. The Eastern Red Hills centre consists of several granitic intrusions, two major gabbroic intrusions and some hybrid rocks in the Kilchrist Vent (Figure 5.4). The Glas Bheinn Mhor granite, one of the earliest rocks of this centre, cuts some of the rocks of the Western Red Hills centre (Figure 5.4) indicating its younger age. The central part of the Eastern Red Hills centre is occupied by conspicuous Beinn na Caillich granite. The Beinn na Dubhaich granite, which is situated south of the Beinn na Caillich granite (Figure 5.4), has been subjected to more detailed investigations compared to other members of the Eastern Red Hills centre. Harker (1904) described this granite as a boss but later work by King (1960) suggested that it has a sheet like structure.

5.2.5 Origin of the Granitic Rocks in Skye

The origin of the Skye granites was first discussed by Harker (1904). According to him these granites were emplaced as a result of crystal fractionation of basaltic magma. Brown (1963) showed that the composition of granitic rocks in Skye can be almost entirely expressed by a $NaAlSi_3O_8$-$KAlSi_3O_8$-SiO_2-H_2O system. By using the position of the composition of Skye granites in the

$NaAlSi_3O_8$-$KAlSi_3O_8$-SiO_2-H_2O system he showed that the granites could have originated from the partial melting of underlying Lewisian basement at a depth of 3-4km. Further evidence for the crustal origin of the Skye granites came from a strontium isotope study of the granites by Moorbath and Bell (1965). In this study, they found that $(^{87}Sr/^{86}Sr)_{initial}$ ratios of Skye basic rocks are different from that of the acidic rocks. This indicates that the source region of acidic rocks cannot be the same as the source region of basic rocks. Moorbath and Bell (1965) therefore concluded that Skye granites must have been produced by the partial melting of underlying Lewisian rocks. Moorbath and Welke (1969) showed both granitic and gabbroic rocks of the Skye complex contain varying amounts of ancient crustal lead. The percentage of crustal lead present in the granitic rocks varies from 35 to 77. Since this variation is too high Moorbath and Welke (1969) came to the conclusion that both the melting of the Lewisian basement and the crystal fractionation of basic magma must have contributed to the production of granitic magma. Most of the rocks in the Skye igneous complex are highly depleted in ^{18}O isotope and Taylor and Forester (1971) showed that this was due to the circulation of heated ground water within the complex during the time it was cooling (see 4.2.3). This hydrothermal circulation could have disturbed the Sr isotope ratio and calculated $(^{87}Sr/^{86}Sr)_{initial}$ ratio from observations may not give the ratio at the time rock was formed. Therefore it is not possible to ignore crystal fractionation as a possible hypothesis for the origin of Skye granites from Sr isotope studies. Dickin (1981) studied lead isotope ratios of Skye granitic rocks using samples selected from sites which are not effected by the hydrothermal circulations and showed that granitic magma has been

generated as a result of both partial melting of crust and basaltic differentiation. The proportion of crustal component varies from 10% to 30% from older to younger rocks.

5.2.6 Age of the Igneous Activity in Skye

Rb-Sr age determinations of Skye granites by Moorbath and Bell (1966) have shown that the mean age of Western and Eastern Red Hills granites is 54±2 m.y. Their work did not show any significant difference in ages of Western and Eastern Red Hills granites. Dickin (1981) determined the age of peridotite rocks of the Cuillin centre by using the same technique and found that the rocks are 60 m.y. old. The lavas of Skye, which predates the Cuillin rocks must be older than 60 m.y.

5.3 Previous Gravity and Magnetic Studies of the Skye Igneous Complex

5.3.1 Gravity Studies

The Bouguer gravity anomaly map over the Skye igneous complex has been prepared by Tuson (1959) and Bott and Tuson (1973) and it is shown in Figure 5.5. This positive gravity anomaly which has a near circular symmetry has a maximum value of 73 mgal over the southern part of the Cuillin centre. Tuson (1959) interpreted the Skye gravity anomaly in terms of a basic cylindrical body which extends to a depth of 17km having a radius of 8km and a density contrast of 0.2 g/cm^3. A large area of the Skye igneous complex is covered with the granitic rocks of the three late centres (Figure 5.4). The effect of these granites was not included in this interpretation. As a result of this and because the shape of the subsurface structure differed from the assumed cylindrical shape, the discrepancy between the observed and calculated anomalies was up to 11 mgal in places. McQuillin and Tuson (1965) presented a similar interpretation of

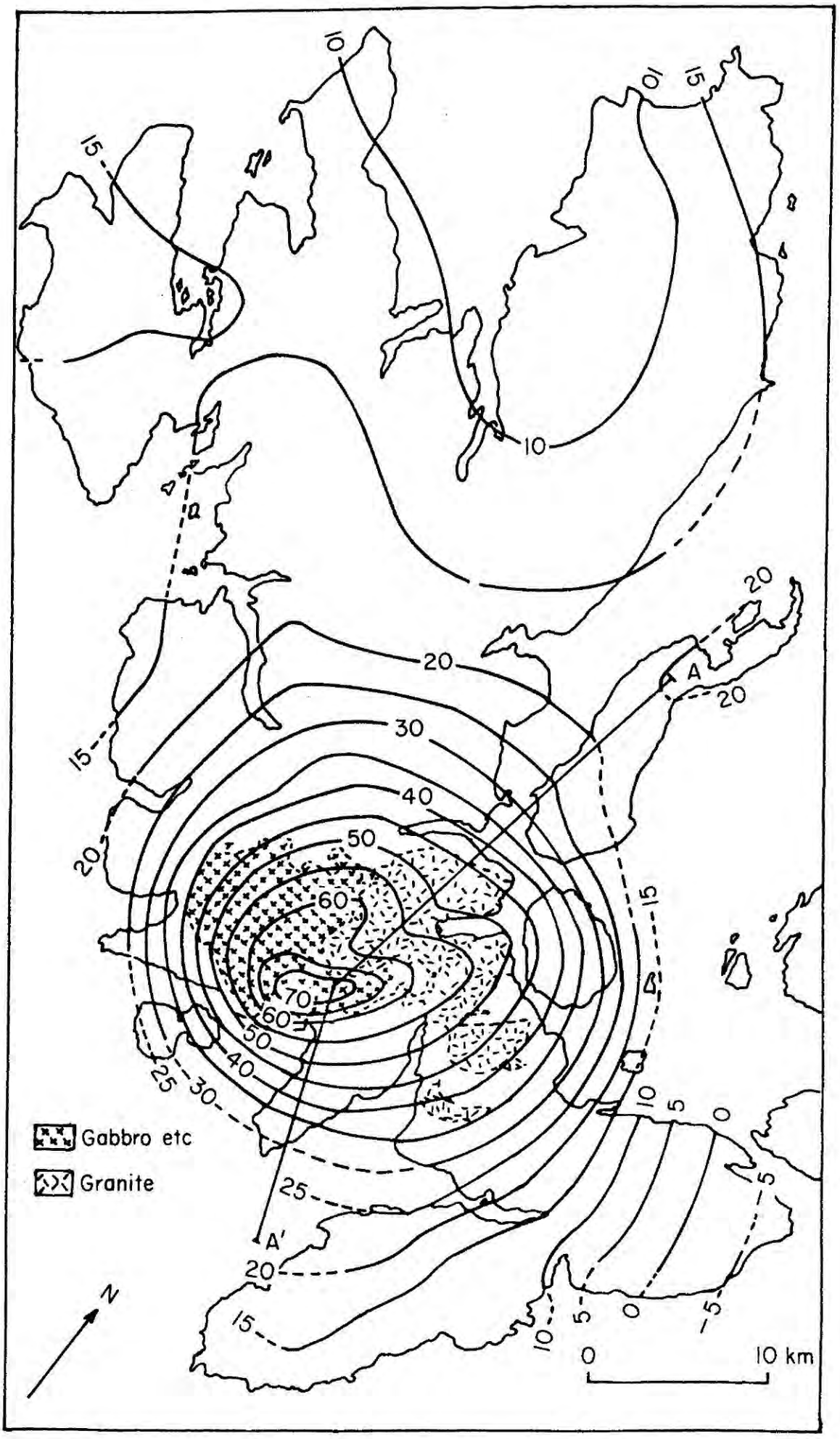

Figure 5.5 Bouguer anomaly map of the Isle of Skye, showing contours at 5 mgal intervals. from Bott and Tuson (1973).

the Skye complex. Bott and Tuson (1973) performed a detailed three dimensional interpretation of the gravity anomaly map of the Skye complex using the end correction method (Nettleton, 1940). They interpreted the profile AA' of Figure 5.5 in terms of a body having a shape similar to a truncated cone which extends to a depth of 14km. The effect due to the subordinate granitic rocks was also included in this interpretation and the depth to which they extend was found to be in the range 1.0 - 1.6km below sea level. A cross-section of the model obtained together with density values used are shown in Figure 5.6. The widths of the body in a direction perpendicular to the profile at the top and bottom surfaces are 12km and 18km respectively. In the model the densities of basic and acidic parts of the body were taken as 3.01 g/cm^3 and 2.61 g/cm^3 respectively and the density of the background rocks as 2.80 g/cm^3. The density used for the basic rocks either corresponds to dense gabbro or to a mixture of 75% gabbro and 25% ultrabasic rocks. Bott and Tuson (1973) produced another model for the Skye igneous complex which extends to a depth of 5.5 km using a density of 3.15 g/cm^3 for the dense rocks. This density value corresponds to almost 100% ultrabasic rocks. The nature of the subsurface structure of the Skye igneous complex must lie between these two models depending on the ratio of basic to ultrabasic rocks present in the complex.

5.3.2 Magnetic Studies

Aeromagnetic anomaly maps over the Skye igneous complex (Figure 5.1) have been published by the Institute of Geological Sciences of Great Britain in one inch to one mile and quarter inch to one mile scales. Brown and Mussett (1976) discussed the nature of the sub-surface structure of the Skye igneous complex using gravity and aeromagnetic anomaly maps and smoothed aeromagnetic anomaly maps which only indicate the effect due to deep seated magnetized bodies.

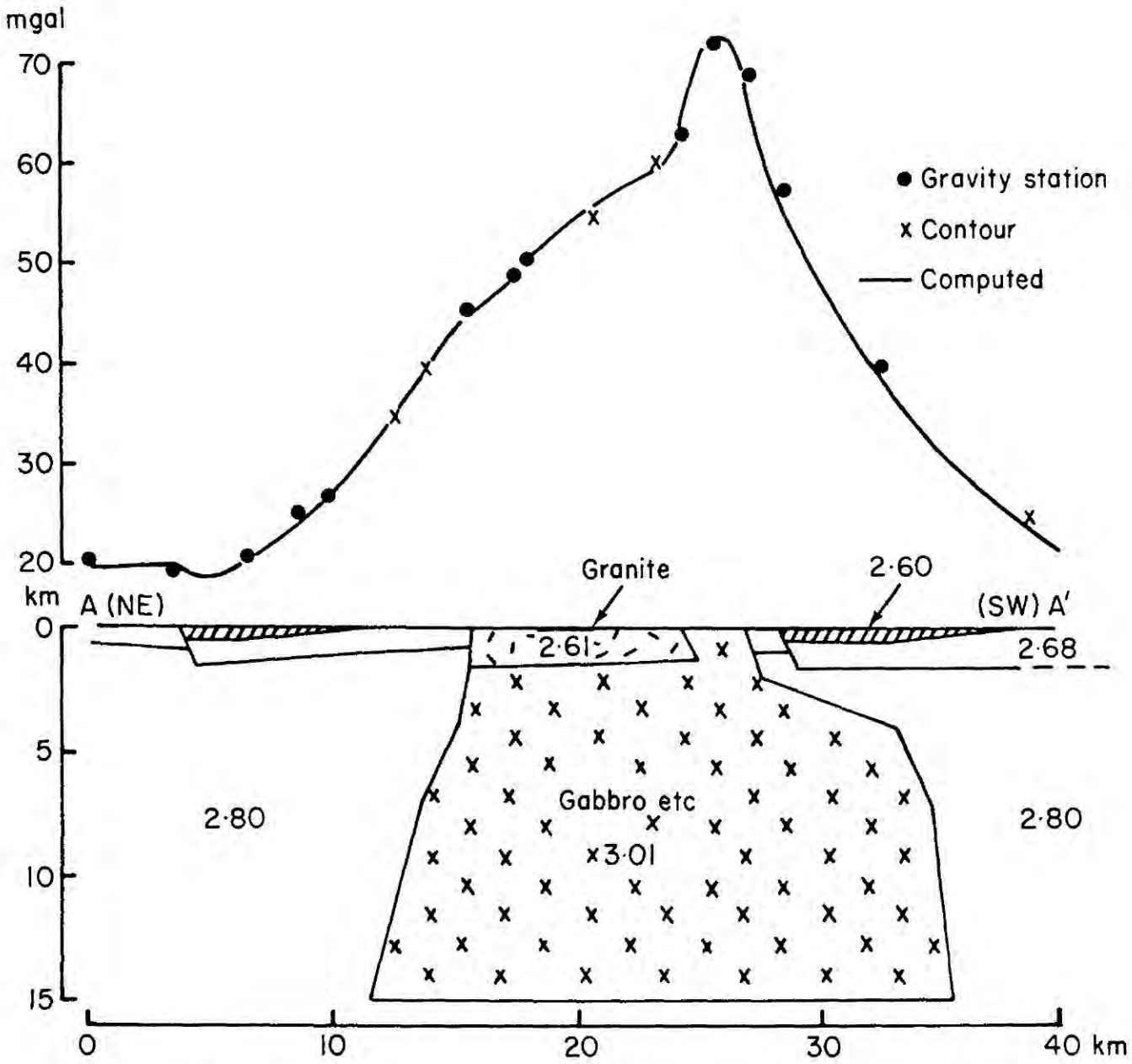

Figure 5.6 Interpretation of the sub-surface structure of the Skye igneous complex along AA'(Figure 5.5), from Bott and Tuson (1973). Density contrast in g/cm^3.

According to them, the Skye igneous complex is underlain by two bodies having opposite magnetic polarities. These two bodies are sufficiently close to produce a single gravity anomaly. Since the positive anomaly over the Red Hills centres appear prominently on the filtered aeromagnetic map, Brown and Mussett (1976) argued that it cannot be due to the shallower Red Hills granites and must be due to a deep seated body. The negative anomaly over the Cuillin centre does not appear as prominently on the smoothed map as the positive anomaly and therefore they concluded that it is caused by the outcropping basic and ultrabasic rocks of the Cuillin centre. Brown and Mussett (1976) further showed that two deep vertical gabbroic cylinders in contact with each other, having opposite polarities produce gravity and magnetic anomalies of similar nature to those observed.

5.4 Interpretation of Magnetic Anomalies Over the Skye Igneous Complex

The aeromagnetic anomaly map over the Skye igneous complex (Figure 5.1) was digitized at 1 km intervals and was transformed into pseudogravimetric anomalies using the method described in chapter 2. In this transformation it was assumed that rocks in the Skye igneous complex are magnetized either along the direction of the present day earth's field or along the opposite direction. Remanent magnetization of rocks in the Mull complex is in a direction fairly close to the direction of the present day earth's field or in a direction fairly close to the opposite direction to the present day earth's field (section 4.4). Therefore it is reasonable to assume that the Skye igneous rocks, which were emplaced in the same period as the Mull igneous rocks, have similar directions of remanent magnetization. In addition, paleomagnetic studies on Skye lavas by Khan (1960) have shown that the average direction of remanent magnetization of the lavas (declination = 186.1^{o}, inclination = -59.7^{o}) is in a direction close to the opposite direction

to the present day earth's field.

Figure 5.7 shows the resulting pseudogravimetric anomaly map when the magnetic anomaly map shown in Figure 5.1 was transformed. The peseudogravimetric anomaly has been superimposed on a geological sketch of Skye (Figure 5.8). This anomaly map consists of pseudo-gravimetric lows over the Cuillin centre and over the basaltic lavas and a pseudogravimetric high over the Western and Eastern Red Hills granites. The negative pseudogravimetric anomaly is most intense over the eucrite rocks of the Cuillin centre and it reaches an equally low value over the submerged lavas situated beyond the western coast of Skye (Figure 5.3). The positive part of the pseudogravimetric anomaly has its maximum value over the north-eastern part of the Western Red Hills centre. The positive pseudogravimetric anomaly over the Red Hills is elongated towards the east coast of northern Skye. This may be due to the presence of normally magnetized lavas and normally magnetized intrusive bodies such as dykes and sills in this area. The pseudogravimetric anomaly over the lavas changes from positive to negative when going from this area to the western coast of northern Skye. This suggests that there is a variation in the direction of magnetization of the lavas from normal to reverse from the east coast to the west coast of northern Skye. However, measurement of the remanent direction of magnetization of the lavas in these areas is required to confirm this idea. As can be seen from Figure 5.7 there is a negative regional gradient in the pseudogravimetric anomaly along a S.W. - N.E. direction. Due to the fact that the pseudogravimetric anomaly consists of positive and negative parts and also due to the above mentioned regional gradient, comparison of the pseudogravimetric anomaly with the gravity anomaly is difficult. A profile of the pseudogravimetric

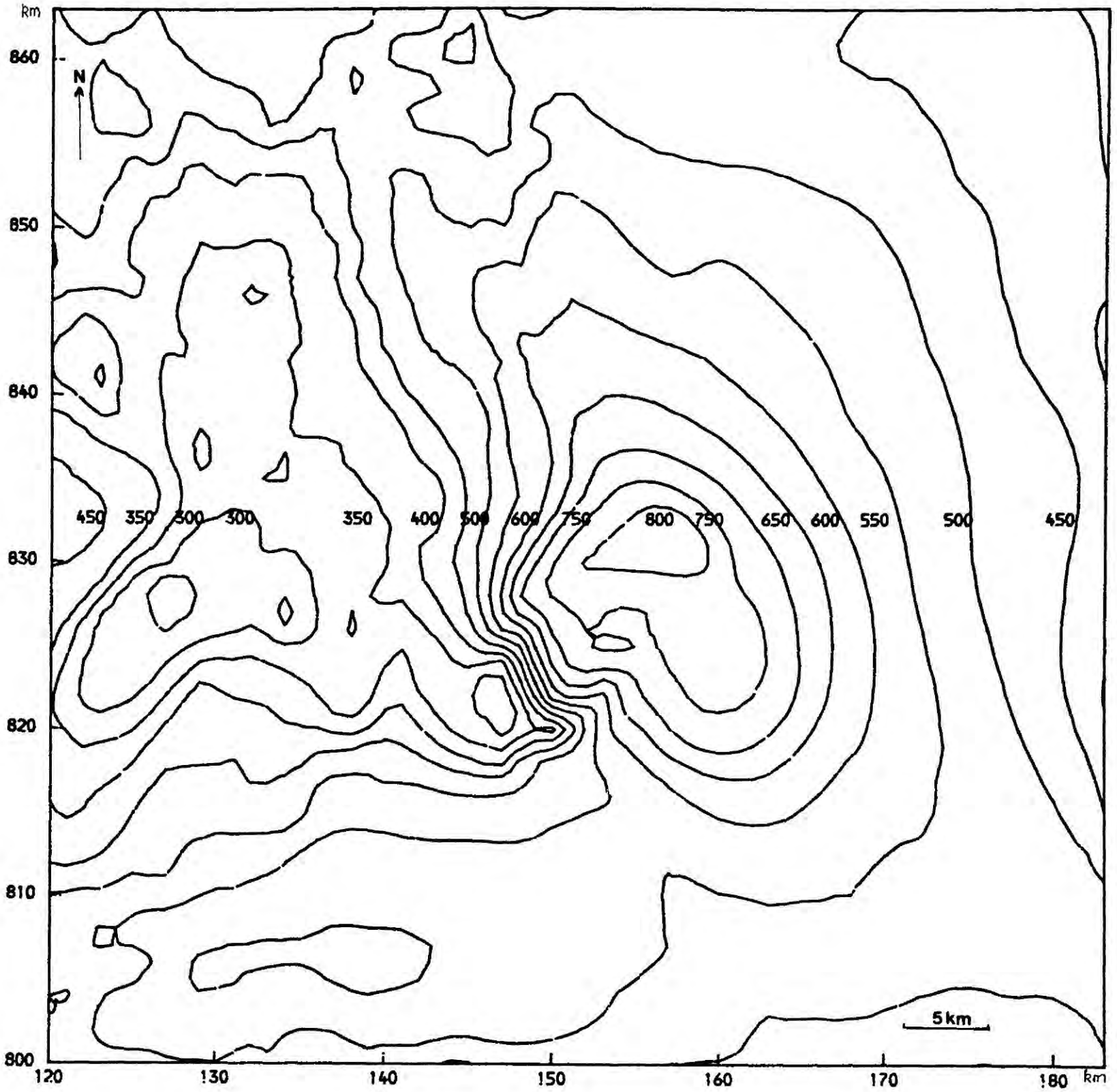

Figure 5.7 Pseudogravimetric anomaly map of the Isle of Skye, showing contours at 5o mgal intervals. On this and subsequent related figures national grid is shown.

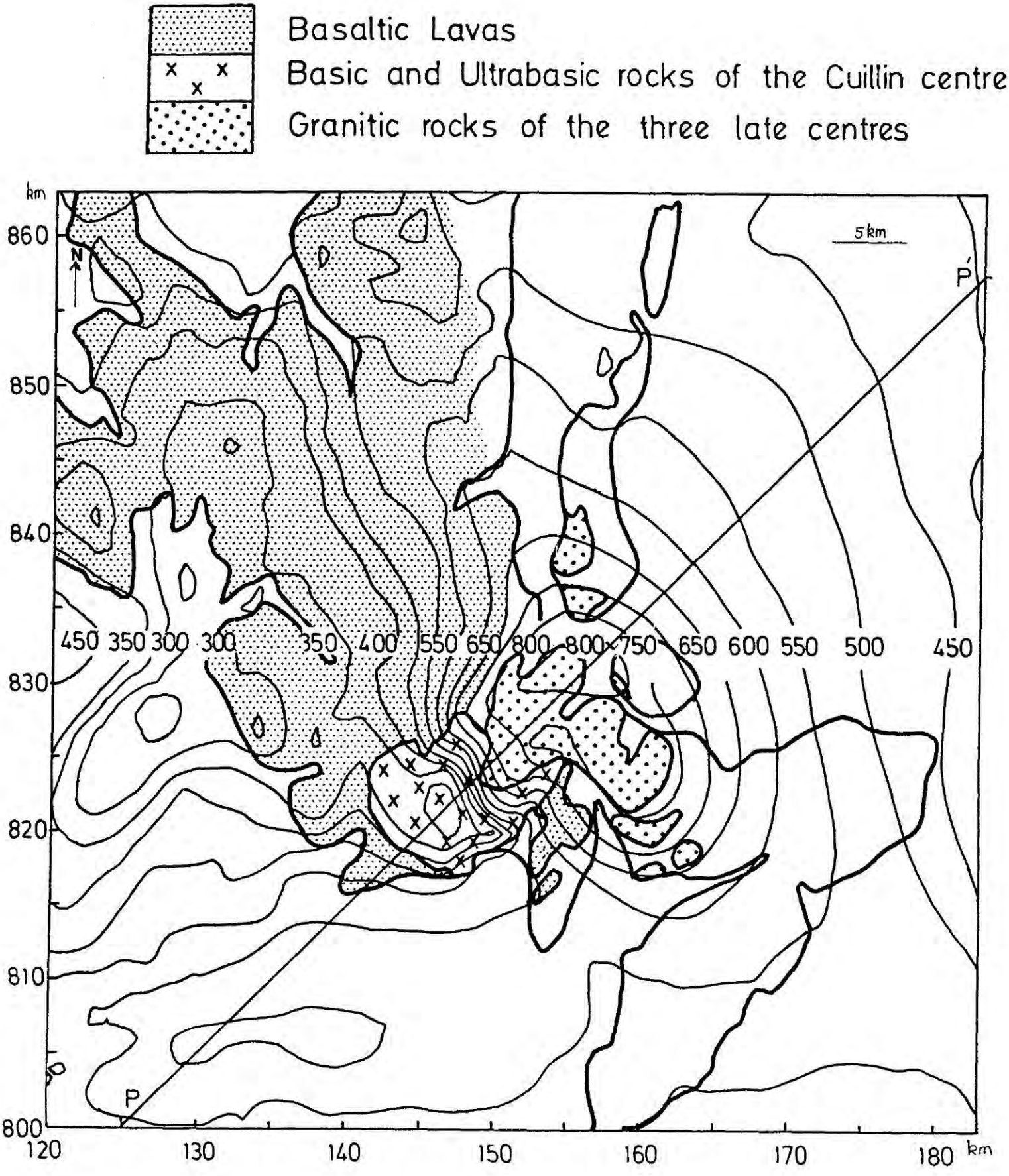

Figure 5.8 Correlation between the pseudogravimetric anomaly and the broad geology of Skye. Contours in mgal.

anomaly along a S.W. - N.E. direction (profile PP', Figure 5.8) passing through the Cuillin centre and the Western Red Hills centre is shown in Figure 5.9. This profile consists of a relatively narrow and intense negative anomaly superimposed on a broad positive anomaly. This negative anomaly which occurs over the Cuillin centre has steep gradients indicating that it is due to a shallow body. The positive anomaly over the Western Red Hills has gentle gradients and therefore it may be caused by a deep seated body. When going north-eastwards from the steep negative anomaly over the Cuillins, the gradient of the positive part of the anomaly becomes shallower over part of the Western Red Hills (section AB of the anomaly) and then the anomaly increases to its maximum with steep gradients. This portion of the positive anomaly having steep gradients indicates the partly shallower nature of the causative body.

A three-dimensional interpretation of the pseudogravimetric profile of Figure 5.9 was performed using the end correction method (Nettleton, 1940). This interpretation was done by using the Fortran routine GREND (see chapter 3) which performs gravity interpretation using the trial and error method. Application of the end correction method requires the trial model to be divided into a series of polygonal prisms (see 3.2) and Figure 5.10 shows the way in which this division was performed. The result of this interpretation is shown in Figure 5.11. The model obtained for the subsurface structure of the Skye complex consists of three different bodies which are labelled as A, B and C in Figure 5.11. The body A can be identified with the Cuillin basic and ultrabasic rocks. This body, which takes a shape close to a truncated cylinder, has widths of 7.5 km and 8.0 km along the direction of the profile and along the perpendicular direction

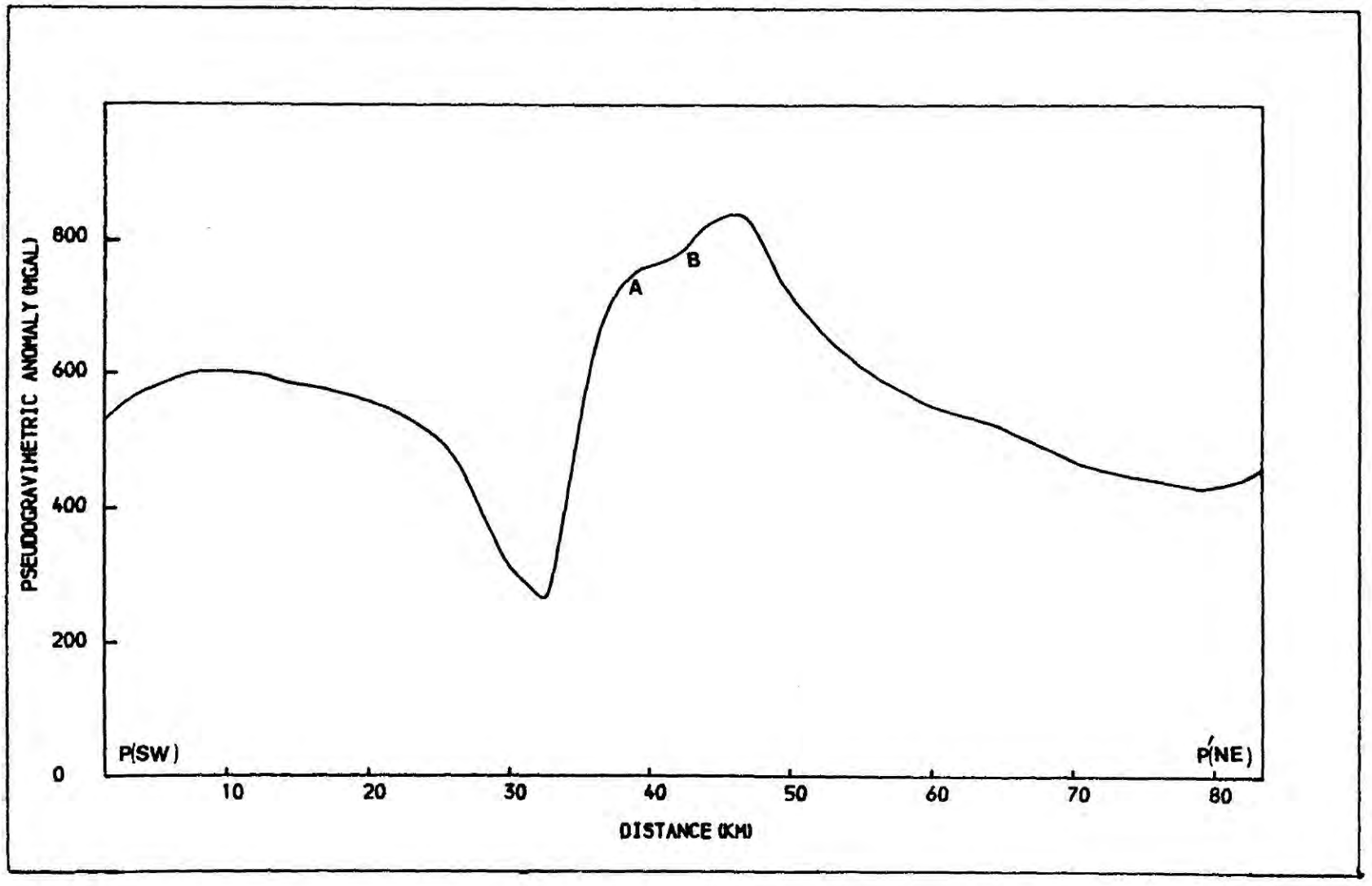

Figure 5.9 Profile of the pseudogravimetric anomaly of Figure 5.8 along PP'.

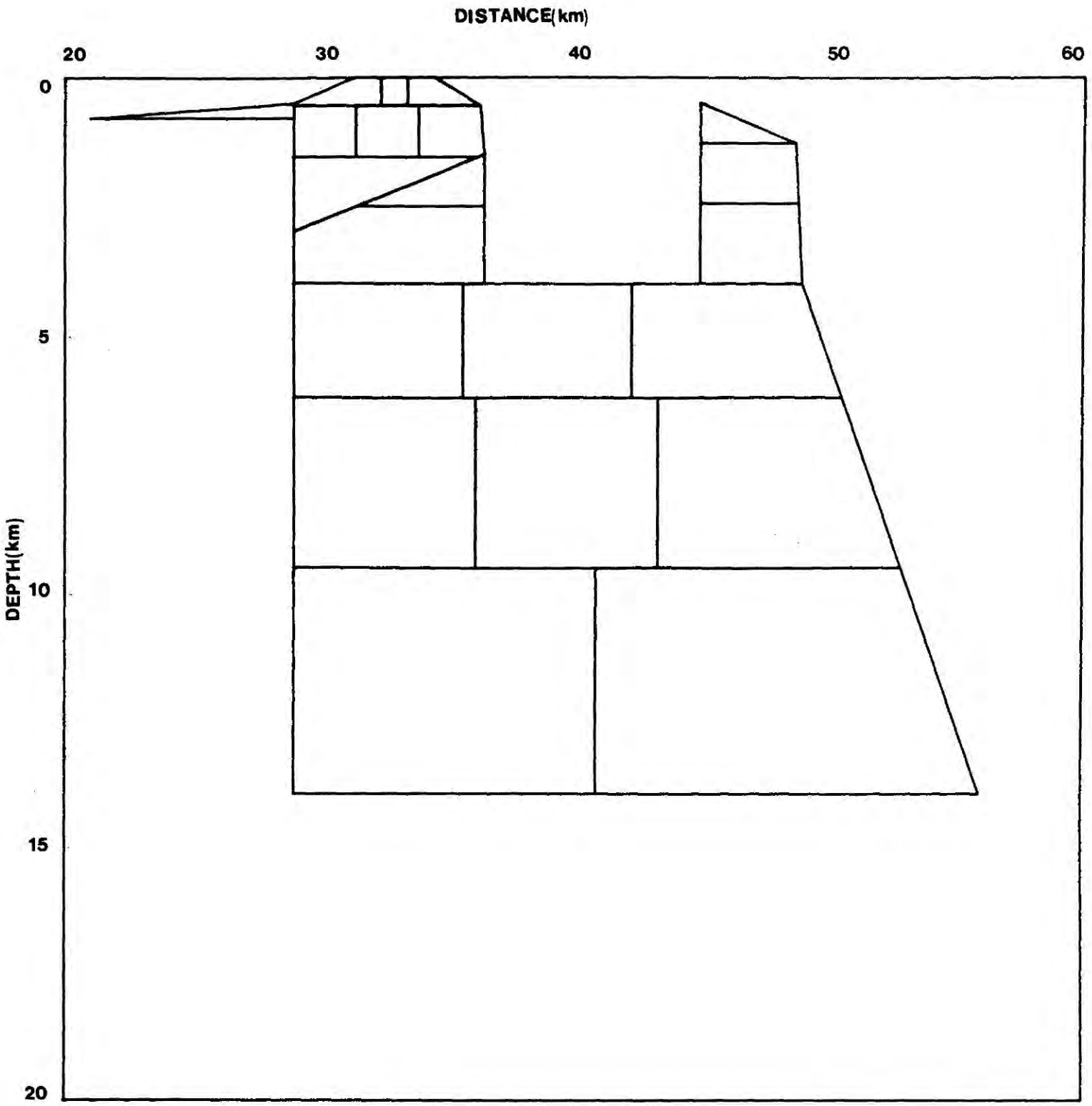

Figure 5.1o Subdivision of the model of Figure 5.11 for application of end corrections.

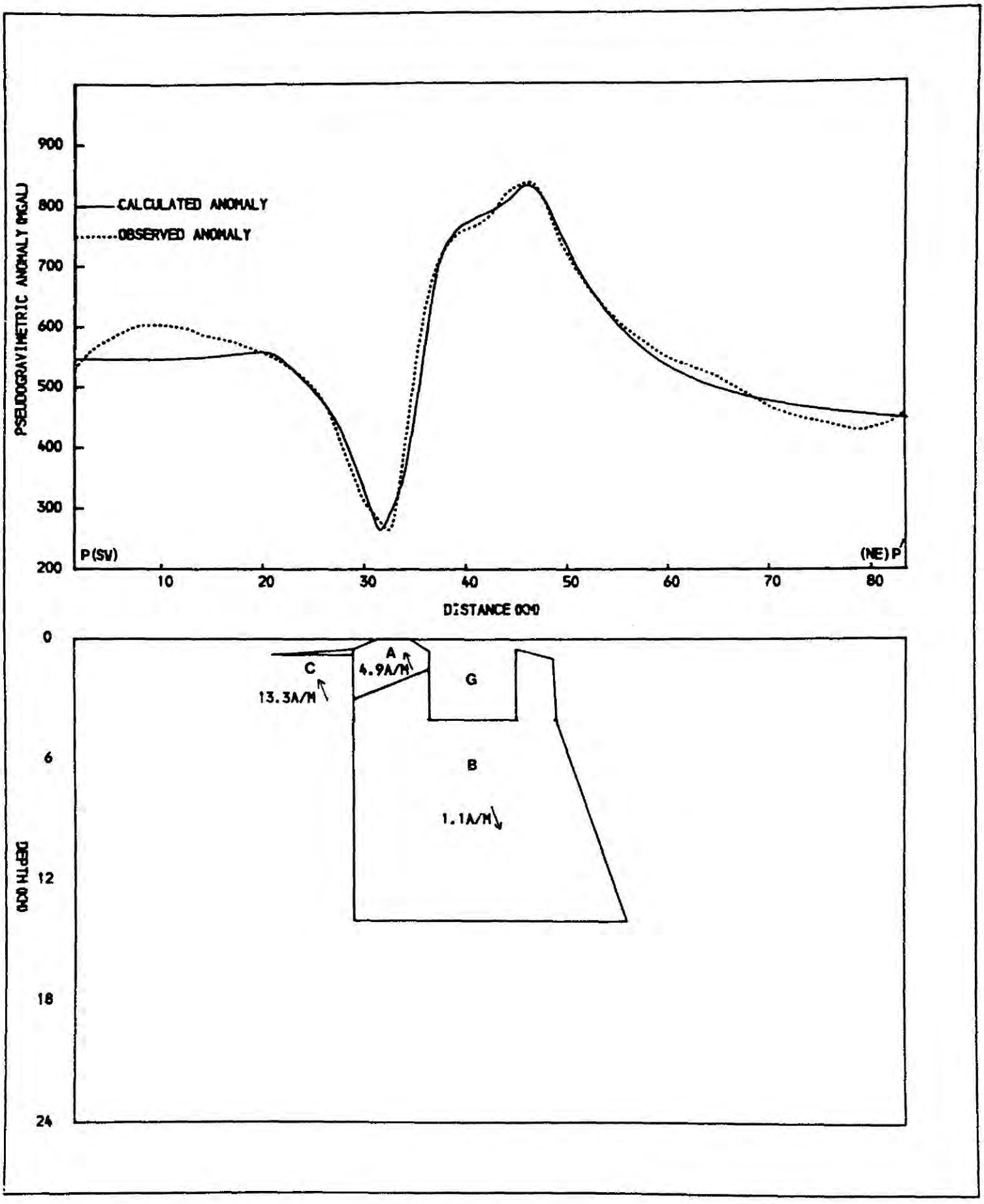

Figure 5.11 Interpretation of the pseudogravimetric profile PP' of Figure 5.8.

respectively. The bottom surface of the body inclines downwards towards the S.W. and the depth to which it extends ranges from 1.5 km to 3.0 km. The body A is reversely magnetized and has a magnetization of 4.9 A/m. The body B, which is situated below the body A, extends to a depth of 14 km and it is normally magnetized with a magnetization of 1.1 A/m. This body which approximately takes the shape of a truncated cone has a diameter of 20 km along the direction of the profile and along the perpendicular direction at the top surface. The dimensions at the base of the body are 27.0 km and 22.0 km respectively. The narrower part of the body which comes closest to the surface is responsible for the section of the positive anomaly having steep gradients. The third body C can be identified with the lavas situated in the S.W. part of Skye. Since these lavas extend through a large distance along the direction perpendicular to the profile (Figure 5.4) they were interpreted in terms of a two-dimensional body. These lavas are reversely magnetized and have a magnetization of 13.3 A/m. The lava pile which takes the shape of a wedge has a maximum thickness of 0.3 km at the place where it is in contact with the Cuillin rocks. To explain part of the anomaly having shallower gradients between the negative anomaly over the Cuillins and the positive peak it was necessary to have the region G in the model (Figure 5.11) with non magnetic rocks. The region G corresponds to the Red Hills granitic rocks in Skye. Microscopic studies of the Red Hills granites have revealed that the exposed granites do not contain a significant amount of magnetite (Emeleus, private communications). The assumption ofa a non-magnetic region G in the model is therefore valid.

It is necessary to mention that the model obtained from this interpretation is only one of several possible models that can satisfy

the observations and are geologically realistic (see 3.4). Whatever the model, it should mainly consist of two bodies having opposite magnetic polarities. The negatively magnetized body must be a shallower one and the positively magnetized body must be of greater depth extent. A weakly magnetized region corresponding to the granites is also required.

5.5 Discussion

It is clear from the interpretation discussed in the last section that the Skye igneous complex consists of a reversely magnetized shallower body which can be identified with the basic and ultrabasic rocks of the Cuillin centre and a normally magnetized body below it. This normally magnetized body in the model extends to a depth of 14 km and it has a relatively low magnetization compared to the reversely magnetized body. The interpretation confirms the results of the gravity interpretation of Bott and Tuson (1973) which showed the existence of a large basic body below the Skye igneous complex.

A detailed comparison between the pseudogravimetric interpretation and the gravity interpretation of Bott and Tuson (1973) is not possible as the two interpretations have considered profiles along different directions. It is however clear from the two interpretations that the bodies causing the magnetic and gravity anomalies have approximately equal magnitudes. The pseudogravimetric interpretation also agrees with the qualitative interpretation of the Skye magnetic anomalies presented by Brown and Mussett (1976). The Cuillin basic and ultrabasic rocks were emplaced about 60 m.y. ago in a period of reverse polarity of the earth's magnetic field. The body below the Cuillin rocks (body B, Figure 5.11) may also have been emplaced together with the

Cuillin rocks and its normal magnetization can be explained as follows. Since the Cuillin rocks were shallower they could cool quicker and could complete the cooling process within the reverse period catching the reverse polarity of magnetization. The body below it extends to a greater depth and therefore should take a relatively longer time to complete the cooling. This cooling process may have continued into the next normal period and may have been completed during that period, giving the body a normal magnetization.

Most recent studies on the origin of Skye granites suggest that they were emplaced as a result of both basaltic fractionation and melting of the continental crust (Dickin, 1981). When a massive body such as that suggested by gravity and magnetic interpretations is emplaced as magma, acid material could be produced by fractionation. At the same time melting of the continental crust may occur due to the large amount of heat present in the body. The above implication of the results of gravity and magnetic interpretations is therefore in agreement with the ideas put forward by Dickin (1981).

CHAPTER 6

INTERPRETATION OF MAGNETIC ANOMALIES OVER THE BLACKSTONES BANK IGNEOUS COMPLEX

6.1 Introduction

Bullerwell (1963) recognized the similarity between aeromagnetic anomalies over the Blackstones Bank situated about 50 km S.W. of Mull and over the other Tertiary igneous centres such as Mull, Skye and Rhum. This similarity led him to propose the existence of a Tertiary igneous centre related to the Islay and Jura dyke swarms at the Blackstones Bank. Geophysical and geological investigations have been carried out by several workers on the Blackstones Bank and their results have generally confirmed Bullerwell's suggestion.

This chapter presents an interpretation of aeromagnetic anomalies over the Blackstones Bank igneous centre. A map of aeromagnetic anomalies over the Blackstones Bank centre is shown in Figure 6.1. The almost circular nature of the anomaly is distorted by its elongation along the N.W. - S.E. axis. The magnetic anomaly over the Blackstones Bank is dominantly negative with a relatively narrow positive anomaly superimposed. This indicates the presence of a reversely magnetized body possibly with a normally magnetized core. The complicated nature of the magnetic anomalies over the Blackstones Bank does not allow an interpretation using normal magnetic interpretation methods. The magnetic anomalies were transformed into the less complicated pseudogravimetric anomalies (chapter 2). The resulting pseudogravimetric anomaly was then interpreted in terms of a three dimensional body using the end correction method (Nettleton, 1940). The results of this interpretation are discussed and compared with the results of a gravity interpretation of the Blackstones Bank. A brief account of previous geophysical and geological studies performed on the Blackstones Bank

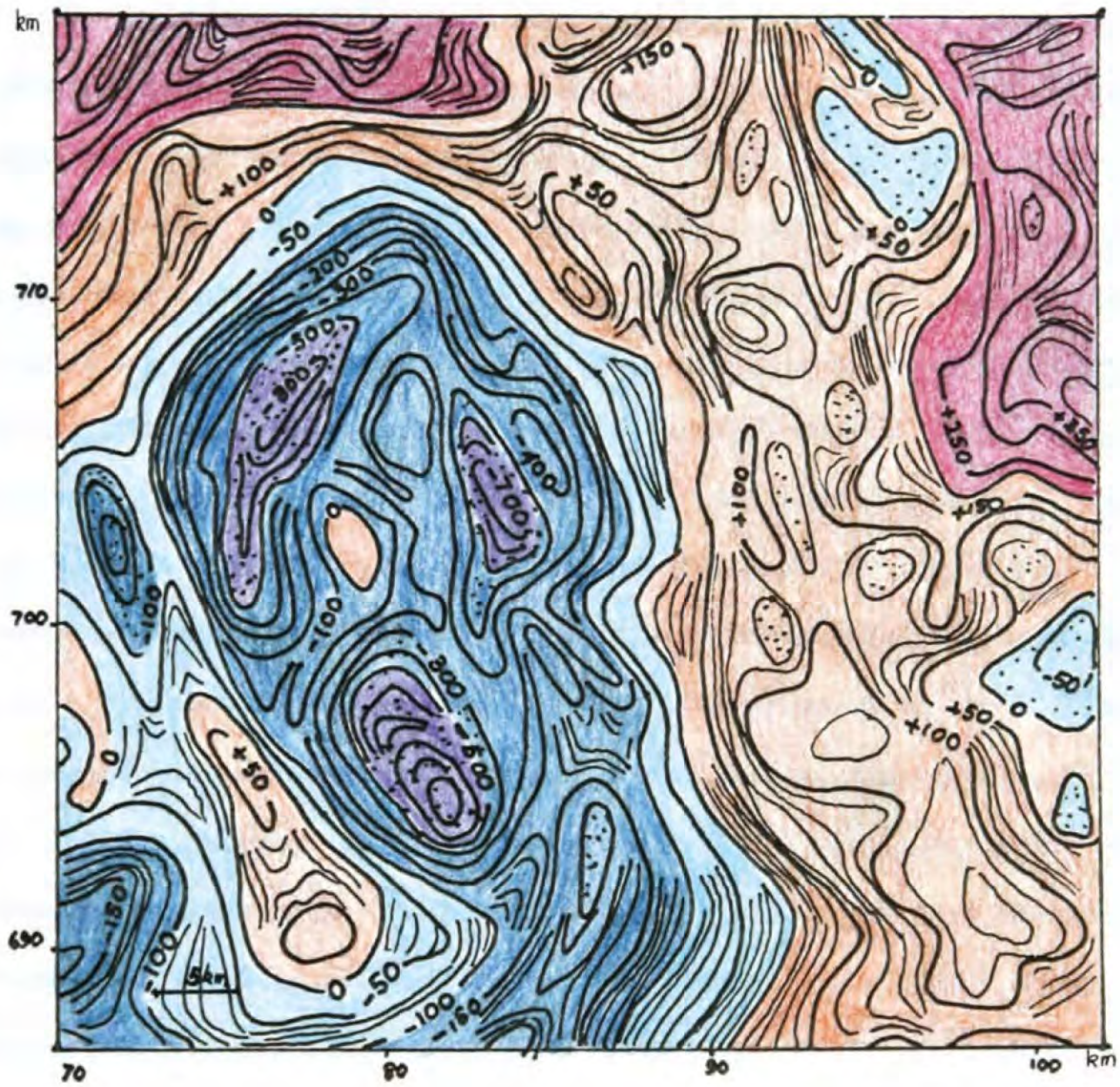

Figure 6.1 Aeromagnetic anomaly map over the Blackstones Bank. Contours in gamma. Coordinates shown are national grid.

o 200 gamma

above 200 gamma

o -100 gamma

-100 -500 gamma

below -500 gamma

igneous centre is first presented.

6.2 Geology of the Blackstones Bank Igneous Centre

Figure 6.2 shows the bathymetry map of the Blackstones Bank and as can be seen the peaks of this igneous centre attain a minimum water depth of 20m. Geological knowledge of the Blackstones Bank is largely confined to results of petrographic studies of many rock samples obtained from the sea bed. Eden et al.(1973) sampled gabbroic rocks from the Blackstones Bank by drilling. Durant et al.(1976) collected about 100 dive samples from the Blackstones Bank and presented a more detailed analysis of rock types found in this centre. Most of these samples were gabbroic and although they were petrographically similar to layered rocks formed elsewhere, the authors observed layering only during a later underwater survey. Other rock types identified from the collected samples were dolerite and metamorphosed sediments. Dolerite samples were collected from dykes and inclined sheets which were intruded into the gabbroic rocks. The presence of these minor intrusions in the southern part of the Blackstones Bank led Durant et al.(1976) to suggest the possible existence of a localized centre of activity in this area. Mitchell et al.(1976) dredged some basaltic rocks from the Blackstones Bank and presented a petrological study of these rocks. The Blackstones Bank igneous centre is situated in a Mesozoic basin in contrast to most of the other igneous centres which are situated on ridges between basins. This may be a possible explanation for the submarine character of this centre.

Some uncertainty exists as regards to age of the Blackstones Bank. Its proximity to the Tertiary centres suggests that it also has a Tertiary age. Samples collected by dives from dolerite dykes intruded into the gabbro yielded a radiometric age of 70 m.y.

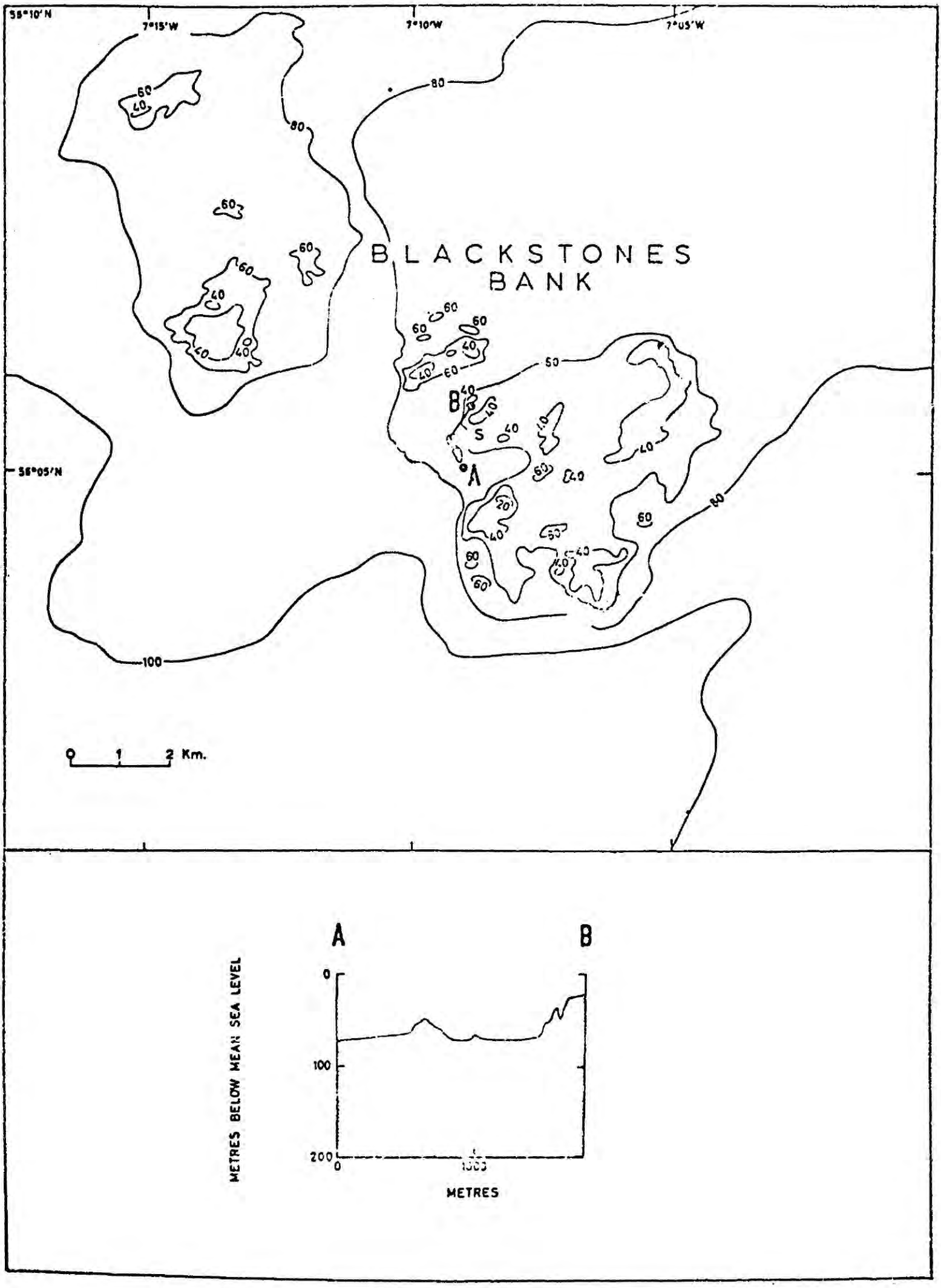

Figure 6.2 Bathymetry map of the Blackstones Bank showing contours at 2o m intervals from Eden et al.(1973).

(Durant et al. 1976). This suggests that the main body of the Blackstones Bank was intruded prior to this date and is therefore of upper Cretaceous age. Michell et al.(1976) dredged basalts from the Blackstones area which were subsequently dated at 57 m.y. Therefore, until further and more accurate sampling and dating is carried out, the age of the Blackstones Bank centre will be in doubt.

6.3 Geophysical Studies of the Blackstones Bank Igneous Centre

Gravity surveys over the Blackstones Bank were carried out by Roberts (1970) and McQuillin et al. (1975). The Bouguer anomaly map prepared by McQuillin et al. (1975) is shown in Figure 6.3. The near circular Bouguer anomaly over the Blackstones Bank reaches a maximum of 140 mgal. This value is almost twice the maximum gravity anomaly observed in Mull and Skye (see Chapters 4 and 5). McQuillin et al. (1975) interpreted the profiles I, II and III of Figure 6.3 in terms of vertical cylinders having a density contrast of 0.35 g/cm^3 (Figure 6.4). The cylindrical models have radii in the range 7-8 km, depth to the base in the range 22-30 km and depth to the top in the range 0-2 km. In the interpretation of the profile III the effect due to the Mesozoic rocks in the south-eastern part of the Blackstones Bank was included. McQuillin et al. (1975) also interpreted the profile I in terms of truncated cones having a density contrast of 0.35 g/cm^3 (Figure 6.5).

McQuillin and Bacon (1974) carried out a deep seismic investigation in sea areas around Scotland. During this investigation they surveyed a reflection line over the Blackstones Bank (line cd, Figure 6.3). McQuillin et al. (1975) presented a processed seismic section of this line which shows the pluton and overlying sedimentary layers (Figure 6.6). They described the layers 1, 2 and 3 of Figure 6.6. as Quaternary, Tertiary and Mesozoic sediments respectively. As can be seen from the

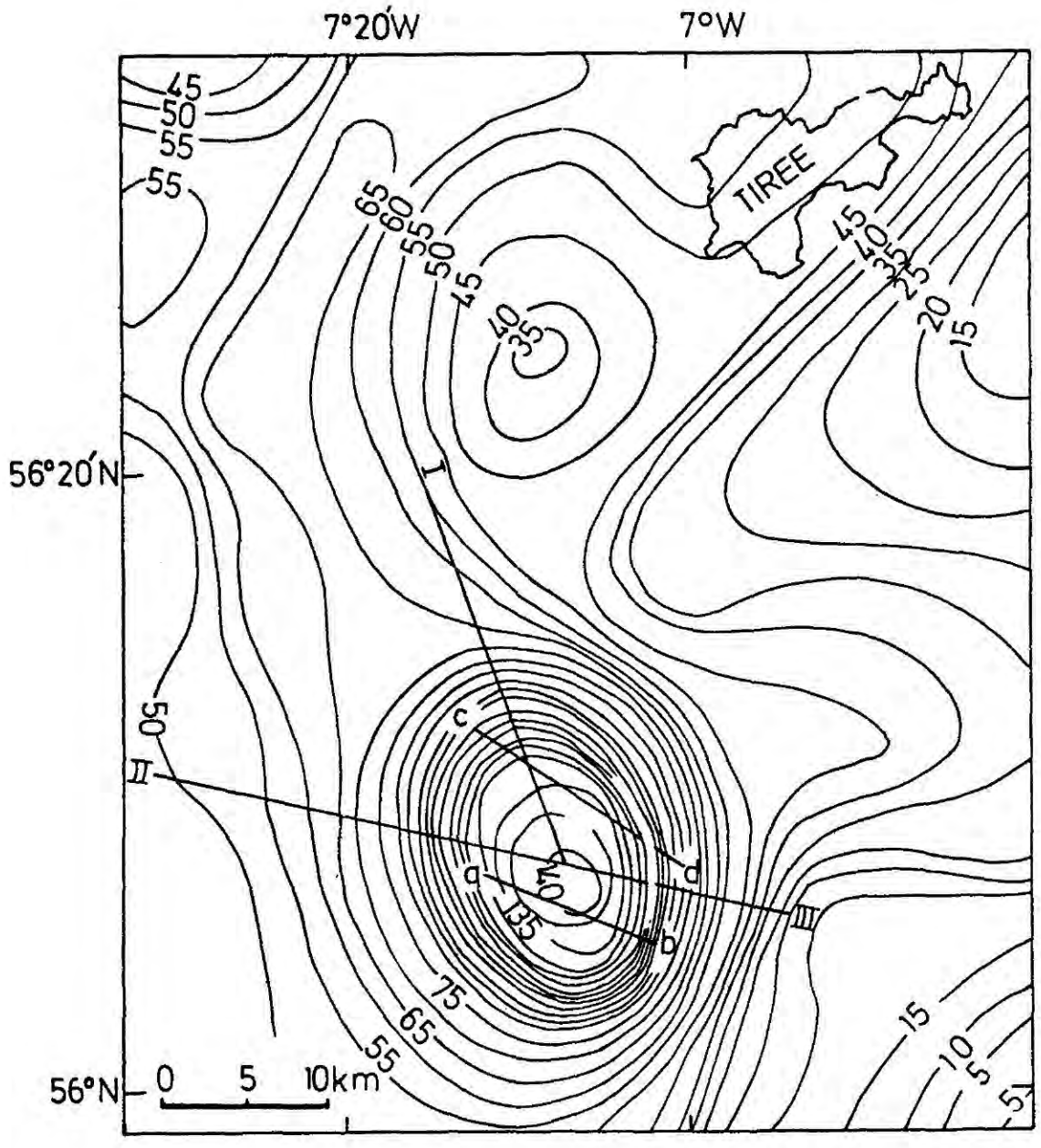

Figure 6.3 Bouguer anomaly map of the Blackstones Bank from McQuillin et al.(1975). Contours in mgal.

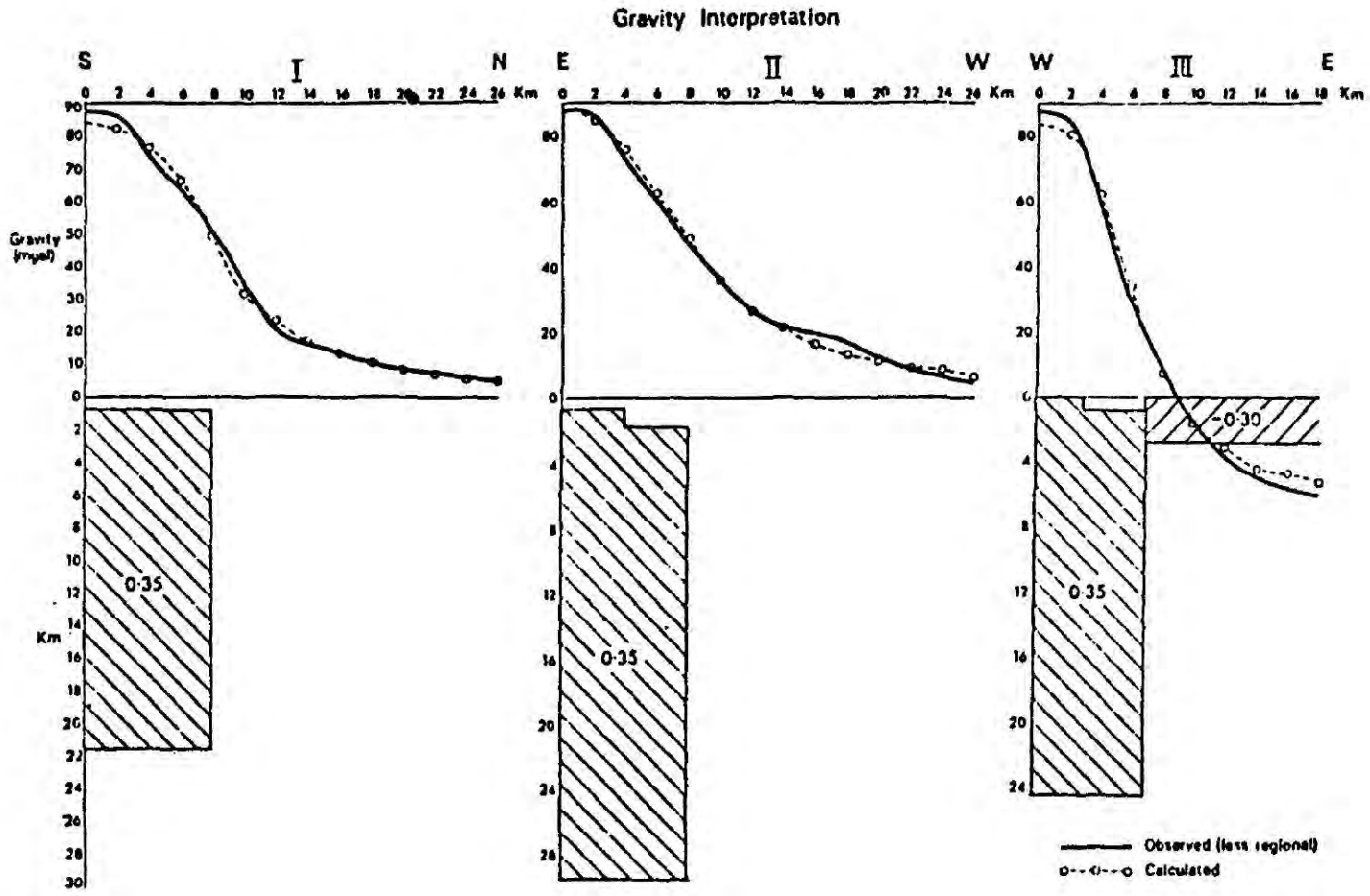

Figure 6.4 Interpretation of gravity profiles I,II,III of Figure 6.3 from McQuillin et al.(1975).Density contrast in g/cm^3.

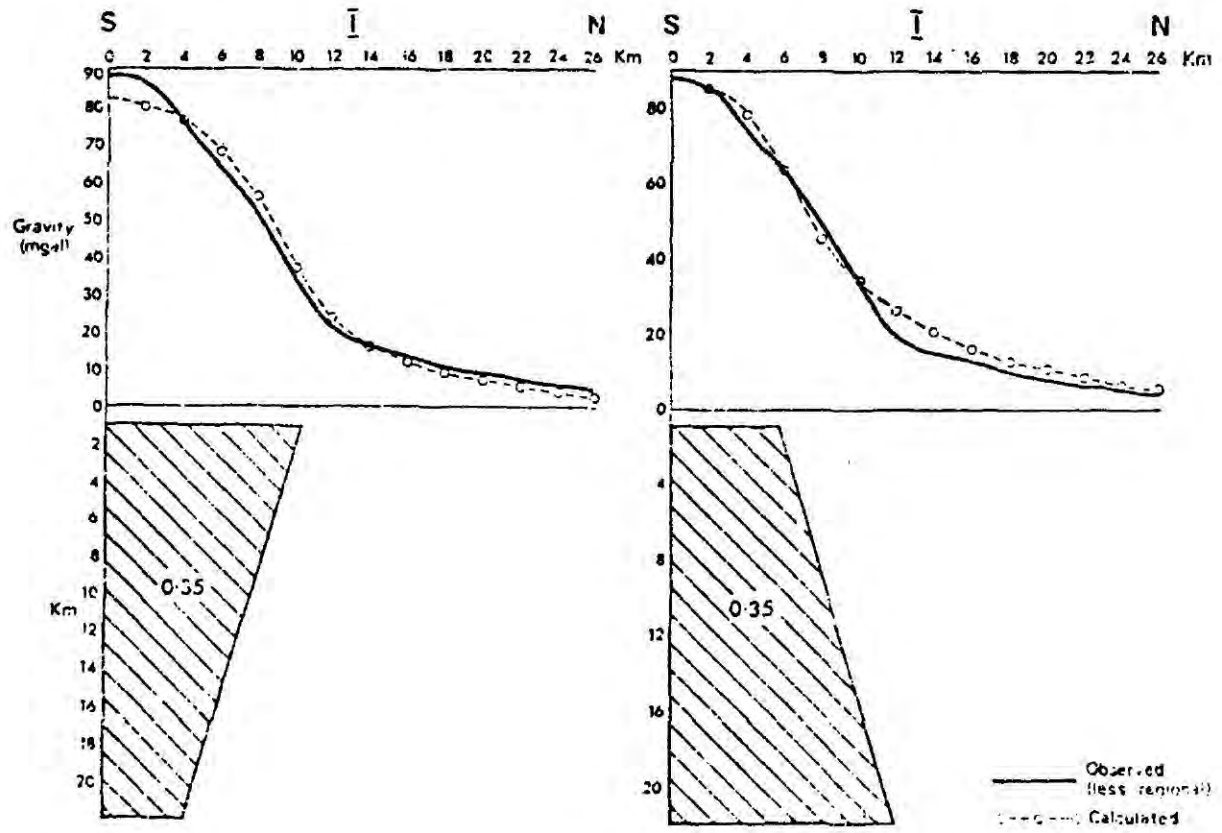

Figure 6.5 Truncated cone interpretation model for gravity profileI of Figure 6.3 from McQuillin et al.(1975). Density contrast in g/cm^3.

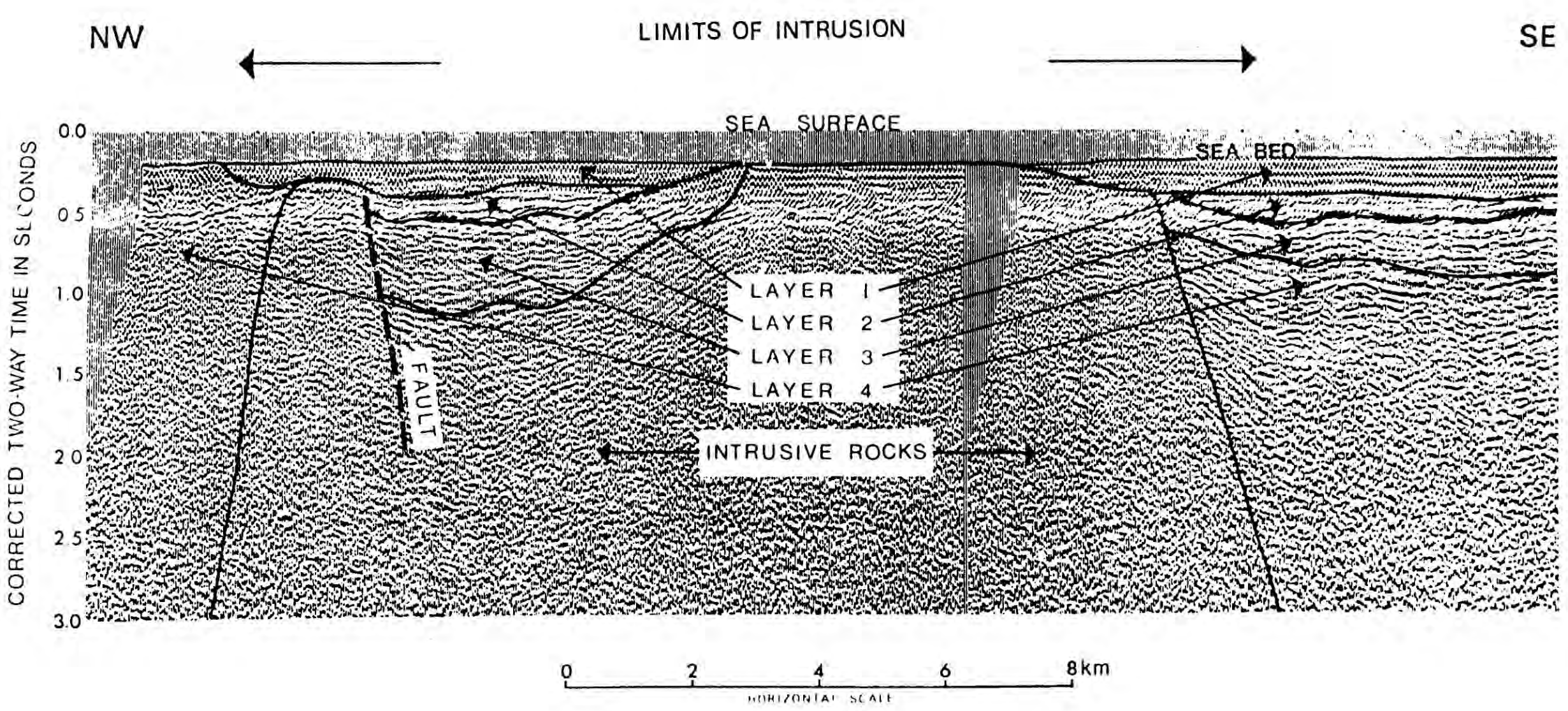

Figure 6.6 Deep seismic section over the Blackstones Bank igneous centre along the line cd of Figure 6.3. *from* McQuillin and Bacon(1974).

seismic section given in Figure 6.6 there is a fault running across the Blackstones pluton and it may postdate the main phase of the intrusion and probably deposition of Tertiary sediments (McQuillin et al. 1975).

McQuillin et al.(1975) also discussed the results of a seismic refraction survey carried out over the Blackstones Bank along the line ab of Figure 6.3. The high velocity material (7.2 km/s), corresponding to a density of 3.09 g/cm^3 was found to lie approximately 0.9 km below the sea level. This is overlain by low velocity material (2.02 km/s). The high velocity material can be identified with the ultrabasic pluton while the low velocity material can be identified with the sedimentary rocks discussed above.

6.4 Interpretation of Magnetic Anomalies over the Blackstones Bank

A pseudogravimetric transformation was performed on the aeromagnetic anomaly map over the Blackstones Bank after digitizing at intervals of 1 km. In this transformation it was assumed that the mean direction of magnetization of rocks in the Blackstones Bank igneous centre is parallel to the present day earth's field, either in the same direction, or reversed, as is the direction of magnetization of rocks of the Mull central intrusive complex (see 4.4). This assumption is made as both complexes may have been emplaced during the same period.

When a pseudogravimetric transformation is performed on a magnetic anomaly map, it is usually arranged that the region of the anomaly under consideration lies in the middle part of map (see 2.7.2). This is because at the edges of the map the anomaly becomes sharply discontinuous and this can give rise to spurious edge effects. In the present work the aeromagnetic anomaly maps prepared by the Institute of Geological Sciences of Great Britain were used. This

aeromagnetic survey was not carried out far to the west of the Blackstones Bank. Therefore in the available aeromagnetic map, the anomalies over the Blackstones Bank appear close to the west boundary. How much this will effect the resulting pseudogravimetric anomaly was examined by transforming magnetic anomalies due to a known sphere shown in Figure 6.7 and Figure 6.8. In Figure 6.7 the prominent features of the magnetic anomaly are in the middle part of the map while in Figure 6.8 these features are close to one of the edges. The pseudogravimetric anomalies of Figure 6.7 and Figure 6.8 are shown in Figure 6.9 and Figure 6.10. Two cross-sections of these pseudogravimetric anomalies are shown in Figure 6.11. As can be seen from these figures there is no serious difference between the two anomalies. The available aeromagnetic anomaly map of the Blackstones Bank is therefore assumed to be suitable for a pseudogravimetric transformation.

The pseudogravimetric anomaly map of the Blackstones Bank is shown in Figure 6.12. This is a negative anomaly having a positive anomaly superimposed on it. This indicates the presence of a large reversely magnetized body possibly with a normally magnetized core. Figures 6.13 and 6.14 show two perpendicular cross-sections of the pseudogravimetric anomaly along AA1 and BB1 and illustrate this further. As can be seen from Figure 6.13 and Figure 6.14 the gradients of the negative part of the pseudogravimetric anomaly decrease gently indicating that the negatively magnetized body extends to a large depth. The positive pseudogravimetric anomaly is superimposed on the central part of the negative anomaly. If the positive part of the anomaly is separated from extrapolated negative anomaly, its amplitude and gradients are accentuated. The body which causes the positive anomaly therefore must be of shallow origin. The corresponding magnetic

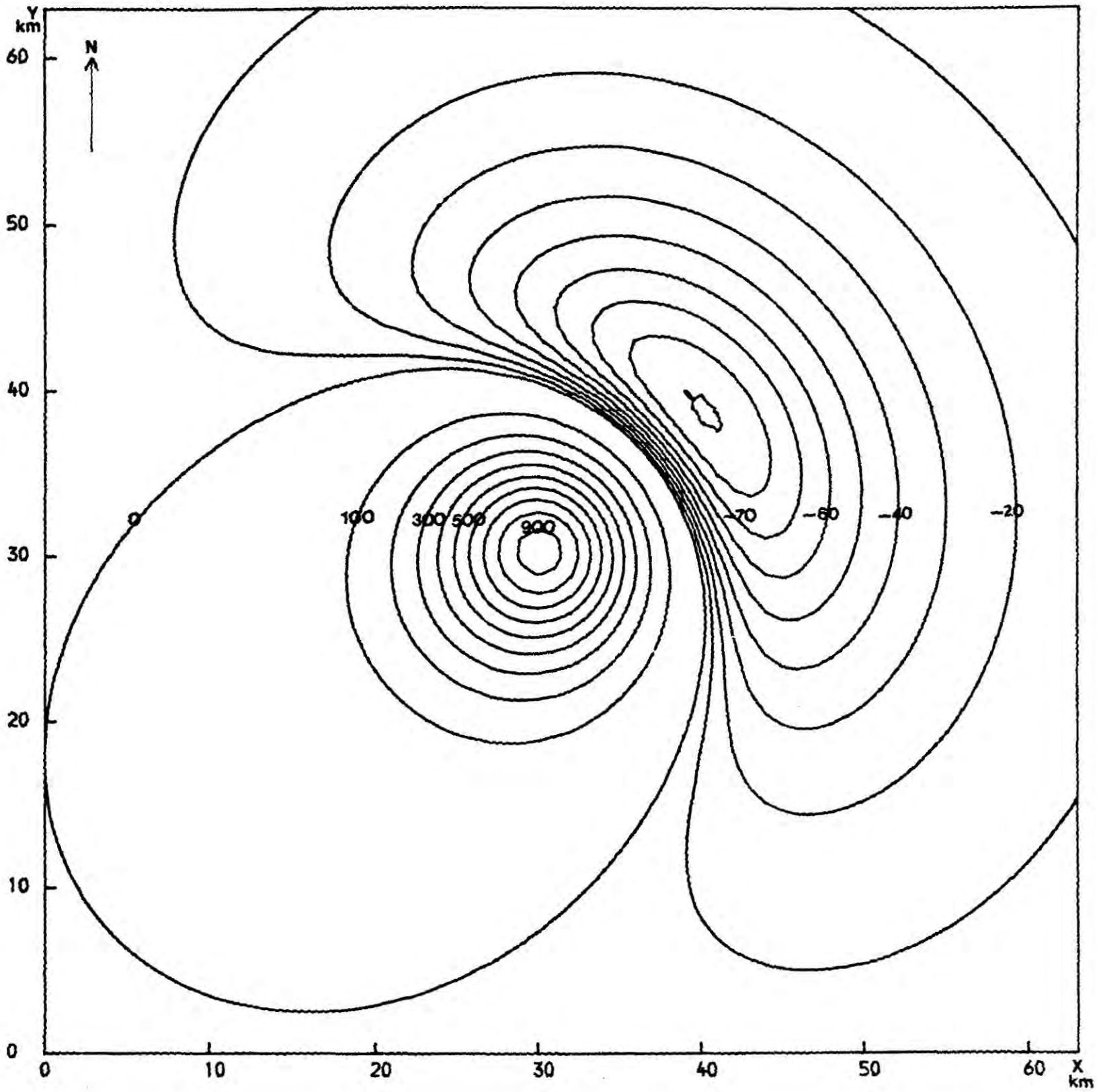

Figure 6.7 Magnetic anomaly due to a sphere having a radius of 5 km and magnetization of 1o A/m. Centre of the sphere is at x=31.5 km, y=31.5 km and z=1o km(vertically downwards). Inclination and declination of the magnetization vector=7o°,4o°. Inclination and declination of the earth's total magnetic field=7o°,4o°. Contours in gamma.

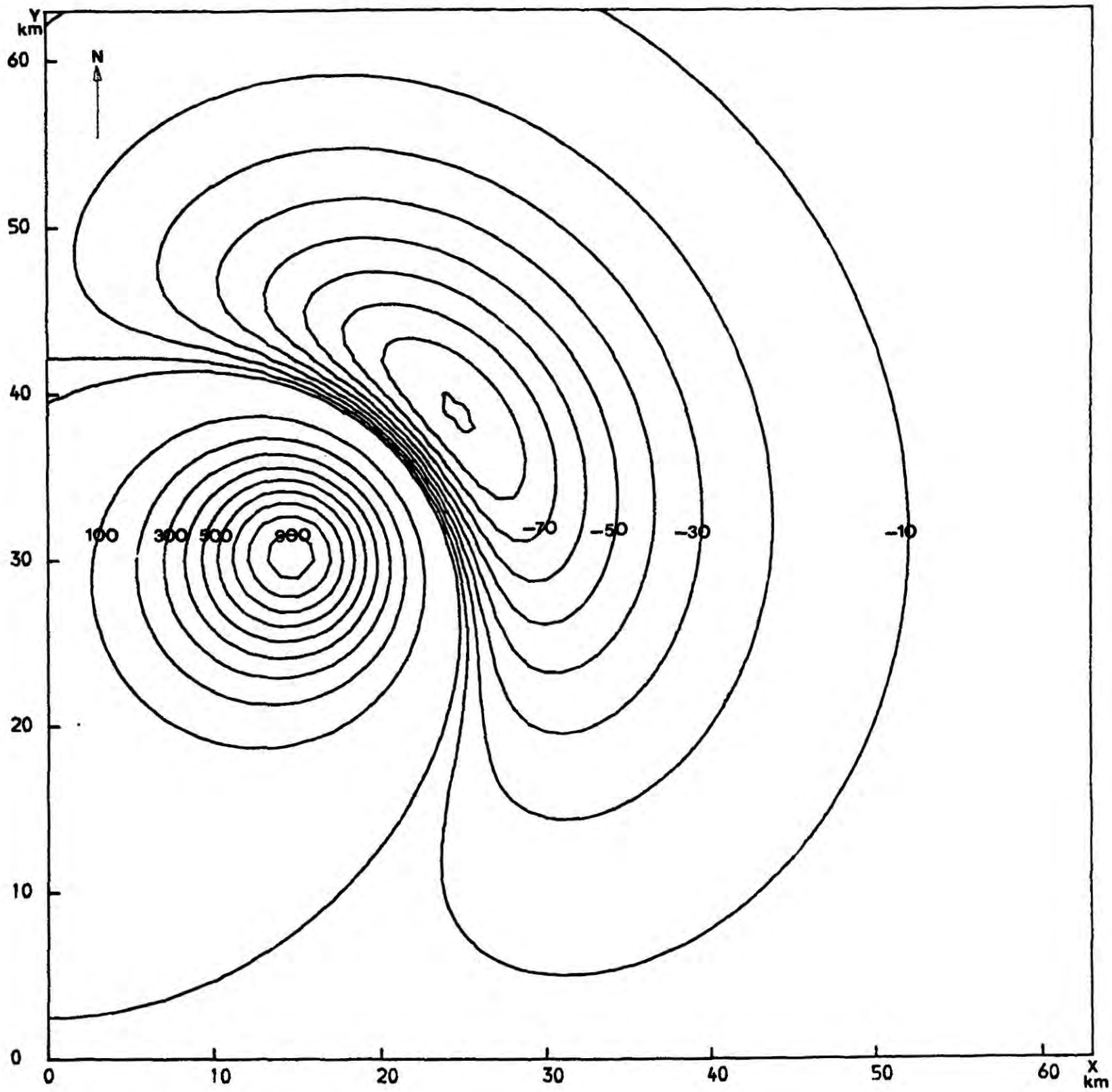

Figure 6.8 Magnetic anomaly due to a sphere having a radius of 5 km and magnetization of 1o A/m. Centre of the sphere is at x=16.o km, y=31.5 km and z=1o km(vertically downwards). Inclination and declination of the magnetization vector=7o°,4o°. Inclination and declination of the earth's total magnetic field=7o°,4o°. Contours in gamma.

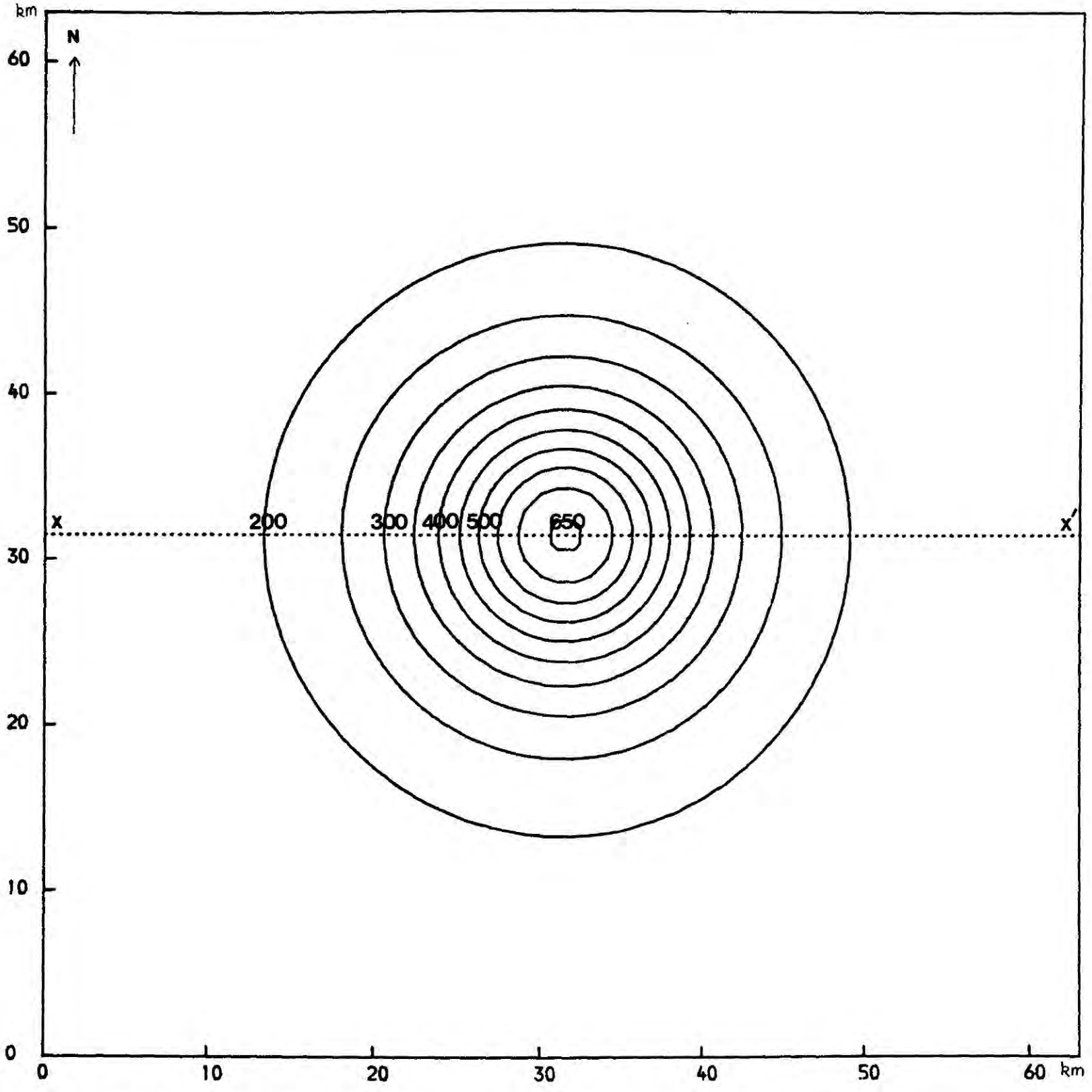

Figure 6.9 Pseudogravimetric anomaly map of the magnetic anomaly shown in Figure 6.7. Contours in mgal.

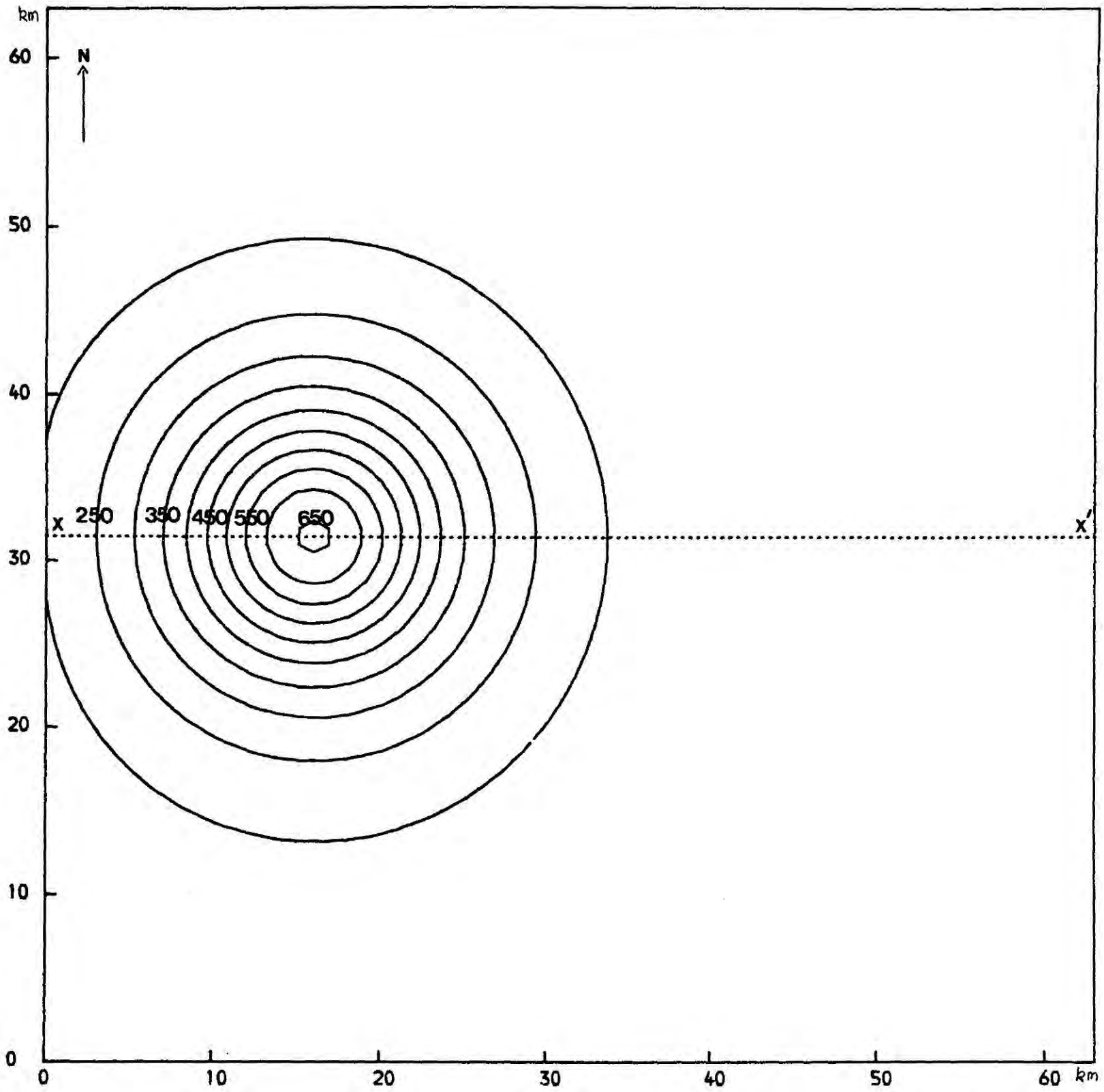

Figure 6.1o Pseudogravimetric anomaly map of the magnetic anomaly shown in Figure 6.8. Contours in mgal.

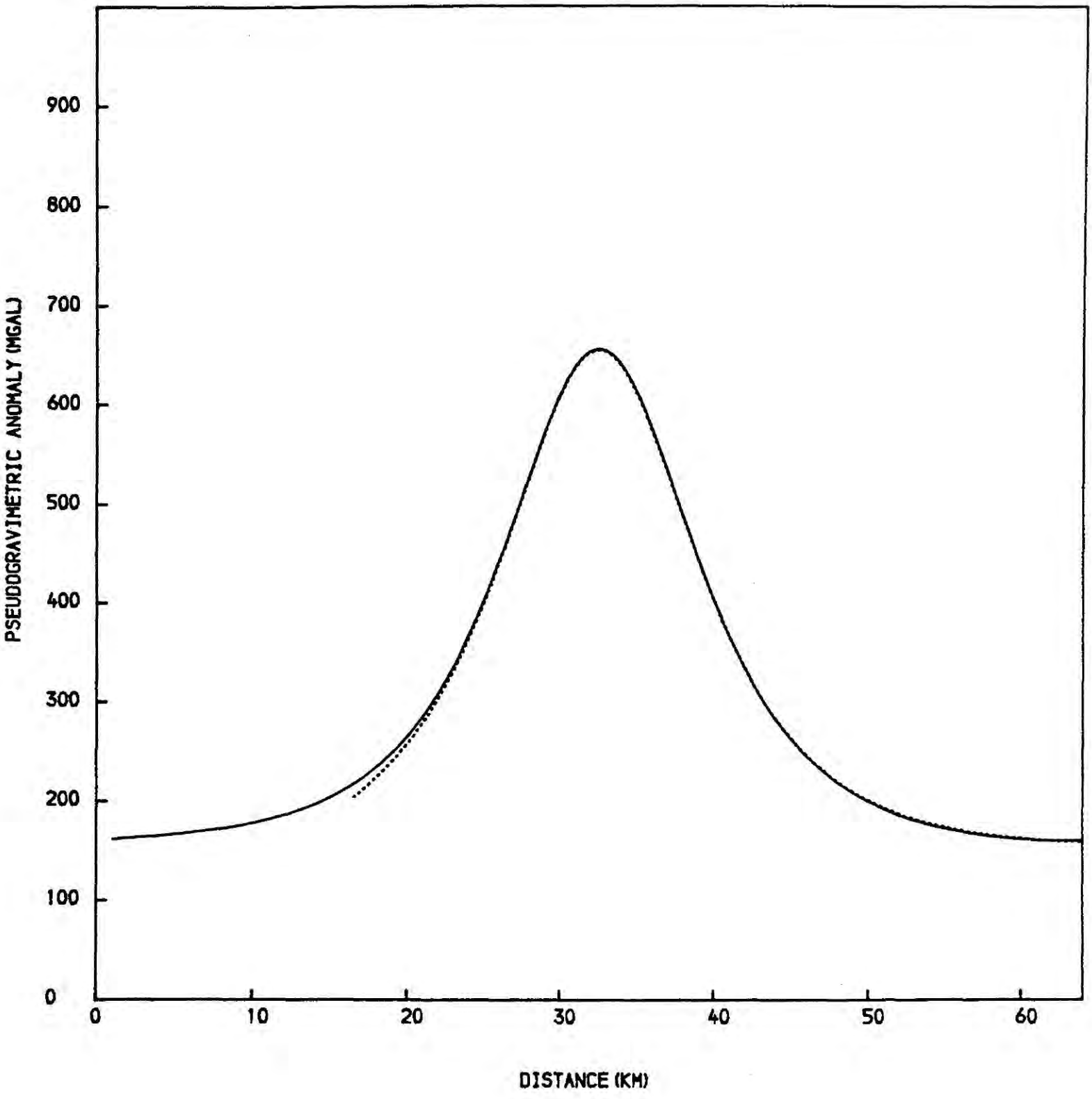

Figure 6.11 —— A cross-section of Figure 6.9 along xx'.

..... A cross-section of Figure 6.1o along xx'.

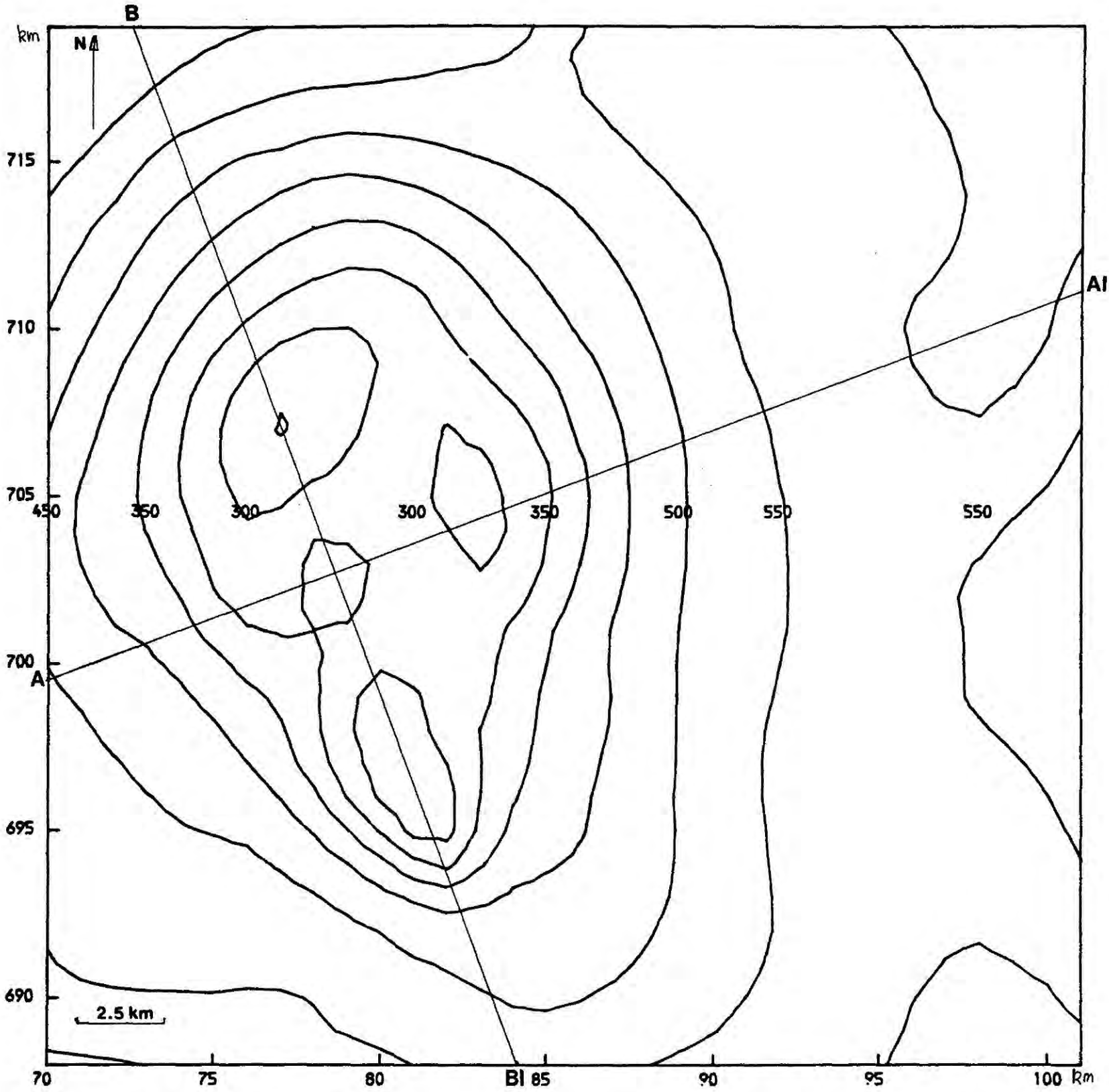

Figure 6.12 Pseudogravimetric anomaly map of the Blackstones Bank, showing contours at 5o mgal intervals. On this and subsequent related figures national grid is shown.

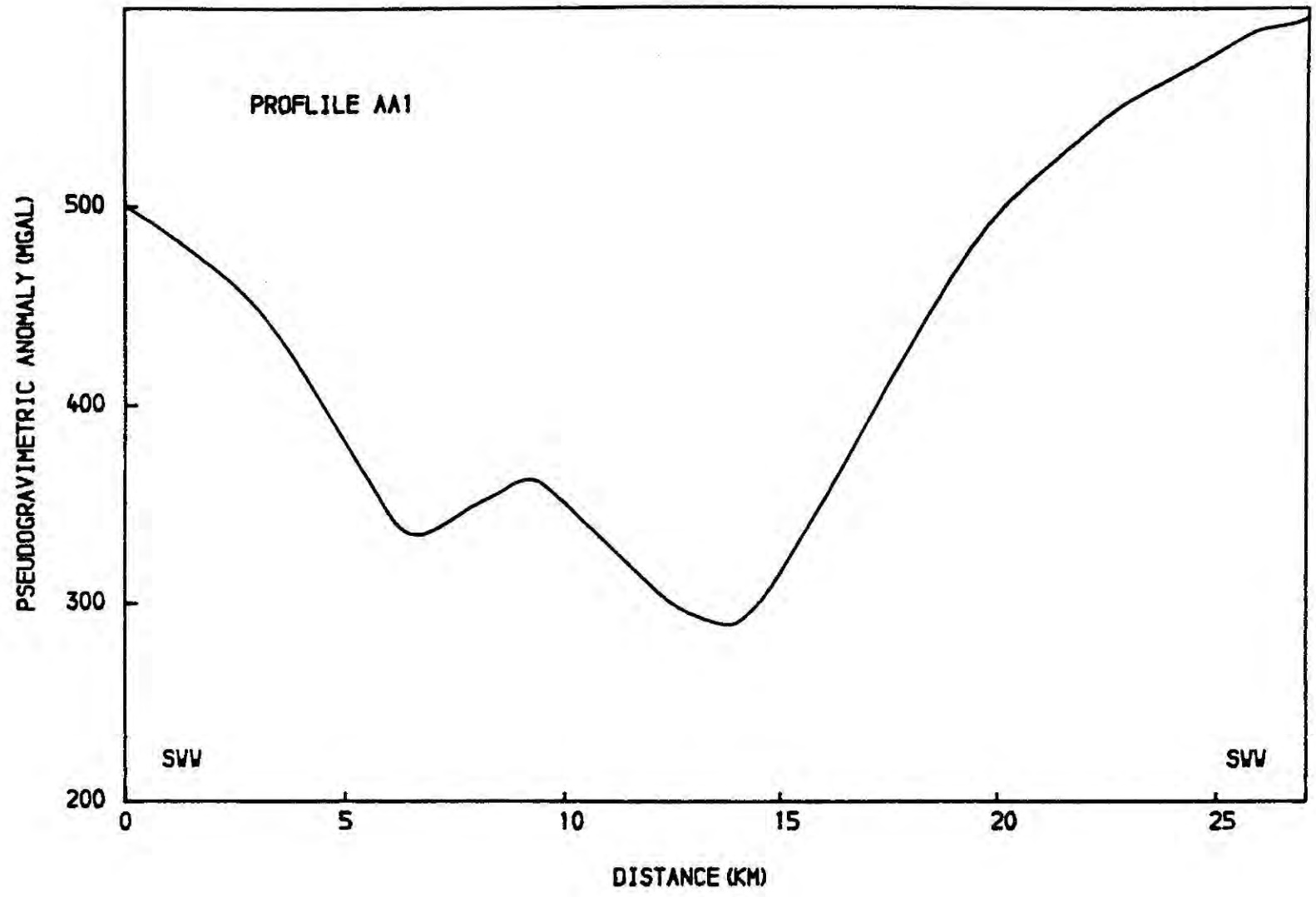

Figure 6.13 A cross-section of the pseudogravimetric anomaly of the Blackstones Bank(Figure 6.12) along AA1.

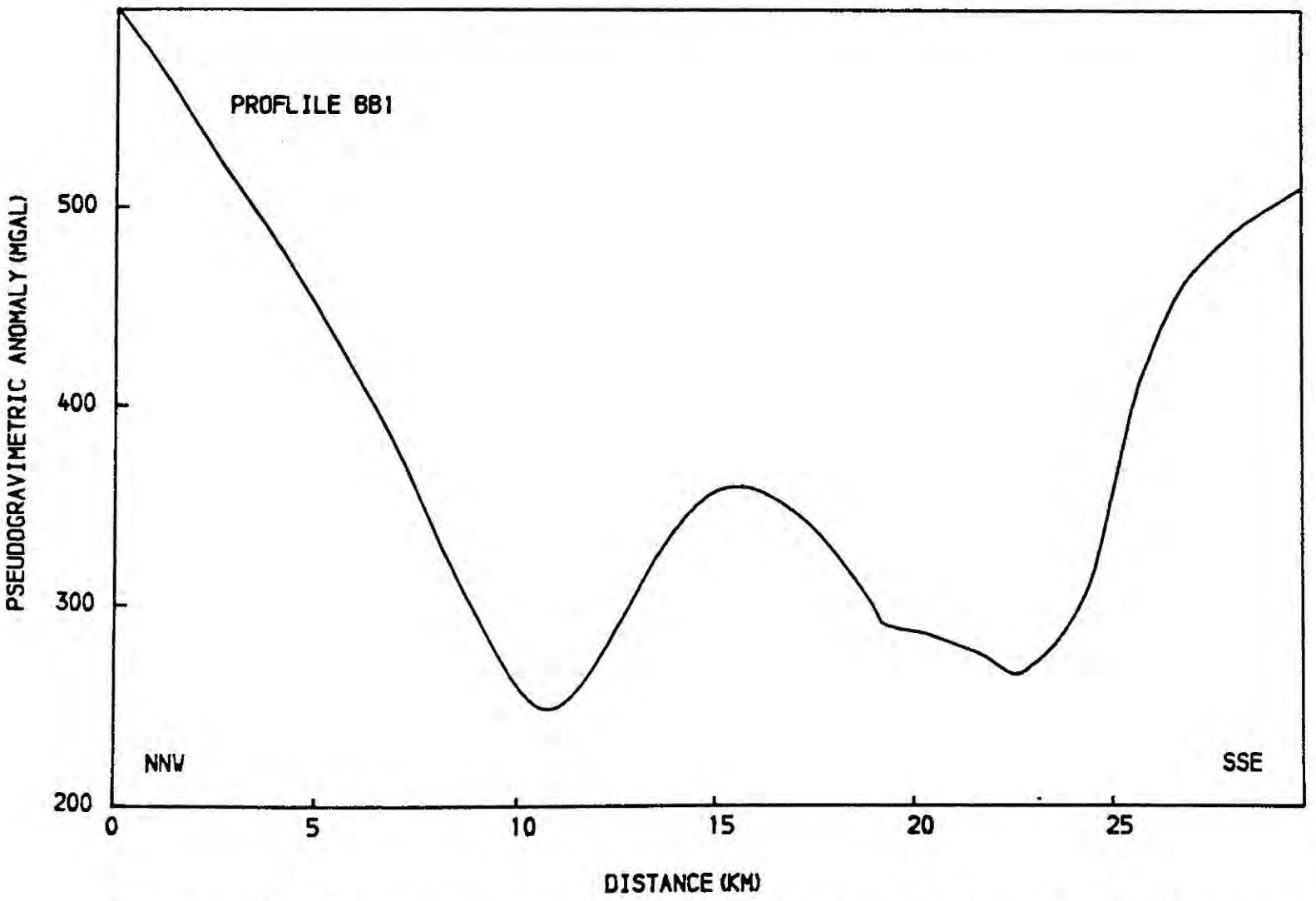

Figure 6.14 A cross-section of the pseudogravimetric anomaly of the Blackstones Bank(Figure 6.12) along BB1.

anomaly of the positive pseudogravimetric anomaly (Figure 6.1) has an irregular shape indicating that it is caused by a body having a variable magnetization.

In Figure 6.15 the pseudogravimetric anomaly and the actual gravity anomaly are shown on the same scale. As can be seen from this figure, both the gravity and pseudogravimetric anomalies extend over approximately equal areas. The gravity and pseudogravimetric profiles along two perpendicular directions are shown in Figure 6.16 and Figure 6.17. Since the gravity anomaly is positive and the pseudogravimetric anomaly is dominantly negative, in Figure 6.16 and Figure 6.17 the pseudogravimetric profiles are drawn after reflecting about the X-axis and scaling by a factor of 0.25. The regional level of the pseudogravimetric profiles was adjusted in such a way that it approximately coincides with the regional level of the gravity profiles. But for the effect of the normally magnetized rocks, both gravity and pseudogravimetric anomalies have approximately equal shapes and wavelengths. This similarity between the two anomalies may indicate the fact that the same rock units are producing both the gravity and magnetic anomalies.

A three-dimensional interpretation of the pseudogravimetric profile AA1 of Figure 6.12 was performed using the end correction method (see chapter 3). This interpretation was first performed by using the Fortran routine GREND which uses the trial and error method. Then the results were improved further using the Fortran routine OPGREND which performs the gravity interpretation using a non-linear optimization technique (see chapter 3). The initial model used for the interpretation consisted of two bodies one inside

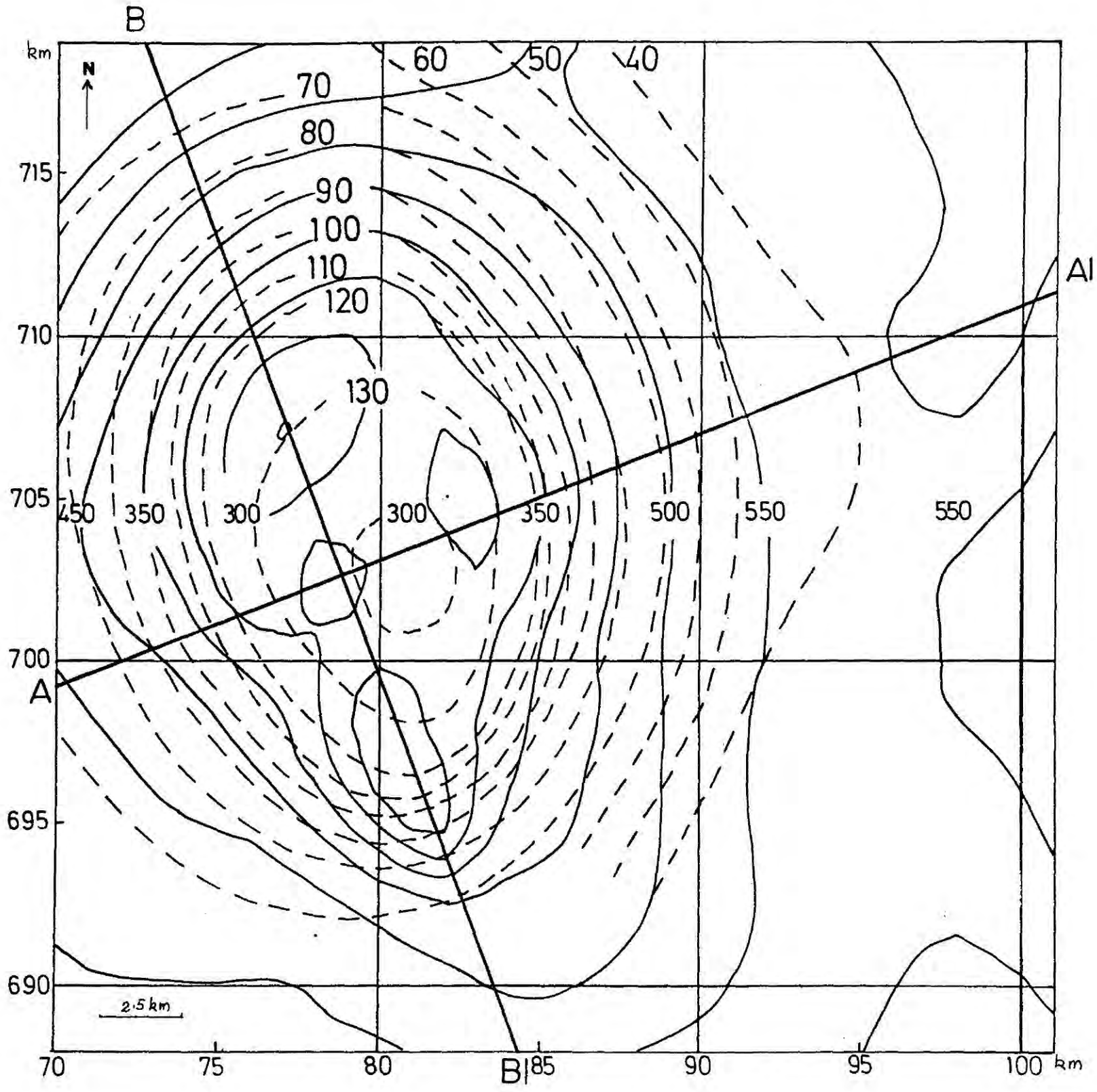

— — Gravity contours (in MGAL)

—— Pseudogravimetric contours (in MGAL)

Figure 6.15 Map showing gravity and pseudogravimetric anomalies over the Blackstones Bank.

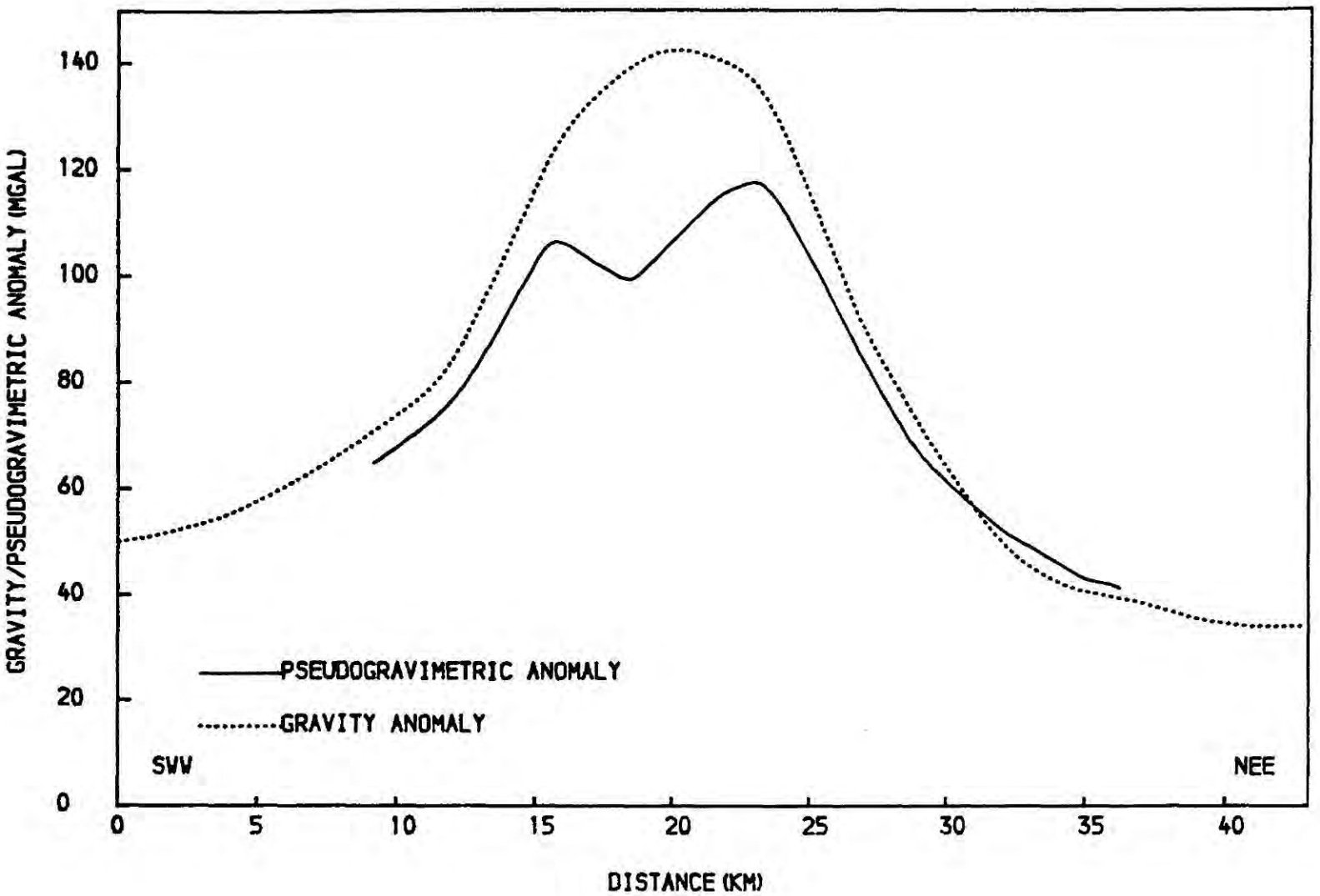

Figure 6.16 Gravity and pseudogravimetric anomaly profiles over the Blackstones Bank(Figure 6.15) along AA1. The pseudogravimetric profile was drawn after reflecting about the x-axis and scaling by a factor of 0.25. The regional level of the pseudogravimetric profile was adjusted in such a way it approximately coincides with that of the gravity profile.

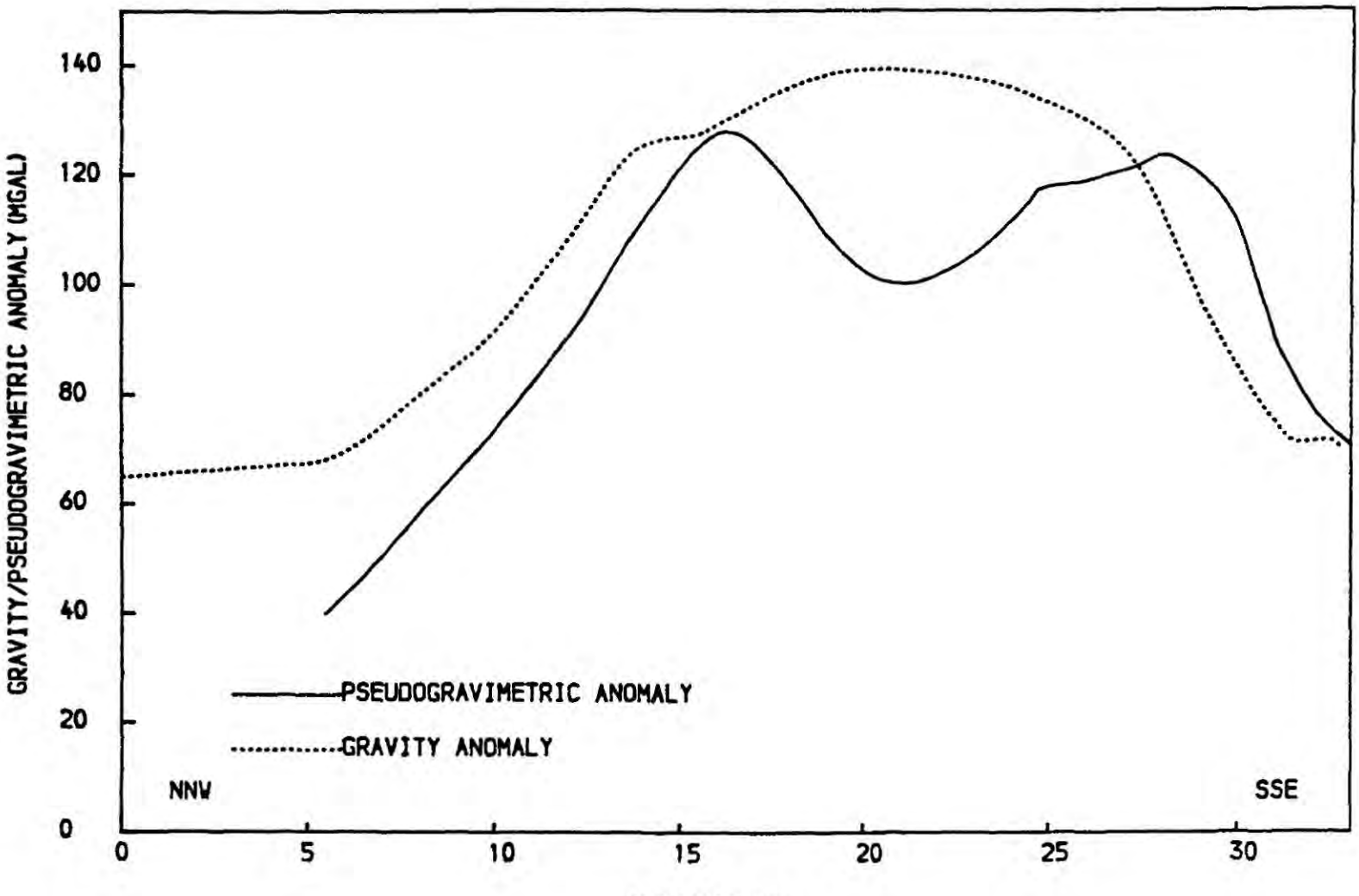

Figure 6.17 Gravity and pseudogravimetric anomaly profiles over the Blackstones Bank(Figure 6.15) along BB1. The pseudogravimetric profile was drawn after reflecting about the x-axis and scaling by a factor of o.25. The regional level of the pseudogravimetric profile was adjusted in such a way it approximately coincides with that of the gravity profile.

the other. It was mentioned in 3.2 that to apply the end correction method it is necessary to divide the body into a number of elements. Figure 6.18 shows how this division was performed. In Figure 6.18 thicker lines divide the body ABCDEF while the lighter lines divide the body PQRS. The total pseudogravimetric anomaly due to the model was calculated as follows. First the pseudogravimetric anomaly due to the reversely magnetized body ABCDE was calculated without considering the normally magnetized inner part PQRS. Then the pseudogravimetric anomaly due to the normally magnetized part was separately calculated and added to the above result. If P_1 and P_2 are the density contrasts used in calculating the anomalies due to ABCDE and PQRS respectively, then the actual density contrast of PQRS is $P_1 + P_2$.

The results of this interpretation are presented in Figure 6.19. The negatively magnetized body in the model takes the approximate shape of a truncated cone having widths of 9.4 km parallel to the profile and 15.0 km in the perpendicular direction at the top surface. The corresponding dimensions at the base are 13.3 km and 18.0 km respectively. This body extends to a depth of 15 km and has a magnetization of 0.93 A/m. The normally magnetized middle part also takes the approximate shape of a truncated cone, has a magnetization of 2.47 A/m. The widths of the body at the top surface along the direction of the profile and along the perpendicular direction are 1.7 km and 6.0 km respectively. At its base these dimensions are 7.5 km and 6.3 km respectively. The body extends to a depth of 1.0 km. This body cannot be shallower than 1 km as the fits obtained for such cases were not good. Another model for the Blackstones Bank igneous centre was obtained by using zero magnetization for the inner body. In this model, the assumed non-magnetic inner body extends to a depth of 5.0 km and the reversely

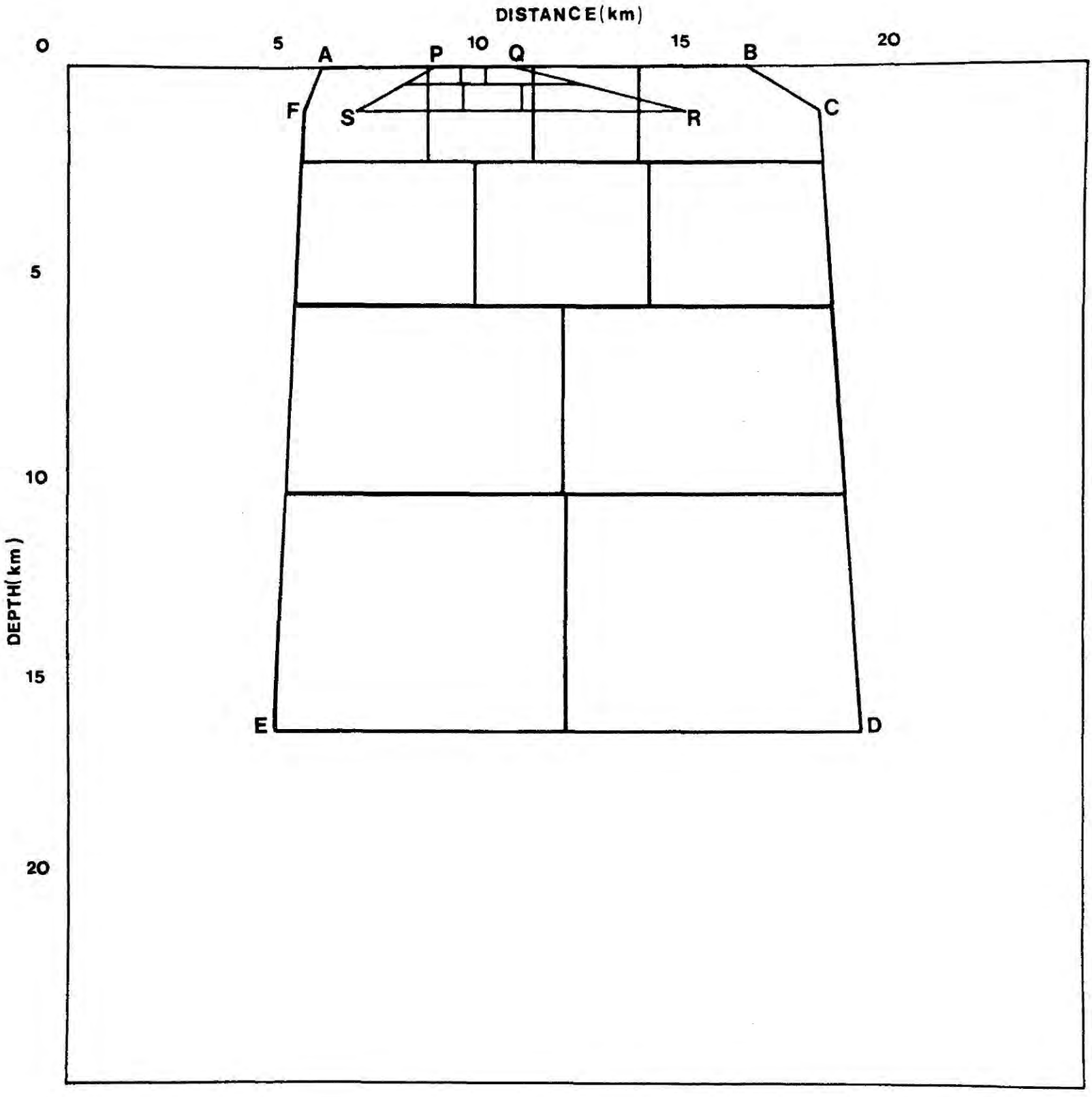

Figure 6.18 Subdivision of the model of Figure 6.19 for application of end corrections.

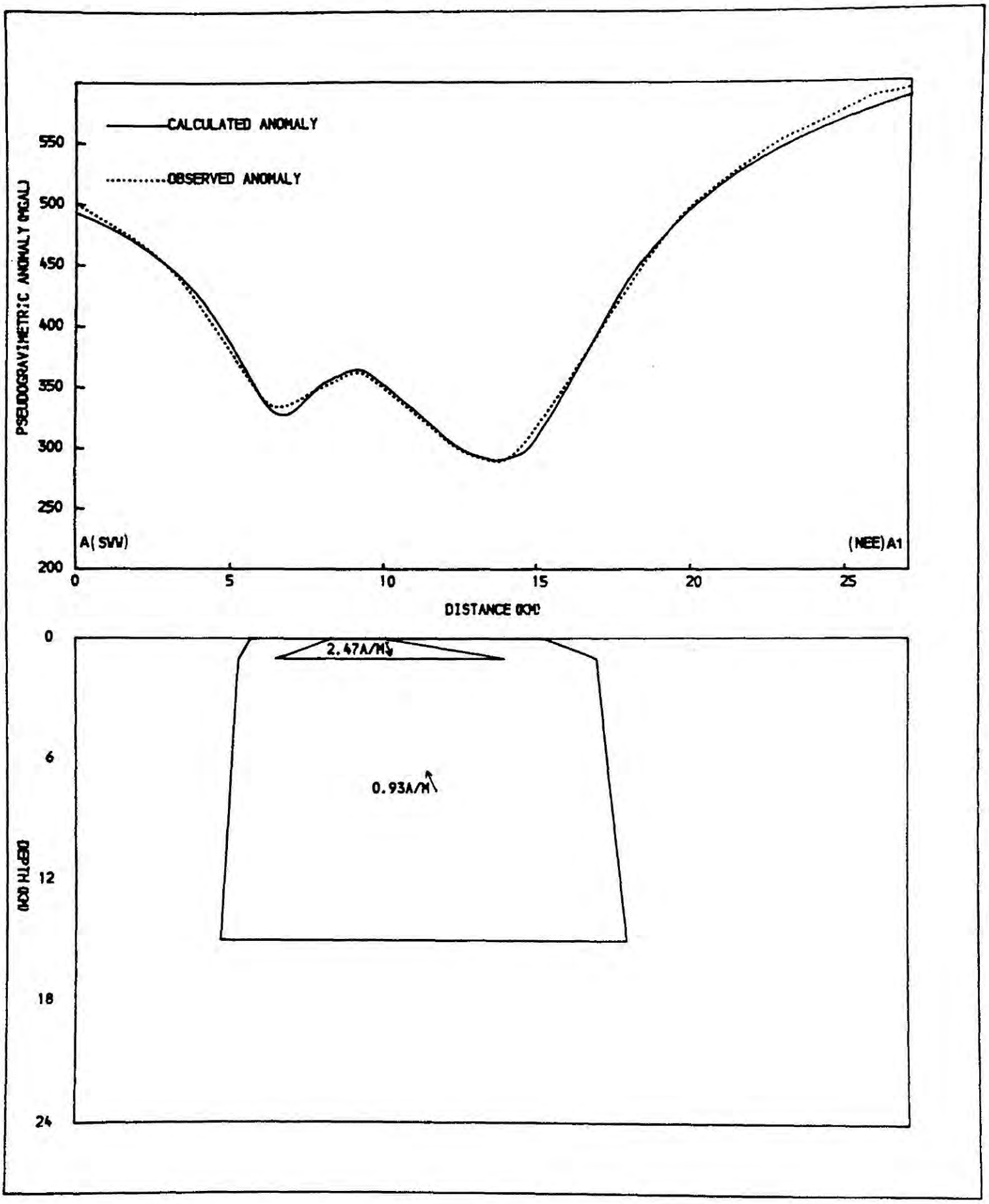

Figure 6.19 Interpretation of the pseudogravimetric profile AA1 of Figure 6.12.

magnetized outer body extends to a depth of 15 km as in the previous model. The depth to which the normally magnetized body extends would therefore be in the range 1.0 - 5.0 km.

It is useful to compare the results of this interpretation with results of a gravity interpretation of the Blackstones Bank igneous centre. McQuillin et al (1975) presented a gravity interpretation of the Blackstones Bank in terms of vertical cylinders and truncated cones which are symmetrical about their axes. As can be seen from Figure 6.3 the gravity anomaly over the Blackstones Bank is not symmetrical. In addition, none of the profiles interpreted by McQuillin et al (1975) lies along the same line as the pseudogravimetric profiles used for the present interpretation. Therefore it was decided to interpret a gravity profile along AA' of Figure 6.15, which lies on the same line as the pseudogravimetric profile used for the interpretation, in terms of a three-dimensional body. This interpretation was also performed by use of the Fortran routines GREND and OPGREND and the results are shown in Figure 6.20. The body which produces the positive anomaly is modelled in terms of a truncated cone which extends to a depth of 20 km having a density contrast of 0.33 g/cm^3. The widths of the body parallel and perpendicular to the profile are 11.5 km and 15 km respectively at the top surface and 19.0 km and 20.0 km respectively at the base. The effect due to the Mesozoic rocks to the S.E. of the Blackstones Bank was also included in this interpretation. These Mesozoic rocks extend over a large area and therefore they were interpreted in terms of a two-dimensional body. The density contrast used for the Mesozoic rocks was -0.3 g/cm^3 (McQuillin et al 1975).

Results of the gravity and pseudogravimetric interpretations are shown in Figure 6.21 at the same scale. The body which produces the

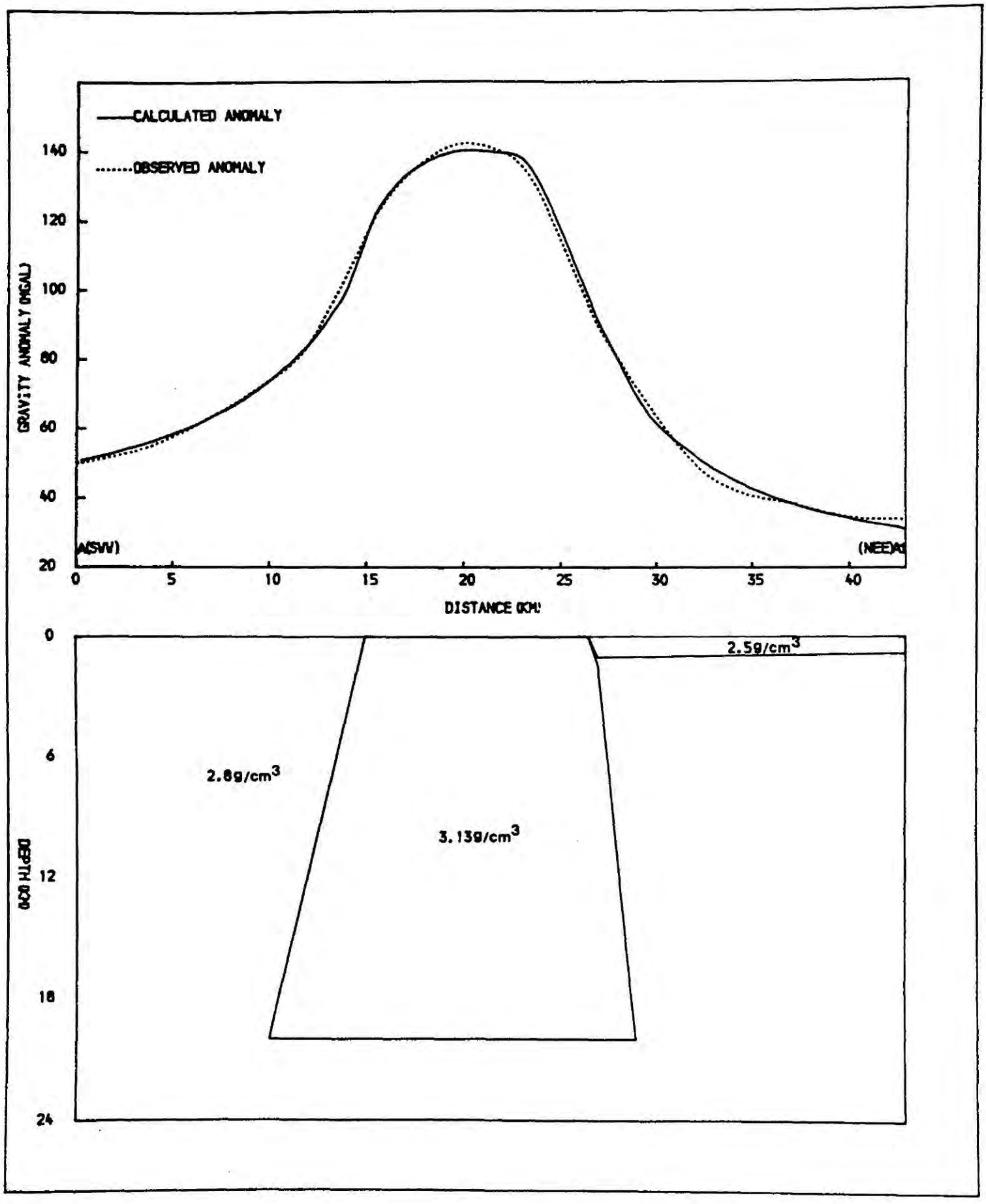

Figure 6.2o Interpretation of the gravity profile AA1 of Figure 6.15.

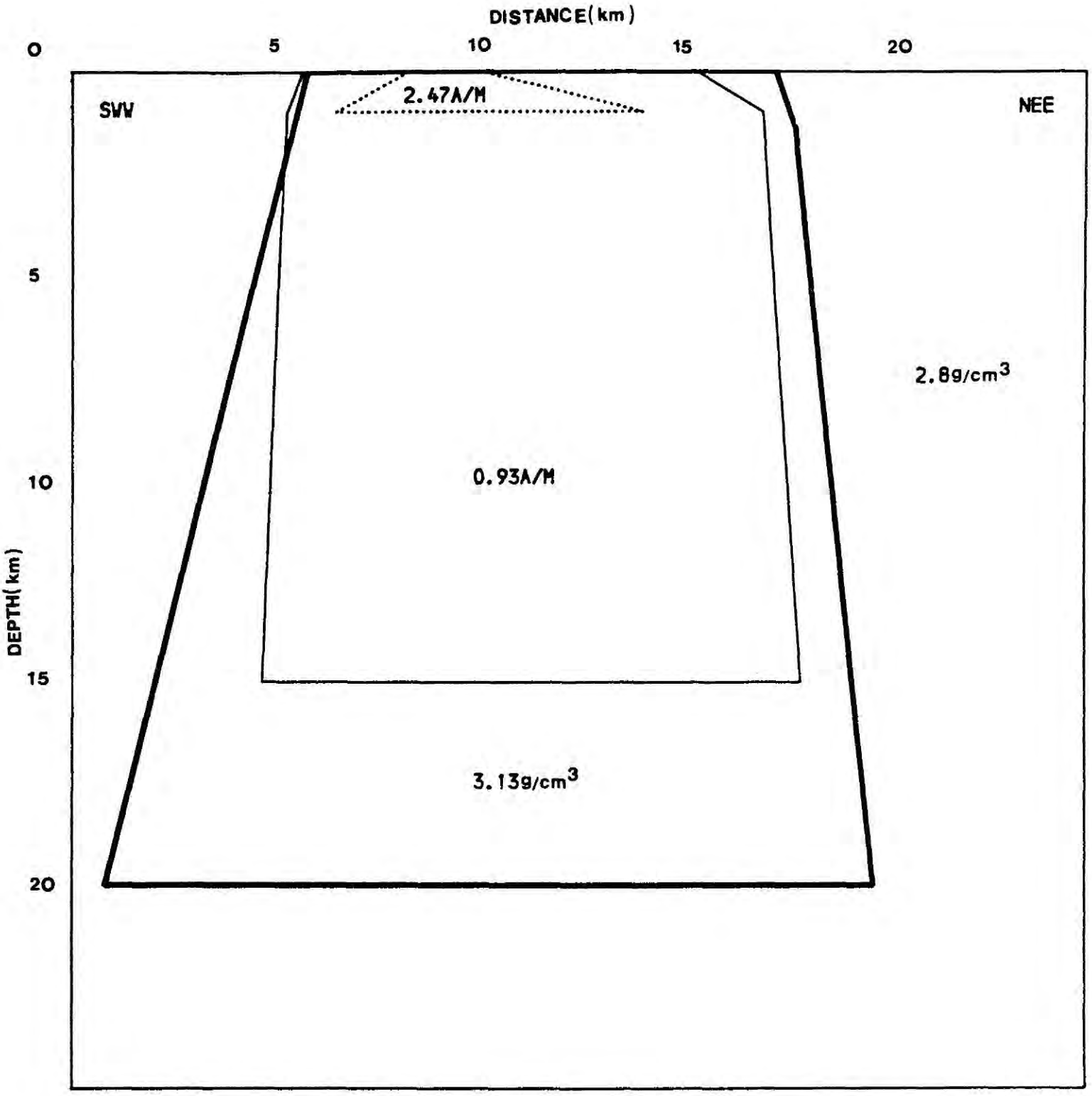

Figure 6.21 Comparison of results of the gravity and pseudogavimetric interpretations of the Blackstones Bank.

..... normally magnetized body,

——— reversely magnetized body,

━━━ body obtained from the gravity interpretation.

gravity anomaly extends to a larger depth than the body which produces the magnetic anomaly. The lateral extent of these two bodies are approximately equal.

6.5 Discussion

The ultrabasic pluton forming the Blackstones Bank subsurface structure was modelled in terms of a body which extends to a depth of 20 km and having a density contrast of 0.33 g/cm^3. Assuming a density of 2.8 g/cm^3 for the surrounding Lewisian rocks, the density of the model body becomes 3.13 g/cm^3. This density is consistent with the observed seismic velocity of 7.2 km/s of the pluton (McQuillin et al, 1975) and it is fairly close to the density of ultrabasic rocks of Rhum (Bott and Tuson, 1973). Only the first 15 km of the body contributes to the observed magnetic anomaly and it is reversely magnetized. This reversely magnetized upper part has a normally magnetized core. The depth to which the normally magnetized core extends is in the range 1.0 - 5.0 km. The presence of bodies with opposite magnetic polarities in the Blackstones Bank igneous centre indicates that it was active at least for two successive reverse and normal polarity periods of the earth's magnetic field. Both the gravity and the pseudogravimetric anomalies of the Blackstones Bank are elongated along N.W. - S.E. axis. This might probably indicate the presence of more than one localized centre in the Blackstones Bank similar to other igneous complexes in the Hebridian province.

CHAPTER 7

SUMMARY AND CONCLUSIONS

7.1 Development of Methods

A method of transforming magnetic anomalies into pseudogravimetric anomalies has been developed. This method first calculates the pseudogravimetric potential by integrating the magnetic anomaly along the direction of the earth's total field and along the direction of magnetization. Then it calculates the pseudogravimetric anomaly by taking the vertical derivative of the pseudogravimetric potential. Using the fact that the magnetic anomaly must satisfy Laplace's equation, it can be shown that these operations of differentiation and integration are equivalent to finding the inverse Fourier transform of the product of the Fourier transform of the magnetic anomaly and an appropriate kernal (Chapter 2). This is illustrated in Figure 7.1. The transformations between the spatial and frequency domains were performed using a fast Fourier transform algorithm.

The pseudogravimetric transformation is useful in interpreting complicated magnetic anomalies as it removes characteristic short wavelength features present in a magnetic anomaly and it makes the anomaly symmetrical with respect to the causative body. It also allows the interpretation to be carried out using gravity methods which are more straightforward to apply compared to magnetic methods.

An automatic end correction method was developed to interpret gravity and pseudogravimetric anomalies in three dimensions. The end correction method has the advantage of approximately calculating the gravity or magnetic anomaly due to a three dimensional body at small expense in computing time compared to the detailed three dimensional calculations. Methods of interpreting magnetic anomalies in two dimensions using non-linear optimization techniques were developed.

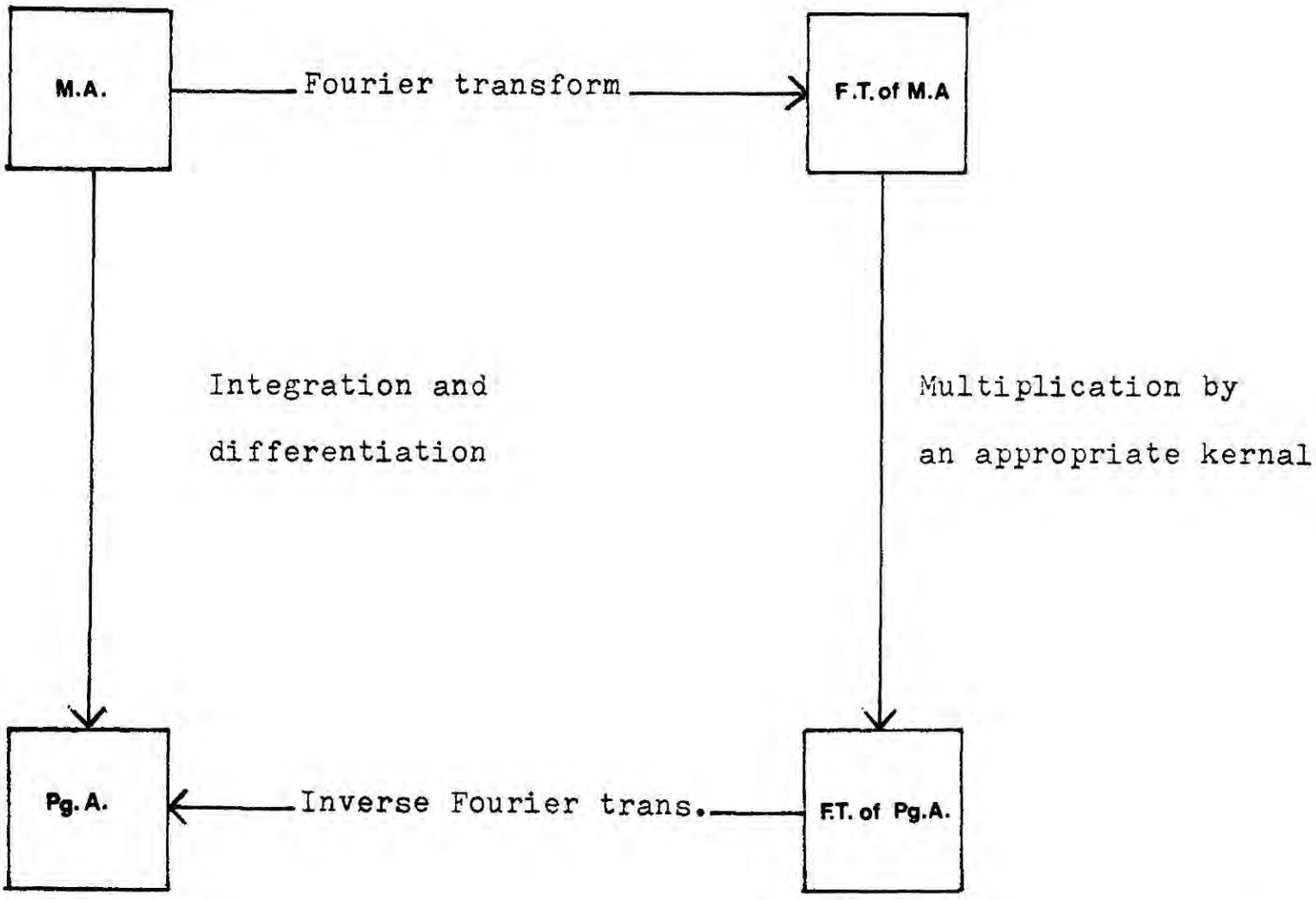

Figure 7.1 The equivalence of direct and Fourier transform procedures for determining the pseudogravimetric anomaly.

M.A. Magnetic anomaly,

F.T. Fourier transform,

Pg.A. Pseudogravimetric anomaly.

The end correction factor for magnetic interpretation was also derived.

7.2 Applications to Tertiary Igneous Centres

Aeromagnetic anomalies over the Mull, Skye and the Blackstones Bank igneous centres were transformed into pseudogravimetric anomalies. The pseudogravimetric anomalies were compared with the actual gravity anomalies of the three igneous centres and interpreted in terms of three dimensional bodies using the end correction method. The results of the interpretations were discussed and compared with previous geophysical and geological studies of the igneous centres. Owing to the ambiguity inherent in the gravity and magnetic interpretation, the models obtained are not unique. There can be other models which equally satisfy the observations as well as being geologically realistic. However, the main features of models obtained by the present interpretation should be common to all the possible models.

The aeromagnetic anomaly map of the Mull igneous complex consists of three main features. These are the large, dominantly positive anomaly over the Mull central intrusive complex, negative anomalies over the basaltic lavas and a ring of narrow positive and negative anomalies outside the central intrusive complex. The prominent feature of the pseudogravimetric anomaly is the large positive anomaly over the central intrusive complex. This anomaly has steep gradients indicating shallow origin of the causative body. The extent of the central positive pseudogravimetric anomaly is small compared to the extent of the actual gravity anomaly. The pseudogravimetric anomaly was interpreted in terms of a body having an approximated shape of a truncated cone which extends to a depth of 2.1 km, having a magnetization of 6.7A/m. The gravity model of the Mull igneous complex (Bott, private communications) extends to a depth of 14km and its horizontal dimensions are larger than that of the model obtained by the pseudogravimetric interpretation. The subsurface structure of the Mull igneous complex therefore must consists

of a highly magnetized core surrounded by more weakly magnetized rocks. The negative anomalies outside the central intrusive complex are caused by the basaltic lavas and the ring of positive and negative anomalies outside the complex is interpreted in terms of a ring of intrusive dyke-like bodies which do not outcrop.

The aeromagnetic anomaly map over the Skye igneous complex consists of intense negative anomalies over the Cuillin centre and over the basaltic lavas situated N.W. of the centre and an extensive positive anomaly over the Eastern and Western Red Hills centres. The pseudogravimetric anomaly obtained by transforming the magnetic anomaly shows similar features at corresponding places. The negative pseudogravimetric anomaly over the Cuillin centre has steep gradients suggesting that it may be due to outcropping basic and ultrabasic rocks of this centre. The positive anomaly over the Red Hills has gentle gradients and therefore it is probably not due to the outcropping rocks of the Red Hills beyond which it extends. The positive anomaly has been attributed to unexposed magnetic rocks situated below the whole complex. A three dimensional interpretation of the pseudogravimetric anomaly was performed using the end correction method. The model obtained essentially consists of two bodies. One of them can be identified with the basic and ultrabasic rocks of the Cuillin centre. This body, which takes an approximate shape of a truncated cylinder, has a width of 8 km and a base which deepens towards the S.W. from 1.5-3.0 km. The body is reversely magnetized and has an interpreted magnetization of 4.9A/m. The other body is situated below the Red Hills and takes the approximate shape of a truncated cone extending to a depth of 14km. This body has a magnetization of 1.1 A/m and it is normally magnetized. The interpretation shows that the Red Hills granites are shallow and weakly magnetized. Basaltic lavas with reverse magnetization situated west of the Cuillin

centre were also incorporated in the interpretation. The pseudogravimetric interpretation confirms the results of the previous gravity interpretation of the Skye igneous complex (Bott and Tuson, 1973) which showed the existence of a large basic body in the subsurface.

The aeromagnetic and pseudogravimetric anomalies of the Blackstones Bank are dominantly negative with a narrow positive anomaly superimposed at the central part. When compared with the actual gravity anomaly over the Blackstones Bank, it can be seen that both the gravity and pseudogravimetric anomalies extend over approximately equal areas and cross-sections have approximately equal widths. This suggests that the same rock units are essentially producing both the gravity and magnetic anomalies. Two extreme models were obtained by interpreting the pseudogravimetric anomaly. These two models consist of two bodies, one inside the other, and both the bodies take the approximate shape of a truncated cone. The outer body which is reversely magnetized extends to a depth of 15 km in both models and its magnetization is 0.93 A/m in both models. In one of the models, the inner body extends to a depth of 1km and has a magnetization of 2.47 A/m. It was found that this is the lower limit of the depth to the base as it was difficult to obtain a good fit when the depth to the base was less than this value. The magnetization of the inner body in the second model is zero and it extends to a depth of 5 km. This is the maximum permissible depth to the base of this body. The depth to which the normally magnetized body extends must therefore be in the range 1.0-5.0 km. The gravity model of the Blackstones Bank takes the approximate shape of a truncated cone extending to a depth of 20 km and having a density contrast of 0.33 g/cm^3. Assuming a density of 2.8g/cm^3 for the surrounding Lewisian

rocks, the density of the gravity model becomes 3.13 g/cm^3 which is fairly close to the density of ultrabasic rocks of Rhum (Bott and Tuson, 1973). Both the gravity and pseudogravimetric models have approximately equal horizontal dimensions.

7.3 Comparison of the Centres

High positive Bouguer gravity anomalies have been observed over the Tertiary igneous centres in N.W.Scotland (Bott and Tuson,1973, McQuillin et al. 1975). The observed maximum Bouguer gravity anomaly of the Mull and Skye igneous centre is about 73 mgal while it is about 150 mgal over the Blackstones Bank igneous centre. The amplitude of the gravity anomalies over the Mull and Skye igneous complexes related to an estimated regional level of 20 mgal is about 53 mgal (Bott and Tuson, 1973). Estimated regional level of the Blackstones Bank igneous complex is 50 mgal and the amplitude is therefore about 90 mgal. These intense positive gravity anomalies suggest the existence of massive basic and ultrabasic bodies in the subsurface beneath the Tertiary igneous complexes. Interpretation of the gravity anomalies over the Mull and Skye igneous complexes have shown that they are underlain by basic and ultrabasic bodies extending to a depth of around 14 km (Bott and Tuson, 1973). Gravity anomalies over the Blackstones Bank igneous complex have been interpreted in terms of a ultrabasic body extending to a depth of 20 km. Gravity studies further show that the granitic rocks in the Mull and Skye igneous complexes are fairly shallow and small in volume compared to the basic and ultrabasic rocks.

Intense magnetic and pseudogravimetric anomalies over the Mull, Skye and the Blackstones Bank igneous centres indicate the presence of massive basic and ultrabasic magnetized bodies of large depth extent beneath the subsurface of the complexes. However, the interpretation

of pseudogravimetric anomalies over these complexes show only the Skye and Blackstones Bank igneous centres consist of magnetized bodies as large as the corresponding gravity models. The magnetic model of the Mull complex is smaller and shallower compared to its gravity model and the magnetic models of other two complexes. The magnetic models of both the Skye and Blackstones Bank igneous complexes consist of two bodies with opposite magnetic polarities while the magnetic model of the Mull complex consists of a normally magnetized single body. Nevertheless, it is surrounded by reversely magnetized lavas as in the Skye igneous complex. The magnetic anomaly map of Mull shows a ring of narrow positive and negative anomalies outside the central intrusive complex. There are no such regular features in the magnetic anomaly maps of Skye and Blackstones Bank. Out of the three magnetic models, the magnetic model of the Mull complex has the highest magnetization. Presence of normally and reversely magnetized bodies in all three complexes indicates that the complexes were active at least for successive reverse and normal periods of the earth's magnetic field. The intense negative anomalies over the lavas and some of the intrusive rocks of the igneous complexes demonstrate their strong remanent magnetization. The reverse remanent magnetization of these rocks and lavas is very large and must outweigh the induced magnetization. As indicated earlier, gravity studies show that the granitic rocks of the igneous complexes are shallow and small in volume. The present pseudogravimetric study further shows that the granitic rocks are weakly magnetized compared to the basic and ultrabasic rocks.

7.4 Suggestions for Further Work

Bott and Stavrev (private communications) transformed the magnetic anomalies over the Arran igneous complex into pseudogravimetric

anomalies and performed an interpretation. The pseudogravimetric anomaly map of the Rhum igneous complex has been prepared by the author. This is a negative pseudogravimetric anomaly. The gradient of the anomaly becomes very steep at its central part. This shows the possible existence of a strongly and reversely magnetized shallower body surrounded by weakly and reversely magnetized deeper body in the subsurface of the Rhum igneous complex. It may be of interest to compare the pseudogravimetric anomaly with the actual gravity anomaly and perform an interpretation to investigate this further. A similar study can be carried out on the aeromagnetic anomaly map of the Ardamurchan igneous centre. The pseudogravimetric anomaly over the basaltic lavas of northern Skye changes its sign from positive to negative when going from the east coast to the west coast of the island. This suggests that the direction of magnetization of lavas changes from positive to negative along this direction. It may be useful to interpret a profile of the pseudogravimetric anomaly over the lavas and perform some measurements of the magnetization of the lavas to investigate this idea further.

It was shown in chapter 4 that there is a zone of highly magnetized rocks in central Mull surrounded by more weakly magnetized rocks. A detailed mineralogical study and measurement of magnetic properties of the intrusive complex would also present a scope for further studies.

REFERENCES

Ade-Hall, J.M., Dagley, P., Wilson, R.L., Evans, A., Riding, A., Smith, P.J., Skelhorn, R. and Sloan, T., 1972. A paleomagnetic study of the Mull regional dyke swarm. Geophys. J.R. astr. Soc., 27, 517-545.

Al-Chalabi, M., 1970. The application of non-linear optimisation techniques in geophysics. Ph.D. thesis, Univ. of Durham.

Al-Chalabi, M., 1971. Some studies relating to non-uniqueness in gravity and magnetic inverse problems. Geophysics, 36, 835-855.

Anderson, F.W. and Dunham, K.C., 1966. The geology of northern Skye. Mem. geol. Surv. Scotland.

Bailey, E.B., Clough, C.T., Wright, W.B., Richey, J.E. and Wilson, G.V., 1924. The Tertiary and post-Tertiary geology of Mull, Loch Aline and Oban. Mem. geol. Surv. Scotland.

Baranov, V., 1957. A new method for interpretation of aeromagnetic maps: pseudo-gravimetric anomalies. Geophysics, 22, 359-383.

Baranov, V., 1975. Potential fields and their transformation in applied geophysics. Gebruder Borntraeger, Berlin.

Baranov, V. and Naudy, H., 1964. Numerical calculation of the formula of reduction to the magnetic pole. Geophysics, 29, 67-79.

Bell, J.D., 1966. Granites and associated rocks of the eastern part of the Western Redhills Complex, Isle of Skye. Trans. R. Soc. Edinb., 66, 307-343.

Bell, J.D., 1976. The Tertiary intrusive complex on the Isle of Skye. Proc. geol. Assoc., 87(3), 247-271

Bennett, J.R.P., 1968. Magnetic investigations of the Tertiary central intrusion complex, Isle of Mull. Proc. geol. Soc. 1647, 61-65.

Bhattacharyya, B.K., 1965. Two-dimensional harmonic analysis as a tool for magnetic interpretation. Geophysics, 30, 829-857.

Bhattacharyya, B.K., 1969. Bicubic spline interpolation as a method of treatment of potential field data. Geophysics, 34, 402-423.

Blackman, R.B. and Tukey, S.W., 1959. The measurement of power spectra. Dover, New York.

Bott, M.H.P., 1960. The use of rapid digital computing methods for direct gravity interpretation of sedimentary basins. Geophys. J.R. astr. Soc., 3, 63-67.

Bott, M.H.P., 1973. The evolution of the Atlantic north of the Faeroe Islands. In Implications of continental drift to the Earth Sciences (edited by Tarling, D.H. and Runcorn, S.K.), 1, 175-189, Academic press, London and New York.

Bott, M.H.P.,1975. MAGN. Durham geophysics computer program specification, 2.

Bott, M.H.P. and Ingles, A., 1972. Matrix methods for joint interpretation of two-dimensional gravity and magnetic anomalies with application to the Iceland-Faeroe ridge. Geophys. J.R. astr. Soc., 30, 55-67.

Bott, M.H.P., Smith, R.A. and Stacey, R.A., 1966. Estimation of the direction of magnetization of a body causing a magnetic anomaly using a pseudo-gravity transformation. Geophysics, 31, 803-811.

Bott, M.H.P. and Tuson, J., 1973. Deep structure beneath the Tertiary volcanic regions of Skye, Mull and Ardnamurchan, north-west Scotland. Nature Physical Science, 242, 114-116.

Box, M.J., 1966. A comparison of several current optimization methods and the use of transformations in constrained problems. Comput. J.,9, 67-77.

Box, J., Davies, D. and Swann, W.H.,1969. Non-linear optimization techniques. I.C.I. Monograph No.5., Oliver and Boyd, Edinburgh.

Bracewell, R., 1965. The Fourier transform and its applications. McGraw-Hill, New York.

Brigham, E.O., 1974. The fast Fourier transform. Prentice-Hall, New Jersey.

Brown, G.C. and Mussett, A.E., 1976. Evidence for two discrete centres in Skye. Nature, 261, 218-220.

Broyden, C.G., 1967. Quasi-Newton methods and their applications to function minimisation. Math. Comp., 21, 368.- 381.

Bruckshaw, J.M. and Vincenz, S.A.,1954. The permanent magnetism of the Mull lavas. Mon. Not. R. astr. Soc. Geophys. Suppl.,6, 580-589.

Bullerwell, W., 1963. Airborne magnetic surveys. Summ. Prog. geol. Surv. Gt Br., 1962, 67.

Cooley, J.W. and Tukey, J.W., 1965. An algorithm for machine calculation of complex Fourier series. Math. Comp., 19, 297-301.

Cordell, L. and Taylor, P., 1971. Investigation of magnetization and density of a north Atlantic seamount using Poisson's theorem. Geophysics, 36, 919-937.

Dickin, A.P., 1981. Isotope geochemistry of Tertiary igneous rocks from the Isle of Skye, N.W. Scotland. J. Petrology, 22, 155-189.

Durant, G.P., Dobson, M.R., Kokelaar, B.P., Macintyre, R. M and Rea, W.J., 1976. Preliminary report on the nature and age of the Blackstones Bank igneous centre, Western Scotland. Jl geol. Soc. Lond., 132, 319-326.

Eden, R.A., Deegan, C.E., Rhys, G.H., Wright, J.E. and Dobson, M.R., 1973. Geological investigations with a manned submersible in the Irish Sea and off western Scotland, 1971. Inst. geol. Sci. Rept. 73/2.

Emeleus, C.H., 1982. The central complexes. In Igneous rocks of the British Isles (Edited by Sutherland, D.S.), 369-414, John Wiley and Sons, Chichester, England.

Evans, A.L., Fitch, F.J. and Miller, J.A., 1973. Potassium-argon age determinations on some British Tertiary igneous rocks. Jl geol. Soc. Lond., 129, 419-443.

Forester, R.W. and Taylor Jr., H.P., 1976. O^{18}-depleted igneous rocks from the Tertiary complex of the Isle of Mull, Scotland. Earth planet. Sci. Lett., 32, 11-17.

Geikie, A., 1897. Ancient volcanoes of Great Britain. 2, Macmillan, London.

Gunn, P.J., 1972. Application of Wiener filters to transformation of gravity and magnetic fields. Geophys. Prospect., 20, 860-871.

Hailwood, E.A., Bock, W., Costa, L., Dupeuble, P.A., Muller, C. and Schnitker, D., 1979. Chronology and biostratigraphy of north east Atlantic sediments, DSDP Leg 48. In Initial reports of deep sea drilling project (edited by Montadert, L. and Roberts, D.G.), 48, 1119-1141, U.S. Government Printing Office, Washington.

Harker, A., 1904. The Tertiary igneous rocks of Skye. Mem. geol. Surv. Scotland.

Judd, J.W., 1874. On the ancient volcanoes of the Highlands and the relations to their products to the Mesozoic Strata. Q. Jl geol. Soc. Lond., 30, 220-301.

Kanasewich, E.R., 1975. Time sequence analysis in geophysics. The University of Alberta Press, Edmonton.

Kanasewich, E.R. and Agarwal, R.G., 1970. Analysis of combined gravity and magnetic fields in wave number domain. J. geophys. Res., 75, 5702-5712.

Khan, M.A., 1960. The remanent magnetization of the basic Tertiary igneous rocks of Skye, Invernessshire. Geophys. J. R. astr. Soc., 3, 45-62.

King, B.C., 1960. The form of the Beinn na Dubhaich granite, Skye. Geol. Mag., 97, 326-333.

Lewis, J.D., 1968. The form and structure of the Loch Ba ring dyke, Isle of Mull, Scotland. Proc. geol. Soc., 1649, 110-111.

Lobjoit, W.M., 1959. On the form and mode of emplacement of the Ben Buie intrusion, Island of Mull, Argyllshire. Geol. Mag., 96, 393-402.

McQuillin, R. and Bacon, M. 1974. Preliminary report on seismic reflection surveys in sea areas around Scotland, 1969-73. Inst. geol. Sci. Rept. 74/12.

McQuillin, R., Bacon, M. and Binns, P.E., 1975. The Blackstones Tertiary igneous complex. Scott. J. Geol., 11, 179-192.

McQuillin,R and Binns, P.E., 1973. Geological structures in the sea areas of the Hebrides. Nature Physical Science, 241, 2-4.

McQuillin, R. and Tuson, J., 1965. An interpretation from gravity measurements of the sizes of some British Tertiary granites. Proc. geol. Soc., 1621, 59-60.

Miller, J.A. and Brown, P.E., 1965. Potassium-Argon age Studies in Scotland. Geol. Mag., 102, 106-134.

Mitchell, J.G., Jones, E.J.W. and Jones G.T., 1976. The composition and age of basalts dredged from the Blackstones igneous centre, western Scotland. Geol. Mag., 113, 525-533.

Moorbath, S. and Bell, J.D. 1965. Strontium isotope abundance studies and rubidium-strontium age determinations on Tertiary igneous rocks from the Isle of Skye, north-west Scotland. J. Petrology, 6, 37-66.

Moorbath, S. and Welke, H., 1969. Lead isotope studies on igneous rocks from the Isle of Skye, north-west Scotland. Earth and Planet. Sci. Lett., 5, 217-230.

Mussett, A.E., Brown, G.C., Eckford, M. and Charlton, S.R., 1973. The British Tertiary igneous province: K-Ar ages of some dykes and lavas, from Mull, Scotland. Geophys. J.R. astr. Soc., 30, 405-414.

Mussett, A.E., Dagley, P. and Skelhorn, R.R., 1980. Magnetostratigraphy of the Tertiary igneous succession of Mull, Scotland. J. geol. Soc. Lond. , 137, 349-357

Nelder, J.A. and Mead, R., 1965. A simplex method for function minimization. Comput. J., 7, 308-313.

Nettleton, L.L., 1940. Geophysical prospecting for oil. McGraw-Hill, New York and London.

Richey, J.E., 1961. British regional geology, Scotland : The Tertiary volcanic districts (3rd Ed., revised by MacGregor, A.G.and Anderson, F.W.). H.M.Geol. Surv.

Richey, J.E., Stewart, F.H. and Wager, L.C., 1946. Age relations of certain granites and marscoite in Skye. Geol. Mag., 83, 293.

Richey, J.E.,Stewart, F.H. and Wager, L.R., 1947. Age relations of certain granites in Skye. Geol. Mag., 84, 128

Roberts, D.G., 1970. Recent geophysical investigations on the Rockall plateau and adjacent areas. Proc. geol. Soc., 1662, 87-93.

Roy, A., 1962. Ambiguity in geophysical interpretation. Geophysics, 27, 90-99.

Savinskiy, I.D., 1976. Conversion of three-dimensional potential fields and computing the pseudo-gravitational field. Phys. Solid Earth, 12, 680-684.

Seward, A.C. and Holttum, R.E.,1924. Tertiary plants from Mull. In Tertiary and post-Tertiary geology of Mull, Loch Aline and Oban (edited by Bailey, E.B., Clough, C.T., Wright, W.B., Richey, J.E. and Wilson, G.V.), 89, Mem. geol. Surv. Scotland.

Shuey, R.T., 1972. Application of Hilbert transforms to magnetic profiles. Geophysics, 37, 1043-1045.

Skeels, D.C., 1947. Ambiguity in gravity interpetation. Geophysics, 12, 43-56.

Skelhorn, R.R., MacDougall, J.D.S. and Longland, P.J.N.,1969. The Tertiary igneous geology of the Isle of Mull. Geol. Assoc. London, Guide No.20.

Smith, R.A., 1961. A uniqueness theorem concerning gravity fields. Proc. Camb. Phil. Soc. Math. Phys. Sci., 57, 865-870.

Smith, R.A., 1978. Non-uniqueness in the inverse gravity problem for finite polygonal cylinders. J. Inst. Maths Applics, 21, 61-65.

Spendley, W., Hext, G.R. and Himsworth, F.R., 1962. Sequential applications of simplex designs in optimisation and evolutionary operation. Technometrics, 4, 441-461.

Stewart, F.H., 1965. Tertiary igneous activity. In The Geology of Scotland (edited by Craig, G.Y.), 417-465 , Oliver and Boyd, Edinburgh and London.

Talwani, M. and Ewing, M., 1960. Rapid computation of gravitational attraction of three-dimensional bodies of arbitrary shape. Geophysics, 25, 203-225

Talwani, M. and Heirtzler, J.R., 1964. Computation of magnetic anomalies caused by two-dimensional structures of arbitrary shape. In computers in mineral industries,part 1, Standford Univ. Publ. Geol. Sci., 9, 464-480.

Talwani,M., Worzel, J.L. and Landisman, M., 1959. Rapid gravity computations for two dimensional bodies with application to the Medocino submarine fracture zone. J. geophys. Res., 64, 49-59.

Taylor, Jr., H.P. and Forester, R.W., 1971. Low-O^{18} igneous rocks from the intrusive complexes of Skye, Mull and Ardnamurchan, Scotland. J. Petrology, 12, 465-497.

Thompson, R.N., 1969. Tertiary granites and associated rocks of the Marsco area, Isle of Skye. Q. Jl. geol. Soc. Lond., 124, 349-385.

Tuson, J., 1959. A geophysical investigation of the Tertiary volcanic districts of western Scotland. Ph.D. thesis, Univ. of Durham.

Vincenz, S.A., 1954. The magnetic properties of some Tertiary intrusives of the Isle of Mull. Mon. Not. R. astr. Soc. Geophys. Suppl.,6, 590-603.

Wager, L.R. and Brown, G.M., 1968. Layered igneous rocks. Oliver and Boyd, Edinburgh and London.

Wager, L.R. and Vincent, E.A., 1962. Ferrodiorite from the Isle of Skye. Mineralog. Mag., 33, 26-36.

Wager, L.R., Vincent, E.A., Brown, G.M. and Bell, J.D., 1965. Marscoite and related rocks of the Western Redhills complex, Isle of Skye. Phil. Trans. R. Soc., A, 257, 273-307.

Walker, G.P.L., 1971. The distribution of amygdale minerals in Mull and Morvern (Western Scotland). In Studies in earth sciences (edited by Murty, T.V.V. G.R.K. and Rao, S.S.), West Commemoration Vol., 181-194, Today and Tomorrow's Printers and Publishers, New Delhi.

Walsh, J.N., Beckinsale, R.D., Skelhorn, R.R. and Thorpe, R.S., 1979. Geochemistry and petrogenesis of Tertiary granitic rocks from the Island of Mull, northwest Scotland. Contrib. Minteral. Petrol., 71, 99-116.

Weedon, D.S., 1961. Basic igneous rocks of the southern Cuillin, Isle of Skye. Trans. geol. Soc. Glasg., 24, 190-212.

Weedon, D.S., 1965. The layered ultrabasic rocks of Sgurr Dubh, Isle of Skye. Scott. J. Geol., 1, 42-68.

Winter, S.R., 1972. The interpretation of magnetic anomalies using two dimensional methods with end corrections. M.Sc. thesis, Univ. of Durham.

Wolfe, M.A., 1978. Numerical methods for unconstrained optimization. Van Nostrand Reinhold, New York.

Zinovieff, P., 1958. The basic layered intrusion and the associated igneous rocks of the central and eastern Cuillin Hills, Isle of Skye. D.Phil. thesis, Univ. of Oxford.

APPENDIX A1

The appendix A1 gives a listing of computer programs developed followed by a brief description of each program.

PSGC transforms a given magnetic anomaly values at nodes of an equally spaced square grid into pseudogravimetric anomalies and produces a contour map of the pseudogravimetric anomaly.

Run Command

```
$ RUN OBJ.+*GHOST+UNSP:DIGLIB   5 = MDATA   4 = MPDATA   9 = PLOTFILE
```

Description of input files

MDATA contains the magnetic anomaly values at the nodes of the grid.

MPDATA contains values of dip and zimuth of magnetization vector and earth's total field, height at which anomaly required to be calculated and information regarding the contour map (see listing of the program).

Description of output file

PLOTFILE contains the information required to plot the contour map of the anomaly.

GREND performs 3D gravity interpretation using the trial and error method. The end correction method is used to calculate the gravity anomaly.

Run Command

```
$RUN OBJ.+*GHOST   5 = BDATA   4 = OBDATA   6 = RES  9 = PLOTFILE
```

Description of input files

BDATA contains information about the trial model such as its body coordinates (see listing of the program).

OBDATA contains the observed anomaly values and their X-coordinates.

Description of output files

RES contains the calculated anomaly at given X-coordinates

PLOTFILE contains information required to draw the diagram which illustrates the subdivision of the model for the use of end correction method and to draw the observed and calculated anomalies together with a cross-section of the body.

OPGREND performs 3D gravity interpretation using a non-linear optimization technique. The end correction method is used in calculating the anomaly as in GREND.

Run Command

$RUN OBJ.+*GHOST+*NAG 5 = BDATA 4 = OBDATA 6 = RES 9 = PLOTFILE

Description of input and output files see the description given for GREND.

MAGI performs 2D magnetic interpretation using a Quasi-Newton method.

Run command

$RUN OBJ.+*NAG 5 = BDATA 7 = OBDATA 6 = RES

Description of input files

BDATA contains information of the body such as its body coordinates (see listing of the program).

OBDATA contains observed anomalies, their X-coordinates and weighting factors.

RES contains information about the optimal body.

MAG2 performs 2D magnetic interpretation using the simplex method.

Run Command

$RUN OBJ.+*NAG 5 = BDATA 7 = OBDATA 6 2 RES 8 = OBF

Description of input and output files

BDATA, OBDATA, RES See description given for MAG1.

OBF contains the values of the objective function at the verticies of the simplex after a specified number iterations.

```
C      PROGRAM PSGC          D.A.TANTRIGODA  1980
C
C THE PROGRAM PSGC CONVERTS A GIVEN MAGNETIC ANOMALY VALUES AT
C THE NODES OF A SQUARE GRID INTO PSEUDOGRAVIMETRIC ANOMALIES
C AND DRAWS A CONTOUR MAP OF THE PSEUDOGRAVIMETRIC ANOMALY.
C
C INPUT DATA
C
C PIN,PD=INCL. AND DECL. OF MAGNETIZATION VECTOR,
C   EI,D=INCL. AND DECL. OF EARTH'S FIELD
C      Z=HEIGHT AT WHICH PSGRV. ANOMALY NEEDED TO BE COMPUTED,
C    LNS=NO. OF NODES OF EACH SIDE OF THE SQUARE GRID,
C     NH=NO. CONTOURS NEEDED TO BE DRAWN,
C   DINT=DIGITIZING INTERVAL,
C   XMIN=MINIMUM X-COORD. OF MAG. ANOMALY MAP,
C   XMAX=MAXIMUM X-COORD. OF MAG. ANOMALY MAP,
C   YMIN=MINIMUM Y-COORD. OF MAG. ANOMALY MAP,
C   YMAX=MAXIMUM Y-COORD. OF MAG. ANOMALY MAP,
C   AINT=INTER. AT WHICH AXES OF PSEGRV. MAP NEEDED TO BE ANOTATED,
C    REG=CONSTANT REGIONAL LEVEL ADDED TO THE PSGRV. ANOMALY.
C     F(2D ARRAY) ARRAY IN WHICH MAG. ANOMALY VALUES ARE STORED.
C     H(1D ARRAY) ARRAY IN WHICH CONTAINS CONTOUR LEVELS.
C ARRAYS X,Y,F,G,A ALL SHOULD BE DECLEARED AS HAVING DIMENSIONS LNS
C OR LNS*LNS APPROPRIATELY.
C
      DIMENSION X(32), Y(32), F(32,32), G(32,32), H(17), YLOC(50)
     $,A(32,32)
      LOGICAL SWITCH(5)/5 *.TRUE. /
      EXTERNAL POSITN,JOIN,LABELR
      CALL PAPER (1)
      READ(4,*)PIN,PD,EI,D,Z,LNS,NH,DINT,AINT
     $,XMIN,XMAX,YMIN,YMIN,REG
      READ(4,*)(H(I),I=1,NH)
      READ(5,*)((F(I,J),J=1,LNS),I=1,LNS)
      DO 10 I=1,LNS
      X(I)=I-1
      Y(I)=I-1
   10 CONTINUE
      LX=LNS
      LY=LNS
      DO 11 I=1,LNS
      DO 11 J=1,LNS
   11 G(I,J)=0.0
      CALL PSGC(LX,LY,F,G,EI,D,PIN,PD,Z,REG,DINT)
      DO 14 I=1,LNS
      DO 12 J=1,LNS
      A(I,J)=F(J,I)
   12 CONTINUE
   14 CONTINUE
      CALL PSPACE(0.1,0.9,0.1,0.9)
      CALL CSPACE(0.0,1.0,0.0,1.0)
      CALL MAP(X(1),X(LNS),Y(1),Y(LNS))
      CALL CONSET(POSITN,JOIN,6)
      DIST=2.0*DINT
      NYL=1
      YLOC(1)=DINT*LNS/2
      NXL=0
```

```
      XLOC=25.5
      CALL CONLBL(LABELR,DIST,NXL,XLOC,NYL,YLOC)
      CALL CONTUR(X,LNS,Y,LNS,A,LNS,H,17,SWITCH)
      CALL MAP(XMIN,XMAX,YMIN,YMIN)
      CALL CTRMAG(7)
      CALL AXESSI(AINT,AINT)
      CALL BORDER
      CALL GREND
      SI=200.0
      N=LNS
      STOP
      END
      SUBROUTINE FURRY(LX,X,Y,SIGNI,S)
C
C FAST FOURIER TRANSFORM SUBROUTINE
C
C A.G.NUNNS 1977,MODIFIED FROM CLAERBOUT (1976),FUNDAMENTALS OF
C GEOPHYSICAL DATA PROCESSING
C
C THE COOLEY-TUKEY ALGORITHM IS USED TO CALCULATE .HE FOURIER TRANSFORM
C OF A COMPLEX TIME SERIES (X(J),Y(J)) OF LX EQUALLY SPACED POINTS WHERE
C LX=2**INTEGER.THE COMPLEX TRANSFORM,(X(K),Y(K)) IS OBTAINED AT LX
C EQUALLY SPACED FREQUENCY POINTS FROM ZERO TO 2*PI.
C
C              LX
C X(K)=SC*(SUM(X(J)*COS(ARG)-Y(J)*SIN(ARG)))
C             J=1                                          FOR K=1,2,....,LX
C              LX
C Y(K)=SC*(SUM(X(J)*SIN(ARG)+Y(J)*COS(ARG)))
C             J=1
C
C WHERE    ARG=2*PI*SIGNI*(J-1)*(K-1)/LX
C
C IF SIGNI=+1.0,THEN SC=1.0 AND FORWARD TRANSFORM IS OBTAINED
C IF SIGNI=-1.0,THEN SC=1.0/LX AND REVERSE TRANSFORM IS OBTAINED
C
C LIST OF SUBROUTINE ARGUMENTS
C LX     THE NUMBER OF DATA POINTS
C X      THE ARRAY X(1),X(2),....,X(LX) WHICH CONTAINS THE REAL PART
C        OF THE TIME SERIES WHEN THE SUBROUTINE IS CALLED AND ON
C        RETURN THE REAL PART OF THE FOURIER TRANSFORM
C Y      THE ARRAY Y(1),Y(2),....,Y(LX) CONTAINING THE IMAGINARY PARTS
C        OF THE TIME SERIES AND TRANSFORM ON CALL AND RETURN RESPECTIVELY
C SIGNI  INDICATOR FOR FORWARD OR INVERSE TRANSFORM
C S      THE ARRAY S(1),S(2),....,S(LX/4+1) CONTAINING TABLE OF
C        SINE VALUES EVALUATED BY SUBROUTINE SINTAB,CALLED FROM MAIN
C
      DIMENSION X(LX),Y(LX),S(LX)
C
      SC=1.0
      IF(SIGNI.LT.0.0) SC=1.0/LX
      NN=LX/2
      N=LX/4
C
C REORDER DATA POINTS BY REVERSING ORDER OF THE BINARY DIGITS OF THEIR
C INDICES(INDEX OF X(J) IS (J-1)) AND MULTIPLY BY SCALE CONSTANT SC
```

```
C
      J=1
      DO 30 I=1,LX
      IF(I.GT.J) GO TO 10
      TEMPX=X(J)*SC
      TEMPY=Y(J)*SC
      X(J)=X(I)*SC
      Y(J)=Y(I)*SC
      X(I)=TEMPX
      Y(I)=TEMPY
   10 M=NN
   20 IF(J.LE.M) GO TO 30
      J=J-M
      M=M/2
      IF(M.GE.1) GO TO 20
   30 J=J+M
C
C COMPUTE TRANSFORM USING DOUBLING PROCEDURE.THE REQUIRED SINE AND
C COSINE VALUES FROM ZERO TO PI ARE ALL OBTAINED BY APPROPRIATE INDEXING
C FROM THE ARRAY S WHICH HAS SINES EVALUATED FROM ZERO TO PI/2
C
      L=1
      NL=NN
   40 ISTEP=2*L
      IND=1
      DO 55 M=1,L
      INDN=IND-N-1
      IF(INDN) 41,42,43
   41 WX=S(1-INDN)
      WY=S(IND)*SIGNI
      GO TO 45
   42 WX=0.
      WY=SIGNI
      GO TO 45
   43 WX=-S(INDN+1)
      WY=S(N+1-INDN)*SIGNI
   45 DO 50 I=M,LX,ISTEP
      TEMPX=WX*X(I+L)-WY*Y(I+L)
      TEMPY=WX*Y(I+L)+WY*X(I+L)
      X(I+L)=X(I)-TEMPX
      Y(I+L)=Y(I)-TEMPY
      X(I)=X(I)+TEMPX
   50 Y(I)=Y(I)+TEMPY
   55 IND=IND+NL
      L=ISTEP
      NL=NL/2
      IF(L.LT.LX) GO TO 40
      RETURN
      END
-     SUBROUTINE SINTAB(LX,S)
C
C SINE TABLE SUBROUTINE
C
C THE SUBROUTINE RETURNS VALUES
C
C S(I)=SIN(2*PI*(I-1/)/LX)   I=1,2,....,LX/4+1
C
```

```
C WHERE LX=2**INTEGER IS THE NUMBER OF POINTS IN THE TIME SERIES IN MAIN
C
      DIMENSION S(LX)
      DOUBLE PRECISION ARG,DELARG
C
      N1=LX/4+1
      ARG=0.0
      DELARG=0.62831853071795860D01/LX
      DO 10 I=1,N1
      S(I)=DSIN(ARG)
      ARG=ARG+DELARG
   10 CONTINUE
      RETURN
      END
      SUBROUTINE TRNS2D (LX,LY,F,G,SIGNI,SX,SY)
C
C  MARY ROGAN 1977.
C
C  THE SUBROUTINE CALCULATES THE 2-DIMENSIONAL TRANSFORM OF AN ARRAY
C  F(X,Y)+I*G(X,Y),X=L*A,L=1,LX, Y=J*B,J=1,LY, BY REPEATED APPLICATION O
C  1-DIMENSIONAL TRANSFORM FURRY TO THE MATRIX F(L,J).
C  MXY= MAX(LX,LY)
C  IF  SIGNI=+1.0 THE FORWARD TRANSFORM IS CALCULATED,
C      SIGNI=-1.0 THE INVERSE TRANSFORM IS CALCULATED.
C
      DIMENSION F(LX,1),G(LX,1),X(128),Y(128),SX(LX),SY(LY)
      DO 10 J=1,LY
      CALL MTOV(LX,LY,J,1,X,Y,F,G)
      CALL FURRY(LX,X,Y,SIGNI,SX)
      CALL VTOM(LX,LY,J,1,X,Y,F,G)
   10 CONTINUE
      DO 20 L=1,LX
      CALL MTOV(LX,LY,L,2,X,Y,F,G)
      CALL FURRY(LY,X,Y,SIGNI,SY)
      CALL VTOM(LX,LY,L,2,X,Y,F,G)
   20 CONTINUE
      RETURN
      END
      SUBROUTINE MTOV(LX,LY,J,NI,X,Y,F,G)
      DIMENSION X(128),Y(128),F(LX,1),G(LX,1)
      IF(NI.EQ.2) GO TO 15
      DO 10 L=1,LX
      X(L)=F(L,J)
      Y(L)=G(L,J)
   10 CONTINUE
      RETURN
   15 CONTINUE
      DO 20 L=1,LY
      X(L)=F(J,L)
      Y(L)=G(J,L)
   20 CONTINUE
      RETURN
      END
      SUBROUTINE VTOM(LX,LY,J,NI,X,Y,F,G)
      DIMENSION X(128),Y(128),F(LX,1),G(LX,1)
      IF(NI.EQ.2) GO TO 15
```

```
      DO 10 L=1,LX
      F(L,J)=X(L)
      G(L,J)=Y(L)
   10 CONTINUE
      RETURN
   15 CONTINUE
      DO 20 L=1,LY
      F(J,L)=X(L)
      G(J,L)=Y(L)
   20 CONTINUE
      RETURN
      END
C
      SUBROUTINE PSGC(LX,LY,F,G,EI,D,PIN,PD,Z,REG,DINT)
C
C THE SUBROUTINE PSGC CONVERTS A GIVEN MANNETIC ANOMALY VALUES AT AN
C EQUALLY SPACED GRID INTO PSEUDOGRAVIMETIC ANOMALIES. THIS SUBROUTINE
C FIRST COPUTES THE FOURIER TRANSFORM OF MAG. ANOMALY USING A F.F.T
C ALGORIHEM. THEN BY MULTIPLYING EACH FOURIER COEFF. BY AN APPROPRIATE
C KERNAL(SEE CHAP. 2) AND TAKING THE INVERSE FOURIER TRANSFORM OF THIS
C PRODUCT, THE PSEUDOGRAVIMETRIC ANOMALY IS COMPUTED.
C
C LIST OF SUBROUTINE ARGUMENTS
C
C  F=ARRAY IN WHICH THE REAL PART OF MAG. AND PSGRV. ANOMALIES ARE STORED
C  G=ARRAY IN WHICH THE IMA. PART OF MAG. AND PSGRV. ANOMALIES ARE STORED,
C LX=LNS
C LY=LNS
C EI,D,PIN,PD,X - SAME AS DEFINED IN MAIN PROGRAM.
C
      DIMENSION F(LX,1), G(LX,1), SX(32), SY(32)
      PI=ATAN(1.0)*4.0
      H=2.0*PI/LX
      DGTORD=PI/180.0
      EI=DGTORD*EI
      D=DGTORD*D
      PIN=DGTORD*PIN
      PD=DGTORD*PD
      CALL SINTAB(LX,SX)
      CALL SINTAB(LY,SY)
      CALL TRNS2D(LX,LY,F,G,1.0,SX,SY)
      F(1,1)=0.0
      G(1,1)=0.0
      LX2=LX/2
      LY2=LY/2
      L1=LX2+1
      L2=LY2+1
      DO 22 I=2,LX2
      K1=I-1
      K2=0
      ARG=K1**2+K2**2
      P12=H*SQRT(ARG)
      S1=H*(K1*COS(D)+K2*SIN(D))*COS(EI)/SIN(EI)
      S2=H*(K1*COS(PD)+K2*SIN(PD))*COS(PIN)/SIN(PIN)
      DE=(P12**2-S1*S2)**2+(S1+S2)**2*P12**2
      E=EXP(P12*Z)
      PR=(P12**4-S1*S2*P12**2)/DE/P12
```

```
      PN=((S1+S2)*P12**3)/DE/P12
      A=(F(I,1)*PR-G(I,1)*PN)*E
      B=(F(I,1)*PN+G(I,1)*PR)*E
      F(I,1)=A
      G(I,1)=B
      I1=LX-I+2
      F(I1,1)=F(I,1)
      G(I1,1)=-G(I,1)
   22 CONTINUE
      DO 24 J=2,LY2
      K1=0
      K2=J-1
      ARG=K1**2+K2**2
      P12=H*SQRT(ARG)
      S1=H*(K1*COS(D)+K2*SIN(D))*COS(EI)/SIN(EI)
      S2=H*(K1*COS(PD)+K2*SIN(PD))*COS(PIN)/SIN(PIN)
      DE=(P12**2-S1*S2)**2+(S1+S2)**2*P12**2
      E=EXP(P12*Z)
      PR=(P12**4-S1*S2*P12**2)/DE/P12
      PN=((S1+S2)*P12**3)/DE/P12
      A=(F(1,J)*PR-G(1,J)*PN)*E
      B=(F(1,J)*PN+G(1,J)*PR)*E
      F(1,J)=A
      G(1,J)=B
      J1=LY-J+2
      F(1,J1)=F(1,J)
      G(1,J1)=-G(1,J)
   24 CONTINUE
      DO 26 I=2,LX2
      K1=I-1
      I1=LX-I+2
      DO 28 J=2,LY2
      J1=LY-J+2
      K2=J-1
      ARG=K1**2+K2**2
      P12=H*SQRT(ARG)
      S1=H*(K1*COS(D)+K2*SIN(D))*COS(EI)/SIN(EI)
      S2=H*(K1*COS(PD)+K2*SIN(PD))*COS(PIN)/SIN(PIN)
      DE=(P12**2-S1*S2)**2+(S1+S2)**2*P12**2
      E=EXP(P12*Z)
      PR=(P12**4-S1*S2*P12**2)/DE/P12
      PN=((S1+S2)*P12**3)/DE/P12
      A=(F(I,J)*PR-G(I,J)*PN)*E
      B=(F(I,J)*PN+G(I,J)*PR)*E
      F(I,J)=A
      G(I,J)=B
      F(I1,J1)=F(I,J)
      G(I1,J1)=-G(I,J)
      K2=-K2
      ARG=K1**2+K2**2
      P12=H*SQRT(ARG)
      S1=H*(K1*COS(D)+K2*SIN(D))*COS(EI)/SIN(EI)
      S2=H*(K1*COS(PD)+K2*SIN(PD))*COS(PIN)/SIN(PIN)
      DE=(P12**2-S1*S2)**2+(S1+S2)**2*P12**2
      E=EXP(P12*Z)
      PR=(P12**4-S1*S2*P12**2)/DE/P12
      PN=((S1+S2)*P12**3)/DE/P12
```

```
      A1=(F(I,J1)*PR-G(I,J1)*PN)*E
      B1=(F(I,J1)*PN+G(I,J1)*PR)*E
      F(I,J1)=A1
      G(I,J1)=B1
      F(I1,J)=F(I,J1)
      G(I1,J)=-G(I,J1)
   28 CONTINUE
   26 CONTINUE
      DO 32 I=1,LX
      F(I,L2)=0.0
      G(I,L2)=0.0
      F(L1,I)=0.0
      G(L1,I)=0.0
   32 CONTINUE
      CALL SINTAB(LX,SX)
      CALL SINTAB(LY,SY)
      CALL TRNS2D(LX,LY,F,G,-1.0,SX,SY)
      HA=SIN(EI)*SIN(PIN)
      DO 80 I=1,LX
      DO 90 J=1,LX
      CC=0.1
      F(I,J)=CC*F(I,J)/HA+REG
      G(I,J)=CC*G(I,J)/HA
   90 CONTINUE
   80 CONTINUE
      RETURN
      END
      SUBROUTINE LABELR(XC,YC,Z)
C
C     THE SUBROUTINE LABLER WRITES VALUES OF CONTOURS AT
C     APPROPRIATE PLACES ON THE PSGRV. MAP.
      M=IFIX(Z)
      CALL CTRMAG(7)
      CALL PLOTNI(XC,YC,M)
      RETURN
      END
```

```
C      PROGRAM GREND        D.A.TANTRIGODA   1981
C
C THE PROGRAM GREND PERFORMAS 3-D GRAVITY INTERPRETATION USING END
C CORRECTINS. WAY IN WHICH THE MODEL IS SUBDIVIDED FOR THE APPLICATION
C OF END CORRECTIONS AND OBS. AND CALC. ANOMALIES TOGETHER WIHTH A
C X-SECTION OF THE MODEL ARE DRAWN AS OUTPUT.
C
C INPUT DATA
C
C      NB=NO. OF BODIES
C      NT=TOTAL NO.OF BODY POINTS
C      NF=NO. FIELD POINTS
C     NBR=NO. DIFFERENT DENSITY VALUES
C      ZS=HEIGHT AT WHICH OBS. ARE MADE(Z-AXIS VERTICALL DOWNWARDS)
C      RL=ASSUMED CONSTANT  REG. LEVEL
C     RLG=ASSUMED REG. GRADIENT(MGAL/KM)
C      NN(1D ARRAY)-NO. OF BODY POINS OF EACH BODY
C     NNZ(1D ARRAY)-NO. OF HORIZONTAL STRIPS EACH BODY IS DIVIDED
C     INTO(SEE CHAPTER3)
C      RR(1D ARRAY)-COM. RATIO OF THE ARITH. PROG. EACH SET OF
C     HORIZONTAL STRIPS FORM
C     RHH(1D ARRAY)-NBR DENSITY VALUES
C      NR(1D ARRAY)-SET OF INDICIES CORROSP. DENSITY VALUES(EG. 1 2 3 3
C       -1ST AND 2ED BODIES HAVE 1ST AND 2ND DENSITY VALUES
C      OF THE ARRAY RHH AND 3RD AND 4TH BODIES HAVE 3RD DENSITY VAL.
C      OF THE ARRAY RHH)
C      SLO(1D ARRAY)-TAN. OF ANGLE BETWEEN VERT. AND SIDES OF THE
C      BODY ALONG A DIRCT. PERPENDICULAR TO THE PROFILE
C     MXX(2D ARRAY)-NO OF ELEMENTS EACH STRIP OF EACH BODY ARE DIVIDED
C     (EG.    5  4   3    2
C     THE BODY IS DIVIDED INTO 4 STRIPS AND 1ST 2ND 3RD AND 4TH
C     STRIPS ARE DIVED INTO 5,4,3 AND 2 ELEMENTS RESPECTIVELY.
C     YY(2D ARRAY)-HALF LENGTH OF PRISMS CORROSPONDIG TO ELEMENTS
C       IN THE FIRST STRIP OF EACH BODY.
C      IT NECESSARY TO WRITE YY VALUES CORRES. EACH BODY
C      IMMEDIATELY AFTER ITS MXX VALUE.I.E. IN THE INPUT DATA
C      SETS OF MXX AND YY VALUES SHOULD APPEAR ALTERNATIVELY.
C     XB,ZB(1D ARRAYS)-X AND Z COODINATES OF ALL BODY POINTS.
C      BODY POINTS ARE SPECIFIED CLOCKWISE STARTING FROM THE  TOP
C      LEFT HAND SIDE BODY POINT.
C      NII(1D ARRAY)-AN ARRAY OF INTIGER NO. WHICH INDICTAES
C      WHETHER EACH BODY POINT
C      IS ON RHS. OR LHS. NII IS 0 FOR POINT ON LHS. AND IT IS 1 FOR
C      POINT ON RHS.
C      XSS(1D ARRAY) X-COORD. OF OBS. AND CALC. ANOMALIES.
C      FO(1D ARRAY) OBS. ANOMALY VALUES AT XSS(I).
C
C
      IMPLICIT REAL*8(A-H,O-Z)
      DIMENSION XB(100),ZB(100),YB(100),XSS(100),FO(100),NII(50),NN(10)
     $,NNZ(10),RR(10),RHH(10),SLO(10),YC(20,20),YY(10,10),MXX(10,10)
     $,F(100),NR(100)
      COMMON/COM1/NB,NT,NN,NNZ,MXX,NII,NR,NBR
      COMMON/COM2/RR,YB,FO,SLO,SC,F,RLG,RL
      COMMON/COM3/NF,NNF,ZS,XSS
      READ(5,*)NB,NT,NF,NBR,ZS,RL,RLG
      READ(5,*)(NN(I),I=1,NB)
      READ(5,*)(NNZ(I),I=1,NB)
```

```
      READ(5,*)(RR(I),I=1,NB)
      READ(5,*)(RHH(I),I=1,NBR)
      READ(5,*)(NR(I),I=1,NB)
      READ(5,*)(SLO(I),I=1,NB)
      JN=0
      JM=0
      DO 32 K=1,NB
      JN=JN+1
      NZ=NNZ(K)
      READ(5,*)(MXX(I,K),I=1,NZ)
      M=MXX(1,K)
      READ(5,*)(YY(I,K),I=1,M)
      DO 34 I=1,M
      JM=JM+1
      YC(I,JN)=YY(I,K)
   34 YB(JM)=YY(I,K)
      DO 36 J=2,NZ
      JN=JN+1
      JN1=JN-1
      J1=J-1
      I1=MXX(J,K)
      I2=MXX(J1,K)
      I3=I2-I1
      DO 36 L=1,I1
      JM=JM+1
      L1=L+I3
      S=0.0D0
      DO 38 I=L,L1
   38 S=S+YC(I,JN1)
      YC(L,JN)=S/(I3+1)
   36 YB(JM)=YC(L,JN)
   32 CONTINUE
      READ(5,*)(XB(I),ZB(I),NII(I),I=1,NT)
      READ(4,*)(XSS(I),FO(I),I=1,NF)
      CALL BD(XB,ZB,RHH)
      CALL PLOT(F,XSS,NF,NN,FO,XB,ZB,NB)
      WRITE(6,33)(XSS(I),F(I),I=1,NF)
   33 FORMAT(1H , 2F10.3)
      STOP
      END
      SUBROUTINE BD(XB,ZB,RH)
C
CC    THE SUBROUTINE BD DIVIDES GIVEN BODY INTO A NUMBER OF ELEMENTS
C     AND CALCULATES THE GRAVITY ANOMALY DUE TO THE BODY USING
C     END CORRECTIONS.
      IMPLICIT REAL*8(A-H,O-Z)
      DIMENSION X(50),Z(50),XR(50),XL(50),NI(50),NZL(50),NZR(50)
     $,ZC(50),XRC(50),XLC(50),GR(50),CR(50),GL(50),CL(50),SLO(10)
     $,ZR(50),ZL(50),XLA(50),ZLA(50),X1(100),X2(100),X3(100),X4(100)
     $,Z1(100),Z2(100),Z3(100),Z4(100),XT(100),MX(50),XB(100),ZB(100)
     $,RR(10),MXX(10,10),NII(50),XG(100),ZG(100),YB(100),FO(100)
     $,KN(10),KNA(10),KNB(10),X5(100),Z5(100),NN(10),NNZ(10),NG(100)
     $,XSS(100),F(100),RH(10),XA(10),ZA(10),EC(80,80),FS(80,80)
     $,NR(100)
      COMMON/COM1/NB,NT,NN,NNZ,MXX,NII,NR,NBR
      COMMON/COM2/RR,YB,FO,SLO,SC,F,RLG,RL
      COMMON/COM3/NF,NNF,ZS,XSS
      COMMON/COMP/X1,Z1,X2,Z2,X3,Z3,X4,Z4,X5,Z5,XG,ZG,NG,K1
```

```
      COMMON/CLAB/FS
      COMMON/CEC/EC
      CALL TIME(0)
C
C     CALCULATE THE RGIONAL ANOMALY AT EACH FIELD POINT.
C
      DO 17 I=1,NF
   17 F(I)=RL+RLG*XSS(I)
      K1=0
      KB1=1
      DO 1 IK=1,NB
      NH=NN(IK)
      NZ=NNZ(IK)
      R=RR(IK)
      SLP=SLO(IK)
      DO 3 I=1,NZ
    3 MX(I)=MXX(I,IK)
      KB2=KB1+NH-1
      J=0
      DO 7 I=KB1,KB2
      J=J+1
      X(J)=XB(I)
      Z(J)=ZB(I)
    7 NI(J)=NII(I)
      KB1=KB2+1
      LR=0
      LL=0
C
C     SELECT COORD. OF BODY PTS. ON RHS. AND LHS.
C
      DO 10 I=1,NH
      IF(NI(I).EQ.0) GOTO 20
      LR=LR+1
      XR(LR)=X(I)
      ZR(LR)=Z(I)
      GOTO 10
   20 LL=LL+1
      XLA(LL)=X(I)
      ZLA(LL)=Z(I)
   10 CONTINUE
      XL(1)=XLA(1)
      ZL(1)=ZLA(1)
      DO 5 I=2,LL
      K=LL+2-I
      XL(I)=XLA(K)
    5 ZL(I)=ZLA(K)
      LRR=LR-1
C
C     CALC. GRAD. AND INTERCPT. OF SIDES ON RHS.
C
      DO 30 I=1,LRR
      J=I+1
      XXR=XR(I)-XR(J)
      XXRA=DABS(XXR)
      IF(XXRA.LT.0.000001D0) GOTO 40
      GR(I)=(ZR(I)-ZR(J))/XXR
      CR(I)=ZR(I)-GR(I)*XR(I)
      GOTO 30
```

```
   40 GR(I)=10.0D+10
      CR(I)=0.0D0
   30 CONTINUE
      LLL=LL-1
C
C     CALC. GRAD. AND INTERCPT. OF SIDES ON LHS.
C
      DO 60 I=1,LLL
      J=I+1
      XXL=XL(I)-XL(J)
      XXLL=DABS(XXL)
      IF(XXLL.LT.0.000001D0) GOTO 70
      GL(I)=(ZL(I)-ZL(J))/XXL
      CL(I)=ZL(I)-GL(I)*XL(I)
      GOTO 60
   70 GL(I)=10.0D+10
      CL(I)=0.0D0
   60 CONTINUE
C
C     CALC. COMMON DIFF. OF ARITHM. PROG. H. STRIPS FORM
C     AND DIVIDE THE BODY INTO H. STRIPS.
C
      R2=R/2.0D0
      SN=NZ+(NZ*NZ-NZ)*R2
      ZZ=ZL(LL)-ZL(1)
      A=ZZ/SN
      ZC(1)=ZL(1)
      NZL(1)=1
      NZR(1)=1
      DO 80 L=1,NZ
      L1=L+1
      SL=L+(L*L-L)*R2
      ZC(L1)=ZL(1)+A*SL
      DO 90 I=1,LLL
      J=I+1
      IF(A.LT.0.0) GOTO 94
      IF(ZC(L1).LT.ZL(J).AND.ZC(L1).GT.ZL(I)) NZL(L1)=I
      IF(ZC(L1).LT.ZL(J)) GOTO 100
      GOTO 90
   94 IF(ZC(L1).GT.ZL(J).AND.ZC(L1).LT.ZL(I)) NZL(L1)=I
      IF(ZC(L1).GT.ZL(J)) GOTO 100
   90 CONTINUE
  100 DO 110 I=1,LRR
      J=I+1
      IF(A.LT.0.0) GOTO 96
      IF(ZC(L1).LT.ZR(J).AND.ZC(L1).GT.ZR(I)) NZR(L1)=I
      IF(ZC(L1).LT.ZR(J)) GOTO 80
      GOTO 110
   96 IF(ZC(L1).GT.ZR(J).AND.ZC(L1).LT.ZR(I)) NZR(L1)=I
      IF(ZC(L1).GT.ZR(J)) GOTO 80
  110 CONTINUE
   80 CONTINUE
      DO 120 I=1,NZ
      JL=NZL(I)
      IF(GL(JL).GT.10.0D+9) GOTO 130
      XLC(I)=(ZC(I)-CL(JL))/GL(JL)
      GOTO 140
  130 XLC(I)=XL(JL)
```

```
  140 JR=NZR(I)
      IF(GR(JR).GT.10.0D+9) GOTO 150
      XRC(I)=(ZC(I)-CR(JR))/GR(JR)
      GOTO 120
  150 XRC(I)=XR(JR)
  120 CONTINUE
      NZZ=NZ+1
      XRC(NZZ)=XR(LR)
      XLC(NZZ)=XL(LL)
      NZL(NZZ)=LLL
      NZR(NZZ)=LRR
      DO 160 J=1,NZ
      M=MX(J)+1
      DO 170 L1=1,M
C
C     DIVIDE EACH H. STRIP INTO ELEMENTS.
C
  170 XT(L1)=XLC(J)+(L1-1)*(XRC(J)-XLC(J))/(M-1)
      J1=J+1
      M=M-1
      DO 180 I=1,M
      IF(I.EQ.1) GOTO 190
      IF(I.EQ.M) GOTO 200
      K1=K1+1
      I1=I+1
      X1(K1)=XT(I)
      Z1(K1)=ZC(J)
      X2(K1)=XT(I1)
      Z2(K1)=ZC(J)
      X3(K1)=XT(I1)
      Z3(K1)=ZC(J1)
      X4(K1)=XT(I)
      Z4(K1)=ZC(J1)
      X5(K1)=0.0D0
      Z5(K1)=0.0D0
      XG(K1)=(X1(K1)+X2(K1)+X3(K1)+X4(K1))/4.0D0
      ZG(K1)=(Z1(K1)+Z2(K1)+Z3(K1)+Z4(K1))/4.0D0
      NG(K1)=4
      GOTO 185
  190 N1=NZL(J)
      N2=NZL(J1)
      IF(N1.NE.N2) GOTO 210
      K1=K1+1
      X1(K1)=XT(1)
      Z1(K1)=ZC(J)
      X2(K1)=XT(2)
      Z2(K1)=ZC(J)
      X3(K1)=XT(2)
      Z3(K1)=ZC(J1)
      X4(K1)=XLC(J1)
      Z4(K1)=ZC(J1)
      IF(M.EQ.1) X3(K1)=XRC(J1)
      X5(K1)=0.0D0
      Z5(K1)=0.0D0
      GOTO 195
  200 N1=NZR(J)
      N2=NZR(J1)
      IF(N1.NE.N2) GOTO 220
```

```
      K1=K1+1
      X1(K1)=XT(M)
      Z1(K1)=ZC(J)
      X2(K1)=XRC(J)
      Z2(K1)=ZC(J)
      X3(K1)=XRC(J1)
      Z3(K1)=ZC(J1)
      X4(K1)=XT(M)
      Z4(K1)=ZC(J1)
      X5(K1)=0.0D0
      Z5(K1)=0.0D0
  195 NG(K1)=4
C
CC    CALC. CMASS OF ELEMENTS HAVING 4 SIDES.
C
      CALL CMASS(X1(K1),Z1(K1),X2(K1),Z2(K1),X3(K1),Z3(K1)
     $,X4(K1),Z4(K1),X5(K1),Z5(K1),NG(K1),XCG,ZCG)
      XG(K1)=XCG
      ZG(K1)=ZCG
  185 ZD=ZG(K1)-ZB(1)
      Y=YB(K1)+ZD*SLP
      RHO=RH(IK)
C
CC    CALC. ENDCR. FOR FACTOR ELEMENTS HAVING 4 SIDES.
C
      CALL ENDCR(XG(K1),ZG(K1),Y,I)
      XA(1)=X4(K1)
      ZA(1)=Z4(K1)
      XA(2)=X1(K1)
      ZA(2)=Z1(K1)
      LAB=1
C
CC    CALC. GRAV. ANOM. DUE TO 2D PRISMS CORRESPONDIG TO
C     ELEM. HAVING 4 SIDES AND MULTIPLY BY THE
C     CORRESPONDING ENDCR. FACTOR.
C
      CALL SLAB(XA,ZA,LAB,I,RHO)
      IF(I.NE.M) GOTO 211
      XA(1)=X3(K1)
      ZA(1)=Z3(K1)
      XA(2)=X2(K1)
      ZA(2)=Z2(K1)
      KR=I+1
      CALL SLAB(XA,ZA,LAB,KR,RHO)
  211 GOTO 180
  210 K1=K1+1
      X1(K1)=XT(1)
      Z1(K1)=ZC(J)
      X2(K1)=XT(2)
      Z2(K1)=ZC(J)
      X3(K1)=XT(2)
      Z3(K1)=ZC(J1)
      X4(K1)=XLC(J1)
      Z4(K1)=ZC(J1)
      X5(K1)=XL(N2)
      Z5(K1)=ZL(N2)
      GOTO 205
  220 K1=K1+1
```

```
      X1(K1)=XT(M)
      Z1(K1)=ZC(J)
      X2(K1)=XRC(J)
      Z2(K1)=ZC(J)
      X3(K1)=XR(N2)
      Z3(K1)=ZR(N2)
      X4(K1)=XRC(J1)
      Z4(K1)=ZC(J1)
      X5(K1)=XT(M)
      Z5(K1)=ZC(J1)
  205 NG(K1)=5
C
C     CALC. CMASS OF ELEMENTS HAVING 5 SIDES.
C
      CALL CMASS(X1(K1),Z1(K1),X2(K1),Z2(K1),X3(K1),Z3(K1)
     $,X4(K1),Z4(K1),X5(K1),Z5(K1),NG(K1),XCG,ZCG)
      XG(K1)=XCG
      ZG(K1)=ZCG
      ZD=ZG(K1)-ZB(1)
      Y=YB(K1)+ZD*SLP
      RHO=RH(IK)
      CALL ENDCR(XG(K1),ZG(K1),Y,I)
C
C     CALC. ENDCR. FACTOR FOR ELEMENTS HAVING 5 SIDES.
C
      IF(I.EQ.M) GOTO 212
      XA(1)=X4(K1)
      ZA(1)=Z4(K1)
      XA(2)=X5(K1)
      ZA(2)=Z5(K1)
      XA(3)=X1(K1)
      ZA(3)=Z1(K1)
      LAB=2
C     CALC. 2D GRAVITY ANOMALY DUE TO PRISMS CORR. ELEMENTS
C     HAVING 5 SIDES AND MULTIPLY BY THE CORRESPONDING
C     ENDCR FACTOR.
      CALL SLAB(XA,ZA,LAB,I,RHO)
      GOTO 180
  212 XA(1)=X5(K1)
      ZA(1)=Z5(K1)
      XA(2)=X1(K1)
      ZA(2)=Z1(K1)
      LAB=1
      CALL SLAB(XA,ZA,LAB,I,RHO)
      XA(1)=X4(K1)
      ZA(1)=Z4(K1)
      XA(2)=X3(K1)
      ZA(2)=Z3(K1)
      XA(3)=X2(K1)
      ZA(3)=Z2(K1)
      LAB=2
      KR=I+1
      CALL SLAB(XA,ZA,LAB,KR,RHO)
  180 CONTINUE
      DO 181 I1=1,NF
      DO 181 J1=1,M
      J2=J1+1
  181 F(I1)=(FS(I1,J1)-FS(I1,J2))*EC(I1,J1)+F(I1)
```

```
  160 CONTINUE
    1 CONTINUE
      CALL TIME(1,1)
      RETURN
      END
      SUBROUTINE CMASS(A1,A2,A3,A4,A5,A6,A7,A8,A9,A10
     $,NS,XCG,ZCG)
C
C     THE SUBROUTINE CMASS CALC. CMASS OF A POLYGONAL SHAPE.
C
      IMPLICIT REAL*8(A-H,O-Z)
      DIMENSION X(10),Z(10)
      X(1)=A1
      Z(1)=A2
      X(2)=A3
      Z(2)=A4
      X(3)=A5
      Z(3)=A6
      X(4)=A7
      Z(4)=A8
      IF (NS.EQ.4) GOTO 5
      X(5)=A9
      Z(5)=A10
    5 N=NS-2
      SA=0.0D0
      SX=0.0D0
      SZ=0.0D0
      DO 10 I=1,N
      M=I+1
      L=I+2
      A=(X(M)*Z(L)-Z(M)*X(L)-X(1)*Z(L)+Z(1)*X(L)+X(1)*Z(M)-Z(1)*
     $X(M))/2.0
      SA=SA+A
      XSS=A*(X(1)+X(M)+X(L))
      SZZ=A*(Z(1)+Z(M)+Z(L))
      SX=XSS+SX
   10 SZ=SZZ+SZ
      XCG=SX/SA/3.0D0
      ZCG=SZ/SA/3.0D0
      RETURN
      END
      SUBROUTINE SLAB(XB,ZB,N,K,RHO)
C
C     THE SUBROUTINE SLAB CALC. GRAV. ANOMALY DUE TO 2D
C     PRISMS AND MULTIPLY BY ENDCR. FACTORS CALCULATED BY
C     THE SUBROUTINE ENDCR.
C
      IMPLICIT REAL*8(A-H,O-Z)
      DIMENSION XSS(100),FS(80,80),XB(5),ZB(5),SI(5),CO(5)
      COMMON/COM3/NF,NFF,ZS,XSS
      COMMON/CLAB/FS
      PI2=2.0D0*DATAN(1.D0)
      CC=RHO*13.34D0
      DO 5 J=1,N
      J1=J+1
      XBD=XB(J)-XB(J1)
      ZBD=ZB(J1)-ZB(J)
      RBD=DSQRT(XBD*XBD+ZBD*ZBD)
```

```
      SI(J)=ZBD/RBD
    5 CO(J)=XBD/RBD
      DO 15 I=1,NF
      SUM=0.0D0
      DO 10 J=1,N
      J1=J+1
      XS=XSS(I)
      X1=XB(J)-XS
      X2=XB(J1)-XS
      Z1=ZB(J)-ZS
      Z2=ZB(J1)-ZS
      AX1=DABS(X1)
      AX2=DABS(X2)
      IF(AX1.LT.0.000001D0) GOTO 20
      T1=DATAN2(Z1,X1)
      GOTO 30
   20 T1=PI2
   30 IF(AX2.LT.0.000001D0) GOTO 40
      T2=DATAN2(Z2,X2)
      GOTO 50
   40 T2=PI2
   50 R1=DSQRT(X1*X1+Z1*Z1)
      R2=DSQRT(X2*X2+Z2*Z2)
      TT=T1-T2
      RL=DLOG(R2/R1)
      SUM=-CC*((Z1*CO(J)+X1*SI(J))*(TT*CO(J)-RL*SI(J))+Z2*T2-Z1*T1)
     $+SUM
   10 CONTINUE
      FS(I,K)=SUM
   15 CONTINUE
      RETURN
      END
      SUBROUTINE ENDCR(XC,ZC,Y,J)
C
C     THE SUBROUTINE ENDCR CALC. ENDCR. FACTOR FOR EACH
C     ELEMENT FOR EACH FIELD POINT.
C
      IMPLICIT REAL*8(A-H,O-Z)
      DIMENSION XSS(100),EC(80,80)
      COMMON/COM3/NF,NNF,ZS,XSS
      COMMON/CEC/EC
      DO 10 I=1,NF
      XE=XC-XSS(I)
      ZE=ZC-ZS
      R=DSQRT(XE*XE+ZE*ZE)
      D=DSQRT(1.0+(R/Y)*(R/Y))
   10 EC(I,J)=1.0D0/D
      RETURN
      END
      SUBROUTINE PLOT(F,XSS,NF,NN,FO,XB,ZB,NB)
C
C     THE SUBROUTINE PLOT DRAWS TWO PLOTS AS OUTPUT.
C     FIRST PLOT SHOWS THE WAY IN WHICH THE BODY IS
C     SUBDIVIDED. 2ND PLOT SHOWS OBS. AND CALC. AND.
C     AND A X-SECTION OF THE BODY ON THE PLANE OF THE
C     PROFILE.
      REAL*8 F,XSS,FO,XB,ZB,X1,X2,X3,X4,X5,Z1,Z2,Z3,Z4,Z5
     $,XG,ZG
```

```
      REAL*4 XA1,XA2,XA3,XA4,XA5,ZA1,ZA2,ZA3,ZA4,ZA5,XGA,ZGA
     $,XXS,X,Z,FOB,FCL
      DIMENSION XSS(100),F(100),FO(100),X(50),Z(50),NN(10),XG(100)
     $,ZG(100),X1(100),Z1(100),X2(100),Z2(100),X3(100),Z3(100)
     $,X4(100),Z4(100),X5(100),Z5(100),NG(100),YY(20),XB(100),ZB(100)
     $,XA1(100),XA2(100),XA3(100),XA4(100),XA5(100),ZA1(100),
     $ZA2(100),ZA3(100),ZA4(100),ZA5(100),XGA(100),ZGA(100)
     $,XXS(100),FOB(100),FCL(100)
      COMMON/COMP/X1,Z1,X2,Z2,X3,Z3,X4,Z4,X5,Z5,XG,ZG,NG,K1
      CALL PAPER(1)
      DO 6 I=1,K1
      XA1(I)=X1(I)
      ZA1(I)=Z1(I)
      XA2(I)=X2(I)
      ZA2(I)=Z2(I)
      XA3(I)=X3(I)
      ZA3(I)=Z3(I)
      XA4(I)=X4(I)
      ZA4(I)=Z4(I)
      XA5(I)=X5(I)
      ZA5(I)=Z5(I)
      XGA(I)=XG(I)
    6 ZGA(I)=ZG(I)
      DO 8 I=1,NF
      XXS(I)=XSS(I)
      FOB(I)=FO(I)
    8 FCL(I)=F(I)
      CALL PSPACE(0.2,0.8,0.2,0.8)
      CALL CSPACE(0.0,1.0,0.0,1.0)
      CALL MAP(15.0, 30.0,5.0,0.0)
      DO 12 I=1,K1
      CALL POSITN(XA1(I),ZA1(I))
      CALL JOIN(XA2(I),ZA2(I))
      CALL JOIN(XA3(I),ZA3(I))
      CALL JOIN(XA4(I),ZA4(I))
      IF(NG(I).EQ.4) GOTO 14
      CALL JOIN(XA5(I),ZA5(I))
   14 CALL JOIN(XA1(I),ZA1(I))
   12 CONTINUE
C     DO 18 I=1,K1
C     CALL POSITN(XGA(I),ZGA(I))
C  18 CALL CIRCLE(0.000005)
      CALL BORDER
C     CALL AXESSI(5.0,5.0)
      CALL GREND
      CALL PAPER(1)
      CALL PSPACE(0.2,0.8,0.55,0.9)
      CALL MAP(XXS(1),XXS(NF),200.0,1200.0)
      CALL CTRMAG(7)
      CALL NSCURV(XXS,FCL,1,NF)
      CALL AXESSI(5.0,5.0)
      CALL POSITN(1.0,800.0)
      CALL JOIN(6.0,800.0)
      CALL CSPACE(0.2,0.8,0.55,0.9)
      CALL PLOTCS(6.1,750.0,'OBSERVED ANOMALY',16)
      CALL PLOTCS(6.1,800.0,'CALCULATED ANOMALY',18)
      CALL BROKEN(1,3,1,3)
      CALL NSCURV(XXS,FOB,1,NF)
```

```
      CALL POSITN(1.0,750.0)
      CALL JOIN(6.0,750.0)
      CALL FULL
      CALL BORDER
      CALL PSPACE(0.2,0.8,0.15,0.5)
      CALL CSPACE(0.2,0.8,0.1,0.5)
      CALL MAP(XXS(1),XXS(NF),24.0,0.0)
      L1=1
      DO 10 M=1,NB
      N=NN(M)
      L2=L1+N-1
      K=0
      DO 20 I=L1,L2
      K=K+1
      X(K)=XB(I)
   20 Z(K)=ZB(I)
      L1=L2+1
      DO 10 I=1,N
      J=I+1
      IF(I.EQ.N) J=1
      CALL POSITN(X(I),Z(I))
      CALL JOIN(X(J),Z(J))
   10 CONTINUE
      CALL BORDER
      CALL POSITN(XXS(1),0.0)
      CALL JOIN(XSS(NF),0.0)
      CALL PSPACE(0.0,1.0,0.0,1.0)
      CALL CSPACE(0.0,1.0,0.0,1.0)
      CALL MAP(0.0,1.0,0.0,1.0)
      CALL PLOTCS(0.47,0.52,'DISTANCE(KM)',12)
      CALL CTRORI(1.0)
      CALL PLOTCS(0.163,0.65,'PSEUDOGRAVIMETRIC ANOMALY(MGAL)',31)
      CALL CTRORI(3.0)
      CALL PLOTCS(0.16,0.35,'DEPTH(KM)',9)
      CALL CTRORI(0.0)
      DO 50 J=1,6
      XP=0.187
      YY(J)=(J-1)*0.35/4.0
      I=(5-J)*6
      Y=YY(J)+0.15
      CALL PLOTNI(XP,Y,I)
   50 CONTINUE
      CALL PSPACE(0.15,0.85,0.1,0.95)
      CALL BORDER
      CALL GREND
      RETURN
      END
```

```
C       PROGRAM OPGREND     D.A.TANTRIGODA      1981
C
C     THE PROGRAM OPGREND PERFORMS 3D GRAVITY INTRPRETATION
C     USING THE END CORRECTION METHOD AND A NON-LINEAR
C     OPTIMIZATION TECHNIQUE. WAY IN WHICH THE MODEL IS
C     SUBDIVIDED FOR THE APPLICATION OF END CORRECTIONS
C     AND OBS. AND CALC. ANOMALIES TOGETHER WITH X-SCETION
C     OF THE BODY ON THE PLANE OF THE PORFILE ARE DRAWN
C     AS OUTPUT. THIS PROGRAM IS SIMILAR TO THE PROGRAM GREND.
C     BUT IT USES A NON-LINEAR OPTIMIZATION TECHNIQUE
C     INSTEAD OF CONVENTIONAL TRAIL-AND-ERROR METHOD.
C
C     INPUT DATA
C
C     NB,NT,NF,NBR,ZS,RL,RLG,NN,NNZ,RR,RHH,NR,MXX,XB,ZB
C     NII,XSS,FO-SAME AS IN GREND.
C     IT IS NECESSARY TO NUMBER ALL X AND Z BODY COORDS.
C     CLOCKWISE STARTING FROM THE FIRST ONE ON THE TOP
C     LEFT SIDE,IF XB1,ZB1,XB2,ZB2,XB3,ZB3,...ARE THE
C     BODY COORDS. IN THE ABOVE MENTION ORDER, THEN THE
C     CORRESPONDING NUMBERS ARE 1,2,3,4,5,6,...RESPECTIVELY.
C
C     NO(1D ARRAY)-IT IS POSSIBLE TO EXCLUDE SOME BODY PTS.
C     IN THE OPT. PROCESS. THIS ARRAY SHOULD CONSIST OF
C     THE NUMBERS CORRESPONDIG TO THESE COORDS.
C
C      NON-NO. OF BODY PTS. DO NOT USE IN THE OPT.
C
C      NE(1D ARRAY)-SOME BODY PTS. HAVE EQUAL VALUES. SOMETIMES
C      IT IS REQUIRED TO MAINTAIN THIS IN THE OPTIMIZATION
C      PROCESS. ARRAY NE CONSISTS OF ABOVE MENTION NUMBERS
C      CORRESPONDING TO SETS OF SUCH BODY POINTS.
C      EACH SET OF NUMBERS CORRESPONDING TO EACH SET
C      OF EQUAL BODY PTS. MUST BE FOLLOWED BY A ZERO.
C      EG.   1   3   5   0   2   8   0
C      BODY PTS. CORRESPONDING TO THE NUMBRES 1 3 AND 5 ARE
C      EQUAL TO EACH OTHER AND BODY POINTS CORRESPONDING TO
C      THE NUMBERS 2 AND 8 ARE EQUAL TO EACH OTHER.
C
C      NEN-NO. ELEMENTS IN THE ARRAY NE INCLUDING ZEROS.
C      RMSEG-WHEN RMS. ERROR OF OBS. AND CALC. ANOM. BECOMES
C      LESS THAN THIS GIVEN VALUE OPTIMIZATION IS STOPED.
C      IPRINT-THIS CAN TAKE VALUES 1 OR 0.IF IRTINT=1
C      VAL. OF THE OBJECTIVE FUNCTION IS PRINTED AFTER
C      A CERTAIN NO OF ITERATIONS.IF IT IS 0 VALS ARE
C      NOT PRINTED.
C      BL,BU,SC(1D ARRAYS)-LOWER AND UPPER BOUNDS OF THE
C      PARAMETERS AND SCALING FACTORS RESPECTIVELY.
C      OR(1D ARRAY)-WEIGHTING COEFFICIENTS.
C
       IMPLICIT REAL*8(A-H,O-Z)
       DIMENSION XB(100),ZB(100),YB(100),XSS(100),FO(100),NII(50),NN(10)
     $,NNZ(10),RR(10),RHH(10),SLO(10),YC(20,20),YY(10,10),MXX(10,10)
     $,F(100),B(100),NO(50),NE(90),SC(20),BL(20),BU(20),X(20),XU(20)
     $,DELTA(20),HESD(20),HESL(200),W(200),OR(100)
     $,ISTATE(20),IW(2),G(20),NR(10)
       COMMON/COM1/NB,NT,NN,NNZ,MXX,NII,NT2,NON,NEN,NO,NE
     $,NU1,NU2,NU,NR,NBR
```

```
      COMMON/COM2/RR,YB,FO,SLO,B,SC,F,RMSEG,OR,RGL
      COMMON/COM3/NF,NNF,ZS,XSS
      LOGICAL LOCSCH
      EXTERNAL E04JBQ,FUNCT,MONIT
      CALL TIME(0)
      READ(5,*)NB,NT,NF,NON,NEN,NBR,ZS,RL,RLG,RMSEG,IPRINT
      READ(5,*)(NN(I),I=1,NB)
      READ(5,*)(NNZ(I),I=1,NB)
      READ(5,*)(RR(I),I=1,NB)
      READ(5,*)(RHH(I),I=1,NBR)
      READ(5,*)(NR(I),I=1,NB)
      READ(5,*)(SLO(I),I=1,NB)
      READ(5,*)(NO(I),I=1,NON)
      READ(5,*)(NE(I),I=1,NEN)
      JN=0
      JM=0
      DO 32 K=1,NB
      JN=JN+1
      NZ=NNZ(K)
      READ(5,*)(MXX(I,K),I=1,NZ)
      M=MXX(1,K)
      READ(5,*)(YY(I,K),I=1,M)
      DO 34 I=1,M
      JM=JM+1
      YC(I,JN)=YY(I,K)
   34 YB(JM)=YY(I,K)
      DO 36 J=2,NZ
      JN=JN+1
      JN1=JN-1
      J1=J-1
      I1=MXX(J,K)
      I2=MXX(J1,K)
      I3=I2-I1
      DO 36 L=1,I1
      JM=JM+1
      L1=L+I3
      S=0.0D0
      DO 38 I=L,L1
   38 S=S+YC(I,JN1)
      YC(L,JN)=S/(I3+1)
   36 YB(JM)=YC(L,JN)
   32 CONTINUE
      READ(5,*)(XB(I),ZB(I),NII(I),I=1,NT)
      NT2=2*NT
      NU=NT2-NON
      N=NU+NB+1
      READ(5,*)(BL(I),BU(I),SC(I),I=1,N)
      DO 10 I=1,NT
      J=2*I
      K=J-1
      B(K)=XB(I)
      B(J)=ZB(I)
   10 CONTINUE
C
C     SELECT THE BODY POINTS THAT WILL BE USED
C     IN THE OPT.
C
      J=0
```

```
      K1=1
      DO 20 I=1,NT2
      DO 25 K=K1,NON
      IF(I.EQ.NO(K)) GOTO 65
   25 CONTINUE
      J=J+1
      XU(J)=B(I)
      GOTO 20
   65 K1=K1+1
   20 CONTINUE
C
C     SCALE THE PARAMETERS OF THE OPT.
C
      DO 30 I=1,NU
   30 X(I)=XU(I)/SC(I)
      NU1=NU+1
      NU2=NU+NBR
      LU=0
      DO 35 I=NU1,NU2
      LU=LU+1
   35 X(I)=RHH(LU)/SC(I)
      X(N)=RL/SC(N)
      DO 33 I=1,N
      BL(I)=BL(I)/SC(I)
   33 BU(I)=BU(I)/SC(I)
      READ(4,*)(XSS(I),FO(I),OR(I),I=1,NF)
      CALL TIME(1,1)
      LH=200
      LIW=2
      LW=200
      IFAIL=0
      CALL E04HBF(N,FUNCT,X,J,DELTA,HESL,LH,HESD,FU,G,IW,
     $LIW,W,LW,IFAIL)
      BIG=HESD(1)
      SMALL=HESD(1)
      DO 21 J=2,N
      IF(BIG.LT.HESD(J)) BIG=HESD(J)
      IF(SMALL.GT.HESD(J)) SMALL=HESD(J)
   21 CONTINUE
      IF(BIG.LT.1.0D+4*SMALL) GOTO 41
      WRITE(6,97)(HESD(J),J=1,N)
      GOTO 61
   41 CONTINUE
      LOCSCH=.FALSE.
      INTYPE=1
      MAXCAL=40*N*(N+5)
      ETA=0.5
      XTOL=0.0D0
      STEPMX=4.0D0
      FEST=0.0D0
      IBOUND=0
      IFAIL=1
      CALL E04JBF(N,FUNCT,MONIT,IPRINT,LOCSCH,INTYPE,E04JBQ,
     $MAXCAL,ETA,XTOL,STEPMX,FEST,DELTA,IBOUND,BL,BU,X,
     $HESL,LH,HESD,ISTATE,FU,G,IW,LIW,W,LW,IFAIL)
      IF(IFAIL.EQ.-2) IFAIL=0
      CALL TIME(1,1)
      CALL PLOT(F,XSS,NF,NN,FO,NB)
```

```
      CALL TIME(1,1)
      IF(IFAIL.EQ.0) GOTO 61
      IF(IFAIL.NE.0) WRITE(6,96)IFAIL
      IF(IFAIL.EQ.1) GOTO 61
      WRITE(6,95)FU
      WRITE(6,94)(X(J),J=1,N)
      IF(IFAIL.NE.2) GOTO 61
      WRITE(6,93)(ISTATE(J),J=1,N)
      WRITE(6,92)(HESL(J),J=1,LH)
      WRITE(6,91)(HESD(J),J=1,N)
   61 STOP
   98 FORMAT(///1H , I3, 38H FUNCTION EVALUATIONS WERE NEEDED BY E,
     $ 5HO4HBF)
   97 FORMAT(///48H TRY RESCALING THE PROBLEM. ELEMENTS OF HESD ARE
     $ /1H , 1P4E15.4)
   96 FORMAT(///16H ERROR EXIT TYPE, I3, 22H - SEE ROUTINE DOCUMEN,
     $ 1HT)
   95 FORMAT(///27H FUNCTION VALUE ON EXIT IS , F12.4)
   94 FORMAT(13H AT THE POINT, 4F12.4)
   93 FORMAT(22H WHERE ISTATE CONTAINS, 4I5, 1H,)
   92 FORMAT(14H HESL CONTAINS/1H , 1P6E20.4)
   91 FORMAT(18H AND HESD CONTAINS, 1P4E20.4)
      END
      SUBROUTINE FUNCT(IFLAG,N,XC,FC,GC,IW,LIW,W,LW)
C     THE SUBROUTINE FUNCT CAL. OBJECTIVE FUNCTION FOR THE
C     OPT. THIS REQUIRS THE CAL. OF THE GRAVITY ANOMALY DUE TO
C     THE MODEL AND THIS IS PERFORMED USING THE END
C     CORRECTION METHOD.
C
      IMPLICIT REAL*8(A-H,O-Z)
      DIMENSION X(50),Z(50),XR(50),XL(50),NI(50),NZL(50),NZR(50)
     $,ZC(50),XRC(50),XLC(50),GR(50),CR(50),GL(50),CL(50),SLO(10)
     $,ZR(50),ZL(50),XLA(50),ZLA(50),X1(100),X2(100),X3(100),X4(100)
     $,Z1(100),Z2(100),Z3(100),Z4(100),XT(100),MX(50),XB(100),ZB(100)
     $,RR(10),MXX(10,10),NII(50),XG(100),ZG(100),YB(100),FO(100)
     $,KN(10),KNA(10),KNB(10),X5(100),Z5(100),NN(10),NNZ(10),NG(100)
     $,XSS(100),F(100),RH(10),XA(10),ZA(10),B(100),NO(50),NE(90)
     $,SC(20),BL(20),BU(20),XUU(20),GC(N),W(LW),XC(N),IW(LIW)
     $,EC(50,50),FS(50,50),OR(100),NR(10),RHH(10)
      COMMON/COM1/NB,NT,NN,NNZ,MXX,NII,NT2,NON,NEN,NO,NE
     $,NU1,NU2,NU,NR,NBR
      COMMON/COM2/RR,YB,FO,SLO,B,SC,F,RMSEG,OR,RGL
      COMMON/COM3/NF,NNF,ZS,XSS
      COMMON/CLAB/FS
      COMMON/CEC/EC
      COMMON/COMP/X1,Z1,X2,Z2,X3,Z3,X4,Z4,X5,Z5,XG,ZG,NG,XB,ZB,K1
C
C     UNSCALE THE PARAMETERS PASSED INTO THE SUBROUTINE
C     FROM THE OPTIMIZATION ROUTINE.
C
      DO 2 I=1,NU
    2 XUU(I)=XC(I)*SC(I)
      LU=0
      DO 9 I=NU1,NU2
      LU=LU+1
    9 RHH(LU)=XC(I)*SC(I)
      RL=XC(N)*SC(N).
      DO 13 I=1,NB
```

```
      J=NR(I)
   13 RH(I)=RHH(J)
C
C     ARRANGE THE OPTIMIZED BODY PTS. WITH OTHER BODY PTS.
C     WHICH WERE NOT INCLUDED IN THE OPT. PROCESS
C     IN THE PROPER ORDER.
C
      J=0
      K1=1
      DO 6 I=1,NT2
      DO 8 K=K1,NON
      IF(I.EQ.NO(K)) GOTO 12
    8 CONTINUE
      J=J+1
      B(I)=XUU(J)
      GOTO 6
   12 K1=K1+1
    6 CONTINUE
      DO 14 I=1,NEN
      J=NE(I)
      IF(J.EQ.0) GOTO 14
      K=I+1
      L=NE(K)
      IF(L.EQ.0) GOTO 14
      B(L)=B(J)
   14 CONTINUE
      DO 18 I=1,NT
      J=2*I
      K=J-1
      XB(I)=B(K)
      ZB(I)=B(J)
   18 CONTINUE
      DO 17 I=1,NF
   17 F(I)=RL+RLG*XSS(I)
      K1=0
      KB1=1
      DO 1 IK=1,NB
      NH=NN(IK)
      NZ=NNZ(IK)
      R=RR(IK)
      SLP=SLO(IK)
      DO 3 I=1,NZ
    3 MX(I)=MXX(I,IK)
      KB2=KB1+NH-1
      J=0
      DO 7 I=KB1,KB2
      J=J+1
      X(J)=XB(I)
      Z(J)=ZB(I)
    7 NI(J)=NII(I)
      KB1=KB2+1
C
C     SELECT CORRDS OF THE B.PTS. WHICH ARE ON RHS. AND LHS.
C
      LR=0
      LL=0
      DO 10 I=1,NH
      IF(NI(I).EQ.0) GOTO 20
```

```
      LR=LR+1
      XR(LR)=X(I)
      ZR(LR)=Z(I)
      GOTO 10
   20 LL=LL+1
      XLA(LL)=X(I)
      ZLA(LL)=Z(I)
   10 CONTINUE
      XL(1)=XLA(1)
      ZL(1)=ZLA(1)
      DO 5 I=2,LL
      K=LL+2-I
      XL(I)=XLA(K)
    5 ZL(I)=ZLA(K)
      LRR=LR-1
C
C     CALC. GRAD. AND INTCEPT. OF SIDES ON RHS.
C
      DO 30 I=1,LRR
      J=I+1
      XXR=XR(I)-XR(J)
      XXRA=DABS(XXR)
      IF(XXRA.LT.0.000001D0) GOTO 40
      GR(I)=(ZR(I)-ZR(J))/XXR
      CR(I)=ZR(I)-GR(I)*XR(I)
      GOTO 30
   40 GR(I)=10.0D+10
      CR(I)=0.0D0
   30 CONTINUE
      LLL=LL-1
C
C     CALC. GRAD. INCEPT. OF SIDES ON LHS.
C
      DO 60 I=1,LLL
      J=I+1
      XXL=XL(I)-XL(J)
      XXLL=DABS(XXL)
      IF(XXLL.LT.0.000001D0) GOTO 70
      GL(I)=(ZL(I)-ZL(J))/XXL
      CL(I)=ZL(I)-GL(I)*XL(I)
      GOTO 60
   70 GL(I)=10.0D+10
      CL(I)=0.0D0
   60 CONTINUE
C
C     CALC. COM. DIFF. OF ARITH. PROG. H. STRIPS FORM.
C
      R2=R/2.0D0
      SN=NZ+(NZ*NZ-NZ)*R2
      ZZ=ZL(LL)-ZL(1)
      A=ZZ/SN
      ZC(1)=ZL(1)
      NZL(1)=1
      NZR(1)=1
      DO 80 L=1,NZ
      L1=L+1
      SL=L+(L*L-L)*R2
      ZC(L1)=ZL(1)+A*SL
```

```
      DO 90 I=1,LLL
      J=I+1
      IF(A.LT.0.0) GOTO 94
      IF(ZC(L1).LT.ZL(J).AND.ZC(L1).GT.ZL(I)) NZL(L1)=I
      IF(ZC(L1).LT.ZL(J)) GOTO 100
      GOTO 90
   94 IF(ZC(L1).GT.ZL(J).AND.ZC(L1).LT.ZL(I)) NZL(L1)=I
      IF(ZC(L1).GT.ZL(J)) GOTO 100
   90 CONTINUE
  100 DO 110 I=1,LRR
      J=I+1
      IF(A.LT.0.0) GOTO 96
      IF(ZC(L1).LT.ZR(J).AND.ZC(L1).GT.ZR(I)) NZR(L1)=I
      IF(ZC(L1).LT.ZR(J)) GOTO 80
      GOTO 110
   96 IF(ZC(L1).GT.ZR(J).AND.ZC(L1).LT.ZR(I)) NZR(L1)=I
      IF(ZC(L1).GT.ZR(J)) GOTO 80
  110 CONTINUE
   80 CONTINUE
C
C     DIVIDE EACH BODY INTO HORIZONTAL STRIPS.
C
      DO 120 I=1,NZ
      JL=NZL(I)
      IF(GL(JL).GT.10.0D+9) GOTO 130
      XLC(I)=(ZC(I)-CL(JL))/GL(JL)
      GOTO 140
  130 XLC(I)=XL(JL)
  140 JR=NZR(I)
      IF(GR(JR).GT.10.0D+9) GOTO 150
      XRC(I)=(ZC(I)-CR(JR))/GR(JR)
      GOTO 120
  150 XRC(I)=XR(JR)
  120 CONTINUE
      NZZ=NZ+1
      XRC(NZZ)=XR(LR)
      XLC(NZZ)=XL(LL)
      NZL(NZZ)=LLL
      NZR(NZZ)=LRR
      DO 160 J=1,NZ
      M=MX(J)+1
C
C      DIVIDE EACH STRIP INTO ELEMENTS.
C
      DO 170 L1=1,M
  170 XT(L1)=XLC(J)+(L1-1)*(XRC(J)-XLC(J))/(M-1)
      J1=J+1
      M=M-1
      DO 180 I=1,M
      IF(I.EQ.1) GOTO 190
      IF(I.EQ.M) GOTO 200
      K1=K1+1
      I1=I+1
      X1(K1)=XT(I)
      Z1(K1)=ZC(J)
      X2(K1)=XT(I1)
      Z2(K1)=ZC(J)
      X3(K1)=XT(I1)
```

```
      Z3(K1)=ZC(J1)
      X4(K1)=XT(I)
      Z4(K1)=ZC(J1)
      X5(K1)=0.0D0
      Z5(K1)=0.0D0
      XG(K1)=(X1(K1)+X2(K1)+X3(K1)+X4(K1))/4.0D0
      ZG(K1)=(Z1(K1)+Z2(K1)+Z3(K1)+Z4(K1))/4.0D0
      NG(K1)=4
      GOTO 185
  190 N1=NZL(J)
      N2=NZL(J1)
      IF(N1.NE.N2) GOTO 210
      K1=K1+1
      X1(K1)=XT(1)
      Z1(K1)=ZC(J)
      X2(K1)=XT(2)
      Z2(K1)=ZC(J)
      X3(K1)=XT(2)
      Z3(K1)=ZC(J1)
      X4(K1)=XLC(J1)
      Z4(K1)=ZC(J1)
      IF(M.EQ.1) X3(K1)=XRC(J1)
      X5(K1)=0.0D0
      Z5(K1)=0.0D0
      GOTO 195
  200 N1=NZR(J)
      N2=NZR(J1)
      IF(N1.NE.N2) GOTO 220
      K1=K1+1
      X1(K1)=XT(M)
      Z1(K1)=ZC(J)
      X2(K1)=XRC(J)
      Z2(K1)=ZC(J)
      X3(K1)=XRC(J1)
      Z3(K1)=ZC(J1)
      X4(K1)=XT(M)
      Z4(K1)=ZC(J1)
      X5(K1)=0.0D0
      Z5(K1)=0.0D0
  195 NG(K1)=4
C
C       CALC. CMASS OF ELEMENTS HAVING 4 SIDES.
C
      CALL CMASS(X1(K1),Z1(K1),X2(K1),Z2(K1),X3(K1),Z3(K1)
     $,X4(K1),Z4(K1),X5(K1),Z5(K1),NG(K1),XCG,ZCG)
      XG(K1)=XCG
      ZG(K1)=ZCG
  185 ZD=ZG(K1)-ZB(1)
      Y=YB(K1)+ZD*SLP
      RHO=RH(IK)
C
C       CALC. ENECR FACTOR FOR ELEMENTS HAVING 4 SIDES.
C
      CALL ENDCR(XG(K1),ZG(K1),Y,I)
      XA(1)=X4(K1)
      ZA(1)=Z4(K1)
      XA(2)=X1(K1)
      ZA(2)=Z1(K1)
```

```
      LAB=1
C
C       CALC. GRAV. ANOM. DUE TO 2D PRISMS CORR. ELEM.
C       HAVING 4 SIDES AND MULTIPLY BY THE CORR. ENDCR FAC.
C
      CALL SLAB(XA,ZA,LAB,I,RHO)
      IF(I.NE.M) GOTO 211
      XA(1)=X3(K1)
      ZA(1)=Z3(K1)
      XA(2)=X2(K1)
      ZA(2)=Z2(K1)
      KR=I+1
      CALL SLAB(XA,ZA,LAB,KR,RHO)
  211 GOTO 180
  210 K1=K1+1
      X1(K1)=XT(1)
      Z1(K1)=ZC(J)
      X2(K1)=XT(2)
      Z2(K1)=ZC(J)
      X3(K1)=XT(2)
      Z3(K1)=ZC(J1)
      X4(K1)=XLC(J1)
      Z4(K1)=ZC(J1)
      X5(K1)=XL(N2)
      Z5(K1)=ZL(N2)
      GOTO 205
  220 K1=K1+1
      X1(K1)=XT(M)
      Z1(K1)=ZC(J)
      X2(K1)=XRC(J)
      Z2(K1)=ZC(J)
      X3(K1)=XR(N2)
      Z3(K1)=ZR(N2)
      X4(K1)=XRC(J1)
      Z4(K1)=ZC(J1)
      X5(K1)=XT(M)
      Z5(K1)=ZC(J1)
  205 NG(K1)=5
C
C       CALC. CMASS OF ELEMTS. HAVING 5 SIDES.
C
      CALL CMASS(X1(K1),Z1(K1),X2(K1),Z2(K1),X3(K1),Z3(K1)
     $,X4(K1),Z4(K1),X5(K1),Z5(K1),NG(K1),XCG,ZCG)
      XG(K1)=XCG
      ZG(K1)=ZCG
      ZD=ZG(K1)-ZB(1)
      Y=YB(K1)+ZD*SLP
      RHO=RH(IK)
C
C       CALC. ENDCR. FACT. FOR ELEM. HAVING 5 SIDES.
C
      CALL ENDCR(XG(K1),ZG(K1),Y,I)
      IF(I.EQ.M) GOTO 212
      XA(1)=X4(K1)
      ZA(1)=Z4(K1)
      XA(2)=X5(K1)
      ZA(2)=Z5(K1)
      XA(3)=X1(K1)
```

```
      ZA(3)=Z1(K1)
      LAB=2
C
C     CALC. 2D GRAVITY ANOMALY DUE TO PRISMS CORR. TO
C     THE ELEMENTS HAVING 5 SIDES AND MULTIPLY BY THE
C     CORR. ENDCR FACT.
C
      CALL SLAB(XA,ZA,LAB,I,RHO)
      GOTO 180
  212 XA(1)=X5(K1)
      ZA(1)=Z5(K1)
      XA(2)=X1(K1)
      ZA(2)=Z1(K1)
      LAB=1
      CALL SLAB(XA,ZA,LAB,I,RHO)
      XA(1)=X4(K1)
      ZA(1)=Z4(K1)
      XA(2)=X3(K1)
      ZA(2)=Z3(K1)
      XA(3)=X2(K1)
      ZA(3)=Z2(K1)
      LAB=2
      KR=I+1
      CALL SLAB(XA,ZA,LAB,KR,RHO)
  180 CONTINUE
C
C     CALC. THE OBJ. FUNCTION.
C
      DO 181 I1=1,NF
      DO 181 J1=1,M
      J2=J1+1
  181 F(I1)=(FS(I1,J1)-FS(I1,J2))*EC(I1,J1)+F(I1)
  160 CONTINUE
    1 CONTINUE
      SUMF=0.0D0
      DO 11 I=1,NF
      SUMF=SUMF+(F(I)-F0(I))*(F(I)-F0(I))*OR(I)
   11 CONTINUE
      FC=SUMF
      RMSE=DSQRT(FC/NF)
      IF(RMSE.LE.RMSEG) IFLAG=-2
      RETURN
      END
      SUBROUTINE CMASS(A1,A2,A3,A4,A5,A6,A7,A8,A9,A10
C
C     THE SUBROUTINE CMASS CALC. CMASS OF EACH ELEMENT.
C
     $,NS,XCG,ZCG)
      IMPLICIT REAL*8(A-H,O-Z)
      DIMENSION X(10),Z(10)
      X(1)=A1
      Z(1)=A2
      X(2)=A3
      Z(2)=A4
      X(3)=A5
      Z(3)=A6
      X(4)=A7
      Z(4)=A8
```

```
      IF (NS.EQ.4) GOTO 5
      X(5)=A9
      Z(5)=A10
    5 N=NS-2
      SA=0.0D0
      SX=0.0D0
      SZ=0.0D0
      DO 10 I=1,N
      M=I+1
      L=I+2
      A=(X(M)*Z(L)-Z(M)*X(L)-X(1)*Z(L)+Z(1)*X(L)+X(1)*Z(M)-Z(1)*
     $X(M))/2.0
      SA=SA+A
      XSS=A*(X(1)+X(M)+X(L))
      SZZ=A*(Z(1)+Z(M)+Z(L))
      SX=XSS+SX
   10 SZ=SZZ+SZ
      XCG=SX/SA/3.0D0
      ZCG=SZ/SA/3.0D0
      RETURN
      END
      SUBROUTINE SLAB(XB,ZB,N,K,RHO)
C
C     THE SUBROUTINE SLAB CALC. GRAV. ANOMALY DUE TO A 2D
C     PRISM AND MULTIPLY BY ENDCR. FACTORS.
C
      IMPLICIT REAL*8(A-H,O-Z)
      DIMENSION XSS(100),FS(50,50),XB(5),ZB(5),SI(5),CO(5)
      COMMON/COM3/NF,NFF,ZS,XSS
      COMMON/CLAB/FS
      PI2=2.0D0*DATAN(1.D0)
      CC=RHO*13.34D0
      DO 5 J=1,N
      J1=J+1
      XBD=XB(J)-XB(J1)
      ZBD=ZB(J1)-ZB(J)
      RBD=DSQRT(XBD*XBD+ZBD*ZBD)
      SI(J)=ZBD/RBD
    5 CO(J)=XBD/RBD
      DO 15 I=1,NF
      SUM=0.0D0
      DO 10 J=1,N
      J1=J+1
      XS=XSS(I)
      X1=XB(J)-XS
      X2=XB(J1)-XS
      Z1=ZB(J)-ZS
      Z2=ZB(J1)-ZS
      AX1=DABS(X1)
      AX2=DABS(X2)
      IF(AX1.LT.0.000001D0) GOTO 20
      T1=DATAN2(Z1,X1)
      GOTO 30
   20 T1=PI2
   30 IF(AX2.LT.0.000001D0) GOTO 40
      T2=DATAN2(Z2,X2)
      GOTO 50
   40 T2=PI2
```

```
   50 R1=DSQRT(X1*X1+Z1*Z1)
      R2=DSQRT(X2*X2+Z2*Z2)
      TT=T1-T2
      RL=DLOG(R2/R1)
      SUM=-CC*((Z1*CO(J)+X1*SI(J))*(TT*CO(J)-RL*SI(J))+Z2*T2-Z1*T1)
     $+SUM
   10 CONTINUE
      FS(I,K)=SUM
   15 CONTINUE
      RETURN
      END
      SUBROUTINE ENDCR(XC,ZC,Y,J)
C
C     THE SUBROUTINE ENDCR CALC. ENDCR. FACTOR FOR EACH
C     PRISM FOR EACH FIELD POINT.
C
      IMPLICIT REAL*8(A-H,O-Z)
      DIMENSION XSS(100),EC(50,50)
      COMMON/COM3/NF,NNF,ZS,XSS
      COMMON/CEC/EC
      DO 10 I=1,NF
      XE=XC-XSS(1)
      ZE=ZC-ZS
      R=DSQRT(XE*XE+ZE*ZE)
      D=DSQRT(1.0+(R/Y)*(R/Y))
   10 EC(I,J)=1.0D0/D
      RETURN
      END
      SUBROUTINE PLOT(F,XSS,NF,NN,FO,NB)
C
C     THE SUBROUTINE PLOT DRAWS 2 PLOTS AS OUTPUT.
C     FIRST PLOT SHOWS THE WAY IN WHICH THE BODY IS
C     SUBDIVISED. 2ED PLOT SHOWS OBS. CALC. AND. AND
C     X-SECTION OF THE MODEL ON PLANE OF THE PROFILE.
C
C
      REAL*8 F,XSS,FO,XB,ZB,X1,X2,X3,X4,X5,Z1,Z2,Z3,Z4,Z5
     $,XG,ZG
      REAL*4 XA1,XA2,XA3,XA4,XA5,ZA1,ZA2,ZA3,ZA4,ZA5,XGA,ZGA
     $,XXS,X,Z,FOB,FCL
      DIMENSION XSS(100),F(100),FO(100),X(50),Z(50),NN(10),XG(100)
     $,ZG(100),X1(100),Z1(100),X2(100),Z2(100),X3(100),Z3(100)
     $,X4(100),Z4(100),X5(100),Z5(100),NG(100),YY(20),XB(100),ZB(100)
     $,XA1(100),XA2(100),XA3(100),XA4(100),XA5(100),ZA1(100),
     $ZA2(100),ZA3(100),ZA4(100),ZA5(100),XGA(100),ZGA(100)
     $,XXS(100),FOB(100),FCL(100)
      COMMON/COMP/X1,Z1,X2,Z2,X3,Z3,X4,Z4,X5,Z5,XG,ZG,NG,XB,ZB,K1
      CALL PAPER(1)
      DO 6 I=1,K1
      XA1(I)=X1(I)
      ZA1(I)=Z1(I)
      XA2(I)=X2(I)
      ZA2(I)=Z2(I)
      XA3(I)=X3(I)
      ZA3(I)=Z3(I)
      XA4(I)=X4(I)
      ZA4(I)=Z4(I)
      XA5(I)=X5(I)
```

```
      ZA5(I)=Z5(I)
      XGA(I)=XG(I)
    6 ZGA(I)=ZG(I)
      DO 8 I=1,NF
      XXS(I)=XSS(I)
      FOB(I)=FO(I)
    8 FCL(I)=F(I)
      CALL PSPACE(0.0,1.0,0.0,1.0)
      CALL CSPACE(0.0,1.0,0.0,1.0)
      CALL MAP(15.0,30.0,10.0,0.0)
      DO 12 I=1,K1
      CALL POSITN(XA1(I),ZA1(I))
      CALL JOIN(XA2(I),ZA2(I))
      CALL JOIN(XA3(I),ZA3(I))
      CALL JOIN(XA4(I),ZA4(I))
      IF(NG(I).EQ.4) GOTO 14
      CALL JOIN(XA5(I),ZA5(I))
   14 CALL JOIN(XA1(I),ZA1(I))
   12 CONTINUE
      DO 18 I=1,K1
      CALL POSITN(XGA(I),ZGA(I))
   18 CALL CIRCLE(0.05)
      CALL BORDER
      CALL GRENDO
      CALL PAPER(1)
      CALL PSPACE(0.2,0.8,0.55,0.9)
      CALL MAP(XXS(1),XXS(NF),0.0,1200.0)
      CALL CTRMAG(7)
      CALL NSCURV(XXS,FCL,1,NF)
      CALL AXESSI(5.0,5.0)
      CALL POSITN(2.0,800.0)
      CALL JOIN(5.0,800.0)
      CALL CSPACE(0.2,0.8,0.55,0.9)
      CALL PLOTCS(5.1,750.0,'OBSERVED ANOMALY',16)
      CALL PLOTCS(5.1,800.0,'CALCULATED ANOMALY',18)
      CALL PLOTCS(5.1,700.0,'J=5.3A/M.',9)
      CALL BROKEN(1,3,1,3)
      CALL NSCURV(XXS,FOB,1,NF)
      CALL POSITN(2.0,750.0)
      CALL JOIN(5.0,750.0)
      CALL FULL
      CALL BORDER
      CALL PSPACE(0.2,0.8,0.15,0.5)
      CALL CSPACE(0.2,0.8,0.1,0.5)
      CALL MAP(XXS(1),XXS(NF),15.0,0.0)
      L1=1
      DO 10 M=1,NB
      N=NN(M)
      L2=L1+N-1
      K=0
      DO 20 I=L1,L2
      K=K+1
      X(K)=XB(I)
   20 Z(K)=ZB(I)
      L1=L2+1
      DO 10 I=1,N
      J=I+1
      IF(I.EQ.N) J=1
```

```
      CALL POSITN(X(I),Z(I))
      CALL JOIN(X(J),Z(J))
   10 CONTINUE
      CALL PLOTCS(2.0,16.0,'WIDTH OF THE',12)
      CALL PLOTCS(2.0,17.5,'CENTRAL BODY=5KM.',17)
      CALL BORDER
      CALL PSPACE(0.0,1.0,0.0,1.0)
      CALL CSPACE(0.0,1.0,0.0,1.0)
      CALL MAP(0.0,1.0,0.0,1.0)
      CALL PLOTCS(0.47,0.52,'DISTANCE(KM.)',13)
      CALL CTRORI(1.0)
      CALL PLOTCS(0.163,0.65,'PSEUDOGRAVIMETRIC ANOMALY(MGAL.)',32)
      CALL CTRORI(3.0)
      CALL PLOTCS(0.16,0.35,'DEPTH(KM.)',10)
      CALL CTRORI(0.0)
      DO 50 J=1,5
      XP=0.187
      YY(J)=(J-1)*0.35/5.0
      I=(6-J)*3
      Y=YY(J)+0.15
      CALL PLOTNI(XP,Y,I)
   50 CONTINUE
      CALL PSPACE(0.15,0.85,0.1,0.95)
      CALL BORDER
      CALL GREND
      RETURN
      END
```

```
      SUBROUTINE MONIT(N,XC,FC,GC,ISTATE,GPJNRM,COND,POSDEF,
     $NITER,NF,IW,LIW,W,LW)
      IMPLICIT REAL*8(A-H,O-Z)
      DIMENSION GC(N),W(LW),XC(N),ISTATE(N),IW(LIW)
      LOGICAL POSDEF
      WRITE(6,99)NITER,NF,FC,GPJNRM
      WRITE(6,98)
   25 FORMAT('MONIT1')
      DO 100 J=1,N
      ISJ=ISTATE(J)
      IF(ISJ.GT.0) GOTO 20
      ISJ=-ISJ
      GOTO(40,60,80),ISJ
   20 WRITE(6,97)J,XC(J),GC(J)
      GOTO 100
   40 WRITE(6,96)J,XC(J),GC(J)
      GOTO 100
   60 WRITE(6,95)J,XC(J),GC(J)
      GOTO 100
   80 WRITE(6,94)J,XC(J),GC(J)
  100 CONTINUE
      IF(COND.EQ.0.0D0) RETURN
      IF(COND.LE.1.0D+6) GOTO 120
      WRITE(6,93)
      GOTO 140
  120 WRITE(6,92)COND
  140 IF(.NOT.POSDEF) WRITE(6,91)
      RETURN
   99 FORMAT(/5HOITNS, 5X, 8HFN EVALS, 11X, 8HFN VALUE, 11X,
     $ 21HNORM OF PROJ GRADIENT/I4, 6X, I5, 2(6X, 1PE20.4))
   98 FORMAT(3HO J, 11X, 4HX(J), 16X, 4HG(J), 13X, 6HSTATUS)
```

```
97 FORMAT(1H , I2, 1X, 1P2E20.4, 5X, 4HFREE)
96 FORMAT(1H , I2, 1X, 1P2E20.4, 5X, 11HUPPER BOUND)
95 FORMAT(1H , I2, 1X, 1P2E20.4, 5X, 11HLOWER BOUND)
94 FORMAT(1H , I2, 1X, 1P2E20.4, 5X, 8HCONSTANT)
93 FORMAT(50HOESTIMATED CONDITION NUMBER OF PROJECTED HESSIAN =,
  $ 4HS MO, 14HRE THAN 1.0D+6)
92 FORMAT(50HOESTIMATED CONDITION NUMBER OF PROJECTED HESSIAN =,
  $ 1H , 1PE10.2)
91 FORMAT(50HOPROJECTED HESSIAN MATRIX IS NOT POSITIVE DEFINITE)
   END
```

```
C       PROGRAM MAG1     D.A.TANTRIGODA      1981
C
C      THE PROGRAM MAG1 PERFORMS 2D MAGNETIC INTERPRETATION
C      USING A NON-LINEAR OPT. TECHNIQUE(A QUASI-NEWTON METHOD)
C
C      INPUT DATA
C      ST=FIRST FIELD POINT.
C      AINT=INTERVALS AT WHICH OBS. ARE MADE.
C      AJ=MAG. OF THE TRIAL MODEL.
C      A=INCL. OF MAG. OF THE TRIAL MODEL.
C      EI=INCL. OF EARTH'S MAG. FIELD.
C      CED=ANG. BETWEEN THE PROFILE AND THE MAG. NORTH.
C      ZS=HEIGHT AT WHICH OBS. ARE MADE.
C      NB=NO. OF BODY PTS.
C      NS=NO. OF FIELD PTS.
C      RL=CONST. REG. LEVEL.
C      XB,ZB(1D ARRAYS) X AND Z BODY COORDS.
C      BL,BU,SC(1D ARRAYS) LOW. AND UPP. LIMITS OF THE
C      PARAMETRES AND SCALING FACTORS.
C      FO,XO,WT(1D ARRAY) OBS. AND. VALS , THEIR X-COORS
C      AND WEIGHTING COEFFICIENTS.
C
      IMPLICIT REAL*8(A-H,O-Z)
      DIMENSION XB(10),ZB(10),T(10),XS(100),F(100),XO(100),FO(100)
     $,BL(11),BU(11),X(11),W(187),IW(13),WT(100),SC(11)
      COMMON/COM1/PI2,XS,F,FO,NS,NB,EI,XB,ZB,CED,AJ,A,RL,NN,NNN
     $,WT,SC
      READ(5,*)ST,AIN,AJ,A,EI,CED,ZS,NB,NS,RL
      READ(5,*)(XB(I),ZB(I),I=1,NB)
      NN=NB*2
      NNN=NN+3
      READ(5,*)(BL(I),BU(I),SC(I),I=1,NNN)
      READ(7,*)(XO(I),FO(I),WT(I),I=1,NS)
      PI=4.0*ATAN(1.0)
      DR=PI/180.0
      PI2=PI/2.0
      A=DR*A
      BL(2)=BL(2)*DR
      BU(2)=BU(2)*DR
      SC(2)=SC(2)*DR
      EI=DR*EI
      CED=DR*CED
      DO 1 I=1,NB
    1 ZB(I)=ZB(I)-ZS
      DO 10 I=1,NS
   10 XS(I)=ST+(I-1)*AIN
      X(1)=AJ/SC(1)
      X(2)=A/SC(2)
      X(3)=RL/SC(3)
      DO 60 I=1,NB
      J=I+3
      K=J+3
      X(J)=XB(I)
   60 Z(K)=ZB(I)
      DO  50 I=1,NNN
      BL(I)=BL(I)/SC(I)
   50 BU(I)=BU(I)/SC(I)
      N=NNN
```

```
      IBOUND=0
      LIW=13
      LW=187
      IFAIL=1
      CALL E04JAF(N,IBOUND,BL,BU,X,F,IW,LIW,W,LW,IFAIL)
      IF(IFAIL.NE.0) WRITE(6,998)IFAIL
      IF(IFAIL.EQ.1) GOTO 25
      WRITE(6,997)F
      WRITE(6,996)(X(J),J=1,N)
      WRITE(6,22)AJ,A,RL
      WRITE(6,22)(XB(I),ZB(I),I=1,NB)
   22 FORMAT(1H , 4F10.4)
   25 STOP
  998 FORMAT(///16H ERROR EXIT TYPE, I3, 22H - SEE ROUTINE DOCUMEN,
     $ 1HT)
  997 FORMAT(///27H FUNCTION VALUE ON EXIT IS , F10.4)
  996 FORMAT(13H AT THE POINT, 4F9.4)
      END
      SUBROUTINE FUNCT1(N,XC,FC)
      IMPLICIT REAL*8(A-H,O-Z)
      DIMENSION XB(10),ZB(10),XX(10),T(10),F(100),FO(100),XS(100)
     $,XC(N),WT(100),SC(11)
      COMMON/COM1/PI2,XS,F,FO,NS,NB,EI,XB,ZB,CED,AJ,A,RL,NN,NNN
     $,WT,SC
      FC=0.0
      AJ=XC(1)*SC(1)
      A=XC(2)*SC(2)
      RL=XC(3)*SC(3)
      DO 65 I=1,NB
      J=I+3
      K=J+NB
      XB(I)=XC(J)
   65 ZB(I)=XC(K)
      XJ=AJ*DCOS(A)
      ZJ=AJ*DSIN(A)
      DO 10 I=1,NS
      DO 20 J=1,NB
      XX(J)=XB(J)-XS(I)
      XSS=DABS(XX(J))
      IF(XSS.LT.0.000001) GOTO 30
      T(J)=DATAN2(ZB(J),XX(J))
      GOTO 20
   30 T(J)=PI2
   20 CONTINUE
      SUM=0.0
      DO 50 J=1,NB
      K=J+1
      IF(J.EQ.NB) K=1
      X1=XX(J)
      Z1=ZB(J)
      T1=T(J)
      X2=XX(K)
      Z2=ZB(K)
      T2=T(K)
      ZA=Z1-Z2
      ZA=DABS(ZA)
      IF(ZA.LT.0.00000001) GOTO 50
      R1=DSQRT(X1*X1+Z1*Z1)
```

```
      R2=DSQRT(X2*X2+Z2*Z2)
      X12=X1-X2
      Z21=Z2-Z1
      T12=T1-T2
      RRX=R2/R1
      RR=DLOG(RRX)
      ZZ=Z21*Z21
      XZ=Z21*X12
      DE=ZZ+X12*X12
      P=(ZZ*T12+XZ*RR)/DE
      Q=(XZ*T12-ZZ*RR)/DE
      V=2.0*(XJ*Q-ZJ*P)
      H=2.0*(XJ*P+ZJ*Q)
      TF=V*DSIN(EI)+H*DCOS(EI)*DCOS(CED)
      SUM=SUM+TF
   50 CONTINUE
      F(I)=100.0*SUM+RL
      FC=FC+(F(I)-FO(I))*(F(I)-FO(I))*WT(I)
   10 CONTINUE
      RETURN
      END
```

```
C          PROGRAM MAG2    D.A.TANTRIGODA     1981.
C
C       THE PROGRAM MAG2 PERFORMS 2D MAGNETIC INTERPRETATION
C       USING A NON-LINEAR OPTIMIZATION TECHNIQUE(SIMPLEX METHOD).
C       BODY COORD. AND THE REG. GRADIENT ARE EVALUATED BY THE
C       OPT. PROCESS. MAGNETIZATION AND THE CONSTANT REG. LEVEL
C       ARE EVALUATED USING THE LEAST SQUARES METHOD.
C
C        INPUT DATA
C
C       ST,AIN,ZS,NS,NB,XB,ZB,XO,FO,SC,CED--AS SAME AS IN MAG1.
C       EI=INCLINATION OF EARTH'S MAG. FIELD.
C       G=INITIAL ESTIMATE OF THE REG. GRAD.
C
        IMPLICIT REAL*8(A-H,O-Z)
        DIMENSION XB(10),ZB(10),XS(100),FO(100),XO(100),
     $X(9),SIM(10,9),W1(9),W2(9),W3(9),W4(9),W5(10),SC(20)
        COMMON/COM/FO,SEI,CEI,CED,PI2,NS,NN
        COMMON/COM1/FS,XSA,XS,NB
        EXTERNAL FUNCT,MONIT
        READ(5,*)ST,AIN,EI,ED,ZS,NB,NS,G
        READ(5,*)(XB(I),ZB(I),I=1,NB)
        NN=2*NB+1
        READ(5,*)(SC(I),I=1,NN)
        READ(7,*)(XO(I),FO(I),I=1,NS)
        PI=4.0D0*DATAN(1.0D0)
        DR=PI/180.0D0
        PI2=PI/2.0D0
        EI=DR*EI
        CED=DR*CED
        SEI=DSIN(EI)
        CEI=DCOS(EI)
        CED=DCOS(CED)
        DO 1 I=1,NB
      1 ZB(I)=ZB(I)-ZS
        XSA=0.0D0
        FS=0.0D0
        DO 10 I=1,NS
        XS(I)=ST+(I-1)*AIN
        XSA=XSA+XS(I)
     10 FS=FS+FO(I)
        N=NN
        DO 60 I=1,NB
        J=I+NB
        X(I)=XB(I)/SC(I)
     60 X(J)=ZB(I)/SC(J)
        X(NN)=G/SC(NN)
        TOL=DSQRT(X02AAF(R))
        N1=N+1
        MAXCAL=500
        IFAIL=0
C
C       EVALUATE BODY COORDS. AND REG. GRAD. USING THE OPT.
C
        CALL E04CCF(N,X,F,TOL,N1,W1,W2,W3,W4,W5,SIM,FUNCT,
      $MONIT,MAXCAL,IFAIL)
        CALL FUNCT(N,XC,FC)
        WRITE(6,998)F
```

```
      WRITE(6,997)(X(I),I=1,N)
      WRITE(6,996)IFAIL
  998 FORMAT(25H FINAL FUNCTION VALUE IS , F12.4)
  997 FORMAT(13H AT THE POINT, 9F6.3)
  996 FORMAT(22H THIS HAS ERROR NUMBER, I3)
      STOP
      END
      SUBROUTINE FUNCT(N,XC,FC)
      IMPLICIT REAL*8(A-H,O-Z)
      DIMENSION XB(10),ZB(10),XX(10),T(10),XS(100),FO(100)
     *,V(100),U(100),XC(N)
      COMMON/COM/FO,SEI,CEI,CED,PI2,NS,NN
      COMMON/COM1/FS,XSA,XS,NB
      DO 15 I=1,NB
      J=I+NB
      XB(I)=XC(I)*SC(I)
   15 ZB(I)=XC(J)*SC(J)
      G=XC(NN)*SC(NN)
C
C     EVALUATE THE X AND Z COMP. OF MAG. AND THE CONSTANT
C     REG. LEVEL USING THE LEAST SQUARES METHOD AND
C     CALCULATE THE MAG. ANOMALY AND THE OBJ. FUN.
C
      FUS=0.0D0
      US=0.0D0
      UUS=0.0D0
      VVS=0.0D0
      UVS=0.0D0
      VS=0.0D0
      FVS=0.0D0
      XSU=0.0D0
      XSV=0.0D0
      DO 10 I=1,NS
      DO 20 J=1,NB
      XX(J)=XB(J)-XS(I)
      XSS=DABS(XX(J))
      IF(XSS.LT.0.000001D0) GOTO 30
      T(J)=DATAN2(ZB(J),XX(J))
      GOTO 20
   30 T(J)=PI2
   20 CONTINUE
      SUMU=0.0D0
      SUMV=0.0D0
      DO 50 J=1,NB
      K=J+1
      IF(J.EQ.NB) K=1
      X1=XX(J)
      Z1=ZB(J)
      T1=T(J)
      X2=XX(K)
      Z2=ZB(K)
      T2=T(K)
      ZA=Z1-Z2
      ZA=DABS(ZA)
      IF(ZA.LT.0.00000001D0) GOTO 50
      R1=DSQRT(X1*X1+Z1*Z1)
      R2=DSQRT(X2*X2+Z2*Z2)
      X12=X1-X2
```

```
      Z21=Z2-Z1
      T12=T1-T2
      RR=R2/R1
      RR=DLOG(RR)
      ZZ=Z21*Z21
      XZ=Z21*X12
      DE=ZZ+X12*X12
      P=(ZZ*T12+XZ*RR)/DE
      Q=(XZ*T12-ZZ*RR)/DE
      UU=2.0D0*(Q*SEI+P*CEI*CED)
      VV=2.0D0*(Q*CEI*CED-P*SEI)
      SUMU=SUMU+UU
      SUMV=SUMV+VV
   50 CONTINUE
      U(I)=SUMV*100.0D0
      V(I)=SUMU*100.0D0
      FUS=FUS+F0(I)*U(I)
      US=US+U(I)
      UUS=UUS+U(I)*U(I)
      VVS=VVS+V(I)*V(I)
      VS=VS+V(I)
      FVS=FVS+F0(I)*V(I)
      UVS=UVS+U(I)*V(I)
      XSU=XSU+XS(I)*U(I)
      XSV=XSV+XS(I)*V(I)
   10 CONTINUE
      PA=NS*FUS-FS*US
      RA=NS*UUS-US*US
      WA=NS*UVS-US*VS
      QA=NS*FVS-FS*VS
      SA=NS*VVS-VS*VS
      AA=(NS*XSU-US*XSA)*G
      BB=(NS*XSV-VS*XSA)*G
      PA=PA-AA
      QA=QA-BB
      D=1.0D0/(WA*WA-RA*SA)
      ZJ=D*(WA*QA-SA*PA)
      XJ=D*(WA*PA-RA*QA)
      B=(FS-ZJ*US-XJ*VS-G*XSA)/NS
      SUM=0.0D0
      DO 70 I=1,NS
   70 SUM=SUM+(F0(I)-B-ZJ*U(I)-XJ*V(I)-G*XS(I))**2
      FC=SUM
      RETURN
      END
      SUBROUTINE MONIT(FMIN,FMAX,SIM,N,N1,NCALL)
      IMPLICIT REAL*8(A-H,O-Z)
      DIMENSION SIM(N1,N)
      WRITE(8,999)NCALL,FMIN
      WRITE(8,998)((SIM(I,J),J=1,N),I=1,N1)
  999 FORMAT(6H AFTER, I5, 30H  FUNCTION CALLS, THE VALUE IS,
     $ F10.4, 14H  WITH SIMPLEX)
  998 FORMAT(10(9F7.3/))
      RETURN
      END
```

```
C          SUBROUTINE ENDCRM   D.A.TANTRIGODA     1982.
C
      SUBROUTINE ENDCRM(SX,SY,SZ,XJ,YJ,ZJ,X,Z,Y1,Y2,EC)
C
C     THE SUBROUTINE ENDCRM CALCULATES END CORRECTION FACTOR
C     FOR THE CALCULATION OF THE MAG. ANOMALY DUE TO A 3D
C     BODY AT POINTS ON THE X-AXIS.
C
C      SUBROUTINE ARGUMENTS
C      SX,SY,SZ-DIRCETIONAL COSINES OF THE EARTH'S MAG. FIELD.
C      XJ,YJ,ZJ=X,Y AND Z COMPONENTS OF MAGNETIZATION.
C      Y1,Y2=Y COORDS. OF THE ENDS OF FINITE LINE OF
C      DIPOLES(SEE 3.2)
C      X,Z=HORIZONTAL AND VERTICAL DISTANCES BETWEEN THE FIELD PT.
C          AND LINE OF DIPOLES.
C       EC=CALCULATED END CORRECTION FACTOR.
C
      IMPLICIT REAL*8(A-H,O-Z)
      RO=DSQRT(X*X+Z*Z)
      R1=DSQRT(RO*RO+Y1*Y1)
      R2=DSQRT(RO*RO+Y2*Y2)
      A=(Y2/R2-Y1/R1)/(RO**4)
      C1=1.0/(R1**3)
      C2=1.0/(R2**3)
      B=(Y2*C2-Y1*C1)/(RO*RO)
      DXX=(2.0*X*X-RO*RO)*A+X*X*B
      DZZ=(2.0*Z*Z-RO*RO)*A+Z*Z*B
      DYY=-(DXX+DZZ)
      DXZ=2.0*X*Z*A+X*Z*B
      DXY=X*(C1-C2)
      DZY=Z*(C1-C2)
      F=SX*XJ*DXX+SY*YJ*DYY+SZ*ZJ*DZZ+(SY*ZJ+SZ*YJ)*DZY
     $+(SX*ZJ+SZ*XJ)*DXZ+(SX*YJ+SY*XJ)*DXY
      DXXI=2.0*(X*X-Z*Z)/(RO**4)
      DZZI=-DXXI
      DXZI=4.0DO*X*Z/(RO**4)
      FI=SX*XJ*DXXI+SZ*ZJ*DZZI+(SX*ZJ+SZ*XJ)*DXZI
      EC=F/FI
      RETURN
      END
```